

D2.2 Good practice criteria for multi-variable risk reduction from restoration/ESS at the Pilots, as a function of projection horizon and domain scale, as enablers to introduce risk products in coastal governance

08/03/24

WP2

Lead beneficiary: UPC

Author/s: Manuel Espino, Vicente Gracia, Xavier S.-Artús, M. Liste, Luis Garrote, David Santillan, Ivan Federico, Salvatore Causio, Fabienne Horneman, Silvia Torresan, Elisa Furlan, Grzegorz Rozynski, Luciana Villa, Joanna Staneva, Benjamin Jacob, Wei Chen, Bas van Maren, Richard Marijnissen, Andreas Wurpts, Pushpa Dissanayake, Rosaria Ester Musumeci, Massimiliano Marino, Petya Eftimova, Nikolay Valchev, Elitsa Hineva, Nataliya Andreeva, Bogdan Prodanov, Remi Caillibotte, Christophe Briere, Soazing Mahe, Julien Fornasari & Agustín S.-Arcilla.

REST-COAST

Large Scale RESToration of COASTal Ecosystems through Rivers to Sea Connectivity



Prepared under contract from the European Commission

Grant agreement No. 101037097

EU Horizon 2020 Coordination and Support Action

Project acronym:	REST-COAST
Project full title:	Large Scale RESToration of COASTal Ecosystems through Rivers to Sea Connectivity
Start of the project:	01.10.2021
Duration:	54 months
Project coordinator:	Prof. Agustín Sánchez-Arcilla, Universitat Politècnica De Catalunya (UPC)
Type:	Restoring biodiversity and ecosystem services
Call:	H2020-LC-GD-2020-3
Deliverable title	Good practice criteria for multi-variable risk reduction from restoration/ESS at the Pilots, as a function of projection horizon and domain scale, as enablers to introduce risk products in coastal governance
Deliverable n°	D2.2
Nature of the deliverable:	Report
Dissemination level:	Public
WP responsible:	WP2
Lead beneficiary:	UPC
Citation:	Espino, M., V. Gracia, X. S.-Artús, M. Liste, L. Garrote, D. Santillan, I. Federico, S. Causio, F. Horneman, S. Torresan, E. Furlan, G. Rozynski, L. Villa, J. Staneva, B. Jacob, W. Chen, B. van Maren, R. Marijnissen, A. Wurpts, P. Dissanayake, R. E. Musumeci, M. Marino, P. Eftimova, N. Valchev, E. Hineva, N. Andreeva, B. Prodanov, R. Caillibotte, C. Briere, S. Mahe, J. Fornasari & A. S.-Arcilla. (2024). <i>Good practice criteria for multi-variable risk reduction from restoration/ESS at the Pilots, as a function of projection horizon and domain scale, as enablers to introduce risk products in coastal governance</i> . Deliverable D2.2. EU Horizon 2020 REST-COAST Project, Grant agreement No 101037097
Due date of deliverable:	Month n° 27
Actual submission date:	Month n° 30

Deliverable status:

Version	Status	Date	Author(s)
1.0	Draft	09 October 2023	Manuel Espino (UPC)
1.1	Ebro Delta	30 Nov. 2023	Xavier S..Artus (UPC)
2.0	Ebro River Venice Lagoon Vistula Lagoon	12 Feb. 2024	Luis Garrote (UPM) Ivan Federico (CMCC) Grzegorz Rozynski (IBW)
2.1	Wadden Sea Sicily Lagoon	16 Feb. 2024	Luciana Villa (Hereon) Rosaria Ester Musumeci (UC)
2.2	Foros Bay Arcachon Bay	21 Feb. 2024	Petya Eftimova (BAS) Remi Caillibotte (EGIS)
3.0	Final document	29 Feb. 2024	Manuel Espino (UPC)
4.0	Final revision	04 March 2024	Agustín S.-Arcilla (UPC)
5.0	Final revision	05 June 2025	Agustín S.-Arcilla (UPC)

The content of this deliverable does not necessarily reflect the official opinions of the European Commission or other institutions of the European Union.

Table of Contents

Table of Contents	4
Preface	8
Summary.....	8
List of abbreviations	9
List of Figures	12
1. General introduction	17
2. Multi-risk projections and climate warnings with ESS in Ebro Delta Pilot (UPC, UPM).....	18
2.1. Ebro Delta Coast.....	18
2.1.1. Risk reduction from different approaches	19
2.1.2. Efficiency at long-term under different climate projections	21
2.1.3. Conclusions	26
2.2. Ebro River (UPM).....	27
2.2.1. Numerical simulations on sediment transport to Ebro Delta.....	27
2.2.2. Parameterization of hydro-morpho-eco interactions to simulate ESS	29
2.2.2.1. Approach to the characterization of sediment transport.....	29
2.2.2.2. Numerical analysis of sediment transport.....	30
2.2.2.3. Sediment transport of clay for other flow rates.....	34
2.2.3. Assessment of current, potential and future sediment transport.....	35
2.2.3.1. Current sediment transport	35
2.2.3.2. Potential sediment transport	36
2.2.3.3. Potential sediment transport under different climate projections	39
2.2.3.3.1. Climate projections	39
2.2.3.3.2. Validation against SIMPA data	40
2.2.3.3.3. Results of annual flows under climate projections	42
2.2.3.3.4. Results of potential sediment transport under climate projections	44
2.2.4. Conclusions	45
3. Multi-risk projections and climate warnings with ESS in Wadden Sea Pilot (DEL, HZG, FSK).	47
3.1. Multi-risk projections for ESS of NBS in the Wadden Sea	47
3.1.1. Criteria to assess risk reduction	48
3.1.2. Risk reduction projection for end of the century future climate conditions under the RCP 8.5 scenario.....	49
3.2. Modeling framework.....	50
3.2.1. Modeling impact of seagrass as Nature-based solution (Hereon)	50
3.2.1.1. Modeling workflow	50
3.2.1.2. Modeling workflow for climate projections	51
3.2.2. Role of morphological feedbacks on the effectiveness of Nature-based solutions (Deltares).....	52

3.2.2.1 Model premise	52
3.2.2.2 Model set-up	53
3.2.2.3 Model calibration and validation	53
3.2.2.4 Ecotope quantification	54
3.3. Efficiency of sea-grass in coastal protection (Hereon)	60
3.3.1. Evaluating the benefit of sea-grass under end of the century climate conditions	60
3.4. Role of morphological feedbacks on the effectiveness of Nature-based solutions (Deltares)	65
3.4.1. Role of SLR on ecotopes and flood risk, without morphodynamic adaptation	65
3.4.1.1. Ecotopes	65
3.4.1.2. Flood risk	67
3.4.2. Scenarios of measures	69
3.4.2.1. Autonomous development	70
3.4.2.2. Measure VLOED	70
3.4.2.3. Sediment trapping	70
3.4.2.4. Extraction of sediment from harbors	71
4. Multi-risk projections and climate warnings with ESS in Venice Lagoon Pilot (CMCC, COR)	72
4.1. Introduction	72
4.2 Methodological approach	73
4.2.1. “What-If” scenarios	73
4.2.2. Climate change scenarios selection and description	74
4.2.3. Numerical implementations	77
4.3. Results	79
4.2.1. Circulation	79
4.2.2. Waves	82
4.2.3. MOSE barriers closure	84
4.3. Conclusions	85
4.4. Annexes	86
5. Multi-risk projections and climate warnings with ESS in Arcachon Bay Pilot (EGIS, INR)	90
5.1. Introduction	90
5.1.1. Context	90
5.1.2. Objectives	90
5.1.3. Methodology	90
5.2. Socio-economic analysis	90
5.2.1. General situation	90
5.2.2. Port activities	91
5.2.2.1. Professional and non-professional fishery	91
5.2.2.2. Dredging	92
5.2.3. Tourism and marine recreational activities	94
5.2.3.1. Pleasure boating and navigation	94

5.2.3.2. Mooring.....	95
5.2.3.3. Residential and general tourism.....	96
5.2.4. Oyster farming.....	96
5.2.5. Conclusion	97
5.3. Impact assessment	98
5.3.1. Method.....	98
5.3.2. Current and climatic forcing conditions	98
5.3.2.1. Water levels	98
5.3.2.2. Wind	99
5.3.2.3. Waves.....	100
5.3.2.4. Bathymetry.....	100
5.3.3. Sediment dynamics	101
5.3.3.1. Impact on seabed stabilization in seagrass areas.....	102
5.3.3.2. Impact in the vicinity of seagrass area	102
5.3.3.3. Impact on sediment size.....	103
5.3.3.4. Erosion/sedimentation of channels	104
5.3.3.5. Impact on modification of draft	105
5.3.3.6. Sedimentation in the vicinity of ports	105
5.3.4. Water quality.....	105
5.3.4.1. Water renewal.....	106
5.4. Sensitivity of ESS to climate forcing and multi-impact chains	107
5.4.1. Sediment management.....	107
5.4.2. Water quality.....	109
5.5. Conclusion	111
6. Multi-risk projections and climate warnings with ESS in Sicily Lagoon Pilot (UC)	112
6.1 Plan of simulations	112
6.2 Performance of the Nature-Based solutions under different climate scenarios	112
6.3 Conclusions	120
7. Multi-risk projections and climate warnings with ESS in Foros Bay Pilot (BAS)	121
7.1. Study framework.....	121
7.2. Data	122
7.2.1. Bathymetry & Topography	122
7.2.2. Waves and surge	122
7.2.3. Bottom sediments	123
7.2.4. Vegetation	123
7.3. Models and methods.....	124
7.3.1. Design of extreme hydrometeorological events	124
7.3.2. Modelling system	126
7.3.3. Nature-based solution (NbS) and related Ecosystem Services (ESS)	130

7.4.Results and discussion.....	131
7.4.1. Hydrodynamic modelling	131
7.4.2. Morphodynamic modelling	135
7.4.3.Assessment of ecosystem services	138
7.5.Conclusions	139
8. Multi-risk projections and climate warnings with ESS in Vistula Lagoon (IBW)	141
8.1 Vistula Lagoon context	141
8.1.1. Criteria to define efficiency of risk reduction	142
8.1.2. Risk reduction.....	142
8.1.2.1. Ad. 1 The rim	142
8.1.2.2. Ad. 2 Placement of the island.....	144
8.1.2.3. Ad. 3 By-effects	146
8.1.3. Efficiency at long term under different climate projections.....	147
8.1.4. Conclusions	148
9. Integrated conclusions.....	149
10. References	151

Preface

The REST-COAST project (Large scale RESToration of COASTal ecosystems through rivers to sea connectivity), funded under the European Union's Horizon 2020 programme (Grant Agreement No. 101037097), aims to advance innovative and science-based solutions for the large-scale restoration of coastal ecosystems. Its central ambition is to improve the delivery of Ecosystem Services (ESS) and reduce coastal risks through nature-based approaches, while reinforcing connectivity from river basins to the sea.

Deliverable D2.2 is the second technical output of Work Package 2 (WP2), building upon the storm-based modelling work presented in D2.1. While D2.1 focused on current hazard conditions and model calibration, this deliverable explores future scenarios of sea level rise, changing sediment dynamics, and increasing storm impacts. It evaluates the long-term performance of Nature-Based Solutions (NbS) through integrated hydro-morpho-eco modelling and assesses their contribution to ESS delivery across seven REST-COAST pilot sites.

This report supports the development of adaptive restoration strategies tailored to local contexts, while contributing to broader coastal management frameworks under climate change. By combining physical process modelling with ecological indicators and socio-economic relevance, D2.2 provides robust evidence to guide nature-based adaptation pathways across Europe's diverse coastal systems.

Summary

Deliverable D2.2 presents an integrated evaluation of future coastal risk reduction supported by Nature-Based Solutions (NbS) and their capacity to deliver multiple Ecosystem Services (ESS) under long-term climate scenarios. Building on the modelling frameworks developed in D2.1—focused on storm forecasting and present-day hazard conditions—this report addresses the performance of restoration strategies under projected sea level rise (SLR), changes in sediment dynamics, and intensified hydrometeorological forcing.

Each REST-COAST pilot site applied calibrated hydro-morpho-ecological models to simulate the evolution of key ESS, including coastal protection, sediment regulation, water quality, and biodiversity support. The pilots assessed the influence of salt marshes, seagrass meadows, dunes, and sediment management measures in mitigating erosion and flooding, enhancing ecological functioning, and supporting socio-economic priorities. The Wadden Sea and Venice Lagoon pilots confirmed the protective role of restored salt marshes in modulating water levels, attenuating waves, and stabilizing sediments. In Foros Bay and Arcachon Bay, seagrass meadows contributed to wave energy dissipation and sediment retention, although their effectiveness decreased under high-energy or advanced SLR scenarios. The Arcachon site also integrated a socio-economic layer to link model outputs with ecosystem-based management strategies.

In Sicily Lagoon and the Ebro Delta, sediment management approaches—such as dune reconstruction and controlled nourishment—were explored to reduce coastal hazards and preserve ecosystem functioning. In Vistula Lagoon, the emphasis was placed on habitat connectivity and biodiversity conservation, given the relatively limited exposure to direct climate impacts.

The modelling results demonstrate that NbS can enhance the delivery of ESS under changing climate conditions, but their performance is highly dependent on spatial configuration, local hydrodynamics, and projected forcing. The deliverable highlights the importance of adaptive design, cross-disciplinary integration, and long-term monitoring in sustaining coastal resilience.

By advancing a framework that combines physical, ecological, and socio-economic indicators within scenario-based simulations, D2.2 provides an evidence-based foundation for the strategic planning of ecosystem-based adaptation pathways. The outcomes support both local restoration actions and broader policy frameworks aimed at integrating ESS into long-term coastal governance.

List of abbreviations

BAS: Institute of Oceanology in Varna

BSS: Brier Skill Score

BHI: Benthic Habitat Index

CEDEX: Centro de Estudios y Experimentación de Obras Públicas (Spain)

CMCC: Centro Euro-Mediterraneo sui Cambiamenti Climatici

CMEMS: Copernicus Marine Environment Monitoring Service

COR: Consorzio coordinamento delle ricerche al Sistema lagunare di Venezia (CORILA)

CORE-PLAT: COastal REstoration PLATform

CWOP-WMO8: Part of the Citizen Weather Observer Program

D: Deliverable

DCSM-FM: Dutch Continental Shelf Model – Flexible Mesh.

DEL: Deltares

DTM: Digital Terrain Model

DWD: German Weather Service

EGIS: EGIS Water and Maritime

ESS: Ecosystem Services

EU: European Union

EUNIS: European Nature Information System

EVA: Extreme Value Analysis

FM: Flexible mesh

FSK: Forschungsstelle Küste (NLWKN, Germany)

GIS: Geographic Information System

HZG: Helmholtz-Zentrum Geesthacht (now HEREON)

IAHR: International Association for Hydro-Environment Engineering and Research.

IBI: Operational Product (<http://marine.copernicus.eu/>)

IBW: Institute of Hydro-Engineering of the Polish Academy of Sciences.

INR: Institut national de recherche pour l’agriculture, l’alimentation et l’environnement INRAE

INSEE: Institut national de la statistique et des études économiques (France)

IO-BAS: Institute of Oceanology, Bulgarian Academy of Sciences

IPCC: Intergovernmental Panel on Climate Change

ISIMIP: Inter-Sectoral Impact Model Intercomparison Project)

IUCN: Red List and as “Threatened” (SPA/BD) Protocol. Annex II under the Barcelona Convention.

JONSWAP: Joint North Sea Wave Project

LiDAR: Light Detection and Ranging

M: Milestone

MHWN: Mean High Water Neap

MLWS: Mean Low Water Neap

MOSE: Modulo Sperimentale Elettromeccanico

MPI-ESM-LR: Max-Planck-Institute Earth System Model Low Resolution

MPIOM-REMO: Regionally Coupled Climate System Model

MSL: Mean Sea Level

NATURA: Network of protected Areas covering Europe's.

NBS: Nature-Based Solutions

NbS: Nature-based Solutions

NLWKN: The Lower Saxony Water Management, Coastal and Nature Protection Agency

NN: NetworkNature

NNW: North northwest wind direction

NTU: Nephelometric Turbidity Unit

PROVV: Provveditorato Interregionale per le Opere Pubbliche per il Veneto, Trentino Alto Adige e Friuli Venezia Giulia

RAMSAR: Convention on Wetlands of International Importance

RCE: Reduction of Coastal Erosion

RCP: Representative Concentration Pathways

REF: Reference configuration without NbS

REMO: Regional climate modelling framework

REST: Restoration configuration with NbS

REST-COAST: Large scale RESToration of COASTal ecosystems through rivers to sea connectivity Project

RMFE: Root Mean Square Error

RFR: Reduction of Flood Risk

SCHISM: Semi-implicit Cross-scale Hydrosience Integrated System Model

SCHISM-WWM: The Semi-implicit Cross-scale Hydrosience Integrated System Model and Waves Model

SCOT: Data Base for new construction (Bassin d'Arcachon)

SIBA: Syndicat Intercommunal du Bassin d'Arcachon

SIMPA: Integrated System for Precipitation-Runoff Modelling

SLR: Sea Level Rise

SMPBA: Syndicat Mixte des Ports du Bassin d'Arcachon

SNS: Coupled climate system model

SPA/BD: Protocol Annex II under the Barcelona Convention

SPM: Suspended Particulate Matter.

SR: Seagrass Meadow Reconstruction

SSC: Suspended Load Concentration

SWAN: Simulating WAVes Nearshore model

SWH: Significant Wave Height

T: Task

TBT: Tributyltin

TDV: Tour du Valat

TMAP: TMAP coastal vegetation (Bouma (2005)).

UAS: Bathymetric Database

UC: University of Catania

UICN: Union internationale pour la conservation de la nature en France

UNESCO: United Nations Educational, Scientific and Cultural organization

UPC: Universitat Politècnica de Catalunya

UPM: Universidad Politécnica de Madrid

VLOED: new intertidal wetland to facilitate sediment extraction

WP: Work Package

WW3: WAVEWATCH III

WWM III: Wind Wave Model III

ZES: Classes for classifying ecotopes

List of Figures

Figure 2.1. a) Ebro Delta b) Placement of an embryonic alternating dune system during 2023 in the Trabucador barrier beach.....	18
Figure 2.2. Flood levels proportional to SLR using SSP3-7.0 a)2050, b)2100 and c)2150 (blue represents flooded and red not flooded).	19
Figure 2.3. Schematisation of mitigation strategies. NP means No protection, AD alternating dunes, CD continuous dunes and CN classical nourishment.	20
Figure 2.4. Final bed level after storm Filomena in +0.27 SLR conditions. a) No protection, b) Alternating dunes and c) Classical nourishment.	21
Figure 2.5. Final bed level after storm Gloria in +0.27 SLR conditions. a) No protection, b) Alternating dunes and c) Classical nourishment.	22
Figure 2.6. Final bed level after storm Isaak in +0.27 SLR conditions. a) No protection, b) Alternating dunes and c) Classical nourishment.	22
Figure 2.7. Final bed level after storm Filomena in +0.57 SLR conditions. a) No protection, b) Alternating dunes and c) Classical nourishment.	23
Figure 2.8. Final bed level after storm Gloria in +0.57 SLR conditions. a) No protection, b) Alternating dunes and c) Classical nourishment.	23
Figure 2.9. Final bed level after storm Isaak in +0.57 SLR conditions. a) No protection, b) Alternating dunes and c) Classical nourishment.	24
Figure 2.10. Final bed level after storm Filomena in +0.75 SLR conditions. a) No protection, b) Alternating dunes and c) Classical nourishment.	24
Figure 2.11. Final bed level after storm Gloria in +0.75 SLR conditions. a) No protection, b) Alternating dunes and c) Classical nourishment.	25
Figure 2.12. Final bed level after storm Isaak in +0.75 SLR conditions. a) No protection, b) Alternating dunes and c) Classical nourishment.	25
Figure 2.13. Three different representations of the efficiency of the measures Alternating dunes and Classical nourishment for present and future conditions.	27
Figure 2.14. Domain of the numerical simulations in the Ebro Delta pilot site.	28
Figure 2.15. Cross sections of the Ebro River	29
Figure 2.16. Suspended sediment concentration for the mean water regime..	31
Figure 2.17. Erosion for the mean water regime	32
Figure 2.18. Suspended sediment concentration for the mean water regime	33
Figure 2.19. Suspended sediment concentration for the mean water regime	34
Figure 2.20. Suspended sediment concentration for several flow rates.	35
Figure 2.21. Figure 3 from Tena et al., 2011 where they show the relationship between turbidity and suspended sediment concentration.....	36
Figure 2.22. Comparison of the estimation of potential sediment transport in Tortosa at the daily and monthly scales. Left: annual flow. Right: sediment transport.....	37
Figure 2.23. Evolution of annual flow and potential sediment transport in the Lower Ebro River under natural and altered conditions. Left: annual flow. Right: sediment transport.....	38
Figure 2.24. Relation between annual flow and potential sediment transport in the Lower Ebro River under natural and altered conditions	38
Figure 2.25. Mean seasonality of flow and potential sediment transport in the Lower Ebro River under natural and altered conditions. Left: annual flow. Right: sediment transport.....	39
Figure 2.26. Comparison of the time sequence of annual flows and potential sediment transport in the Ebro River produced by SIMPA model and ISIMIP global hydrologic models. Left: Annual flows. Right: Potential sediment transport.....	40

Figure 2.27. Comparison of annual flows in the Ebro River produced by ISIMIP global hydrologic models and SIMPA model. Left: H08 model. Right: CWatM model.....	41
Figure 2.28. Comparison of potential sediment transport in the Ebro River produced by ISIMIP global hydrologic models and SIMPA model. Left: H08 model. Right: CWatM model	41
Figure 2.29. Comparison of seasonality of flows and potential sediment transport in the Ebro River produced by ISIMIP global hydrologic models and SIMPA model. Left: Seasonality of flows. Right: Seasonality of potential sediment transport.	42
Figure 2.30. Comparison of bias-corrected potential sediment transport in the Ebro River produced by ISIMIP global hydrologic models and SIMPA model. Left: H08 model. Right: CWatM model	42
Figure 2.31. Projection of mean annual flow in the Ebro River under ISIMIP climate scenarios.....	44
Figure 2.32. Projection of mean potential sediment transport in the Ebro River under ISIMIP climate scenarios	45
Figure 2.33. Projected changes of mean annual flow and potential sediment transport in the Ebro River under ISIMIP climate scenarios.....	46
Figure 3.1. Model domains.....	47
Figure 3.2. Domain and bathymetry of the SCHISM-WWM model (right) and the magnified box shows the study site, Norderney (left, red box)	51
Figure 3.3. Flowchart of model scenarios	53
Figure 3.4. Observed sedimentation- erosion patterns in the Dollard (Elias, 2021).....	54
Figure 3.5. Modelled sedimentation and erosion patterns after 24 years of morphological simulation initializing the model with a thin (15 cm) initial layer of mud	54
Figure 3.6. Modeled mud fraction in the top soil after initial calibration compared to the sediment atlas of the Wadden Sea as dots	54
Figure 3.7. EUNIS map of the Ems estuary produced in WP4.1 of RESTCOAST, based on Baptist (2019)	59
Figure 3.8. EUNIS map produced by output from the Ems-Dollard model	60
Figure 3.9. 95 th Annual percentile in significant Wave Height (HS) and its reduction due to seagrass	62
Figure 3.10. 95 th Annual percentile in depth averaged velocity and its reduction due to seagrass	63
Figure 3.11. 95 th Annual percentile in reduction due to seagrass for erosion proxy variables bottom stress and bottom layer sediment concentration	64
Figure 3.12. Eunis maps for A) 2030, B) 2050, and C) 2100.	66
Figure 3.13. Changes in maximum wave height during storm Herwart compared to the same storm event simulated without sea-level rise and changes in ecotopes for the years A) 2030, B) 2050, and C) 2100 in climate scenario ssp 585	68
Figure 3.14. Changes in maximum wave height during storm Xaver compared to the same storm event simulated without sea-level rise and changes in ecotopes for the years A) 2030, B) 2050, and C) 2100 in climate scenario ssp 585	69
Figure 3.15. Additional intertidal wetland created for sediment extraction in the measure VLOED	70
Figure 3.16. Pilot for sediment trapping on the intertidal flats as (source: Rijkswaterstaat)	71
Figure 4.1. Location of the REST-COAST pilot site in the Venice Lagoon	72
Figure 4.2. Schematic representation of the workflow adopted in this deliverable. The diagram summarizes all the simulations, variables, scenarios and configurations.....	73
Figure 4.3. Wave and wind climate for the Venice lagoon pilot. Sub-plot (a) shows the location for the climate analysis, (b) shows the 99th percentile of SWH, (c) shows the 99th percentile for wind.	76
Figure 4.4. Significant wave height and related trends for past (1990-2020), RCP8.5 (2041-2070) and RCP4.5 (2071-2100) scenarios	77
Figure 4.5. Magnification of the numerical grids and bathymetry on the pilot site. a) shows the REF configuration, b) shows the REST configuration	78
Figure 4.6. Comparison of extreme sea level with open (a) and closed MOSE (b) and corresponding current (c,d).....	79

Figure 4.7. Location of the comparison between numerical configurations: the black dot indicates the pilot area, and the red dot shows the location of the Adriatic Sea.....	79
Figure 4.8. Timeseries of water level (a-b) and currents (c-d) at Adriatic Sea (a-c) and the pilot site (b-d) for the six scenarios. The difference between REST and REF configurations is shown in sub-plots (e) for sea level and (f) for currents.	80
Figure 4.9. Sea level difference computed as REST - REF simulations for H3 during the ebb phase (a) and the flooding phase (b).....	81
Figure 4.10. Currents difference for REST and REF configuration in the H3 simulation both on the slack phase (a) and the flooding phase (b).	81
Figure 4.11. Significant wave height difference (expressed in percentage) computed as REST - REF configurations for the scenarios a) W1a, b) W1b, c) W4a and d) W4b.....	83
Figure 4.12. Significant wave height for the REF configuration and for the scenarios a) W1a, b) W1b, c) W4a, and d) W4b	84
Figure 4.13. Water level difference between REST and REF configurations when MOSE barriers are closed.	84
Figure 4.14. Currents difference for REST and REF configuration and closed MOSE barriers in the H3 simulation both on the slack phase (a) and the flooding phase (b).	85
Figure 4.15. Annex 1: What-if scenarios of significant wave height at the pilot site	87
Figure 4.16. Annex 2: Currents for REST configuration	88
Figure 4.17. Annex 3: Currents for REF configuration	88
Figure 4.18. Annex 4: Water level for REST configuration	89
Figure 4.19. Annex 5: Maximum flooded area at lagoon scale for each of the six scenarios	89
Figure 5.1. Land cover around the Bay (Corine Land Cover).....	91
Figure 5.2. Hydraulic dredge (left) and mechanical dredge (right) [SIBA].	92
Figure 5.3. Location of the dredging works identified on the SMPBA website (SMPBA 2023).....	93
Figure 5.4. Sediment settling basin (left) and their location (right) [SIBA].	94
Figure 5.5. Location of moorings (mooring buoy in blue, anchor in red) observed in an afternoon in July 2008 (Le Corre N. et al., 2015).....	95
Figure 5.6. Sea level rise projections (m), median and likely range, for two climate scenarios: SSP2-4.5 and SSP5-8.5. Extracted from "https://sealevel.nasa.gov"	99
Figure 5.7. Surface wind projections (% of change). Ensemble mean (solid line) and confidence interval are represented for climate scenarios SSP2-4.5 (blue) and SSP5-8.5 (red).....	99
Figure 5.8. Storm events analysis in term of number (a), duration (b) and intensity (c). From Ganthly F., Ifremer (personal communication).	100
Figure 5.9. Initial bathymetry applied in the model (m with respect to current MSL).	101
Figure 5.10. Morphological changes (m), calculated over 3 years for future horizons and corresponding SLR.	104
Figure 5.11.. Evolution of tracer concentration (1 initially) for 5 harbors and 4 horizons over 10 days of simulation.	106
Figure 5.12. Multi-impact chain and climate sensitivity for ESS erosion.	108
Figure 5.13. Multi-impact chain and climate sensitivity for ESS water quality	110
Figure 6.1. Schematization of the terms used within the efficacy indicators: Flooded areas without or with NbS (a and b respectively); shoreline retreat (c).....	114
Figure 6.2. Inundation map for present scenario (SP), $T_r = 100$ years, no-NbS, $H_s = 6.01$ m, $T_p = 10.56$ s, SLR = 0.000 m.....	115
Figure 6.3. Inundation map for simulation S4.5-2100 ($T_r = 100$ years) scenario, current state, $H_s = 7.75$ m, $T_p = 11.39$ s, SLR = 0.369 m	116
Figure 6.4. Inundation maps for simulation scenario S4.5-2100, $T_r = 100$ years ($H_s = 7.75$ m, $T_p = 11.39$ s, SLR = 0.369 m): a) current state, b) dune revegetation, c) seagrass revegetation.....	117

Figure 6.5. a) Flooded areas due to wave storm ($T_r = 100$ years) in the city area; b) Flooding reduction efficiency percentage due to proposed NbS	118
Figure 6.6. Position of the 30 transects along which the shoreline retreat is computed	118
Figure 6.7. Shoreline retreat for no-NbS (NN, black dots), dune revegetation (DR, orange circles) and for seagrass meadow reconstruction (SR, green squares) along transects T1-30 (location in Figure 6.7c) for present (a) and future (c,e,g,i) hydrodynamic scenarios	119
Figure 7.1. Schematization of the study framework	121
Figure 7.2. Bathymetry and topography compiled datasets used in the study	122
Figure 7.3. Location of points for which wave and wind properties were extracted from a hindcast dataset	122
Figure 7.4. Location of bottom sediment samples collected for the needs of REST-COAST Project (red dots) and those of supplementary samples (green dots).....	123
Figure 7.5. Location of the seagrass meadow present in Foros Bay (light green polygon A) and the envisioned area of seagrass restoration (dark green polygons B and C).....	124
Figure 7.6. Extreme events' pattern for selected return periods.....	125
Figure 7.7. Sea level rise scenarios and projections (https://sealevel.nasa.gov/ipcc-ar6-sea-level-projection-tool)	125
Figure 7.8. Modelling system scheme.	126
Figure 7.9. Burgas Bay Delft3D-FM FLOW&WAVE domain and location of the other elements of the modelling chain	127
Figure 7.10. Foros Bay Delft3D-FM domain setup. Unstructured flow grid and regular wave grid (left). Water depths (wave module) and bathymetry (flow module) and a fragment of the unstructured flow grid (right). The offshore boundary conditions points (water levels) for the flow grid are depicted by blue dots (left).	127
Figure 7.11. Location of the seagrass meadows within Foros Bay Delft3D-FM domain existing to present delineated by light green polygon (A) and the planned area of seagrass restoration delineated by dark green polygons (B and C).	128
Figure 7.12. Location of XBeach model domain within Foros Bay delineated by red line (left) and bathymetry of the domain (right). The blue dot at the XBeach boundary allocates the output model location of Foros Bay Delft3D-FM model used for XBeach boundary conditions.....	129
Figure 7.13. Distribution of seagrasses into the XBeach domain (red polygon). The seagrass meadow existing to present is delineated by light green polygon (A) and the planned area of seagrass restoration is delineated by dark green polygon (B).	130
Figure 7.14. Flow pattern calculated for TR020 design event (present climate conditions) for the case of no vegetation (left) and in presence of existing and restored seagrass meadows.	131
Figure 7.15. Significant wave height (upper panel) and wave energy dissipation (lower panel) for TR020 design event (present climate conditions) for the case of no vegetation (left) and in presence of existing and restored seagrass meadows.....	132
Figure 7.16. Flooded areas for considered return periods concerning present conditions and two considered horizons of RCP4.5 and RCP8.5.	134
Figure 7.17. Sedimentation – erosion patterns calculated for TR020 storm event for present climate conditions and future climate change under RCP4.5 and RCP8.5, horizons 2070 and 2100	136
Figure 7.18. Sedimentation – erosion patterns calculated for TR100 storm event for present climate conditions and future climate change under RCP4.5 and RCP8.5, horizons 2070 and 2100.....	137
Figure 7.19. Flood areas concerning present conditions and two considered horizons of RCP4.5 and RCP8.5 calculated for all design events.	138
Figure 7.20. Erosion volumes for cases of no vegetation, present and planned for restoration concerning present conditions and two considered horizons of RCP4.5 and RCP8.5 calculated for all design events. .	138
Figure 7.21. Erosion area for cases of no vegetation, present and planned for restoration concerning present conditions and two considered horizons of RCP4.5 and RCP8.5 calculated for all design events.....	139

Figure 8.1. Location of artificial island – study site in the Polish part of Vistula Lagoon: source – public domain, adapted by G. Różyński.	141
Figure 8.2. Initial concept of rim employing geo-tubes with local sediment, source Maritime Office Gdynia	142
Figure 8.3. Rim under construction, made of two rows of sheet piles with stone armor gradually forming the crest between them: source - courtesy NDI group.	143
Figure 8.4. The rim of artificial island, Sept. 2023: source - REST-COAST	144
Figure 8.5. Wave heights for wind $v = 10$ m/s from NE: (a) without artificial island, (b) with the island, (c) differences in wave height: source – IBW PAN.	145
Figure 8.6. Surface currents for wind $v = 10$ m/s from NE: (a) without artificial island, (b) with the island, (c) differences in currents – IBW PAN.	146
Figure 8.7. Denitrification by jute rollers containing reeds that denitrify effluent returning to Vistula Lagoon after deposition of sediment.....	147

1. General introduction

Coast is facing increasing risks of flooding and coastal erosion from extreme storms, which are becoming more frequent and intense in the context of global climate change. These risks pose a significant threat to the region's coastal communities and ecosystems, and we are committed to finding solutions to mitigate them. A unique challenge in all RESTCOAST Pilot Sites, is that the implementation of conventional hard and grey engineering solutions such as dams and breakwaters are less attractive. This reflects the need to preserve the ecological integrity and aesthetic values of the coast, and underlines the delicate balance between conservation and the need for adaptive strategies. Therefore, the need for innovative, Nature-Based Solutions has received more attention in recent years.

Restoration scenarios have been defined in WP1 for each Pilot and their analysis requires high resolution modelling suites at each site, with different levels of discretizations and suited to simulate different types of hydro-morpho-eco dynamics and interactions.

For the present deliverable report D.2.2, risk reduction in relation to flooding and erosion during future hydrodynamics and extreme wave condition at the Pilot Sites is the focus of the work developed. And with the aim to mitigate coastal risk and restore biodiversity value, a range of Nature-based Solutions (NBS) are investigated considering a current state (with actual active restoration measures) and proposed additional restoration measures.

Using their respective modelling frameworks previously described in D 2.1, the RESTCOAST partners address respectively:

- The restoration of seagrass areas as a coastal protection measure to provide ecosystem buffers and attenuate wave energy, reduce near-shore currents and stabilize the seabed (e.g. Foros Bay and Arcachon Bay);
- The development of saltmarshes which include actions such as the excavation of channels, the creation of tidal flats, re-naturalisation and seagrass transplantation (e.g. Venice Lagoon and Wadden Sea);
- And effective sediment management strategies as dune reconstruction and revegetation to stabilize the dune and improve wave dissipation capabilities of the system (e.g. Ebro Delta, Sicily Lagoons, and Vistula Lagoon);

as NBS with respect to potential improvements for different aspects of the ESS at concern.

RESTCOAST/Task 2.2 has defined (M2.3) future conditions under the commonly agreed climate scenarios and the Pilot restoration scenarios, in order to consistently forecast restoration effects on ESS delivery. Downscaled climate projections have been derived from the commonly agreed global climate scenarios (business-as-usual SSP2-RCP4.5 and pessimistic SSP5-RCP8.5, mean and upper limits) for horizons 2070 and 2100 at least. These scenarios, together with the commonly agreed return period for extreme events, define mean sea level, waves and wind projections for our Pilots, with the site to site variability introduced by the managed restoration scenarios.

2. Multi-risk projections and climate warnings with ESS in Ebro Delta Pilot (UPC, UPM)

2.1. Ebro Delta Coast

UPC is working within different mitigation strategies to reduce the impacts of storms in the Ebro Delta Coast under climate changes scenarios. The approach is based on a selection from more classical interventions to more new strategies to see the efficiency of each one in present (Deliverable 2.1) and future conditions (D2.2). Specifically, they have been tested on the Trabucador Barrier beach, which has been affected with episodes of breaching during the last decades (Jiménez and Sánchez-Arcilla, 2004). The barrier beach connects the mainland with an arrow-shape end (Banya Spit), where a salt industry is located. This corridor, jointly with a high tourism rate in the barrier makes the zone important in terms of the economy of the region (Figure 2.1). Besides, the Fangar bay situated on the back of the barrier beach was designated as a RAMSAR site, with the presence of the mollusk species *Pinna nobilis* (Rodríguez-Santalla and Navarro, 2021) classified as “Critically Endangered” by IUCN Red List and as “Threatened” according to the SPA/BD Protocol Annex II under the Barcelona Convention. For all these reasons, the aim of UPC is to develop a strategy that is able to bare the storm effects in the barrier beach for present and future conditions. During the last decades, some strategies as dune systems have been tried. It has been seen that even if they work for a short amount of time, the constant hit of the waves jointly with the littoral sand transport produce a destruction of the structure at long-term. UPC is trying to be able to use a mitigation approach that can last during these long-term scenarios with few additional actions at the same time that greatly reduces the hazards on the area.

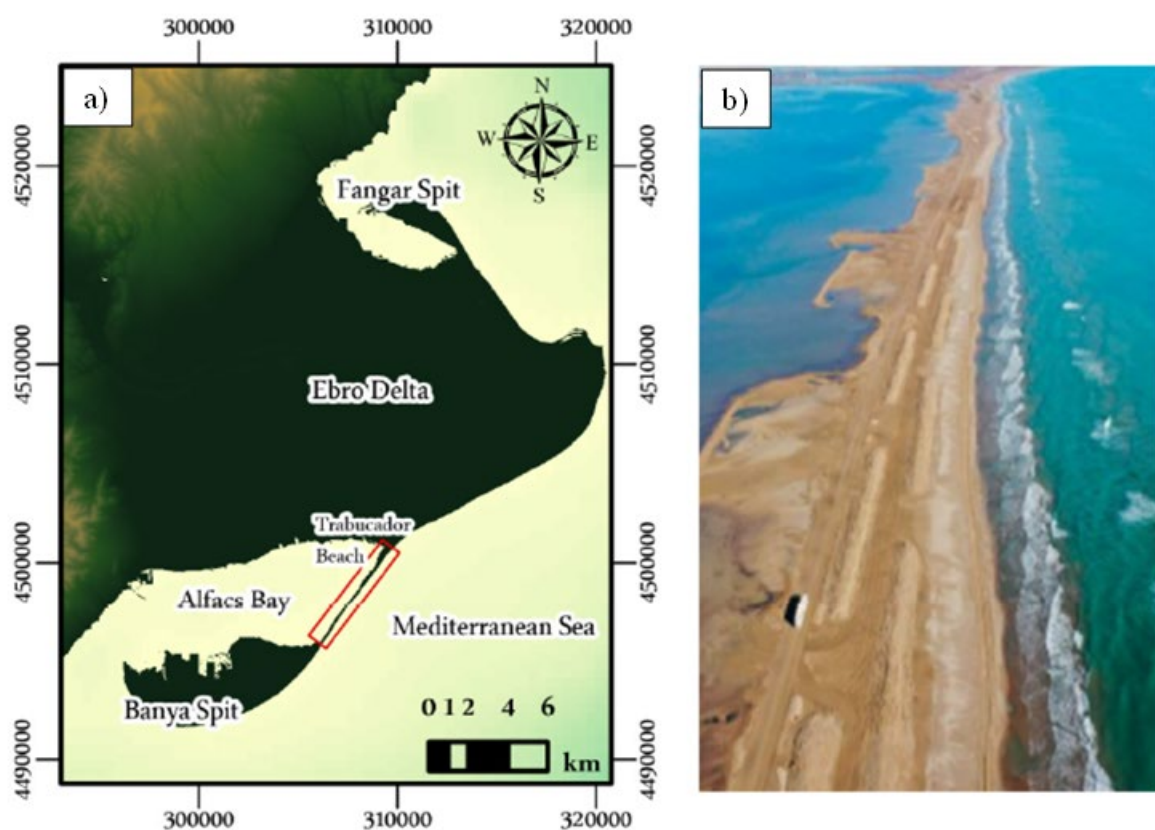


Figure 2.1. a) Ebro Delta. The red rectangle shows the study area which corresponds to the Trabucador barrier beach. b) Placement of an embryonic alternating dune system during 2023 in the Trabucador barrier beach.

Due to Ebro Delta being a low-lying environment (Grases *et al.*, 2010), sea level rise (SLR) will produce a huge impact on the area. As it can be seen in Figure 2.2, even without taking into account the worst scenario SSP5-8.5, the area suffers high flooding rates and within 2150, almost all the study area could be affected. Instead, it is supposed that the beach will adapt and change his equilibrium profile to bare the effects of climate change and not to be totally disappeared. Even so, to simulate or replicate these dynamics is too difficult and inexact so only the increment of SLR, without changing the topo-bathymetry of the barrier beach, has been considered in this study. Because of that, the use of SSP5-8.5 would have relied in a totally disappear of the barrier beach before the arrival of the storms when studying the horizon 2100 for example, being unable to study the efficiency of the mitigation strategies in climate change scenarios. For this reason, we decided to use SSP3-7.0 which is also an extreme scenario to see the effects of the actions on the area. While this scenario is still a negative pronostic, it allows to simulate the beach without its total flooding. In the future, some other scenarios as SSP2-4.5 or the introduction of methodologies as the Brunn rule to try to replicate the evolution of the barrier beach during the increasing of the mean water level could be discussed although the general conclusions about the efficiency of the strategies would not vary in a great extent.

In order to be able to see the effects in climate change conditions, the model had been validated in the area as well as check that the mitigation actions work on the present conditions (D2.1). Following this, we will present some results of the proposed strategies for the current conditions to see if it is worth to simulate them within climate change scenarios and will show the simulated efficiency of the strategies at long-term under different climate projections and discuss about possible issues that each strategy could face.

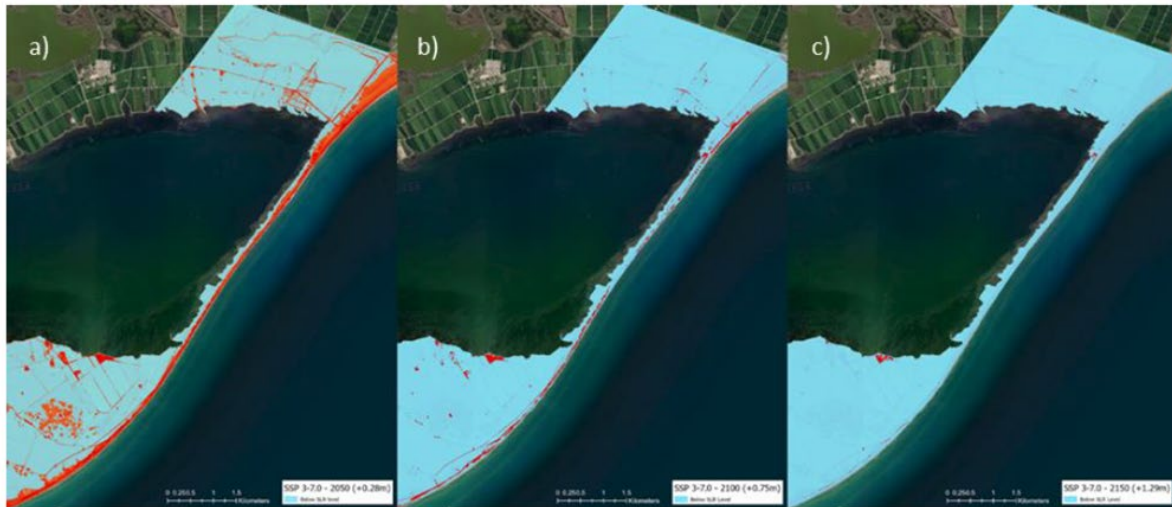


Figure 2.2. Flood levels proportional to SLR using SSP3-7.0 a)2050, b)2100 and c)2150 (blue represents flooded and red not flooded).

2.1.1. Risk reduction from different approaches

As stated at the start of Section 2, four different scenarios were simulated. First, the benchmark corresponded to the strategy where no protection was placed in the study area. Then, following an action done in the barrier during the start of 2023, an embryonic alternating dune system was placed into the mesh (Figure 2.1). Finally, the introduction of a continuous dune and classical nourishment approaches were created to have a more general view about the response of the beach to a series of different strategies (Figure 2.3). Besides from selecting different mitigation strategies, they were also tested under three different storm conditions in order to get storm of the three highest categories defined by Mendoza *et al.* (2011) to classify a storm in the Catalan coast. Then, in addition to Filomena, used for calibration/validation, and that

corresponds to a category IV out of V, also Gloria and Isaak storms were studied. Gloria was the most important storm ever recorded on Catalonia (category V/V) and Isaak was selected because was the storm hitting the barrier beach just after the placement of the alternating dunes on the field (with a category III/V).

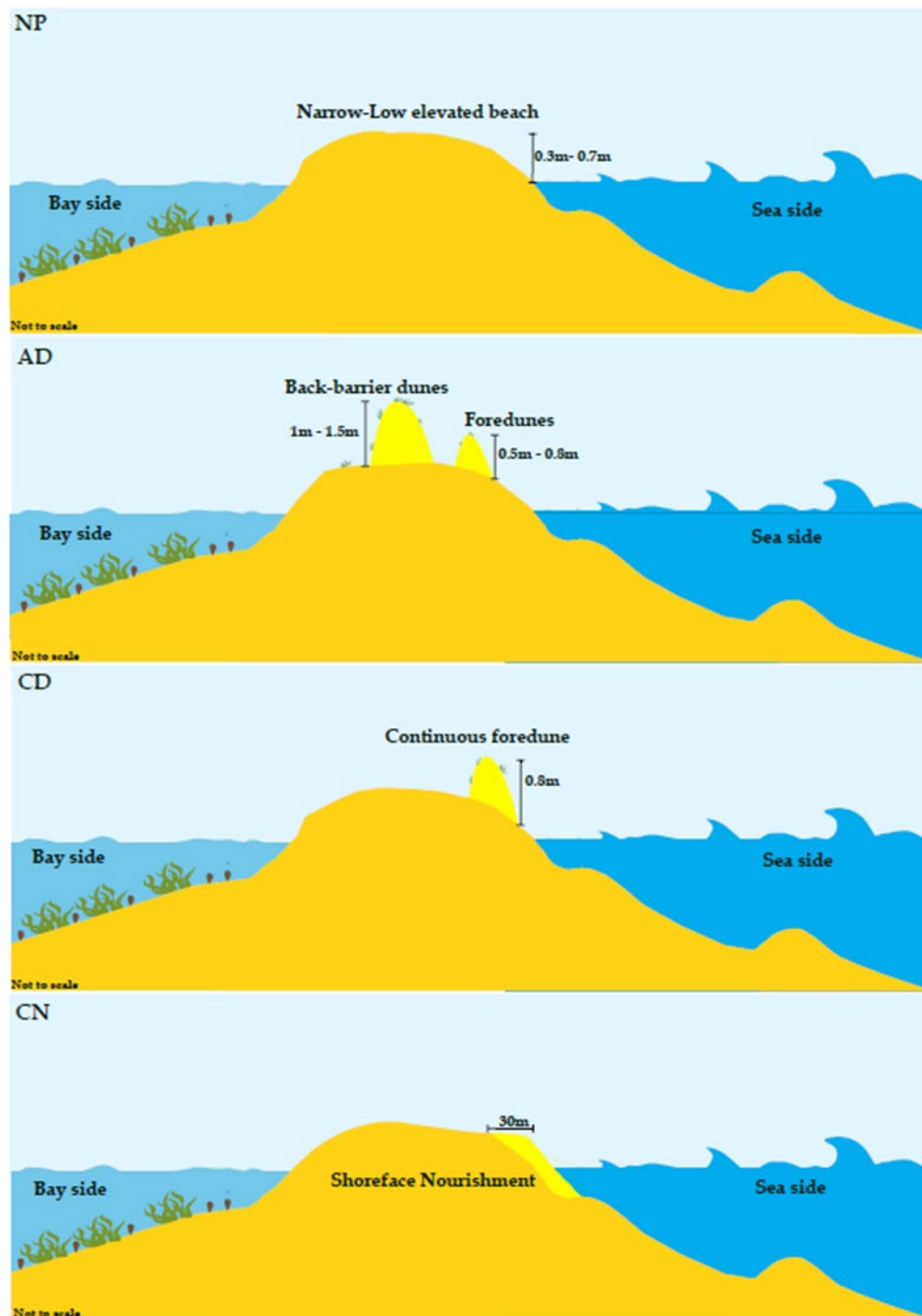


Figure 2.3. Schematisation of mitigation strategies. NP means No protection, AD alternating dunes, CD continuous dunes and CN classical nourishment.

2.1.2. Efficiency at long-term under different climate projections

As stated in Section 2.1.2, the efficiency at long-term under different climate projections will be based on the IPCC AR6 SSP3-7.0 scenario since more negative scenarios as SSP5-8.5 would rely in a complete flooding of the area for the longest horizons. Then, this scenario will be simulated under 2050, 2090 and 2100 projections. Following the estimates of IPCC AR6, the increase of sea level for the area will be +0.27m, +0.57m and +0.75m respectively. Moreover, the continuous dune strategy will not be longer studied since previous results showed similar results with alternating dunes and we consider the latter better in terms of ecology and long-term persistence. In Figures 2.4 - 2.12, the graphical results for the simulations are presented, where it can be seen the effect of each storm for all three different climate projections and within each mitigation action. It can be observed that for the period 2050 the changes are not so important although some more breaching is detected for the three storms. Then, when simulating in the 2090, the response of the beach for the Filomena storm seems like the same as Gloria in the present and Isaak is more similar to actual Filomena response. Finally, within 2100 horizon, all three storms produce heavy breaching damages and no mitigation strategy is able to sufficiently reduce the damages. Besides, all of them seems closer to Gloria's effects nowadays, concluding that within these worse-case scenarios at long-term, the proposed approaches seem inefficient.

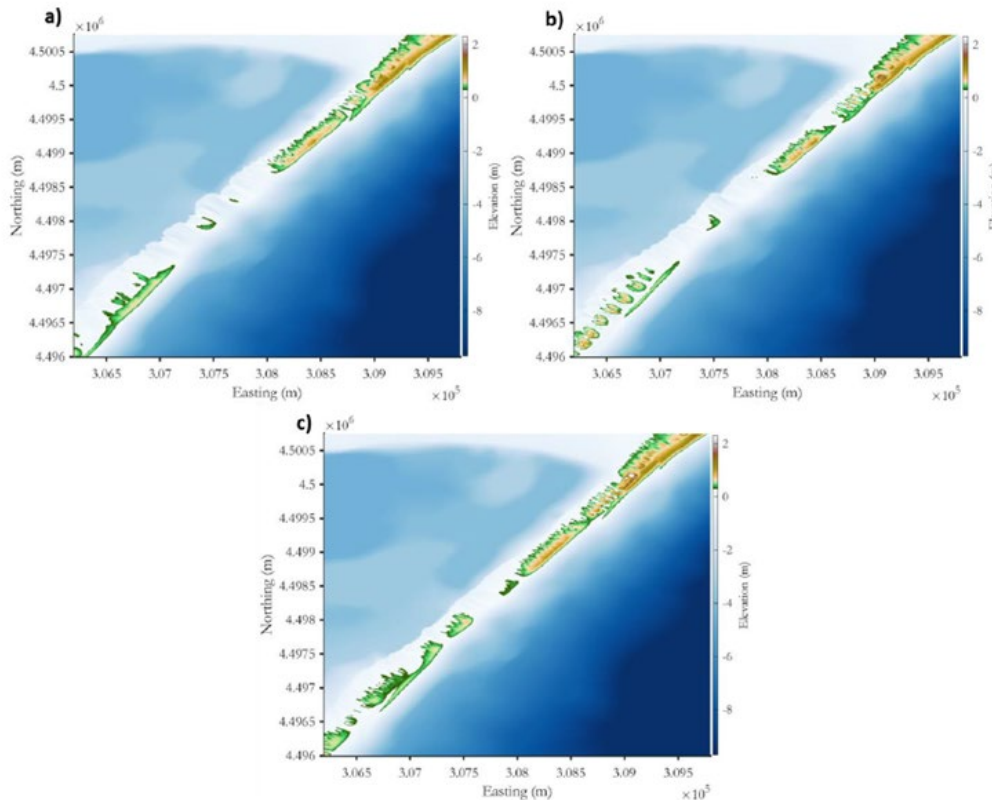


Figure 2.4. Final bed level after storm Filomena in +0.27 SLR conditions. a) No protection, b) Alternating dunes and c) Classical nourishment.

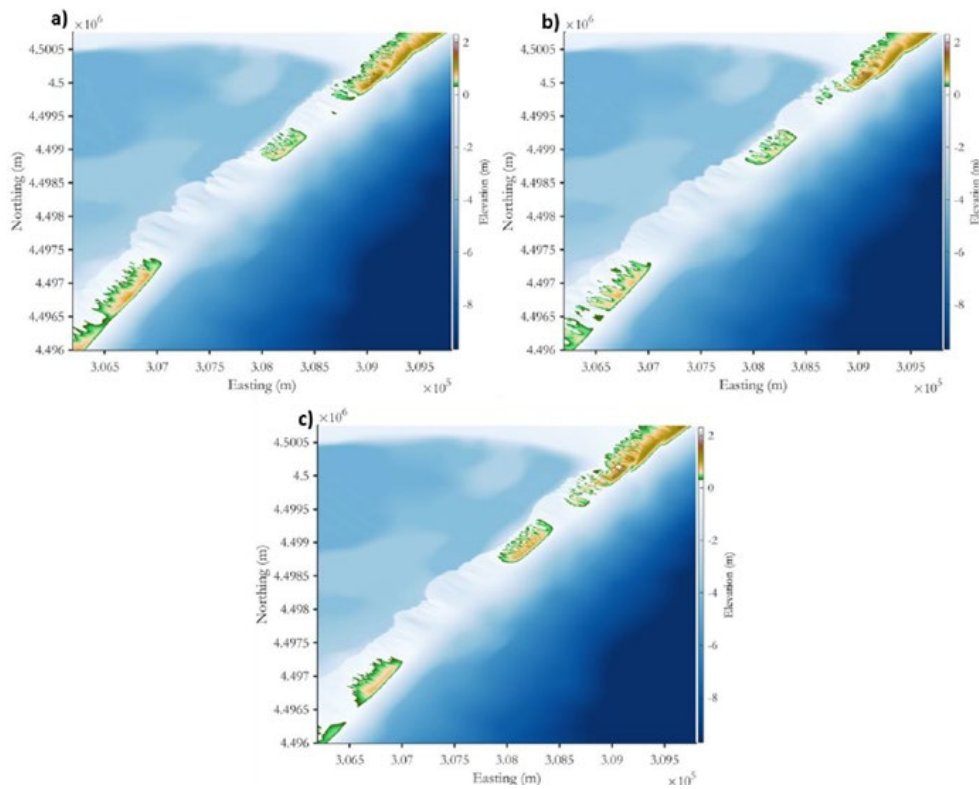


Figure 2.5. Final bed level after storm Gloria in +0.27 SLR conditions. a) No protection, b) Alternating dunes and c) Classical nourishment.

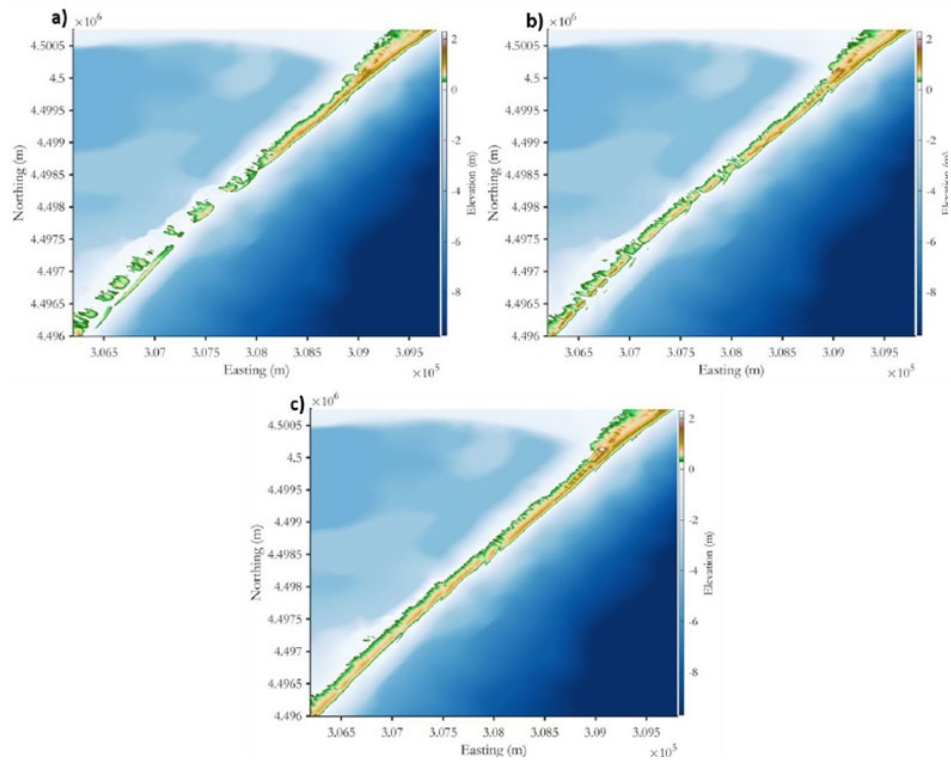


Figure 2.6. Final bed level after storm Isaak in +0.27 SLR conditions. a) No protection, b) Alternating dunes and c) Classical nourishment.

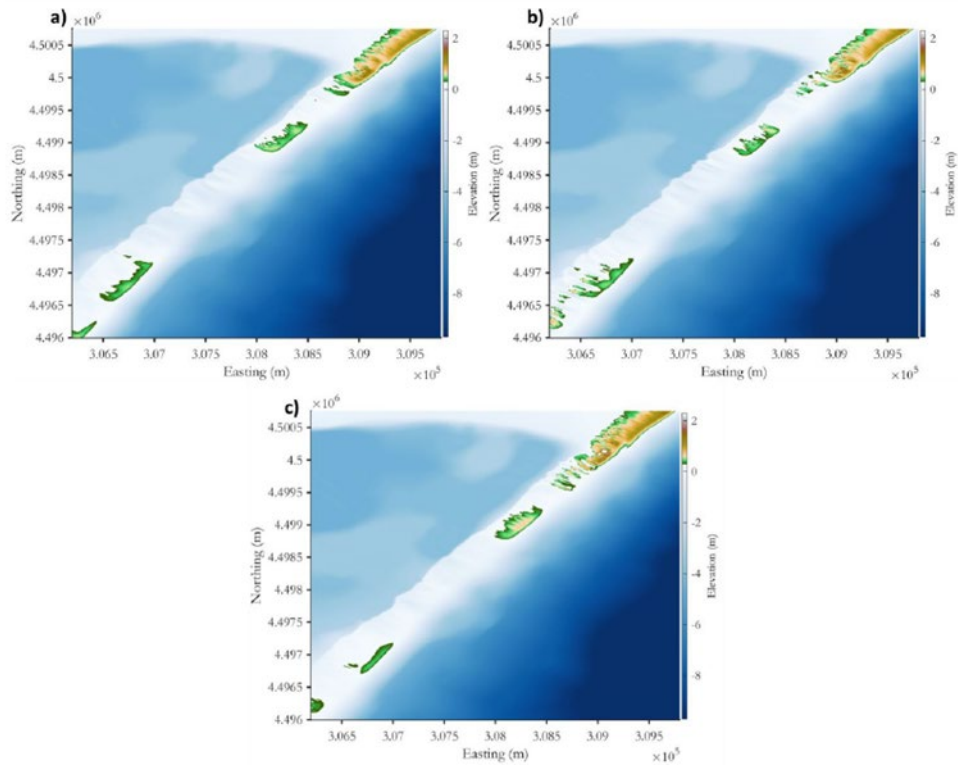


Figure 2.7. Final bed level after storm Filomena in +0.57 SLR conditions. a) No protection, b) Alternating dunes and c) Classical nourishment.

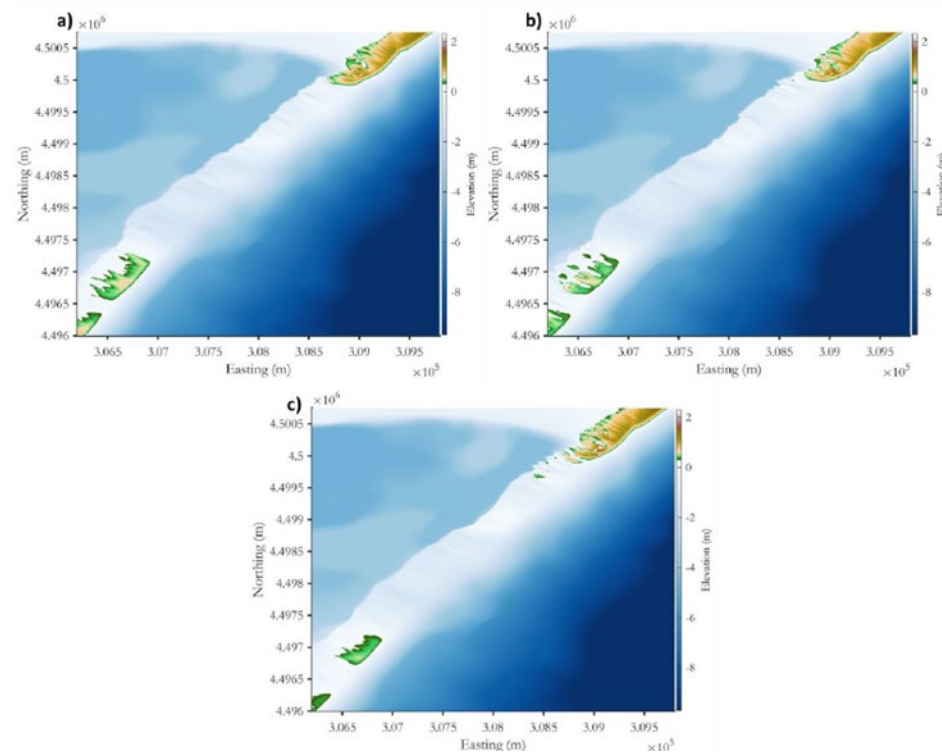


Figure 2.8. Final bed level after storm Gloria in +0.57 SLR conditions. a) No protection, b) Alternating dunes and c) Classical nourishment.

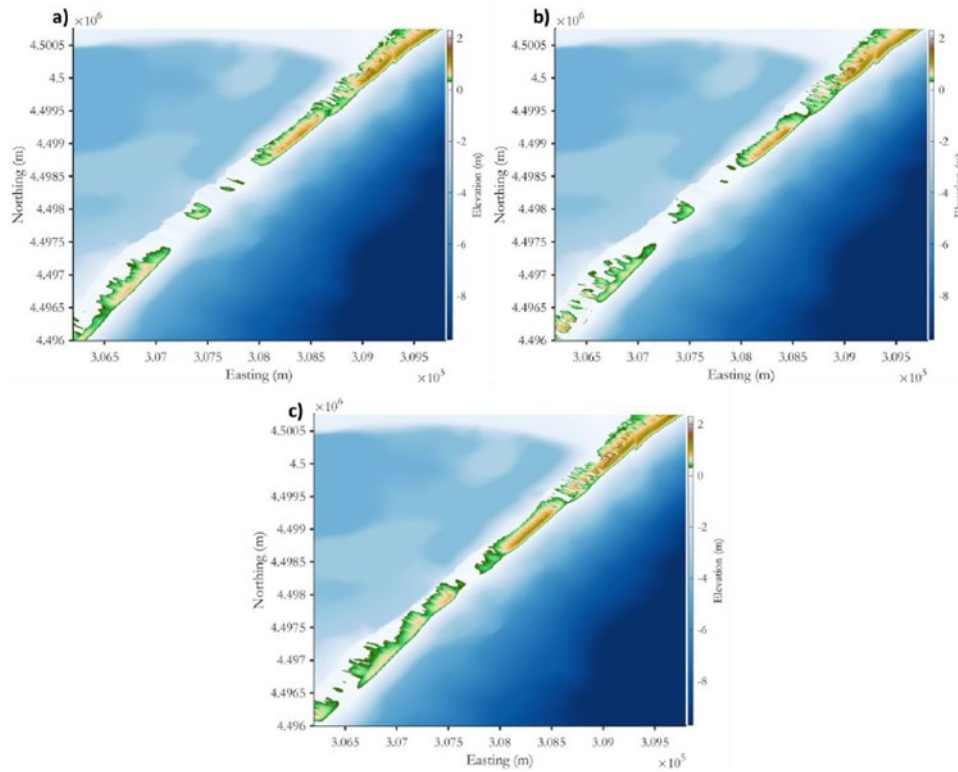


Figure 2.9. Final bed level after storm Isaak in +0.57 SLR conditions. a) No protection, b) Alternating dunes and c) Classical nourishment.

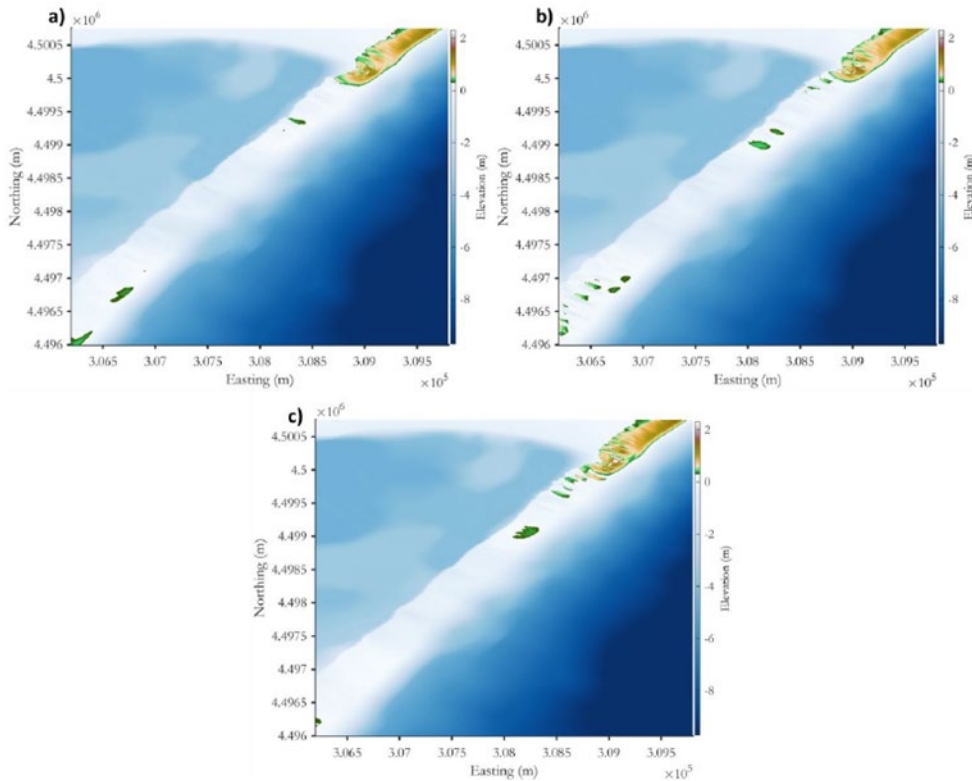


Figure 2.10. Final bed level after storm Filomena in +0.75 SLR conditions. a) No protection, b) Alternating dunes and c) Classical nourishment.

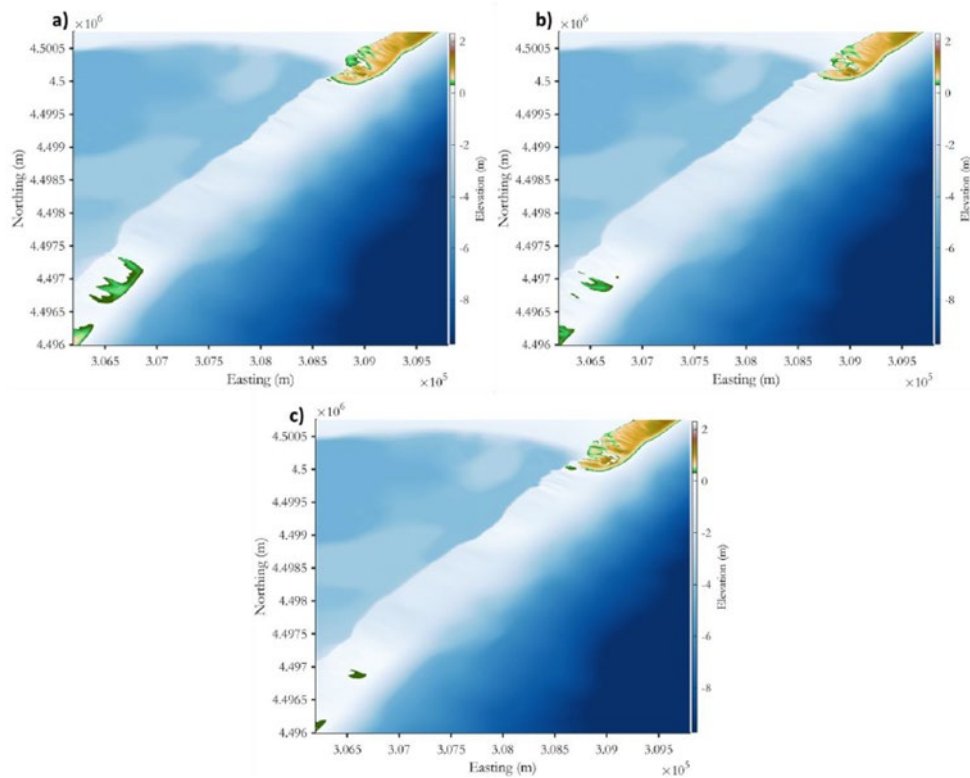


Figure 2.11. Final bed level after storm Gloria in +0.75 SLR conditions. a) No protection, b) Alternating dunes and c) Classical nourishment.

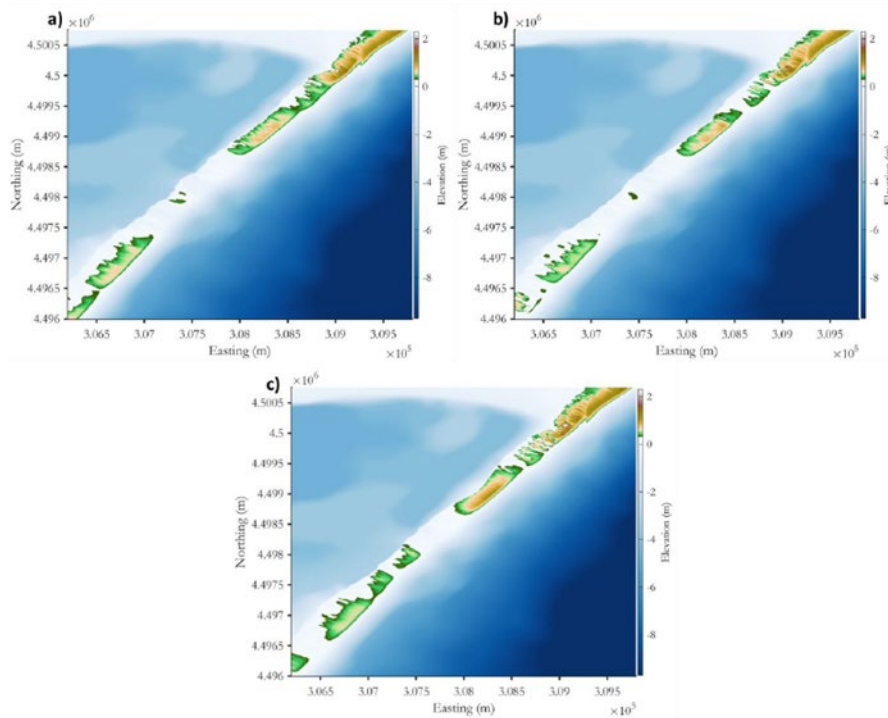


Figure 2.12. Final bed level after storm Isaak in +0.75 SLR conditions. a) No protection, b) Alternating dunes and c) Classical nourishment.

Again, to be able to see the real efficiency in future climate projections, it is necessary to use the metrics instead of the graphical information. In Figure 2.13, this general efficiency for all the studied case scenarios is provided. Comparing the alternating dune system with classical nourishment at the present and future conditions, we can see how the efficiency is reducing while going further into the future horizons. For the classical nourishment, under storm conditions like Gloria and Filomena the efficiency even reaches negative values because the input of sediment is also considered as breached. It can be also observed that for future projections, embryonic alternating dunes seems to work better for the higher storms meanwhile for Isaak, since the effects are not so strong, classical nourishment continues to perform better. Moreover, it can be discussed that when these thresholds are reached, the mitigation strategies would not be enough to protect the barrier beach.

2.1.3. Conclusions

To conclude, in the present conditions, classical nourishment seems to be the best strategy followed by the continuous dune, with alternating dunes being the worst mitigation action although all of them heavily protect the beach from suffering damages. Nevertheless, this has to be put in a long-term view where alternating dune ends being the best strategy for several reasons. First, the simulations show that within future projections, the efficiency gap is reduced until at the end alternating dunes perform better even better than classical nourishment. Besides, classical nourishment has a huge associated problem when planned as long-term action derived from the littoral sediment transport (Dean and Yoo, 1992; Benedet *et al.*, 2016). This effect produces a known loss of sediment through time, being necessary to re-nourish the area to maintain its effectiveness. The continuous dune has been used during the last decades in different tests and although it reduces the hazard, the constant hit of waves produces the destruction of the structure at long-term. Also, the continuous dune is very weak against consecutive events for the same reason. Instead, the embryonic alternating dune system is a more stable strategy since the waves hit the front dunes and the back ones are maintained intact, increasing their efficiency though time (Houser *et al.*, 2008; Pries *et al.*, 2008). The best strategy then would be to use alternating dune and reconstruct the front dunes if necessary and even create some small nourishments to help the structure. These small nourishments have been proved to be more ecological and stable than big nourishments (de Schipper *et al.*, 2021). Even so, when simulating future horizons with the worst climate change scenarios, the mitigation actions don't seem enough to protect the barrier beach from the combined effect of the SLR and the storms.

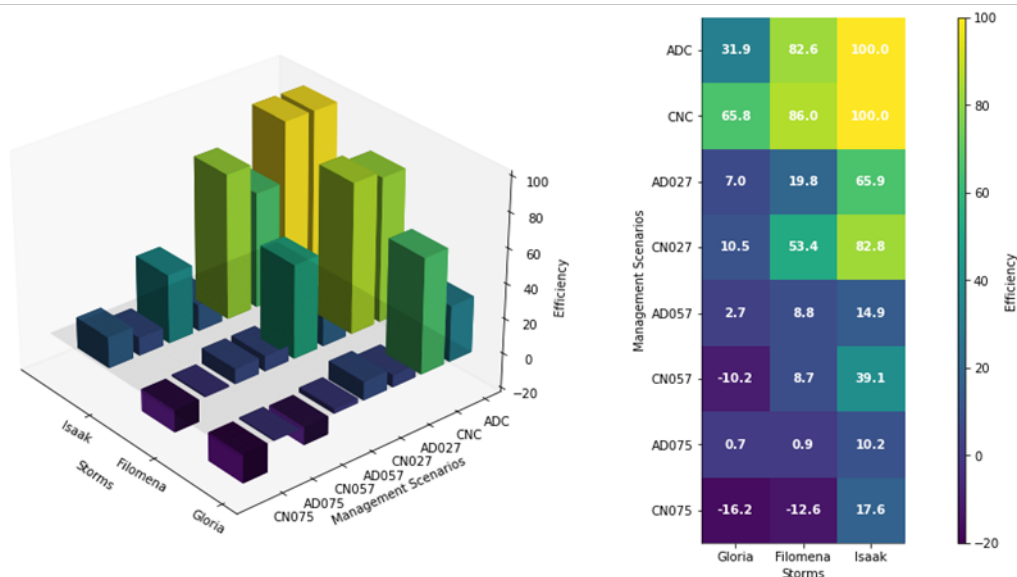
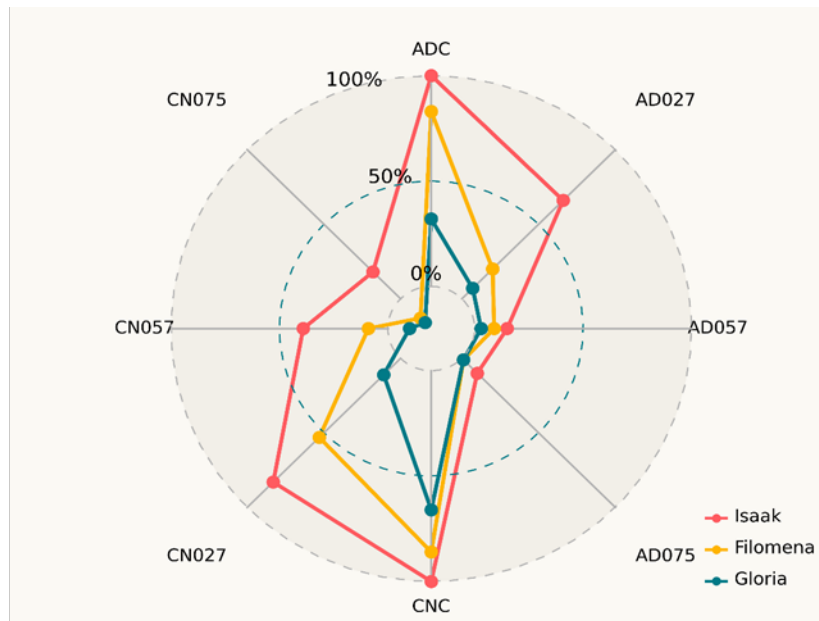


Figure 2.13. Three different representations of the efficiency of the measures Alternating dunes and Classical nourishment for present and future conditions.

2.2. Ebro River (UPM)

2.2.1. Numerical simulations on sediment transport to Ebro Delta

The numerical model used is the one described in Deliverable 2.1. Some modifications have been made to this model, as new bathymetric data of the Ebro River became available, providing a more accurate representation of the channel geometry and offering better resolution. The model calibration has been updated in light of the new bathymetry, and the necessary simulations have been carried out to estimate the river's potential sediment transport capacity.

In our previous study, numerical simulations were conducted using a 1-meter resolution Digital Terrain Model (DTM) of the Ebro basin, provided by the Spanish National System for Flood Risk Mapping. However, this DTM did not capture the riverbed itself; instead, it represented the water surface. For the new set of simulations in this work package, the “Centro de Estudios y Experimentación de Obras Públicas” (CEDEX) supplied a high-resolution DTM of the Ebro basin with a 0.5-meter resolution that includes detailed bathymetric data of the riverbed. Using this updated DTM, we generated a Triangulated Irregular Network (TIN) model of the river with a 0.1-meter vertical tolerance, a maximum triangle side length of 2000 meters, and a minimum side length of 12 meters. The TIN model was then imported into Iber for hydraulic simulations. Figure 2.14 (left) shows the TIN model of the Ebro topography in blue as visualized in Iber. On the right, two detailed snapshots of the topography are provided. The model covers approximately 100 kilometers of the Ebro River and consists of around 4,923,448 triangular elements.

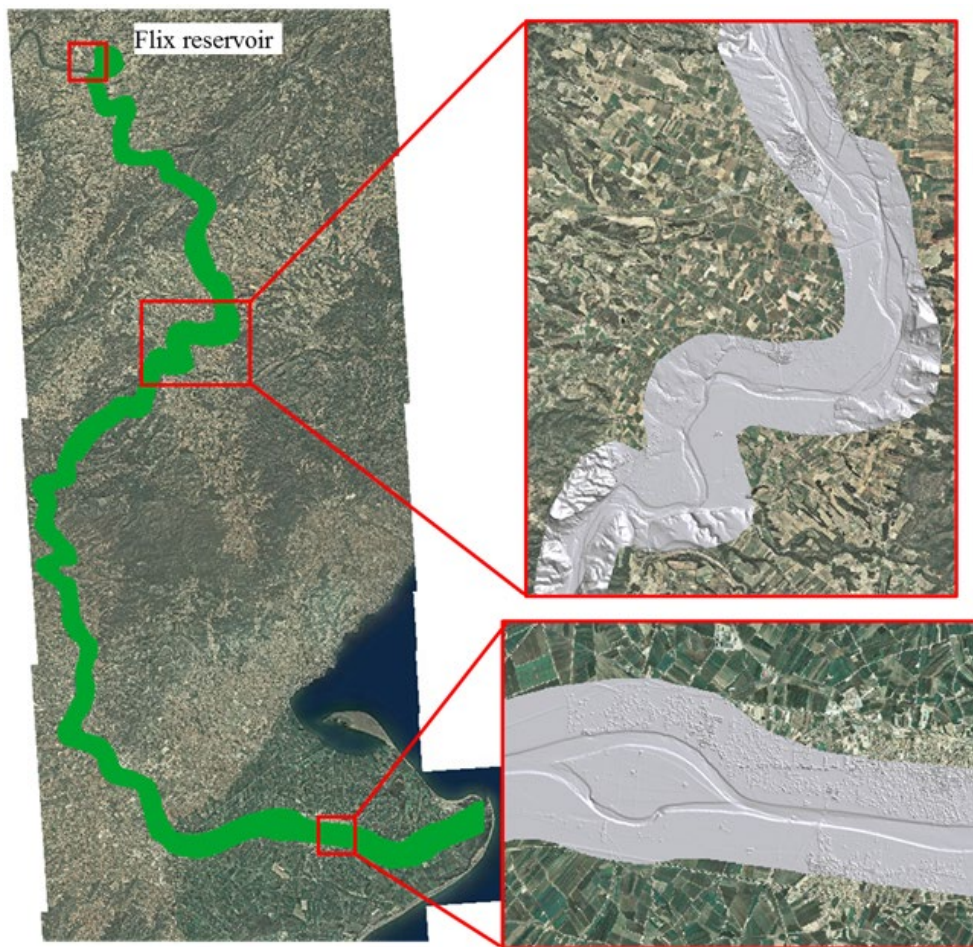


Figure 2.14. Domain of the numerical simulations in the Ebro Delta pilot site.

Figure 2.15 presents a comparison between the two DTMs: (a) the 1-meter resolution DTM provided by the Spanish National System for Flood Risk Mapping, labeled as “Old bathymetry” in the snapshots, and (b) the 0.5-meter resolution DTM provided by CEDEX, labeled as “New bathymetry.” The figure shows three river cross-sections derived from both DTMs. Notably, the new DTM from CEDEX captures the riverbed in greater detail, as clearly illustrated in the southern cross-section.

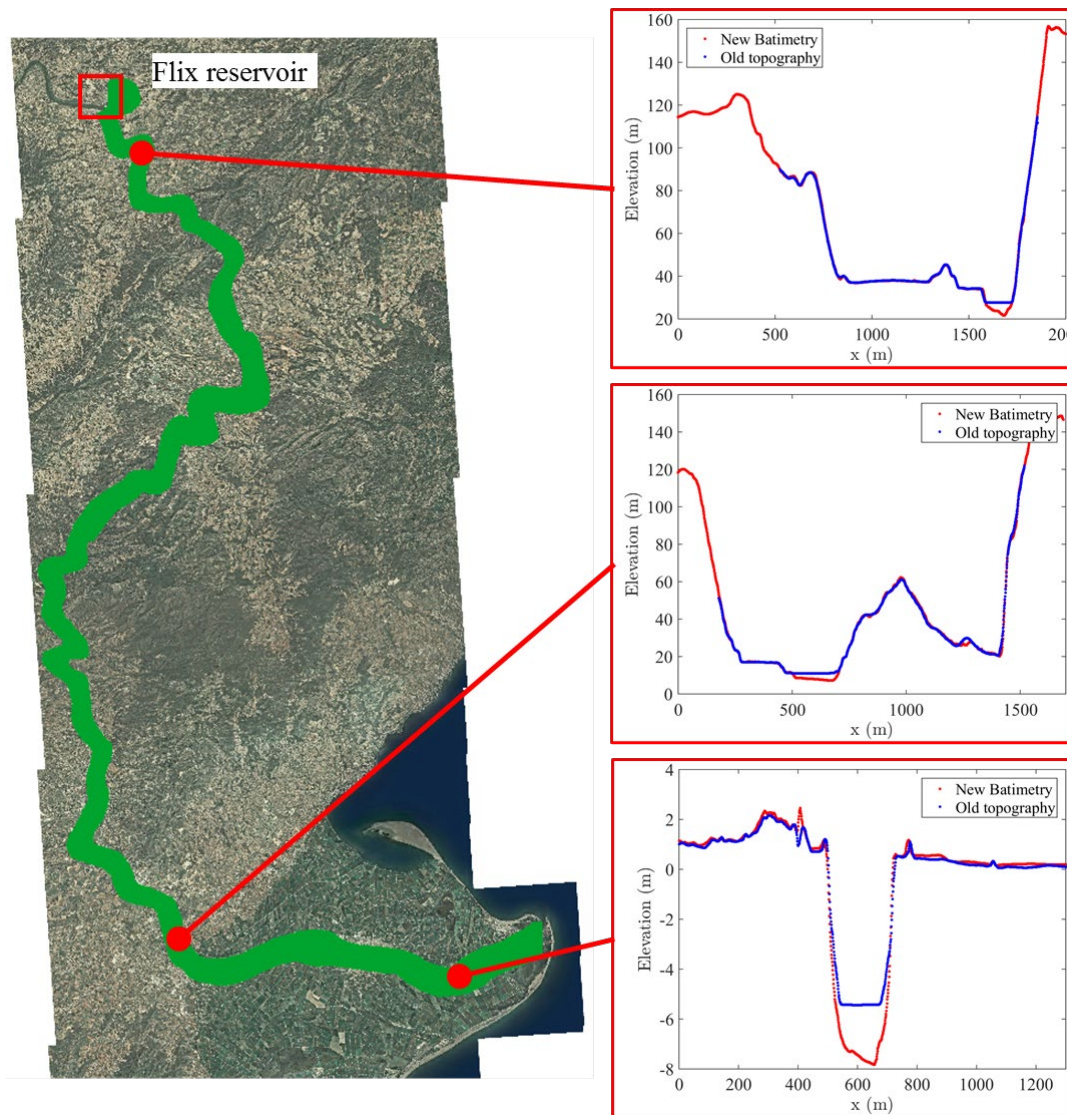


Figure 2.15. Cross sections of the Ebro River

2.2.2. Parameterization of hydro-morpho-eco interactions to simulate ESS

2.1.3.1. Approach to the characterization of sediment transport (based on historical observations)

For the characterization of sediment transport, we followed the approach presented in Deliverable 2.3, based on data compiled by Ibañez et al. (1996) about sediment transport in the lower Ebro River and its estuary. They provided estimates of the annual transport of suspended sediments for several flow ranges in the Ebro. Data were obtained from Gorria's experiments, conducted in 1877, well before the dam construction period. They identified two representative regimes: nor-mal flow, between $300 \text{ m}^3/\text{s}$ and $1500 \text{ m}^3/\text{s}$, with an estimated mean flow of $710 \text{ m}^3/\text{s}$ and a duration of 256 days and an average sediment concentration of 0.9 g/L , and annual flood, for discharge larger than $1500 \text{ m}^3/\text{s}$, with a mean flow of $1764 \text{ m}^3/\text{s}$, a mean duration of 11 days and an estimated sediment concentration of 7.2 g/L . Sediment transport was estimated to be 14.1 Mton/yr for normal flow and 12.1 Mton/yr for annual flood. They added a contribution to the mean sediment transport of 1.7 Mton/yr from exceptional floods. The remaining 0.2 Mton/yr corresponds to flows of less

than 300 m³/s. These values imply a total annual volume of 19.29 km³/yr and sediment transport of 28.1 Mton/yr.

2.2.2.2. Numerical analysis of sediment transport

We performed two numerical simulations corresponding to the two flow regimes characterized by Ibàñez et al. (1996). Each simulation accounts for both river flow hydrodynamics and suspended sediment transport. The objective of these simulations is to assess whether the Ebro River is capable of transporting the given sediment concentrations all the way to the Ebro Delta.

The size of the suspended particles, characterized in the model by their median diameter (D50), is not known a priori. To estimate D50, we carried out a calibration process based on the two flow and concentration values characterized by Ibàñez et al. (1996). This involved running a series of simulations with varying D50 values and selecting the largest diameter that does not result in net sedimentation along the river, while maintaining the suspended sediment concentration specified in the reported data for both flow regimes. The sediment properties used in the simulations are as follows: relative density of 2.65, friction angle of 30 degrees, suspended sediment dispersion coefficient of 0.001 m²/s, and Schmidt number of 1.1. The best match with the observed behavior was obtained for a D50 value of 0.0005 mm, corresponding to clay. Figure 2.16 presents contour plots of the suspended sediment concentration after 1.5 days for two different D50 values: 0.005 mm (silt) and 0.0005 mm (clay). These results are drawn from the calibration simulations, all conducted with a constant flow of 710 m³/s.

As shown in Figure 2.16(a), the flow is unable to transport the coarser silt particles effectively. As a result, sedimentation occurs along the river, and the concentration decreases to approximately 0.5 g/L at the delta. In contrast, the finer clay particles (Figure 2.16(b)) are fully transported by the flow, maintaining the prescribed concentration of 0.9 g/L throughout the river and reaching the delta without significant sedimentation.

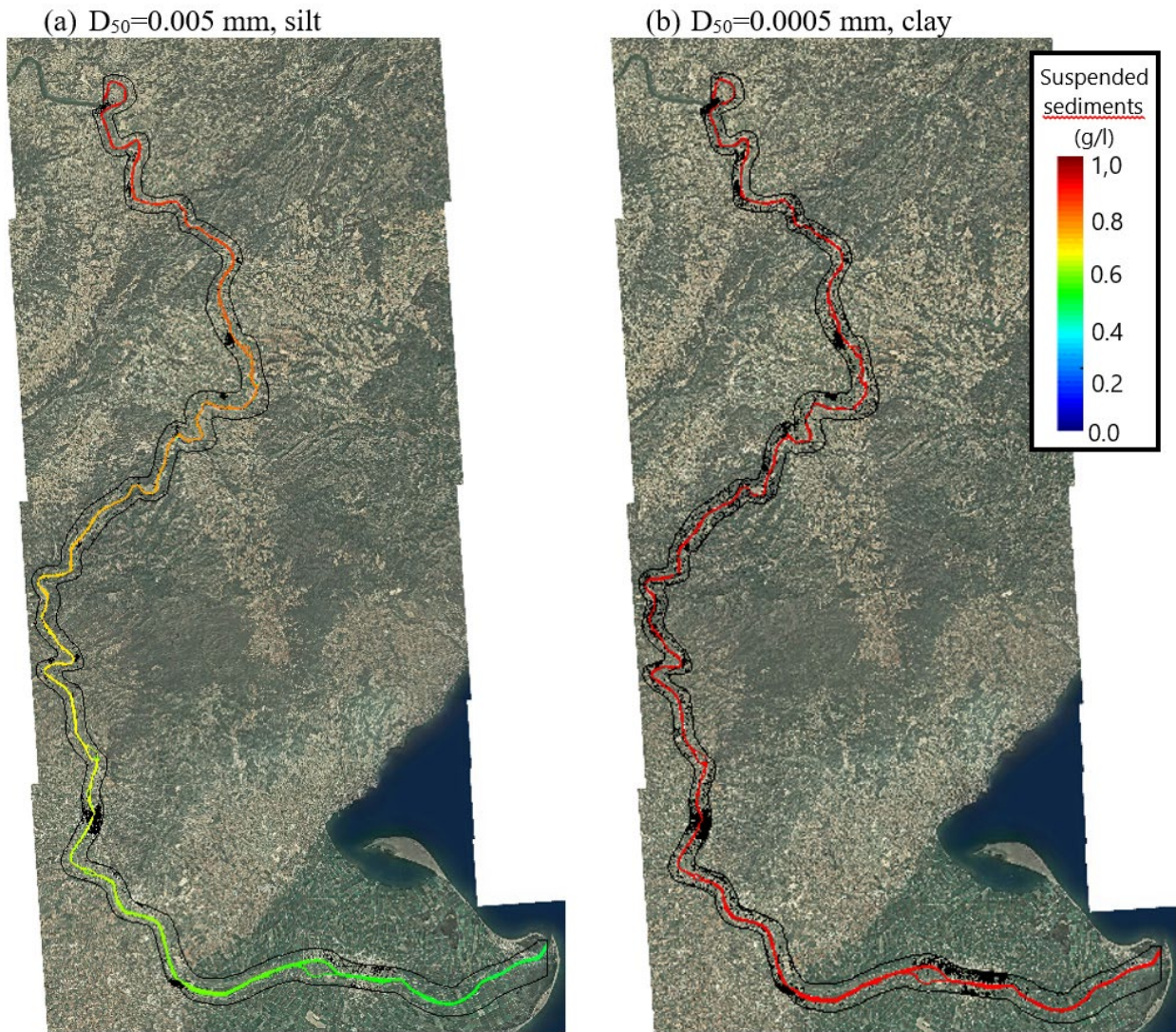


Figure 2.16. Suspended sediment concentration for the mean water regime given in Table 2.2 after 1,5 days. Flow water is $710 \text{ m}^3/\text{s}$ and the sediment concentration at the inlet is 0.9 g/l . In the contour plot (a) we plot the sediment concentration for the simulation with a median diameter of the sediment equal to 0.005 mm , whereas in the contour plot (a) the median diameter of the sediments is 0.0005 mm , ten times smaller.

Figure 2.17 shows the computed erosion results for the simulations using silt and clay. In these plots, negative erosion values indicate net sediment deposition. Figure 2.17(a) presents the results for the silt case. As the sediment concentration decreases along the river, sedimentation increases accordingly. After 1.5 days of simulation, the thickness of the deposited layer reaches approximately 2 mm near the inlet and gradually decreases downstream. In contrast, the simulation with clay exhibits no significant erosion or deposition, as shown in Figure 2.17(b). This indicates that the flow is capable of fully transporting clay particles, while the silt particles are prone to sedimentation along the river course.

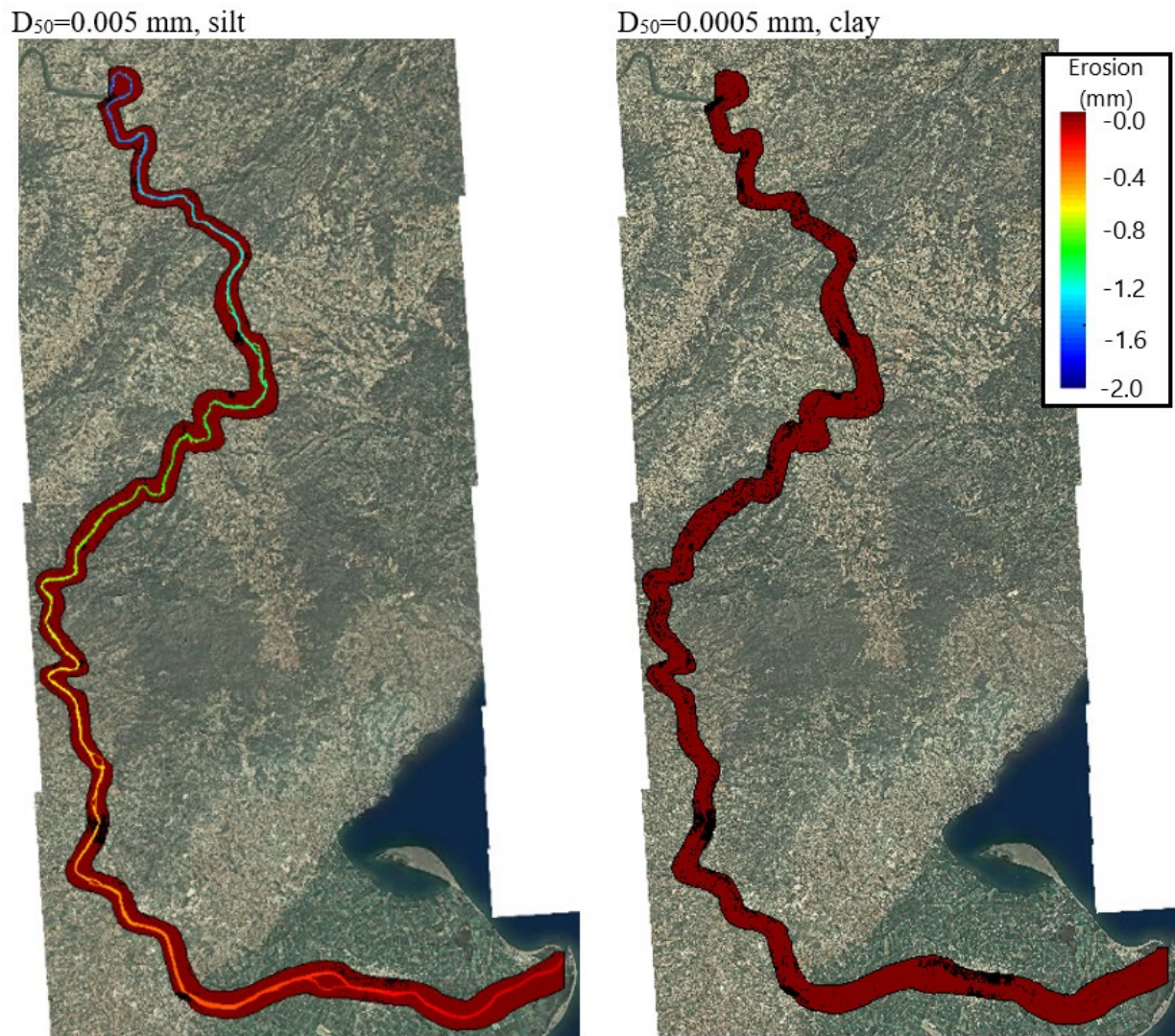


Figure 2.17. Erosion for the mean water regime given in Table 2.2 after 1,5 days. Flow water is $710 \text{ m}^3/\text{s}$ and the sediment concentration at the inlet is 0.9 g/l . In the contour plot (a) we plot the erosion for the simulation with a median diameter of the sediment equals to 0.005 mm , whereas in the contour plot (a) the median diameter of the sediments is 0.0005 mm , ten times smaller. Negative values of erosion mean deposition of sediments.

In the following paragraphs, we present results from the sediment transport simulations under the mean water flow regime. Initially, the riverbed is dry, with zero water depth, and water is introduced at the inlet located at the outlet of the Flix reservoir. The inflow is set to $710 \text{ m}^3/\text{s}$, with a suspended sediment concentration of 0.9 g/L . As the flow propagates downstream, a steady-state regime is eventually established. Figure 2.18 shows the evolution of suspended sediment concentration at three time steps. After 3 hours (Figure 2.18a), the flow has traveled approximately 11 km downstream, reaching the town of Ascó. At this stage, the suspended sediment concentration remains uniform at 0.9 g/L along the entire simulated reach of the Ebro River. After 12 hours (Figure 2.18b), the flow approaches the vicinity of Xerta, and the sediment concentration continues to be consistent at 0.9 g/L throughout the river. No net sediment deposition is observed at this time step (not shown), confirming that the flow can transport the specified sediment load without deposition under the given conditions.

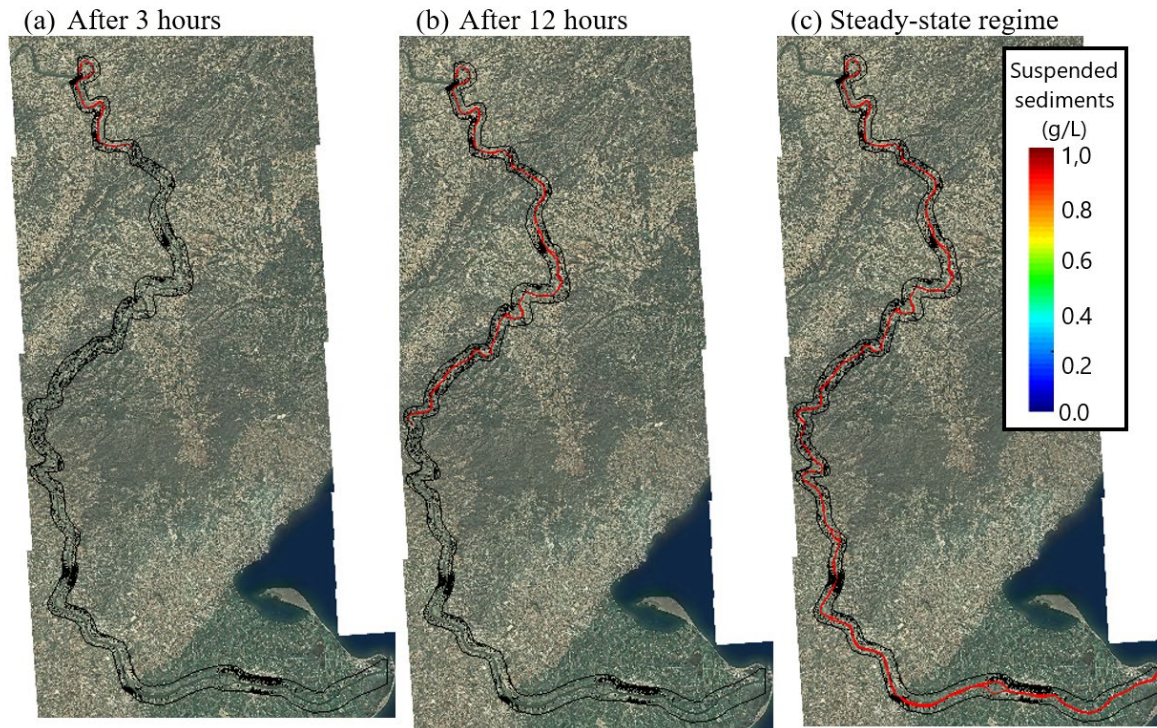


Figure 2.18. Suspended sediment concentration for the mean water regime given in Table 2.2. Flow water is $710 \text{ m}^3/\text{s}$ and suspended sediment concentration at the inlet is 0.9 g/L . We depict the contour plots of the concentration of suspended sediment after 3 hours in (a), after 12 hours in (b), and under the steady-state regime in (c).

We present results from sediment transport simulations under the annual flood conditions. As in the previous scenario, the riverbed is initially dry, and water is introduced at the inlet located at the outlet of the Flix reservoir. In this case, the inflow is set to $1,760 \text{ m}^3/\text{s}$, with a suspended sediment concentration of 7.2 g/L . As the flow propagates downstream, a steady-state regime is eventually established. Figure 2.19 illustrates the evolution of suspended sediment concentration at three time steps. After 3 hours (Figure 2.19a), the flow has advanced further downstream compared to the mean flow regime, maintaining a uniform sediment concentration of 7.2 g/L along the entire simulated reach of the Ebro River, with no deposition observed. After 12 hours (Figure 2.19b), the flow approaches the vicinity of Tortosa, and the sediment concentration remains consistent at 7.2 g/L throughout the river. Finally, Figure 2.19c depicts the steady-state regime, confirming that the river can transport the specified sediment concentration to the delta during the annual flood without significant deposition.

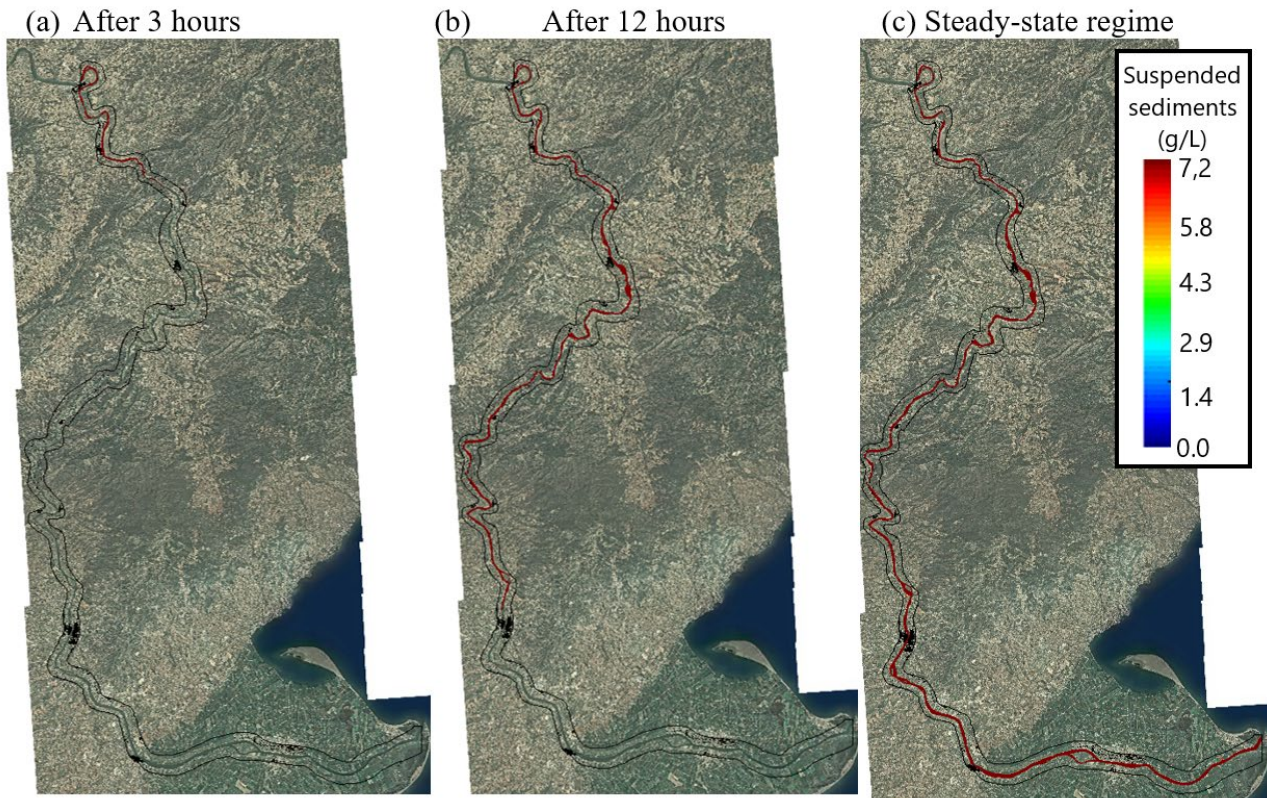


Figure 2.19. Suspended sediment concentration for the mean water regime given in Table 2.1. Flow water is $1764 \text{ m}^3/\text{s}$ and suspended sediment concentration at the inlet is 7.2 g/L . We depict the contour plots of the concentration of suspended sediment after 3 hours in Figure (a), after 12 hours in (b), and under the steady-state regime in (c).

2.2.2.3. Sediment transport of clay for other flow rates

We assess the capacity of the flow to transport suspended sediments for other flow rates different from the values provided by Gorria (1877) and Ibañez et al. (1996). In the previous section, we estimated the features of the sediments for the concentration and flow rates observed by Gorria (1877). The features of the sediment are: the median diameter of the grains, D_{50} , is 0.005 mm , the relative density is 2.65 , the friction angle is 30 degrees, the suspended sediment dispersion is $0.001 \text{ m}^2/\text{s}$, and the Schmidt number is 1.1 .

We estimate the concentration of the sediments that Ebro river can transport to the delta for other flow rates without sedimentation. We include the results in Figure 2.20 where a log-linear trend line is fitted to the data. We recall that concentration values for 710 and $1764 \text{ m}^3/\text{s}$ flow rates are given values by Gorria (1877) and Ibañez et al. (1996).

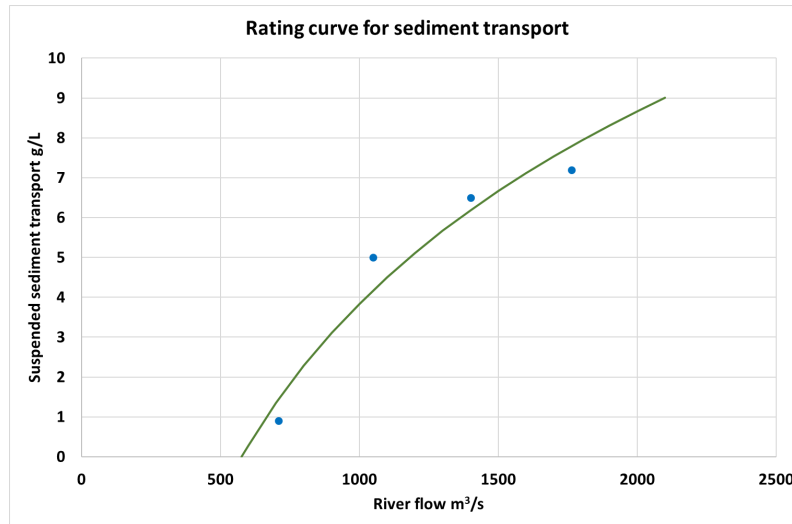


Figure 2.20. Suspended sediment concentration for several flow rates.

2.2.3. Assessment of current, potential and future sediment transport

In this section we evaluate current and potential sediment transport in the lower Ebro River to identify risks and assess the potential effects of mitigation actions.

2.2.3.1. Current sediment transport

We performed a simple analysis of current sediment transport using data available at the Ebro River streamflow and water quality measurement stations, reported in Deliverable 2.1. Turbidity data are available at Ascó and Tortosa monitoring stations. The data's continuity is compromised due to frequent gaps, with Ascó providing records since 1996 and Tortosa since 2011. The analysis performed in Deliverable 2.1 showed that the data exhibits significant dispersion, resulting in low R^2 values and indicating a weak linear correlation.

The relationship between turbidity and suspended sediment concentration was taken from (Tena et al., 2011), who obtained an excellent correlation for the data they collected in Mora de Ebro (Figure 2.21), with an R^2 value of 0.90. Although this empirical relationship may be station specific due to the local characteristics of suspended particles, it can be used to obtain a rough estimate of sediment flow values from available measurements. The equation used is as follows:

$$SSC = 0,83NTU - 1,3 \quad (2.24)$$

Where SSC is the suspended load concentration in mg/L and NTU are the turbidity units. From the concentration and the average daily flow at the corresponding station, the daily sediment load was estimated for the days when both data were available. The resulting mean values are presented in Table 2.3. The results obtained are highly uncertain. The mean flow can be used as an indicator of the representativeness of the analyzed sample by comparing the mean flow for days with both the data available and the average flow in the stations for the period analyzed. The error in Ascó is less than 10% and that in Tortosa exceeds 30%. The values obtained are extremely low compared to the average sediment flow under natural conditions estimated by Gorriá. These values are of the same order of magnitude as the results presented by other

researchers, who obtained somewhat lower loads downstream of the Mequinenza and Ribarroja reservoirs (for example, 0.055 Mton/year in Ascó).

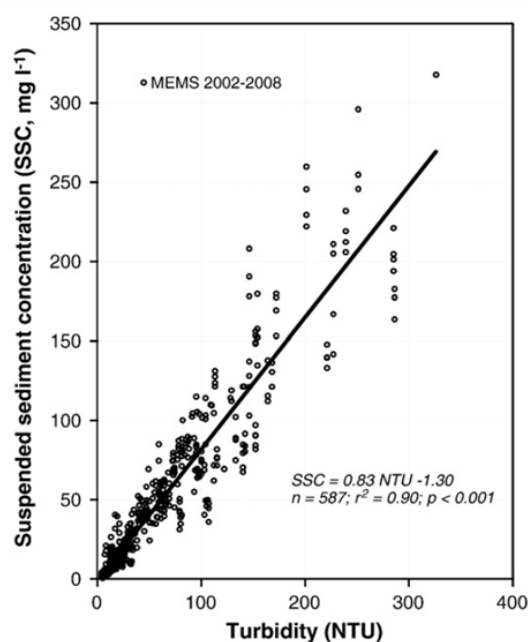


Fig. 3. Rating curve between turbidity (NTU) and suspended sediment concentration (SSC) at the Móra d'Ebre monitoring section (MEMS).

Figure 2.21. Figure 3 from Tena et al., 2011 where they show the relationship between turbidity and suspended sediment concentration

Table 2.3. Estimated average values of sediment transport from the flow and turbidity data in the stations of Ascó and Tortosa

Location	Mean flow 1997-2015 (m ³ /s)	Days with data	Mean flow for days with data (m ³ /s)	Turbidity NTU	Concentration (mg/L)	Sediment transport (Mton/yr)
Ascó	320.2.6	3923	291.6	15.5	11.6	0.120
Tortosa	284.9	981	372.1	32.6	25.9	0.500

2.2.3.2. Potential sediment transport

The low transport rate observed is due to the lack of availability of sediments. In this section, we estimate the potential sediment transport that would be available if the reservoirs can be bypassed. The estimate is based on flow data and on the sediment transport rating curve derived from numerical simulations. Flow data under actual conditions is obtained from the Tortosa gauging station. Data are available from 1913, but there are several small gaps and a larger one from 1936 to 1951. The period when data are continuously available spans from the hydrological year 1953-34 to 2019-20. Potential sediment transport was estimated for that period by applying the sediment transport rating curve to daily flows measured in the Tortosa station. The average potential sediment transport is 24.36 Mton/yr, much larger than the observed sediment flow.

Flow data under natural conditions are obtained from the results of the SIMPA model, Spanish acronym for Integrated System for Precipitation-Runoff Modelling. SIMPA is a conceptual distributed hydrological model that simulates the average monthly flows in the natural regime at any point of the hydrographic network of

Spain. The available simulated period is between the hydrological year 1940-41 and the year 2019-20. We obtained the monthly time series of the flow corresponding to the entire Ebro basin. Naturalized flows are only available at the monthly time scale, but observed flows are available at daily time scale. To compare potential sediment transport under natural and altered conditions, average monthly flows must be used. An error will be introduced in the results because the sediment transport rating curve is nonlinear. To estimate the order of magnitude of the error, we compared the annual sediment transport rates computed at the daily and the monthly scales in the Tortosa gauging station. The results are presented in Figure 2.22, which shows the comparison of the time sequence of both series and the scatter plot of the values, together with a linear fit. The difference does not appear to be very large. The slope of the linear fit is 1.22 and the coefficient of determination is 0.98. Therefore, it is acceptable to work at the monthly time scale, but sediment transport rates obtained at the monthly scale should be increased by 20% to account for the averaging.

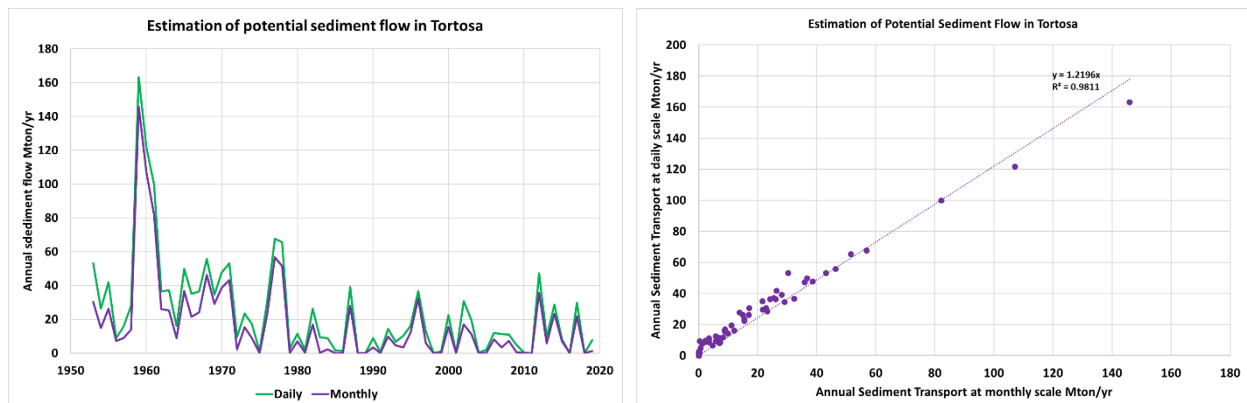


Figure 2.22. Comparison of the estimation of potential sediment transport in Tortosa at the daily and monthly scales. Left: annual flow. Right: sediment transport

Figure 2.23 shows the time series of annual flows and potential sediment transport in the Lower Ebro River under natural and altered conditions. Natural flows were taken from the SIMPA model and altered flows from the Tortosa streamflow gauge. The values begin to diverge in the 1960s decade, when reservoir constructions in the Ebro basin allowed the development of irrigation and the corresponding water extraction. Although some irrigation is still being developed in the basin, the large irrigation districts were finished in the 1980s. The average flow measured in Tortosa in the last 40 years with data is 9.09 km³/yr, while the estimate under natural conditions from the SIMPA model is 15.13 km³/yr. The difference, 6.04 km³/yr, can be mainly attributed to irrigation abstractions. The Ebro River Basin Management Plan for the cycle 2021-2027 considers 924,400 ha of irrigated land with an annual demand of 8.141 km³/yr. The difference between natural and measured flow would correspond to a net loss of water to evapotranspiration of 75% of the bulk abstraction, which is a reasonable Figure

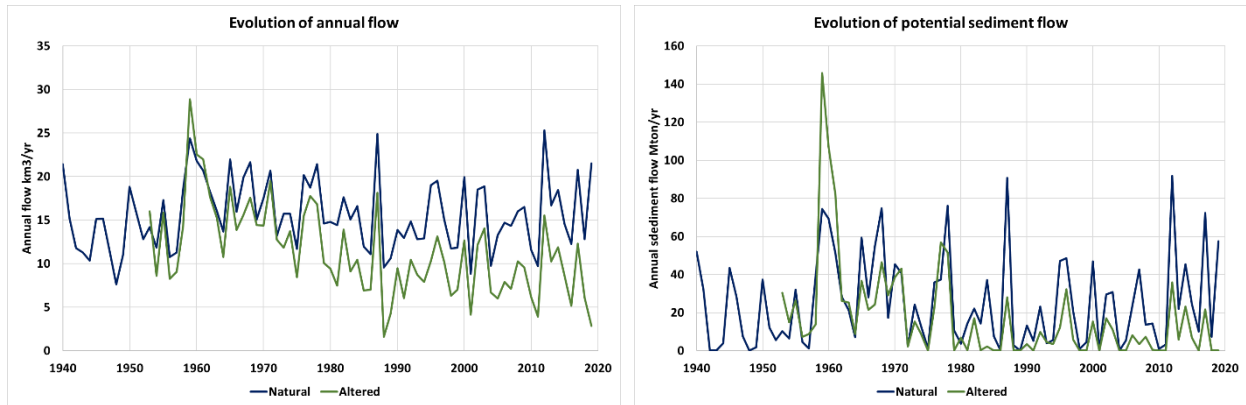


Figure 2.23. Evolution of annual flow and potential sediment transport in the Lower Ebro River under natural and altered conditions. Left: annual flow. Right: sediment transport

The impact of water abstractions on potential sediment transport is much greater than that of annual flow. Potential sediment transport was estimated by applying the sediment transport rating curve to monthly flows. The average value in the last 40 years is 22.39 Mton/yr under natural conditions and 6.93 Mton/yr under actual altered conditions, a 70% reduction versus 42% for annual flow. The rating curve shows that sediment transport requires a minimum flow of approximately 575 m³/s. This threshold was exceeded in 146 months in the last 40 years under natural conditions (30% of the time) and only 59 months under altered conditions (12% of the time). Figure 2.24 shows the relation between annual flow and potential sediment transport in the Lower Ebro River under natural and altered conditions. Although both relationships were obtained from the same rating curve on the monthly scale, the representation on the annual scale shows slightly larger sediment transport under altered conditions for the same annual flow, particularly for low annual flow values.

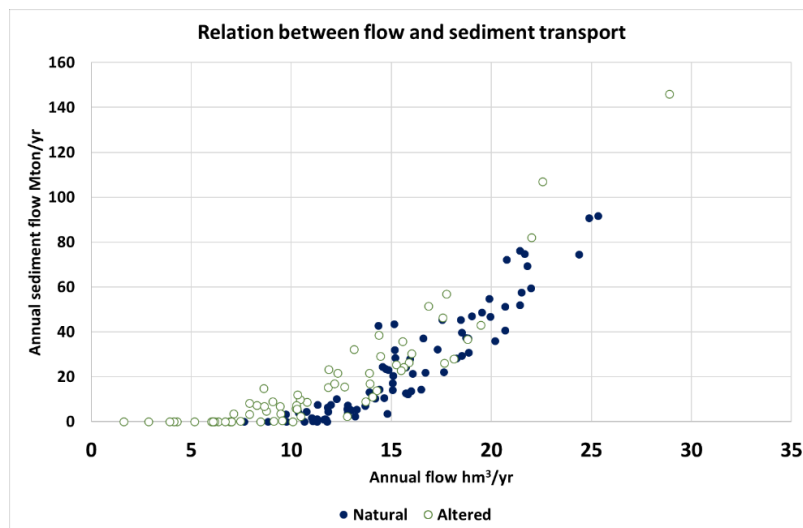


Figure 2.24. Relation between annual flow and potential sediment transport in the Lower Ebro River under natural and altered conditions

Figure 2.25 presents the monthly average values of flow and potential sediment transport under natural and altered conditions. The figure shows that, in addition to water abstractions, flow regulation is also relevant to determine the potential transport of sediments under altered conditions. The seasonality of flows shows that most water abstractions occur during the spring, summer, and autumn months, leaving the average winter flows almost unchanged. However, altered winter flows are concentrated in wet years, when

reservoirs release excess water. This leads to an increase in potential sediment transport in altered conditions during the winter months, which can be used to effectively manage the sediment bypasses in the reservoirs.

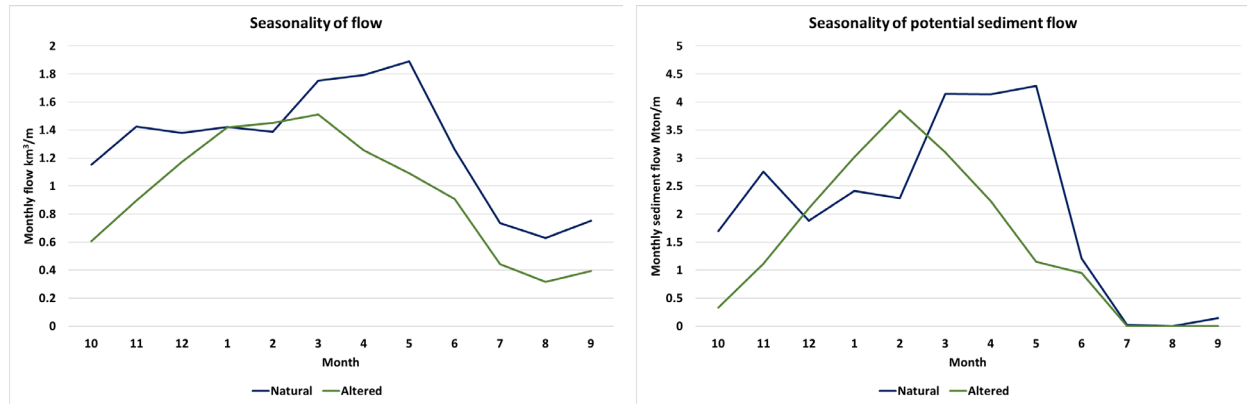


Figure 2.25. Mean seasonality of flow and potential sediment transport in the Lower Ebro River under natural and altered conditions. Left: annual flow. Right: sediment transport

In conclusion, the potential for sediment transport is significantly reduced under current conditions of water management in the Ebro River basin, but there is still capacity to transport almost 7 Mton/yr, which is a figure much larger than current observed sediment transport and exceeds what can be realistically expected to be bypassed from the reservoirs. However, it should be noted that in 14 of the 40 years analyzed there would be no sediment transport because discharges measured in Tortosa do not reach the transport activation threshold.

2.2.3.3. Potential sediment transport under different climate projections

In this section we obtain estimates of potential sediment transport for future scenarios using climate projections. The scenarios considered were taken from IPCC AR6. We selected the SSP1-2.6, SSP3-7.0 and SSP5-8.5 scenarios. The required data was obtained from the ISIMIP repository. The ISIMIP (Inter-Sectoral Impact Model Intercomparison Project) initiative is a collaborative research effort that aims to assess the impacts of climate change on various sectors of society and the environment.

2.2.3.3.1. Climate projections

The hydrological regime of the Ebro basin was taken from the results of global hydrological models H08 and CWatM, available in the ISIMIP repository. Two sets of climate scenarios were used: historical scenarios, for past times and future scenarios, for future times. Selected historical scenarios from ISIMIP are of two types: obsclim and historical. The denomination obsclim corresponds to impact models forced with observed climate in the actual time sequence. They are based on reanalysis data. This option was selected to validate the runoff obtained with the two global climate models against the results of the SIMPA model in the historical period. The denomination historical corresponds to impact models forced with results from climate models. This option was selected as a control reference to estimate changes of potential sediment transport in the future. Future scenarios correspond to the three emission scenarios of AR6 selected: SSP1-2.6, SSP3-7.0 and SSP5-8.5. In these options, climate models were forced with the emission patterns expected in each emission scenario. The simulations for future time periods start in 2015 and end in 2100. The hydrological

models were forced with climate drivers in the corresponding scenarios. There are two types of climate drivers: based on observations and based on climate models. The climate driver based on observations is gswp3 and is used in the obsclim scenario. The climate drivers based on models are gfdl-esm4, mri-esm2, ipsl-cm6a-1r, mpi-esm1-2hr and ukesm1-0-11. They are used in the historical and future scenarios.

2.2.3.3.2. Validation against SIMPA data

The comparison of the time sequence of annual flows and potential sediment transport in the Ebro River produced by the SIMPA model and the two ISIMIP hydrologic models is shown in Figure 2.26. Potential sediment transport was estimated from monthly average flows using the rating curve derived from numerical simulations. Both ISIMIP models show a good agreement with SIMPA in the overlapping period 1940-2019 for annual flows. The agreement of the CWatM model appears to be better. However, the comparison for potential sediment transport shows that both ISIMIP models produce much higher sediment transport than SIMPA model. The time sequence of potential sediment transport is very similar for the two ISIMIP hydrologic models.

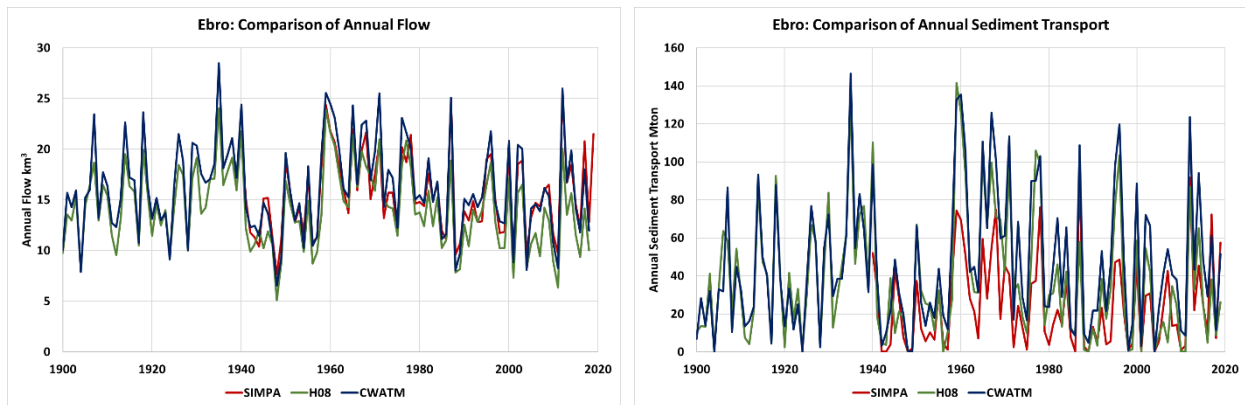


Figure 2.26. Comparison of the time sequence of annual flows and potential sediment transport in the Ebro River produced by SIMPA model and ISIMIP global hydrologic models. Left: Annual flows. Right: Potential sediment transport

Figure 2.27 shows the scatter plot of annual flows in the Ebro River. The plot on the left shows the comparison between H08 model and SIMPA model and the plot on the right shows the comparison between CWatM model and SIMPA model. For the H08 model, the slope of the linear regression fit is 0.89, suggesting underestimation of annual flow values for the H08 model compared to the SIMPA model. The coefficient of determination is very high, 0.986. For the CWatM model, the results are much better. The slope of the linear regression fit is 1.04, suggesting only a small bias. The coefficient of determination is excellent, 0.994.

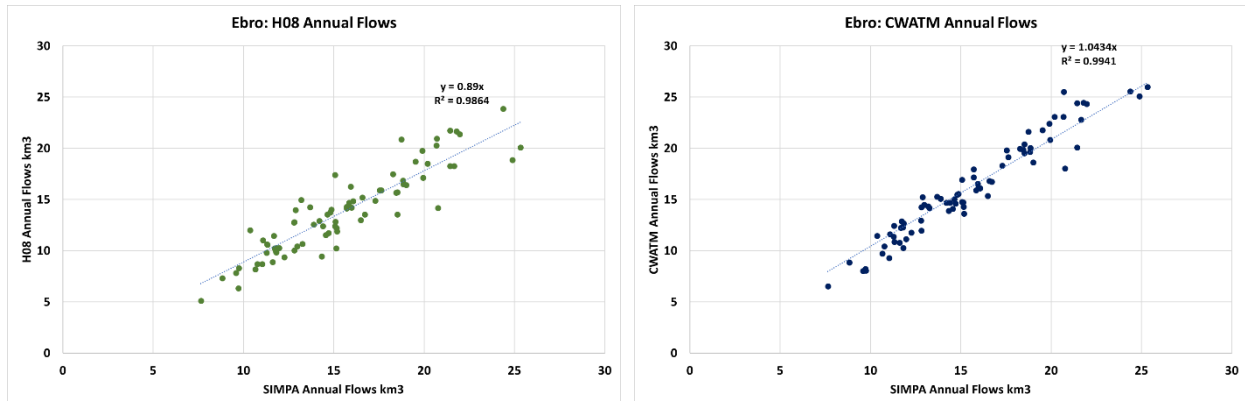


Figure 2.27. Comparison of annual flows in the Ebro River produced by ISIMIP global hydrologic models and SIMPA model. Left: H08 model. Right: CWatM model

Figure 2.28 shows the scatter plot of potential sediment transport in the Ebro River. The plot on the left shows the comparison between H08 model and SIMPA model and the plot on the right shows the comparison between CWatM model and SIMPA model. The scatter is much larger than in the case of annual flows. For the H08 model, the slope of the linear regression fit is 1.32, suggesting a significant overestimation of annual flow values for the H08 model compared to the SIMPA model. The coefficient of determination is low, 0.802. For the CWatM model, the overestimation is even larger. The slope of the linear regression fit is 1.70. The coefficient of determination is better than in the case of the H08 model, 0.907. These results are surprising, because the agreement for annual flows is very good, especially for the CWatM model, and potential sediment transport is derived from annual flows using the same rating curve for all models.

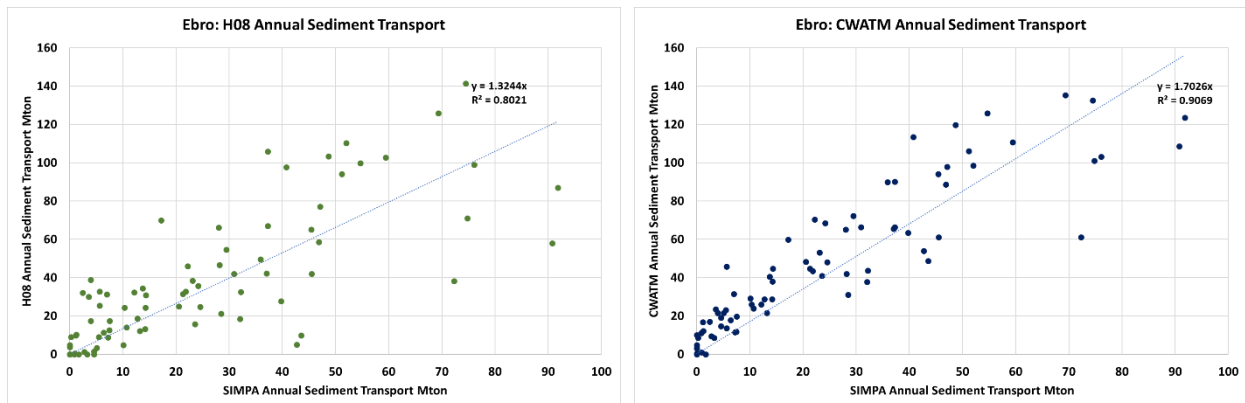


Figure 2.28. Comparison of potential sediment transport in the Ebro River produced by ISIMIP global hydrologic models and SIMPA model. Left: H08 model. Right: CWatM model

The causes for the disagreement in potential sediment transport can be identified by analyzing the seasonality, which is shown in Figure 2.29. The plot on the left shows the monthly flow averages for the overlapping period and the plot on the right shows the monthly averages of potential sediment transport. The comparison of the distribution of monthly flows shows that ISIMIP models tend to overestimate flow in autumn and winter months and to underestimate flow in spring and summer months. The disagreement is probably due to a failure to properly capture the snow accumulation in winter and the snowmelt processes that produce the high flows of the Ebro River in spring. The overestimation of the winter flows is amplified by the nonlinearity of the sediment transport process and leads to a large overestimation of sediment transport.

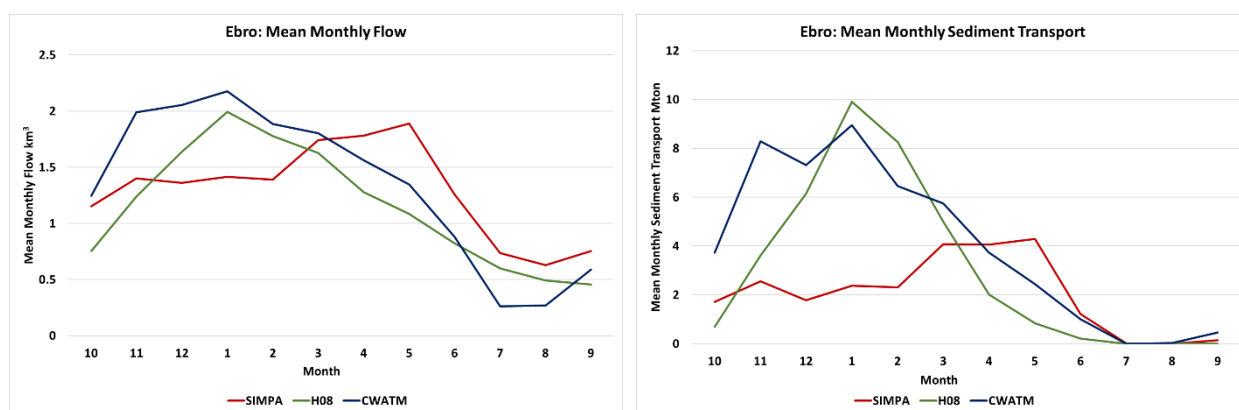


Figure 2.29. Comparison of seasonality of flows and potential sediment transport in the Ebro River produced by ISIMIP global hydrologic models and SIMPA model. Left: Seasonality of flows. Right: Seasonality of potential sediment transport.

The large disagreement between sediment transport estimated by the SIMPA model and by ISIMIP models suggest that a bias correction is required. The values of monthly flows of ISIMIP were corrected for monthly bias. The results of the effect of bias correction on potential sediment transport are shown in Figure 2.30. The scatter is still significantly larger than that of annual flows. For the H08 model, the slope of the linear regression fit is 0.89 and the coefficient of determination is 0.850. For the CWatM model, the slope of the linear regression fit is 1.28 and the coefficient of determination is 0.881. These results improve the agreement for potential sediment transport between SIMPA model and ISIMIP models.

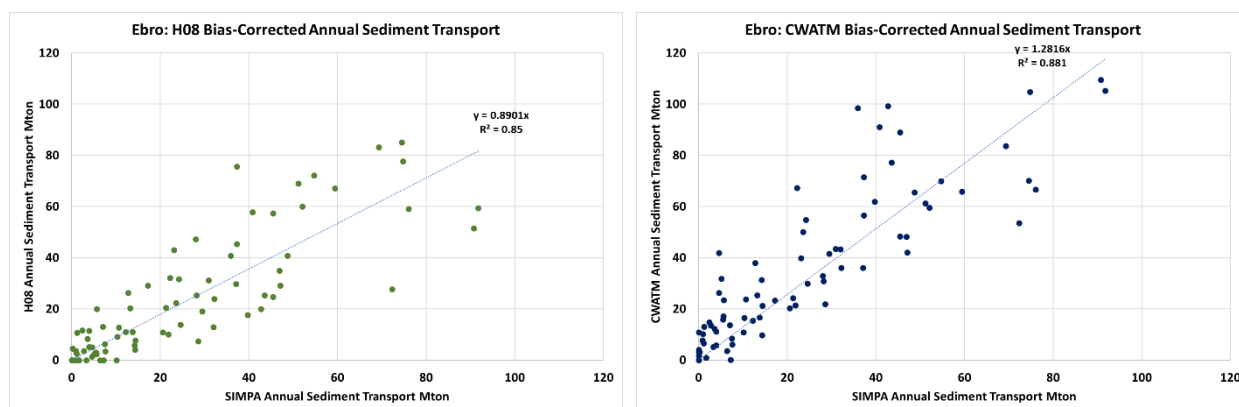


Figure 2.30. Comparison of bias-corrected potential sediment transport in the Ebro River produced by ISIMIP global hydrologic models and SIMPA model. Left: H08 model. Right: CWatM model

2.2.3.3.3. Results of annual flows under climate projections

The results produced by SIMPA model and ISIMIP hydrologic models for mean annual flow in all scenarios analyzed are presented in Table 2.4. The values correspond to averages taken over 40-year periods. The time period for SIMPA and the obsclim scenario spans from 1979-80 to 2018-19. The time series of the historical scenario only cover up to year 2014, so the time period selected for this scenario is 1974-75 to 2013-2014. Two time periods were selected for the climate projections: 2020-21 to 2059-60 and 2060-61 to 2099-2100. The table presents the values of mean annual flow obtained for the SIMPA, the two ISIMIP models, and the average of the two ISIMIP models, in all scenarios considered. It also presents the average values obtained with all climate drivers in each scenario.

The results show a significant difference between the mean annual flow estimated with the two global hydrologic models. For the obsclim scenario, H08 provides a mean annual flow for the Ebro River of 12.63 km³/yr, while the estimate of CWatM is 15.17 km³/yr. The estimate of the SIMPA model, 14.97 km³/yr, is almost coincident with that of the CWatM model. The values for the average over the five climate drivers of the historical scenario are 13.49 km³/yr for the H08 model and 15.62 km³/yr for the CWatM model. The corresponding values of the obsclim scenario for the historical period, 1974-75 to 2013-2014, are 13.19 km³/yr for the H08 model and 15.63 km³/yr for the CWatM model, which means that there is an excellent agreement between the obsclim and the average of the results obtained with the five climate drivers used in the historical scenario.

The projections for future scenarios show some sensitivity to the climate drivers used, but they provide a consistent picture of the expected evolution of mean annual flow in the Ebro basin. Mean annual flow is expected to decrease in the Ebro basin for most scenarios. Only the mri-esm2 climate driver produced an increase in mean annual flow in some scenarios.

Table 2.4. Mean annual flow obtained in the simulations of the scenarios for the Ebro basin, in km³/yr

Scenario	obsclim 80-19	obsclim 75-14	historical 75-14	ssp126 20-59	ssp370 20-59	ssp585 20-59	ssp126 60-99	ssp370 60-99	ssp585 60-99
SIMPA	14.97	15.19							
h08_gswp3	12.63	13.19							
h08_gfdl			13.45	12.12	10.61	11.64	12.20	10.22	9.14
h08_mri			13.40	12.37	11.33	12.97	13.62	11.45	9.94
h08_ipsl			13.61	10.91	10.42	9.83	10.57	8.10	7.27
h08_mpi			13.03	10.95	10.33	10.61	11.39	8.80	8.55
h08_ukesm1			13.98	11.63	9.63	9.24	10.62	7.64	7.97
mean h08	12.63	13.19	13.49	11.59	10.46	10.86	11.68	9.24	8.57
cwatm_gswp3	15.17	15.63							
cwatm_gfdl			15.84	15.31	13.66	14.98	15.46	13.88	12.66
cwatm_mri			15.59	15.81	15.28	16.90	16.78	15.81	14.03
cwatm_ipsl			15.84	13.95	13.98	12.81	13.84	11.82	10.60
cwatm_mpi			15.44	14.02	12.90	13.71	14.49	11.73	11.87
cwatm_ukesm1			15.40	14.92	13.82	12.13	14.30	11.89	11.38
mean cwatm	15.17	15.63	15.62	14.80	13.93	14.11	14.98	13.03	12.11
gswp3	13.90	14.41							
gfdl			14.64	13.72	12.13	13.31	13.83	12.05	10.90
mri			14.49	14.09	13.31	14.93	15.20	13.63	11.98
ipsl			14.72	12.43	12.20	11.32	12.21	9.96	8.94
mpi			14.24	12.49	11.62	12.16	12.94	10.27	10.21
ukesm1			14.69	13.28	11.72	10.69	12.46	9.77	9.67
mean	13.90	14.41	14.56	13.20	12.20	12.48	13.33	11.13	10.34

The average values of projected mean annual flow obtained with the two hydrologic models for the five climate drivers in each scenario are shown in Figure 2.31. To facilitate comparison, the figure shows the actual flow values obtained in the simulations and the bias-corrected values of mean annual flow. Both hydrologic models provide a similar picture of annual flow projection, but with different intensity. The SSP12.6 shows the least reduction of mean annual flow. The SSP37.0 predicts the largest reduction for the first time window 2020-2059, reaching -10% for the CWatM model and exceeding -20% for the H08 model. For the second time window, the largest reduction is predicted by the scenario SSP58.5: more than -20% for the CWatM model and more than -35% for the H08 model.

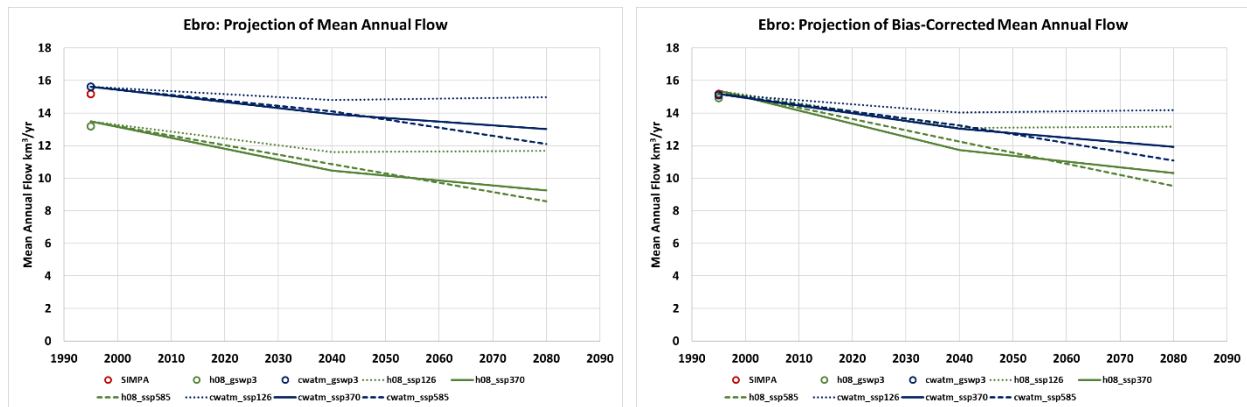


Figure 2.31. Projection of mean annual flow in the Ebro River under ISIMIP climate scenarios. Left: Actual value of mean annual. Right: Bias-corrected mean annual flow

2.2.3.3.4. Results of potential sediment transport under climate projections

The time series produced by SIMPA model and ISIMIP hydrologic models in all scenarios analyzed were processed using the sediment transport rating curve to obtain projections of potential sediment transport in natural conditions. The analysis was performed on the bias-corrected series. The results are presented in Table 4. The values correspond to the same periods shown in Table 2.4. Table 2.5 presents the values of mean annual potential sediment transport obtained for the SIMPA, the two ISIMIP models, and the average of the two ISIMIP models, in all scenarios considered. It also presents the average values obtained with all climate drivers in each scenario.

Table 2.5. Mean potential sediment transport obtained in the simulations of the scenarios for the Ebro basin, in Mton/yr

Scenario	obsclim 80-19	obsclim 75-14	historical 75-14	ssp126 20-59	ssp370 20-59	ssp585 20-59	ssp126 60-99	ssp370 60-99	ssp585 60-99
SIMPA	22.68	21.60							
h08_gswp3	15.61	19.06							
h08_gfdl			20.50	14.34	10.81	11.84	13.82	7.37	5.63
h08_mri			23.33	19.20	10.32	25.54	25.13	19.36	9.85
h08_ipsl			23.92	12.46	11.34	7.50	14.98	8.32	3.81
h08_mpi			21.54	14.04	10.40	11.17	15.23	6.29	7.16
h08_ukesm1			26.93	15.81	6.78	7.02	11.55	5.54	7.36
mean h08	15.61	19.06	23.24	15.17	9.93	12.61	16.14	9.38	6.76
cwatm_gswp3	31.01	34.48							
cwatm_gfdl			36.95	33.65	26.38	30.74	35.93	26.43	23.38
cwatm_mri			39.95	44.13	35.42	50.28	43.20	43.91	33.19
cwatm_ipsl			36.95	32.29	33.27	21.72	37.62	26.76	18.49
cwatm_mpi			40.00	33.88	23.82	26.86	34.13	19.21	21.15
cwatm_ukesm1			36.72	38.12	27.42	20.78	35.66	25.46	22.54
mean cwatm	31.01	34.48	38.11	36.41	29.26	30.08	37.31	28.35	23.75
gswp3	23.31	26.77							
gfdl			28.73	23.99	18.60	21.29	24.87	16.90	14.51
mri			31.64	31.66	22.87	37.91	34.16	31.63	21.52
ipsl			30.44	22.38	22.30	14.61	26.30	17.54	11.15
mpi			30.77	23.96	17.11	19.01	24.68	12.75	14.15
ukesm1			31.83	26.96	17.10	13.90	23.60	15.50	14.95
mean	23.31	26.77	30.68	25.79	19.60	21.35	26.72	18.86	15.26

The results show a significant difference between the mean potential sediment transport estimated with the SIMPA model and those estimated with the two global hydrologic models, despite the bias correction. For the obsclim scenario, the estimate of the SIMPA model is 22.68 Mton/yr. H08 provides a mean sediment transport for the Ebro River of 15.61 Mton/yr (31% less than SIMPA), while the estimate of CWatM is 31.01 Mton/yr (36% more than SIMPA). These estimations are, therefore, highly uncertain. The values for the average over the five climate drivers of the historical scenario are 23.24 Mton/yr for the H08 model and 38.11 Mton/yr for the CWatM model. The corresponding values of the obsclim scenario for the historical period, 1974-75 to 2013-2014, are 19.06 Mton/yr for the H08 model and 34.48 Mton/yr for the CWatM model. The projections for future scenarios show more variability than in the case of annual flows. The potential for sediment transport under natural conditions is expected to decrease dramatically in some scenarios. The average values of projected mean potential sediment transport obtained with the two hydrologic models for the five climate drivers in each scenario are shown in Figure 2.32. Despite the difference in absolute values, the two ISIMIP hydrologic models provide a similar picture of the expected evolution of potential sediment transport, intensifying the effects observed in annual flow. The SSP12.6 shows the least reduction of potential sediment transport. The SSP37.0 predicts the largest reduction for the first time window 2020-2059, reaching -23% for the CWatM model and exceeding -55% for the H08 model. For the second time window, the largest reduction is predicted by the scenario SSP58.5: more than -70% for the CWatM model and more than -35% for the H08 model.

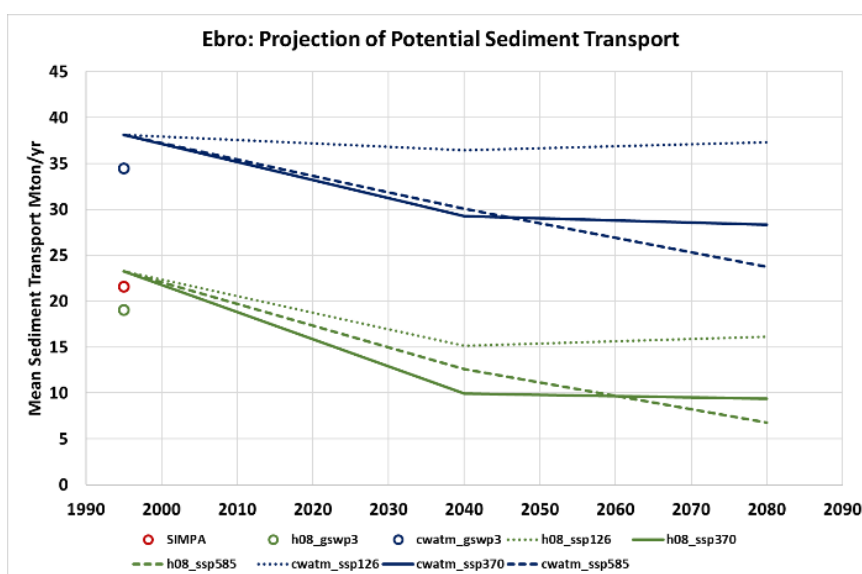


Figure 2.32. Projection of mean potential sediment transport in the Ebro River under ISIMIP climate scenarios

2.2.4. Conclusions

The projected reductions in mean annual flow will dramatically reduce the sediment transport capacity of the Ebro River under natural conditions, due to the nonlinearity of the sediment transport rating curve. The results of the analysis are summarized in Figure 2.33, which shows the projected changes of mean annual flow and potential sediment transport in the Ebro River for the two hydrologic models of ISIMIP. Although the H08 and CWatM models produce different absolute figures, the relative projected evolution is very similar in both models. In the most likely scenario, SSP37.0, the expected reduction in the first time period, 2020-2059, ranges between 10% and 22% for mean annual flow and between 23% and 57% for sediment transport.

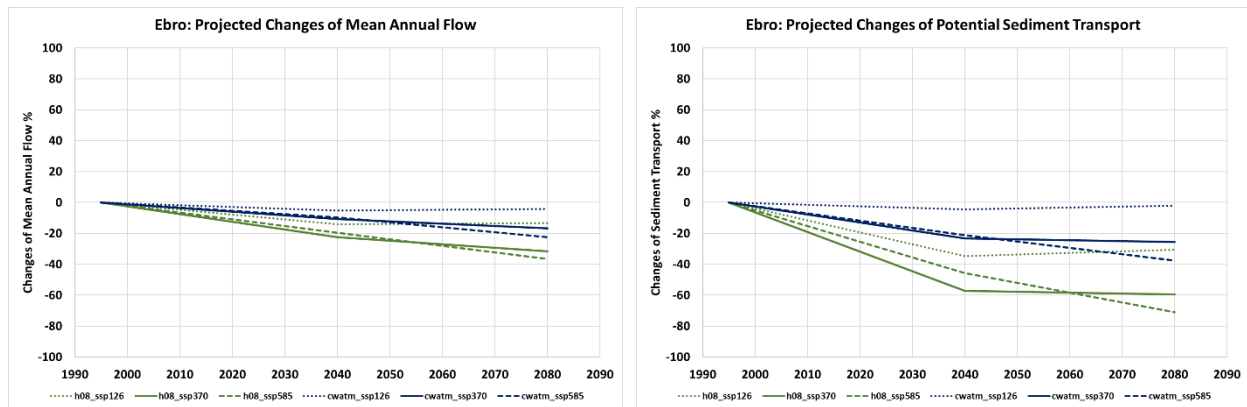


Figure 2.33. Projected changes of mean annual flow and potential sediment transport in the Ebro River under ISIMIP climate scenarios. Left: Changes of mean annual. Right: Changes of potential sediment transport

The impact of such reductions on the potential sediment transport capacity of the Ebro River under altered conditions will depend on how the Ebro River is managed in the future. Under the current management strategy, roughly 6 km³/yr are abstracted from the 15 km³/yr of natural flow, leaving 9 km³/yr in Tortosa. This reduces the potential sediment transport capacity from 22 Mton/yr under natural conditions to 7 Mton/yr, but this figure is still enough to convey the sediment required by the Delta. The projected reductions suggest a future mean annual flow between 12 km³/yr and 13.5 km³/yr. The potential sediment transport capacity for the natural regime is expected to be reduced to between 10 Mton/yr and 17 Mton/yr. If the potential sediment transport under altered conditions was similarly reduced, it would fall to a range between 3.5 km³/yr and 5 km³/yr and some carrying capacity would still remain in the river. However, if current abstractions of 6 km³/yr were maintained in the future, available flow would be reduced to 6 km³/yr to 7.5 km³/yr, which represent a larger reduction than that of natural flow. Therefore, it is very likely that the potential for sediment transport under altered conditions will be reduced more than that under natural conditions.

3. Multi-risk projections and climate warnings with ESS in Wadden Sea Pilot (DEL, HZG, FSK).

The Wadden Sea, located in the south-eastern part of the North Sea, is facing increasing risks of flooding and coastal erosion from extreme storms, which are becoming more frequent and intense in the context of global climate change. These risks pose a significant threat to the region's coastal communities and ecosystems, and we are committed to finding solutions to mitigate them.

A unique challenge in the Wadden Sea, a UNESCO World Heritage Site, is that the implementation of conventional hard and grey engineering solutions, such as dams and breakwaters, are less attractive. This reflects the need to preserve the ecological integrity and aesthetic values of the Wadden Sea, and underlines the delicate balance between conservation and the need for adaptive strategies. Therefore, the need for innovative, nature-based solutions has received more attention in recent years.

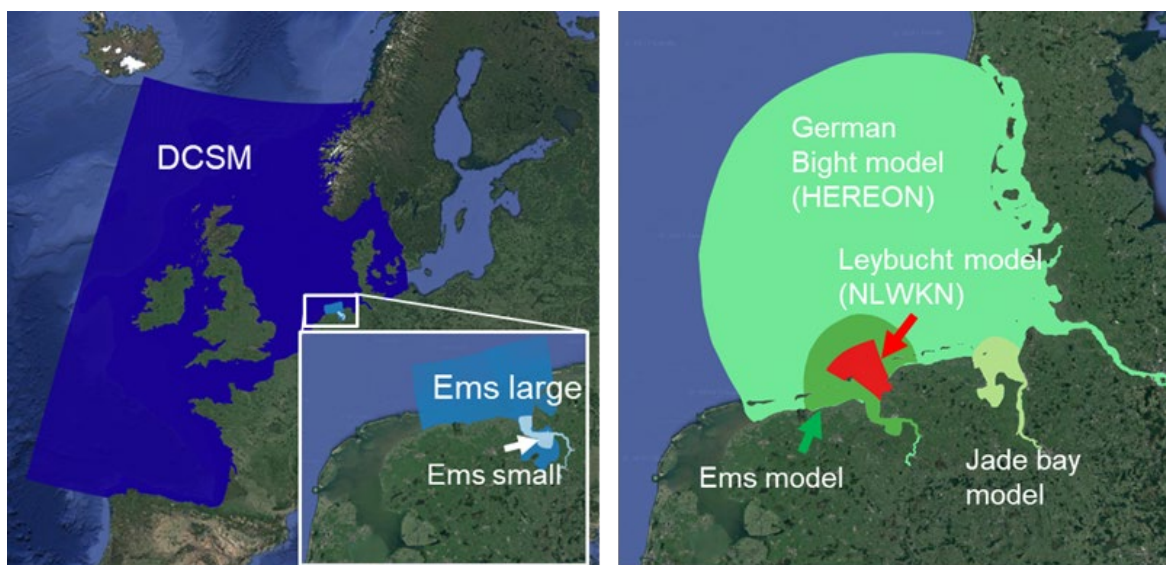


Figure 3.1. Model domains

Seagrass restoration as a coastal protection measure could provide ecosystem buffers and has been shown to be effective in attenuating wave energy, reducing near-shore currents and stabilising the seabed. Recent studies have shown a positive trend in the natural recovery of seagrass meadows in the Wadden Sea area over the last two decades (Dolch, et al., 2017). Therefore, in the Wadden Sea case, we perform what-if scenarios on the size, location and layout of seagrass meadows to investigate the effectiveness of seagrass planting as a nature-based approach to mitigate coastal erosion caused by storm events.

3.1. Multi-risk projections for ESS of NBS in the Wadden Sea

Within Rest-Coast project the pilot case partners of the Wadden Sea are concerned with the assessment of different Nature Based Solutions (NBS) that could provide an enhanced functioning of the following ecosystem services (ESS):

- Flood risk reduction
- Erosion risk reduction
- Carbon storage
- Water quality improvement
- food provisioning

For the present deliverable report D.2.2, risk reduction in relation to flooding and erosion is the focus of the work developed.

Using their respective modelling frameworks developed within Rest-Coast, the partners of Hereon, NLWKN and Deltares address respectively:

- the restoration of seagrass areas;
- the development of saltmarshes;
- and effective sediment management strategies;

as NBS with respect to potential improvements for different aspects of the ESS at concern.

As part of the risk projections strategy the evaluated measures for NBS are explored for different environmental and climatic conditions, involving the present-day conditions as baseline for the ESS including an analysis on the seasonal variability; and different climate projections towards the end of the century that involve significantly elevated sea levels thus affecting coastal dynamics that might be steered differently by the applied NBS.

3.1.1. Criteria to assess risk reduction

For the five essential ESS provided by the NBS a set of key indicators was identified to evaluate the ESS performance based on the parameters that are provided by the partners modeling suits (described in 3.3) and are presented in Table 3.1.

Table 3.1. Key metrics of risk reduction analyses for different scenarios

ESS	Model parameter	Indicator system specific
Reduction coastal erosion	Erosion volumes	Annual mean erosion volume for a user-defined area
	Shoreline (where applicable as saltmarsh edge) retreat Vegetation/biotope cover on foreshore	Mean, min and max annual shoreline change for a user-defined area Area (in m2) per EUNIS ecotope in a user-defined area at the end of a time horizon
Water purification	Mineral suspended solids Basic water quality parameters (T, O2, pH, salinity)	Annual mean and max per user-defined area (not in this deliverable)
Carbon sequestration	C-sequestration based on biotope (salt marsh, grassland, etc.) C-sequestration based on deposition volume	kg per year per user-defined area (not in this deliverable)
Food provisioning	Food production based on biotope	kg per year per user-defined area (not in this deliverable)

These metrics -as far as applicable for the respective case- are utilized to assess the multi risk factor related ESS efficiency within the environmental condition and climatic projections that are layout within the following.

For the pilot case the risks (3.2) and reduction are explored based on system specific key indicator metrics (Table 3.1) derived from the model parameters for investigated ESS.

3.1.2. Risk reduction projection for end of the century future climate conditions under the RCP 8.5 scenario

Future risk projections are undertaken under the RCP8.5 scenario, which assumes a continuing growth of greenhouse gas emissions towards the end of the 21st century.

The probability of this emission trajectory has been doubted (Hausfather and Peters, 2020), yet it retains scientific value due to its high signal-to-noise ratio and is employed here to delineate the emerging signals of climate change. Policy-wise it represents the upper limit worst case scenario. Globally, the scenario indicates a rise in mean sea level by nearly 40 cm, with higher values regionally, such is the case in our study area. Within this scenario sea level can increase by up to 1m.

To cover the spread within this scenario, in the RCP 8.5 ensemble simulations, out of the climate forcing scenarios, the 5th, 50th and 95th percentiles ensemble members are chosen to derive the downscaled forcing, for our regional models.

To cover the spread within this scenario, in the RCP 8.5 ensemble simulations, out of the climate forcing scenarios, the 5th, 50th and 95th percentiles ensemble members are chosen to derive the downscaled forcing, for our regional models.

Table 3.2. RCP scenarios considered by the partners

Time	Scenario	Seagrass (Hereon)	Sediment strategies (Deltares)
2020	RCP 8.5 50%		+ 0.07 m (Garner et al., 2021)
2030	RCP 8.5 50%		+ 0.12 m (Garner et al., 2021)
2050	RCP 8.5 50%		+ 0.26 m (Garner et al., 2021)
2100	RCP 8.5 50%	+ 0.8 m in 2090 (Palmer et al., 2020)	+ 0.78 m (Garner et al., 2021)

As a preliminary study, the sensitivity of sediment transport and morphological evolution to sea level rise (SLR) was investigated by NLWKN using an established model setup (Delft3D) by Dissanayake and Wurpts (2013). The model setup consists of 3 domains to downscale forcing from German Bight-, coastal- to the tidal basin-scale. Five SLRs were hypothesized: No SLR, 2, 5, 10, 15 mm/year. These SLRs were implemented in the models considering a 100-year mean sea level rise. It should be noted that SLR is the only variable among simulations: to get the first insights of SLR effects.

Sediment transport and morphological changes were simulated at the tidal-basin scale domain by forcing with water levels, currents and waves. Both water level and current were extracted by simulating the model chain of 3 domains, in which the German Bight domain was first simulated with the astronomical tide and increased mean sea level corresponding to the SLR scenarios. Wave propagation (Delft3D-SWAN) was simulated from the coastal domain to the tidal basin by forcing with the measured wave conditions at around 20 m water depth and increased mean sea level. Bed sediment composition consists of three sediment fractions representing mud, fine and coarse sediments, which vary spatially.

The main drawback applying the existing model setup is that the tidal basin domain consists of only the area behind the barrier islands in the Wadden sea. Therefore, the communication with respect to sediment transport is missing between Wadden Sea and North Sea. Hence, a new model setup is inevitable to cope with this issue. Our new basin-scale model encompasses backbarrier basin and ebb-tidal delta, and extends up to about 20 m offshore depth. At the moment, this setup is calibrated and validated against measured water levels and wave data.

3.2. Modeling framework

3.2.1. Modeling impact of seagrass as Nature-based solution (Hereon)

3.2.1.1. Modeling workflow

Numerical simulations of seagrass recovery scenarios in the Wadden Sea are conducted with the semi-implicit cross-scale hydroscience integrated system model (SCHISM, Zhang et al. 2016) and run in coupled mode with the 3rd-generation wave model WWMIII (Roland et al. 2012) in a configuration for the German Bight to evaluate the potential impact on hydrodynamics. The designated setup, which was already introduced and validated in D2.1, comprises 476,000 nodes and 932,000 triangular and quadrangular elements. The horizontal resolution varies, reaching a maximum of 1.5 km at the open boundary and decreasing to a minimum of 50 m in the estuaries. The vertical aspect is represented using 21 terrain-following sigma coordinates. Specifically, within the East Frisian Wadden Sea, the resolution spans between 100 and 300 m.

Model initialization and ocean boundary forcing are derived from the CMEMS AMM15/IBI (<http://marine.copernicus.eu/>) operational product as hourly time series for temperature, salinity, sea surface elevation, and 3D velocities. Atmospheric forcing is from the German Weather Service (DWD) (Kaspar et al. 2022), and spectral wave forcing from a Wave Watch 3 configuration of the North Atlantic.

To assess the impact of seagrass on morphodynamics north of the Norderney coast, we used the process-based morphodynamic model XBeach (Roelvink et al., 2009), which was regionally nested (one-way) to the SCHISM setup (see Figure 3.2). The model domain extends 4.5 km along the shore and 14 km across the shore, with a horizontal spatial resolution of 10 × 10 m. Hourly resolved sea surface elevations and variance density spectra from the SCHISM-WWM coupled model are used to force the model. The SCHISM-WWM coupled model is applied along the open boundaries of the XBeach domain (Chen et al. 2024).

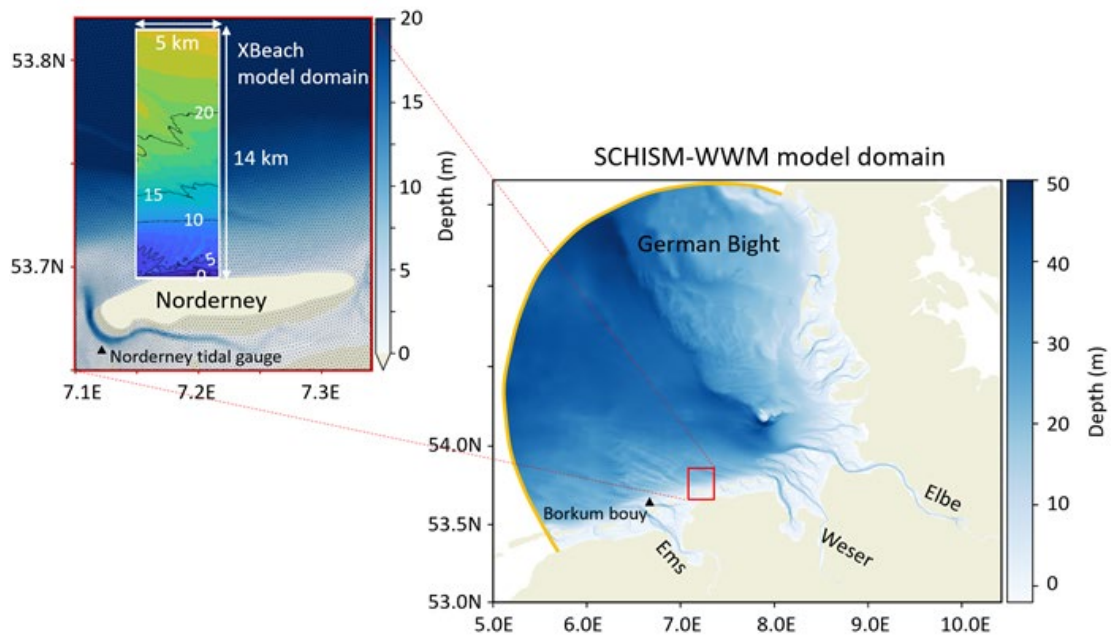


Figure 3.2. Domain and bathymetry of the SCHISM-WWM model (right) and the magnified box shows the study site, Norderney (left, red box). The white box indicates the domain and bathymetry of the XBeach model. The open boundary of the SCHISM-WWM model is illustrated with an orange curve

3.2.1.2. Modeling workflow for climate projections

For future climate scenarios, the boundary forcing is derived from downscaled regionalized projections of mean sea level (MSL) and coupled Remo climate scenario simulation output (Pein et al., 2023). The dynamical drivers in our study of future climate scenarios are global mean sea level change and coupled ocean-atmosphere variability. Global mean sea level rise is caused by thermosteric expansion, melting of polar ice caps and glaciers, and gravitational responses induced by the ice masses becoming liquid (Church et al., 2013; Gollledge, 2020). Regional exacerbation or mitigation of global MSL rise may be caused by vertical land movements such as postglacial isostatic rebound. Probabilistic estimates under the RCP8.5 scenario from the UKCP18 project are used for the prescription of MSL rise (Palmer et al., 2018; 2020).

The regionalised simulations of the Max-Planck-Institute Earth System Model Low Resolution (MPI-ESM-LR) ensemble runs under the RCP8.5 scenario were used to sample the coupled ocean-atmosphere dynamics. The downscaling of the global climate ensemble was performed by a regionally coupled climate system model with a nominal resolution of 5 km in the SNS (MPIOM-REMO, see Mayer et al., 2022; Mikolajewicz et al., 2005; Mathis et al., 2020; Lang and Mikolajewicz, 2020). The REMO atmospheric module has a resolution of approximately 7 km. In addition to atmospheric variables, this model predicts daily surface runoff, which serves as river input. The ensemble simulation dataset represents changes in ocean density and currents, as well as meteorological conditions, including atmospheric water transport, due to enhanced radiative forcing under climate change. The ensemble was created by initiating the global model from various historical states of the years 1950-1959 from three previous simulations using the same model system (Mathis and Mikolajewicz, 2020). The 6-hourly outputs of the global simulations were used as a forcing for the MPIOM-REMO regional climate modelling framework, which in turn provided the boundary forcing for the SCHISM simulations analyzed in this study. These ensemble simulations allow for the exploration of the internal variability of the climate system by varying the initial states across the 30 ensemble members. However, they do not account for MSL rise. Therefore, it is added here, along with the forcing data, using the probabilistic estimates (Palmer et al., 2018; 2020).

For the focus of this study on scenario spread, it is important to note that the spread of MSL is influenced by the variability of the global climate system, while ensemble spread is due to internal variability resulting from local synergies and feedbacks between geometry, density distribution, wind, and tidal forcing.

3.2.2. Role of morphological feedbacks on the effectiveness of Nature-based solutions (Deltares)

3.2.2.1 Model premise

The Ems Estuary is a strongly engineered system, of which the high turbidity leads to large maintenance dredging volumes and negatively influences primary production (van Maren et al., 2015). One of the drivers for high turbidity values is the loss of natural sediment sinks (van Maren et al., 2016). Reclamation of the various natural tidal inlets and salt marshes along the Wadden Sea Coast has resulted in a loss of environments for natural sedimentation. As a consequence, the Ems-Dollard estuary experiences gradually increasing suspended sediment concentrations. This has motivated the development of measures to (1) promote settling of sediment (through constructions or vegetation; reducing local hydrodynamic energy), and (2) extract sediments (either through dredging and landward transport, or by inundating land). Both are expected to reduce the turbidity in the Ems Estuary. Settling of sediment may also have additional benefits, such as wave dissipation and trapping of carbon.

Predicting the effect of nature-based solutions in the Ems estuary on reducing flooding, reducing turbidity, and promoting carbon storage therefore revolves around the prediction of sediment dynamics on short timescales and on long timescales. On short timescales the trapping effects of vegetation and/or interventions are relevant, requiring modeling of waves and currents. Long-term modeling requires coastal adaptation to Sea Level Rise (SLR) under the influence of both waves and currents. Most previous studies investigating the adaption of tidal basins to SLR were limited to tidal forcing only (i.e. Elmilady et al., 2020). Ignoring waves has two clear benefits: it saves computational time (which is important for long-term simulations) and it simplifies numerical modeling because introducing waves requires parameterisations for development of strength of the intertidal flats (using consolidation models as in Winterwerp et al., 2018 or inundation frequency as Nguyen et al., 2022). These flats typically develop during tide-dominated conditions when fine, easily erodible particles are transported landward. After deposition these sediment beds develop strength through consolidation, which prevents excessive erosion during periods of higher wave conditions (Colosimo et al., 2023).

The prediction of morphological change in the Ems estuary is crucial for understanding how ecosystems evolve in the estuary. The presence of ecosystems may be estimated from physical boundaries (inundation frequency, salinity, hydrodynamic energy, and substrate) and shown in ecotope maps (Baptist et al., 2019). While such ecotope maps exist for the Wadden Sea in its current state, there is limited knowledge on how ecotopes will evolve over time (especially in relation to Sea Level Rise), and even less so if NBS considered in the Ems Estuary can significantly contribute to preserving or effectively restoring such ecosystems.

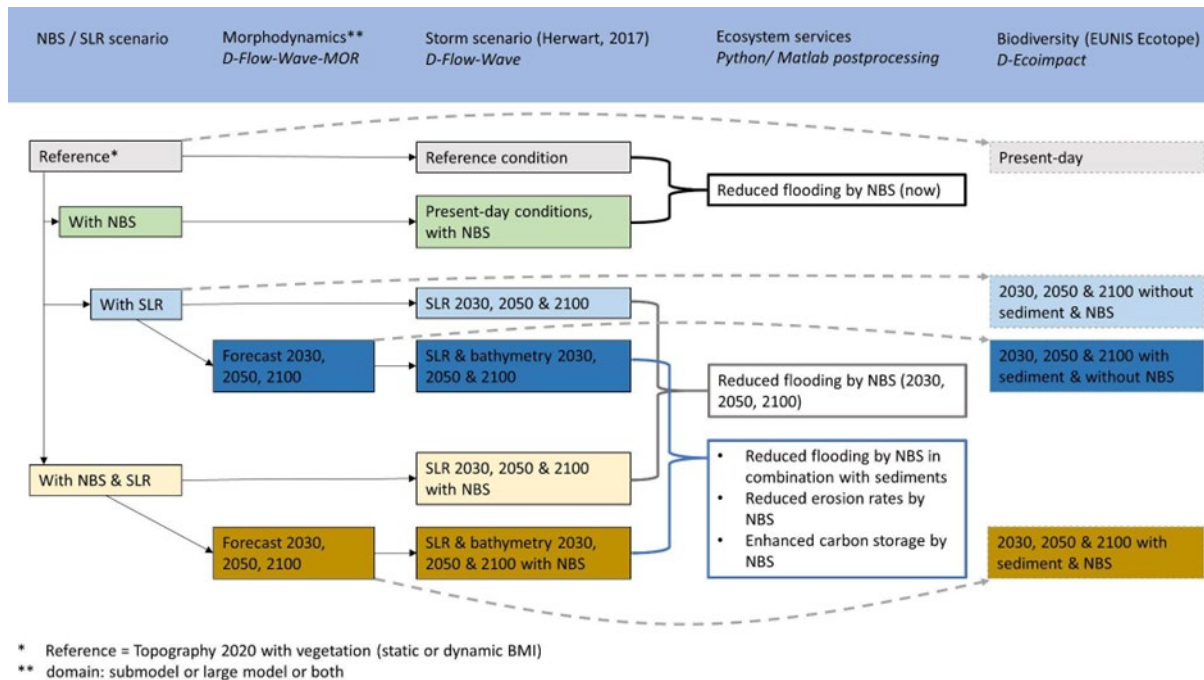


Figure 3.3. Flowchart of model scenarios

We develop a model framework (Figure 3.3) in which we compute the impact of various nature-based solutions on four ecosystem services (reduced flooding, reduced erosion, and increased food provisioning and carbon storage) through quantification of ecotopes. We develop a morphodynamic model accounting for sediment accretion with SLR under the influence of tides, waves, vegetation and nature-based solutions. This model will predict bed levels in the year 2030, 2050, and 2100. These morphodynamic simulations are post-processed 1) into ecotopes and scored on ecosystem services provided. Additionally, the predicted bed levels are used as input for models in which storm scenarios are evaluated for different SLR and nature-based solutions. The reduction in flood risk is herein defined as a reduction in wave height per dike segment.

3.2.2.2 Model set-up

The hydrodynamic set-up of the model was detailed in D2.1. The set-up simulating the morphological change of the estuary, including the local ecotopes, is further discussed here.

3.2.2.3 Model calibration and validation

Morphodynamics

The model is calibrated by comparing sedimentation and erosion patterns that develop within one year of hydrodynamic simulation (=24 years of morphological change) and the mud fraction in the top layer. While initial results look promising, further validation of sedimentation rates and comparison with known sediment sinks (e.g. by comparing dredging volumes) is required.

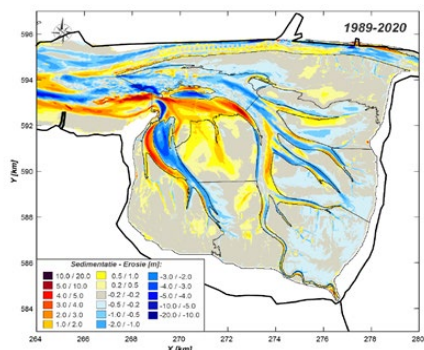


Figure 3.4. Observed sedimentation- erosion patterns in the Dollard (Elias, 2021)

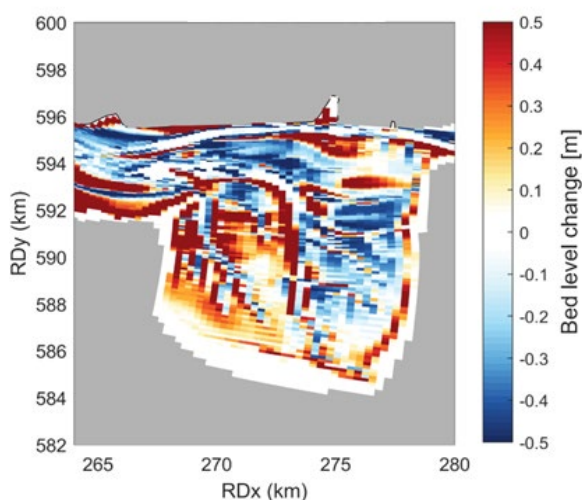


Figure 3.5. Modelled sedimentation and erosion patterns after 24 years of morphological simulation initializing the model with a thin (15 cm) initial layer of mud

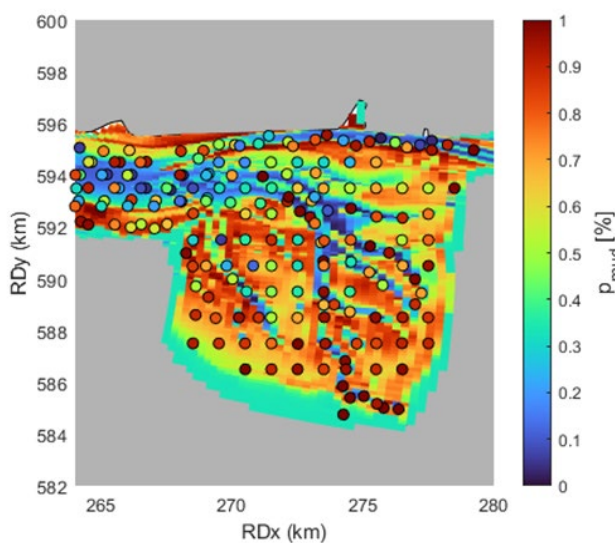


Figure 3.6. Modeled mud fraction in the top soil after initial calibration compared to the sediment atlas of the Wadden Sea as dots https://svn.oss.deltares.nl/repos/openearthrawdata/trunk/rijkswaterstaat/sedimentatlas_waddenzee/

3.2.2.4 Ecotope quantification

Conversion of model results into ecotopes and ESS

The main goal of the morphological model is to quantify the effect of nature-based solutions on ecosystem services. Some of these ecosystem services are quantified with the change in ecotopes over time, both due to sea-level rise and in response to measures implemented in the area. The conversion of modelling output into ecotopes is based on the ZES.1 classes for classifying ecotopes (Bouma, 2005). In cooperation with task 4.1 of REST-COAST these classes are adapted into EUNIS ecotopes based on the Delft3D-FM model output (Table 3.3, Table 3.4).

Table 3.3. Adapted ecotope class boundaries from the ZES.1 system into variables for classification in EUNIS using Delft3D-FM output. Abbreviations in table: MLWS = Mean Low Water Spring, MHWN= Mean High Water Neap, = silt fraction, = average bed shear stress, TMAP coastal vegetation S.X = coastal vegetation classes, see Bouma (2005)

Variables	Classes	Class boundaries	Adapted for Delft3d-FM output and EUNIS classification	Code
		ZES.1		
Mean salinity	Fresh	yearly mean < 0.5 ppt	yearly mean < 0.5 ppt	0
	Brackish	0.5 ppt ≤ yearly mean < 18 ppt	0.5 ppt ≤ yearly mean < 18 ppt	1
	Marine	yearly mean ≥ 18 ppt	yearly mean ≥ 18 ppt	2
Salinity variability	Stable	st. dev./mean ≤ 0.25	st. dev./mean ≤ 0.25	0
	Variable	st. dev./mean > 0.25	st. dev./mean > 0.25	1
Substratum	Sediment	soft sediment	<i>Determined in post-processing</i>	0
	Hard	dikes, dams, quays, etc.		1
Littoral zone	Deep sublittoral (Circalittoral zone)	depth < -5 m MLWS	depth < -5 m MLWS	0
	Shallow sublittoral (Infralittoral zone)	-5 m MLWS ≤ depth < 4% mean exp.	-5 m MLWS ≤ depth < 4% mean exp.	1
	Low littoral	4% ≤ mean exposure < 25%	4% ≤ mean exposure < 25%	2
	Middle littoral	25% ≤ mean exposure < 40%	25% ≤ mean exposure < 40%	3

	High littoral	$40\% \leq \text{mean exposure} < 85\%$	$40\% \leq \text{mean exposure} < 85\%$	4
	Supralittoral	$\text{mean exposure} \geq 85\%$	$\text{mean exposure} \geq 85\%$	5
Hydrodynamics	Low dynamic	$\text{max. current velocity} < 0.8 \text{ m/s}$	$\text{max. current velocity} < 0.8 \text{ m/s}$	0
	High dynamic	$\text{max. current velocity} \geq 0.8 \text{ m/s}$	$\text{max. current velocity} \geq 0.8 \text{ m/s}$	1
Sediment	Silt	$\text{Silt content} \geq 25\%$		1
	Fine sand	$D50 < 250 \mu\text{m}$	and	2
	Coarse sand	$250 \mu\text{m} < D50 < 2000 \mu\text{m}$	and	3
Salt marsh	No vegetation	TMAP vegetation S.0	coastal Depth > MHWN	0
	Potential pioneer zone	TMAP vegetation S.1	coastal Depth < MHWN; inundation frequency > 300 times yr^{-1}	1
	Low salt marsh	TMAP vegetation S.2	coastal 300 times $\text{yr}^{-1} \leq$ inundation frequency < 150 yr^{-1*}	2
	upper-mid marsh	TMAP vegetation S.5	coastal 150 times $\text{yr}^{-1} \leq$ inundation frequency < 50 yr^{-1*}	3
	High salt marsh	TMAP vegetation S.3	coastal 50 times $\text{yr}^{-1} \leq$ inundation frequency < 5 yr^{-1}	4

Table 3.4. Conversion of class boundary codes into EUNIS ecotopes

Litoral zone code	Sediment code	Salinity code	Salt marsh code	EUNIS2019C	EUNIS2019D
0				MC521	Faunal communities of Atlantic circalittoral sand
1		2		MB523	Faunal communities of full salinity Atlantic infralittoral sand
1		1 or 0		MB524	Faunal communities on variable salinity Atlantic infralittoral sand
2, 3, 4 or 5	0 or 2			MA52	Atlantic littoral sand
2, 3, 4 or 5	1	2		MA621	Faunal communities of full salinity Atlantic littoral mud
2, 3, 4 or 5	1	1 or 0		MA622	Faunal communities of variable salinity Atlantic littoral mud
2, 3, 4 or 5	3	2		MA321	Faunal communities on full salinity Atlantic littoral coarse sediment
2, 3, 4 or 5	3	1 or 0		MA322	Faunal communities on variable salinity Atlantic littoral coarse sediment
2, 3	1, 2		1	MA225	Atlantic pioneer saltmarshes
3, 4	1, 2		2	MA224	Atlantic mid-low saltmarshes
4, 5	1, 2		3	MA223	Atlantic upper-mid saltmarshes and saline and brackish reed, rush and sedge beds
6	1, 2		4	MA222	Atlantic upper saltmarshes

The distribution of ecotopes is calculated for each modelled sea-level rise scenario and implementation of an NBS measure. The ecotopes are derived from the bed level and bed composition at the specified morphological year and a hydrodynamic simulation of two spring-neap cycles to derive the classes as expressed in Table 3.6 using the software D-EcoImpact (<https://github.com/Deltares/D-EcoImpact>). From the ecotope map, the location of salt-marsh is determined. Two storm events (Herwart from 2018 and Xaver from 2013) are simulated to test how the new distribution of (salt marsh) ecotopes affects the distribution of wave heights on coastal defenses in the estuary.

The effect of salt marsh ecotopes on wave dampening is implemented in the DWaves module in Delft3D-FM through the formula of Suzuki et al. (2019). In it, vegetation properties such as plant height, stem density, and stem diameter are used to calculate an additional energy loss term for waves in vegetated areas. Vegetation parameters for each marsh ecotope are based on a representative plant species with parameters from Vuik (2017) as measured at the end of the growing season when storms are most likely to occur. The vegetation parameters used are presented in Table 3.5.

Table 3.5 Vegetation parameters used per ecotope

EUNIS Code	Representative species	Vegetation height (cm)	Stem diameter (mm)	Stem density (n. of stems /m2)
MA225	Spartina anglica	47	3.3	232
MA224	Suaeda maritima	57	2.7	274
MA223 & MA222	Elymus athericus & repens	50	1.3	405

3.2.2.4.1. Validation of ecotope classification

The map produced from the Delft3D-FM model for the year 2020 (Figure 3.8) was compared with the most recent EUNIS ecotope map of the Wadden Sea produced by Martin Baptist in WP4.1 of RESTCOAST (Figure 3.7). This map was in turn based on an earlier study by Baptist (2019).

The Delft3D-FM model is able to reproduce the current extent of ecotopes remarkably well despite a relatively coarse resolution (about 100 m) and only depth-averaged velocities. Crucially, the salt marsh, the main ecosystem of interest for its flood risk, is well represented. As expected, there is a perfect correspondence between the location of circalittoral and infralittoral zones since no morphological changes have been simulated yet. Nevertheless, the inundation frequency and exposure boundaries (Table 3.3) are well captured in the modeling.

There are also key differences between the two maps. The most notable is that ecotopes MA525 (bivalve-dominated littoral muddy sand) and MA523 (barren or amphipod-dominated littoral mobile sand) are not classified from the model. With only one sand fraction in the model available for transport, inherent uncertainties in the mud content of the sandy soil, and no further information aside from the boundaries in Table 3.11 to estimate the presence of bivalves or amphipods, it was considered classification beyond littoral sand (MA52) and saline / brackish littoral mud (MA621, MA622) would not be sufficiently reliable. This is seen in Figure 3.8 where littoral mud and littoral sand replace MA525 from Figure 3.7. The mobile sand (MA523) is replaced by coarse sediment (MA321) because it was assumed no fine sand could accumulate in areas with high bottom stresses. It should be considered to replace MA321 with MA523 in the future as the considered ecotope boundary of bed shear stress does not distinguish areas of mobile (fine) sand and stable coarse sand taking into consideration that large areas of littoral coarse sediment are rare inside the Ems estuary (Figure 3.7). Finally, the 2D simulation of salinity means that the spread of fresh water across the Geisedam from the Ems into the Dollard is not well-represented. However, this discrepancy is an acceptable trade-off to considerably speed up the model during morphological simulations.

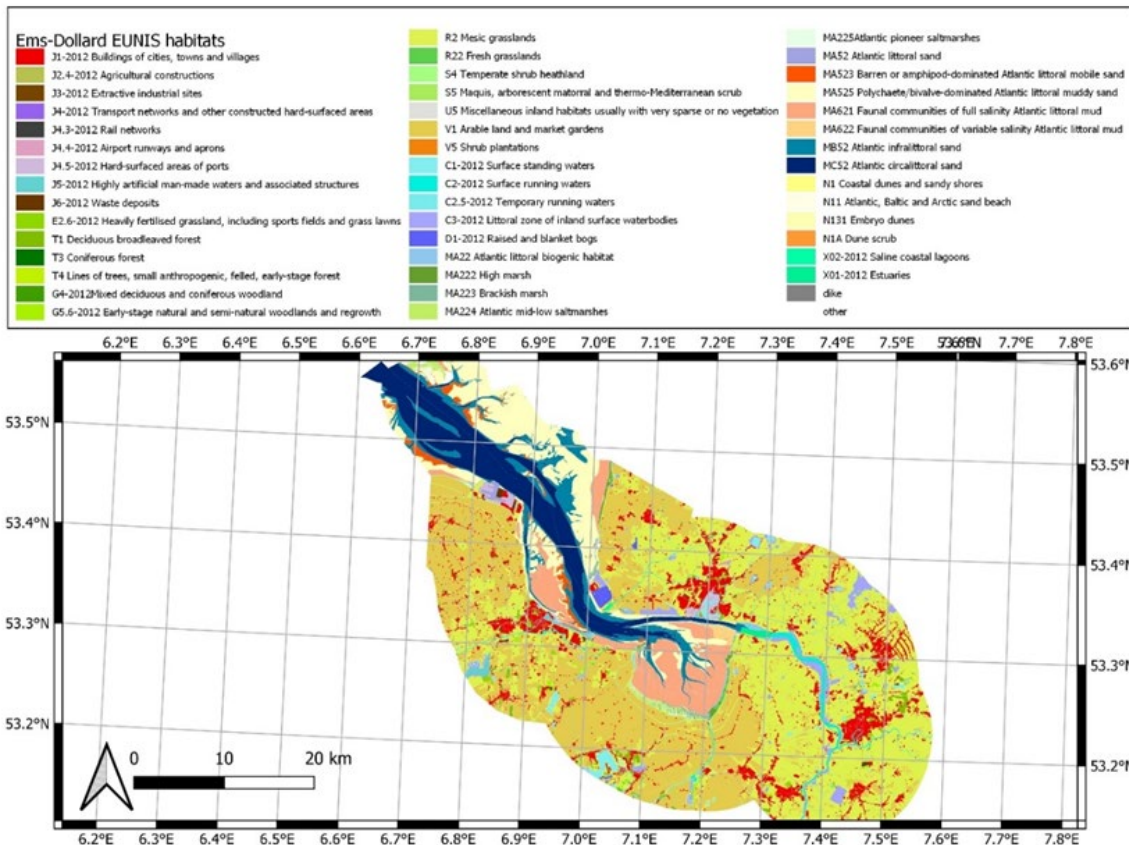


Figure 3.7. EUNIS map of the Ems estuary produced in WP4.1 of RESTCOAST, based on Baptist (2019)

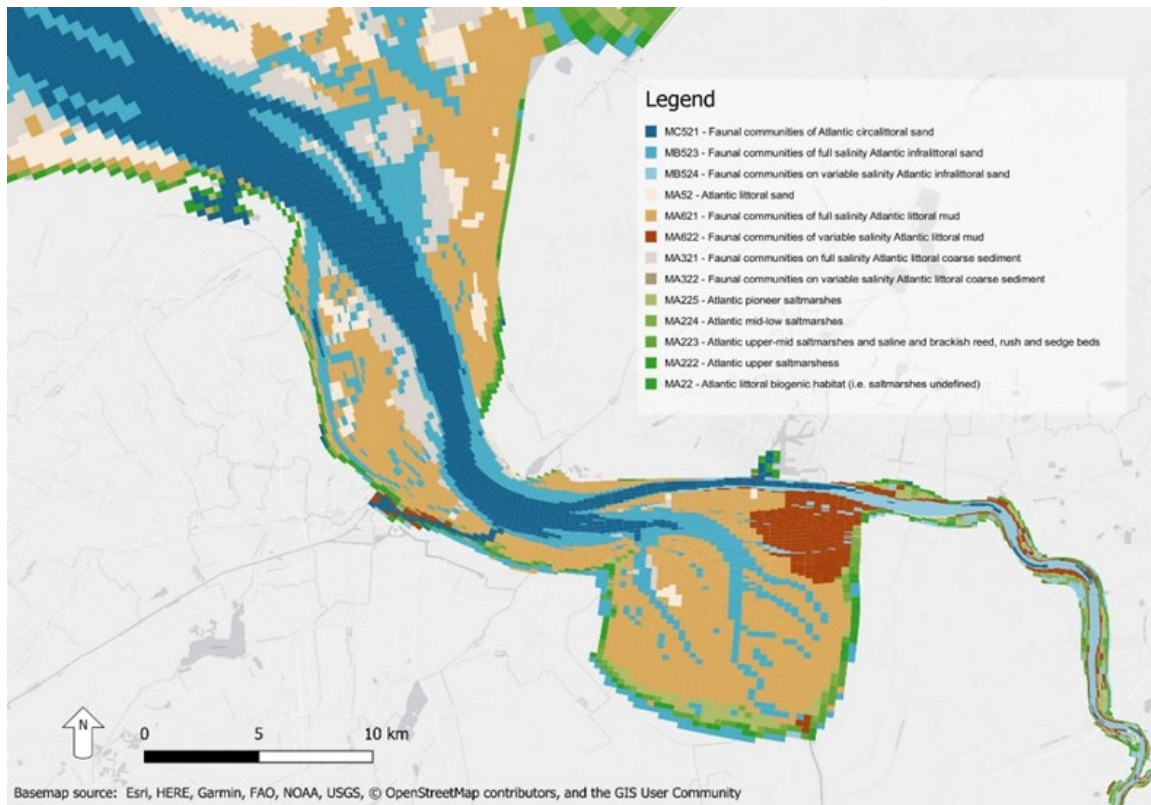


Figure 3.8. EUNIS map produced by output from the Ems-Dollard model

3.3. Efficiency of sea-grass in coastal protection (Hereon)

3.3.1. Evaluating the benefit of sea-grass under end of the century climate conditions

After the efficiency of seagrass under current conditions was demonstrated in D.2.1, it is important to consider to what extent the hydraulic engineering capabilities of seagrass will remain under future climate conditions. This is particularly relevant as sea levels are expected to rise significantly, and seagrass will occupy less space vertically in the water column.

To limit the computational costs of running the German Bight SCHISM configuration for multiple seagrass scenarios over several years, we had to restrict the number of simulations. Therefore, we focus solely on the RCP8.5 scenario ensemble mean realization of regionalized sea level rise and ocean-atmosphere variability for the year 2090, which was available to us. In relation to the seagrass scenarios, we compare the scenarios with no seagrass and maximum seagrass coverages (3.2.1) without altering the scenario configuration used under present day conditions.

As we are only simulating a one-time slice, it is important to maintain objectivity and avoid subjective evaluations. Therefore, we will use the bathymetry identical to present day conditions, as any future changes are highly speculative. However, given a sediment supply, an accumulation of sediment in the tidal flats would be expected.

The simulations based on the RCP 8.5 projection for the year 2090 were compared to the reference simulations for 2017. The maximum aerial coverage seagrass scenario (Vegmax) was contrasted with the no seagrass scenario (VegCntrl) in the SLR scenario. In the EFWS area, the average sea level is expected to rise

by approximately 0.7m, which is about 0.9m higher than the 95th percentile and almost 1.8m higher than the annual maximum. As demonstrated by the present-day baseline analysis, seagrass has only a marginal impact on peak water levels. Therefore, this analysis focuses solely on the impact of seagrass on waves, currents, bottom stress, and sediment concentrations in bottom layers, which serve as erosion proxies.

Wave Heights

Under the projected wind climate, the 95th quantiles in significant wave heights are reduced in the North Sea seaward of the Barrier islands. However, among the tidal flats in the back barrier Wadden Sea future scenario, the 95th percentiles

in HS appear increased, albeit only slightly by a few centimetres while being slightly decreased coastward in the embayments of Ems and Jade (see Figure 3.9). On a large scale, the wave damping effect of seagrass remains similarly strong between the present and future sea level scenarios. Seagrass tends to dampen the 95th quantile HS by around 5-10 near the channels and between 20 and 50% among the flats. The increased future tidal flat wave heights are damped by the intertidal seagrass, leading to an increase in absolute attenuation of around 5 cm. In relative terms, the efficiency is almost the same, but there is a minor reduction of 5-10%.

In the coastal supra littoral, the efficiency is further reduced. However, these areas experience waves mostly during strong wind events, even at present-day sea level.

Current Velocities

The 95th percentiles baseline level for depth averaged velocities is slightly increased by about up to 0.2 m/s in the future sea level rise scenarios (s. Figure 3.9). The attenuation slightly enhances within the majority of the seagrass covered tidal flat areas, as the seagrass on average interacts with larger velocities there while SLR decreases the frictional damping. However the impact for damping on the channel velocities weakens. Overall the structure of velocity reductions do not change strongly, the velocity attenuation strengths for the tidal flat Wadden Sea is reduced by about 5-10%

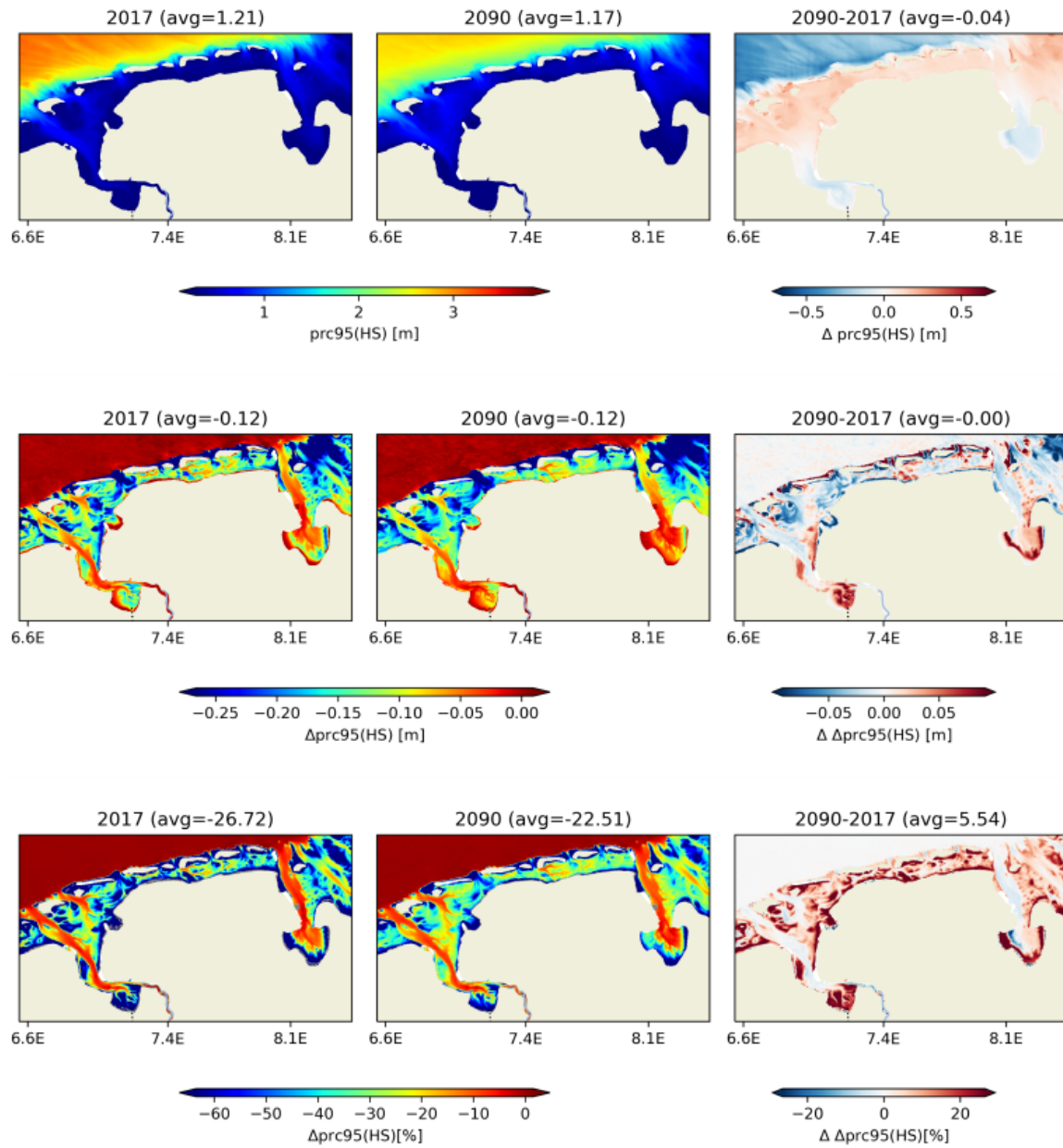


Figure 3.9. 95th Annual percentile in significant Wave Height (HS) and its reduction due to seagrass (Veg_max scenario): Top row shows peak values in 2017 and 2090 and the differences. The middle row depicts the respective difference for the maximum coverage seagrass scenario - the no seagrass scenario, and the difference in differences (positive values in the 3rd column denote a weaker reduction in 2090). The bottom row is analogous to the middle row comparing reductions relative to the absolute values without seagrass instead. Number in the respective title denotes the spatial average for the depicted domain

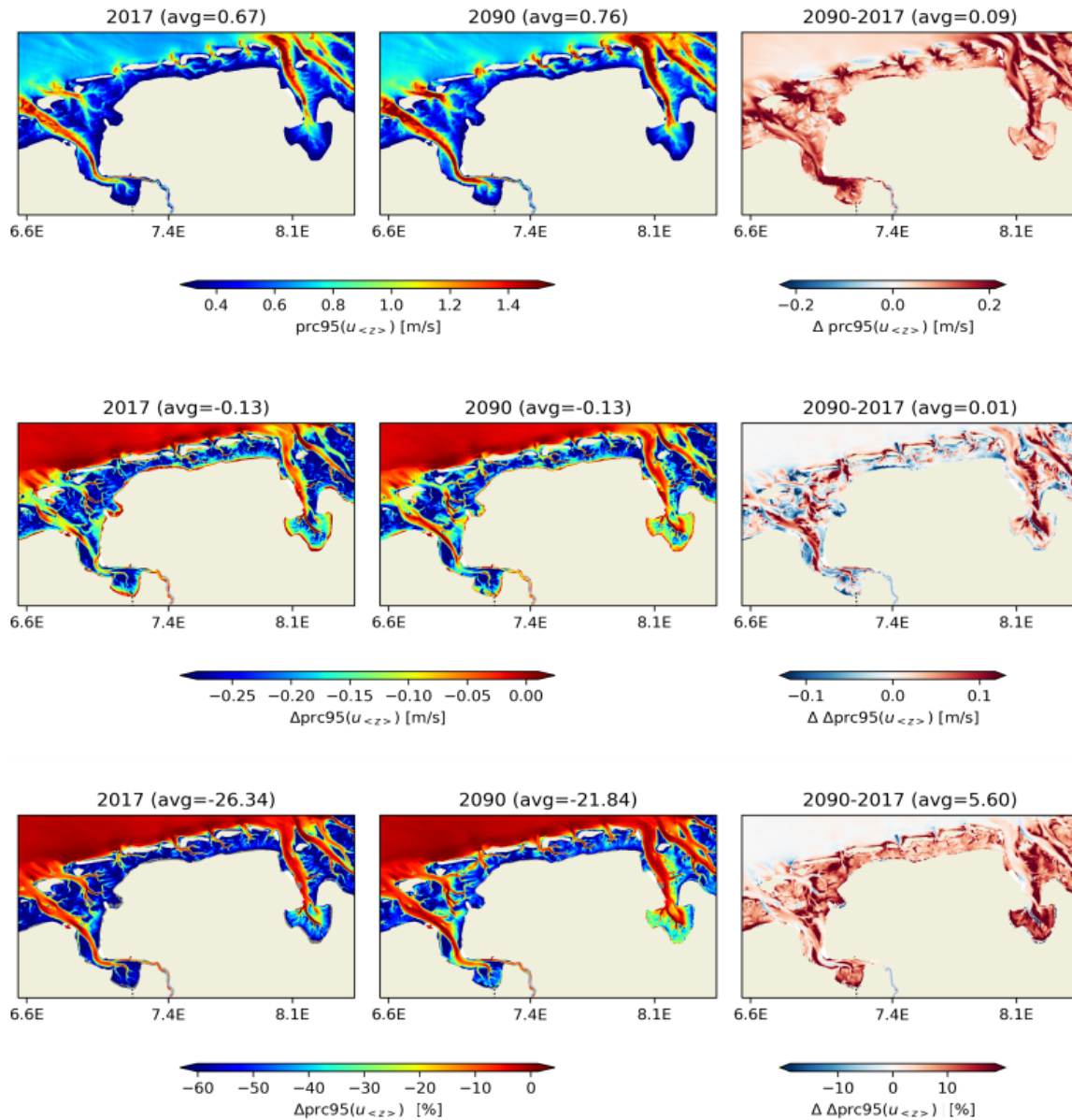


Figure 3.10. 95th Annual percentile in depth averaged velocity and its reduction due to seagrass (Veg_max scenario): Top row shows peak values in 2017 and 2090 and the differences. The middle row depicts the respective difference for the maximum coverage seagrass scenario - the no seagrass scenario, and the difference in differences (positive values in the 3rd column denote a weaker reduction in 2090). The bottom row is analogous to the middle row comparing reductions relative to the absolute values without seagrass instead. Number in the respective title denotes the spatial average for the depicted domain

Bed shear stress and sediments

With the SLR in 2090, there is an increase in the baseline of the bottom stress percentiles, which is more like a week in the shallow areas, but reaches 1 Pa within the tidal channels as a result of the increased flow velocities. Overall, eelgrass remains similarly effective in reducing stress in the covered zones, reducing bottom stress there by up to 0.5 Pa or more than 80% in relative terms. The effect is less pronounced in the transition zone from the seagrass-covered flats to the larger main channels (especially the Jade and Ems channels), where the reduction falls below 40%, i.e. 20% less than at present sea level.

In relative terms, this results in a similar localised reduction in erosion control efficiency as proxied by the 95th percentile total spm concentrations, while within the seagrass meadows the reduction efficiency remains almost the same, reducing sediment resuspension by 80% and more.

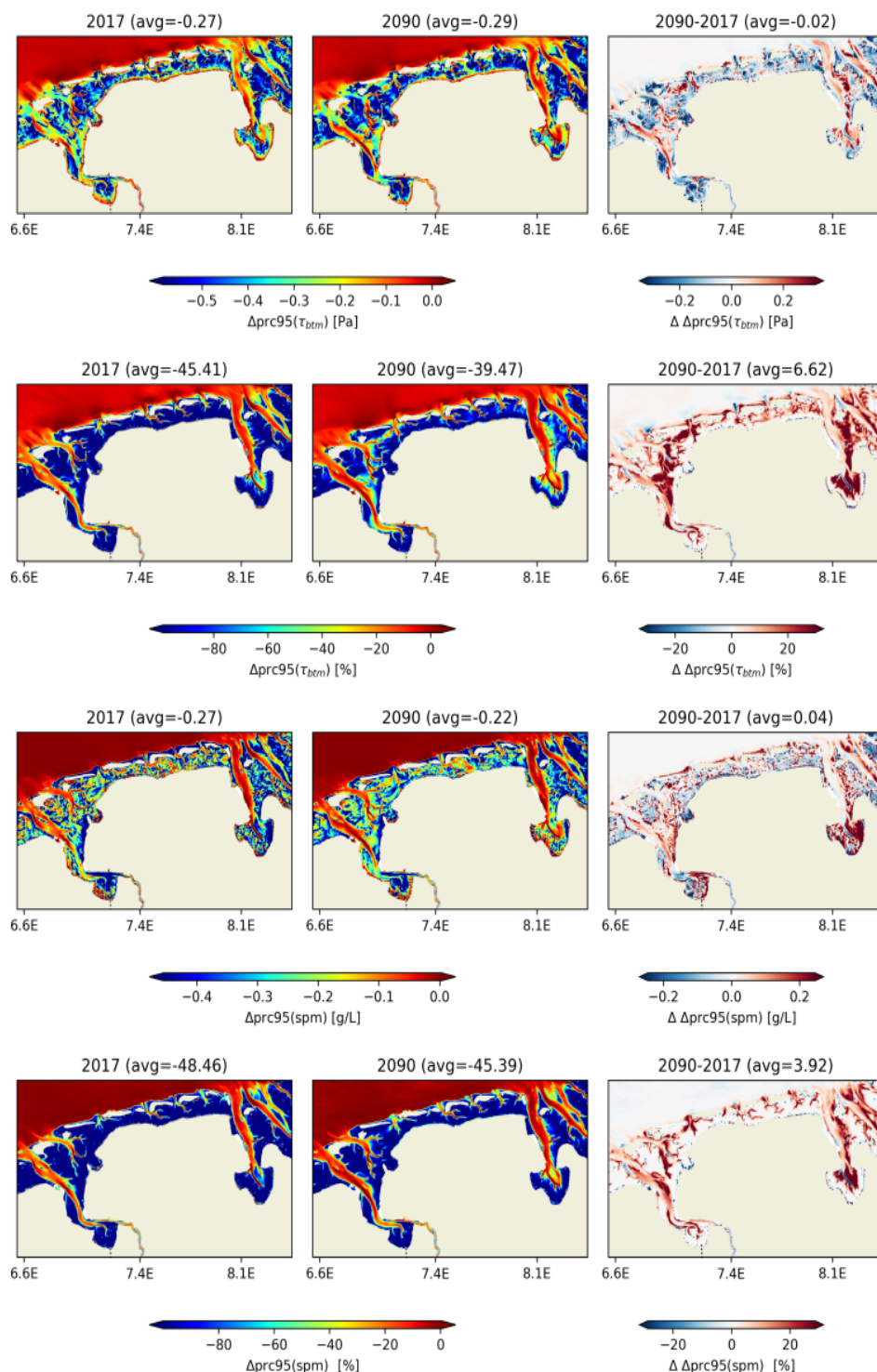


Figure 3.11. 95th Annual percentile in reduction due to seagrass for erosion proxy variables bottom stress and bottom layer sediment concentration. (Veg_max scenario): Top row shows peak values in 2017 and 2090 and the differences. The middle row depicts the respective difference for the maximum coverage seagrass scenario - the no seagrass scenario, and the difference in differences (positive values in the 3rd column denote a weaker reduction in 2090). The bottom row is analogous to the middle row comparing reductions relative to the absolute values without seagrass instead. Number in the respective title denotes the spatial average for the depicted domain

Overall, the future projections show that for the same seagrass restoration scenarios, the overall efficiency of kinematic reduction is reduced and in particular the extended effect of how the flats affect the adjacent channels is reduced. Nevertheless, it remains an effective solution, especially in terms of reducing bottom stress and sediment mobilisation.

3.4. Role of morphological feedbacks on the effectiveness of Nature-based solutions (Deltares)

3.4.1. Role of SLR on ecotopes and flood risk, without morphodynamic adaptation

3.4.1.1. Ecotopes

To establish a baseline for the delivery of ecosystem services provided, model simulations for the sea-level rise scenario ssp 585 (median) are simulated in the absence of morphodynamic adaptation. Below are the projected changes in ecotopes.

The most sensitive ecotope to the change in sea-level are the marshes. Already in 2030 there is clear loss of pioneering marsh visible. By 2100 no more marsh is present aside from areas that had been high marsh in 2020. However, it should be noted that around the edges of the model due to the model's resolution the elevation is influenced by the height of flood defences. Therefore, the perseverance of marsh around the model edged may no longer reflect an actual marsh being present.

Another change relevant for the ecotopes is an increasing salinity in the Dollard in response to sea-level rise. Even though this is less obvious from the ecotope classification where only the area classified as "brackish" around the Geisedam appears affected. Nevertheless, the shift in the 18 ppt salinity boundary reflects a general increase in salinity of the Dollard. Not unexpected but still notable is the increase in the infralittoral ecotopes at the expense of littoral sand and mud ecotopes by 2100.

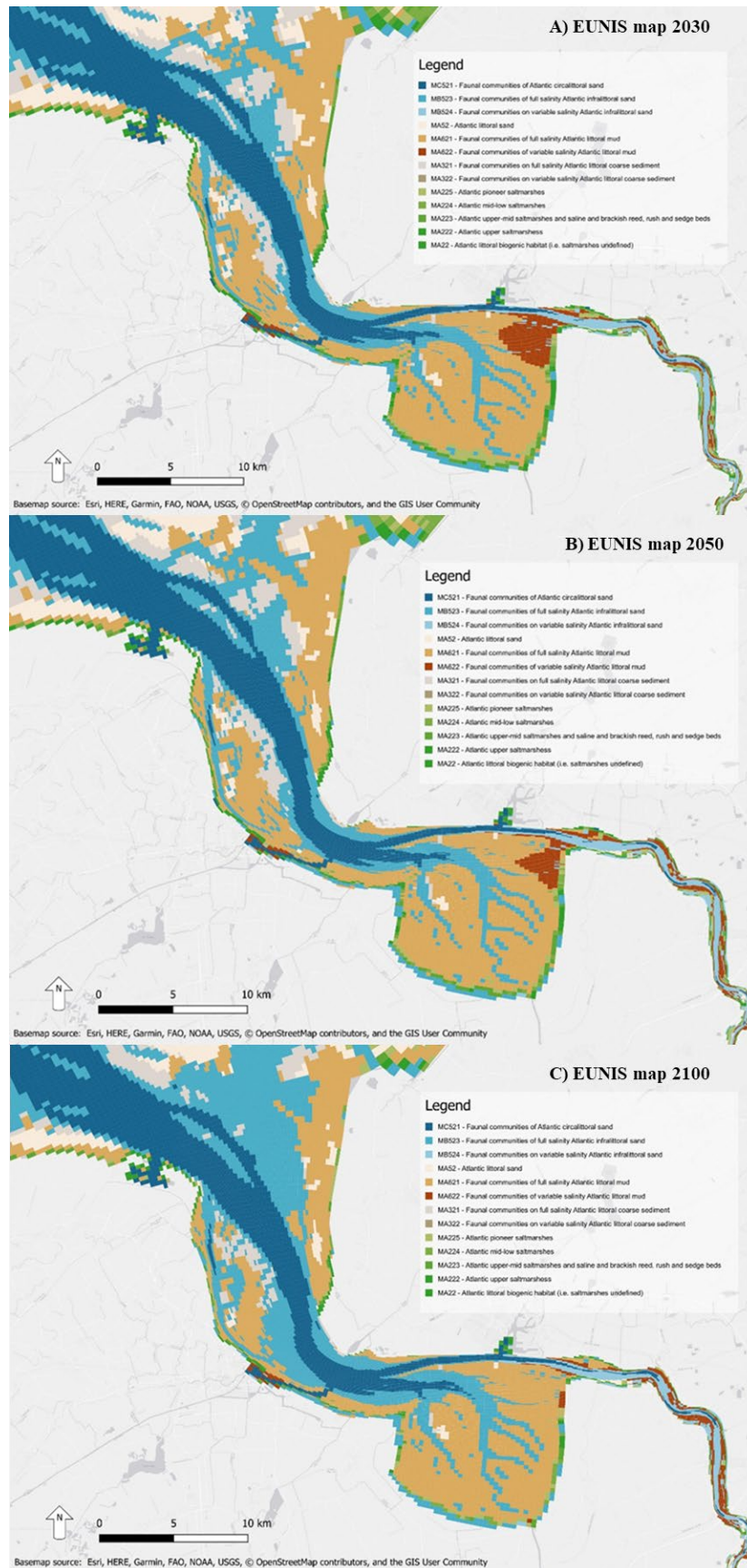


Figure 3.12. Eunis maps for A) 2030, B) 2050, and C) 2100.

3.4.1.2. Flood risk

As a proxy for changing flood risk the change in maximum wave height relative to 2020 is plotted for storms Herwart (Figure 3.13) and Xaver (Figure 3.14) in the years 2030, 2050, and 2100. The main finding even in the absence of morphological feedbacks is that not all areas are equally affected by sea-level rise. In general, the southern areas of the estuary along the Dutch coast are more sensitive to climate change than the German side of the estuary. The main hotspots of increasing wave height are the stretch east of Delfzijl, and the flood defences along the southern stretch of marshes at the Dollard. Storm Xaver featured slightly higher waves and storm surge than storm Herwart. Sea-level rise and ecotope changes affect wave heights slightly less for storm Xaver compared to Herwart. This is most noticeable for the stretch along the Dollard marshes.

A) Change in wave height during storm Herwart by 2030



B) Change in wave height during storm Herwart by 2050



C) Change in wave height during storm Herwart by 2100



Figure 3.13. Changes in maximum wave height during storm Herwart compared to the same storm event simulated without sea-level rise and changes in ecotopes for the years A) 2030, B) 2050, and C) 2100 in climate scenario ssp 585. The color represents the change as % compared to 2020. The size of each dot represents the associated wave height.

A) Change in wave height during storm Xaver by 2030



B) Change in wave height during storm Xaver by 2050**C) Change in wave height during storm Xaver by 2100**

Figure 3.14. Changes in maximum wave height during storm Xaver compared to the same storm event simulated without sea-level rise and changes in ecotopes for the years A) 2030, B) 2050, and C) 2100 in climate scenario ssp 585. The color represents the change as % compared to 2020. The size of each dot represents the associated wave height.

3.4.2. Scenarios of measures

Several scenarios of measures are being developed to be simulated as part of D2.3, the portfolio of restoration measures. These include:

- Autonomous development / business as usual: no new measures are implemented.
- The plan VLOED: the creation of new intertidal wetland to facilitate sediment extraction.
- Sediment trapping: increase sedimentation in the Dollard with brushwood dams.
- Disposal of dredged material on Paap island: generating new habitat on Hond Paap by disposal of sand on the island

It is important to note that these measures are still being discussed with the stakeholders in RESTCOAST as part of the portfolio for restoration measures in D2.3. The final measures being simulated may therefore be different.

3.4.2.1. Autonomous development

Autonomous development is a reference scenario. It is the expected change in the absence of any measures so the effect of measures can be assessed.

3.4.2.2. Measure VLOED

The measure VLOED comprises three phases after which a total area of approximately 300 hectares will be converted into new tidal wetland. The idea behind the measure is that sediment will accumulate in the area from where it can be extracted for beneficial use in heightening agricultural land and improving flood defenses.

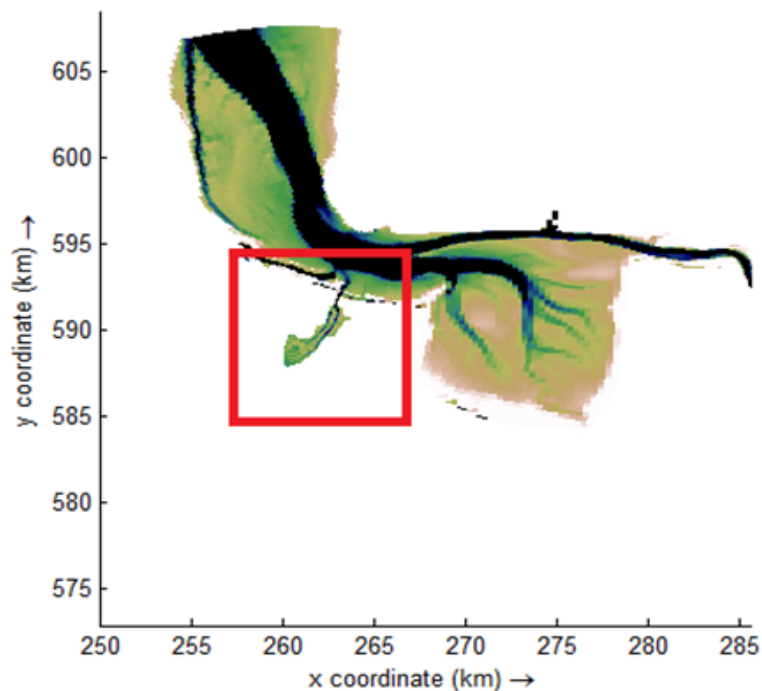


Figure 3.15. Additional intertidal wetland created for sediment extraction in the measure VLOED

3.4.2.3. Sediment trapping

Brushwood dams have been used for centuries in the Ems estuary and beyond to reclaim land from the sea. This old technique could be used to help facilitate sedimentation again, but with the purpose of enhancing the resilience of wetlands against sea-level rise instead of land reclamation. This part of a pilot currently being considered (Figure 3.16).

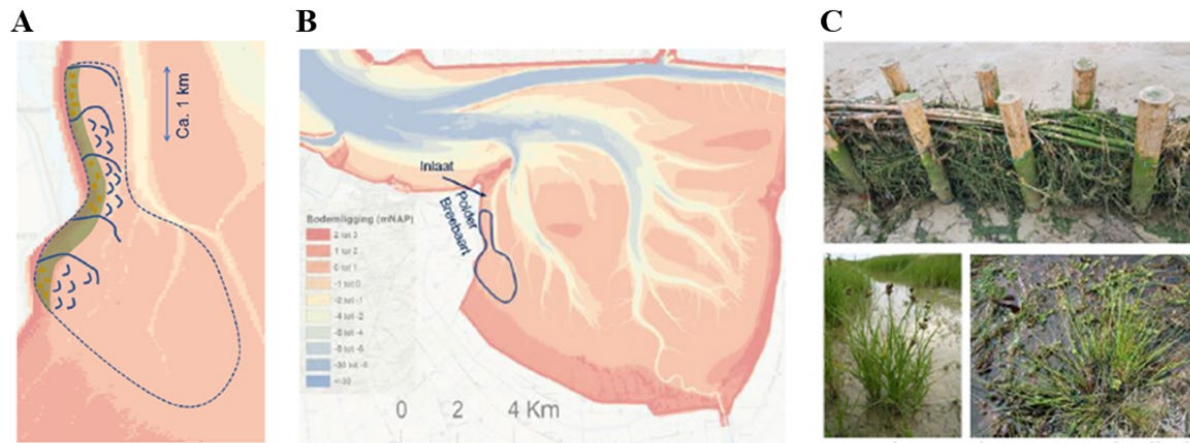


Figure 3.16. Pilot for sediment trapping on the intertidal flats as (source: Rijkswaterstaat)

3.4.2.4. Extraction of sediment from harbors

This measure is considered part of the wider sediment strategy outlined in the EmsDollard2050 program, where sediment dredged from the harbors is extracted. In turn, this sediment could be re-used beneficially in raising low-lying polders or as a material for dyke construction.

4. Multi-risk projections and climate warnings with ESS in Venice Lagoon Pilot (CMCC, COR)

4.1. Introduction

This Deliverable aims to evaluate the ecosystem services (ESS) provided by the restoration of degraded salt marshes in the Venice lagoon, which can be intended as a Nature-Based Solution (NBS). The document specifically focuses on the future climate scenarios for hydrodynamics and extreme wave conditions at the Venice pilot. The numerical simulations were conducted using the modelling framework previously described and validated in Deliverable 2.1, with a focus on a specific area of the Venice Lagoon, hereafter referred to as the “pilot site”. Due to the unique characteristics of the Venice Lagoon, we also carried out a set of simulations that include the MOSE barrier system, which is designed to protect the lagoon from extreme storm surge events.

The pilot site is located in the central-southern lagoon and includes the restoration of 8 salt marshes (Figure 4.1). To simplify the further discussion, we organized the salt marshes in northern (orange box in Figure 4.1) and southern (blue box in Figure 4.1). The restoration of these salt marshes follows two phases: i) the creation of a containment barrier (designed and adjusted to the features of the area restored – e.g., containment barrier with fascines, piles or mattresses), and ii) the refilling of the perimeter with dredged materials. These type of restoration activities are being executed as part of the Piano Morfologico, a lagoon wide plan executed by the Provveditorato Interregionale per le Opere Pubbliche per il Veneto, Trentino Alto Adige e Friuli Venezia Giulia (PROVV.) since 1992 to reverse the degradation of the lagoon morphology, and in addition to salt marsh restoration include actions such as the excavation of channels, the creation of tidal flats, re-naturalisation and seagrass transplantation (Tagliapietra et al., 2018).

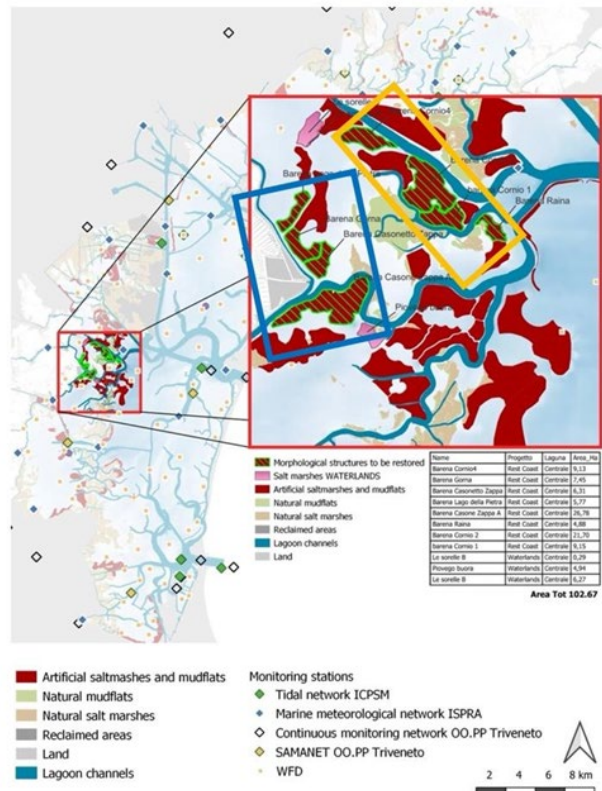


Figure 4.1. Location of the REST-COAST pilot site in the Venice Lagoon, highlighting the 8 salt marshes subjected to restoration in green. Blue box highlights the southern salt marshes, while orange box the northern salt marshes.

Climate change is one of the main drivers of extreme flooding in Venice and is projected to increase with rising sea levels in Venice expected by the end of the 21st century (Alberti et al., 2023). The Venice Lagoon, and the city of Venice, are affected by Acqua Alta. Three of the most devastating events occurred on 04/11/1966, 29/10/2018, and 12/11/2019, causing significant damage to the city (Faranda et al., 2023). In 2003 the construction of the MOSE (MODulo Sperimentale Elettromeccanico: Experimental Electromechanical Module) started, and responds to the objectives set by the Law of Venice 798/84 to protect the lagoon from high tides (<https://www.mosevenezia.eu/>). The structure consists of 79 elements of mobile barriers at the Lagoon inlets that are raised if tides are expected to surpass 1.10 m – and is functional up to 3 m (Janowski et al., 2020). Since its activation at the end of 2020, barriers' closures have an average closing time of $\pm [4, 5]$ h and have been activated more than 50 times (Alberti et al., 2023).

4.2 Methodological approach

In this section the methodological approach is described, introducing the datasets, "what-if" scenarios, the scenario selection, and the numerical implementations, detailing not only their individual composition, but also how they are linked together. Additionally, the influences of the MOSE system are described as well as how this relates to this deliverable. Before going through each of the sections, we graphically summarized the workflow in the following diagram (Figure 4.2). Starting from the Copernicus Climate Change Service (C3S) datasets we defined two groups of simulations, for waves and hydrodynamics respectively. We identified 8 "what-if" scenario for waves and 6 scenarios for hydrodynamics. Each scenario has been simulated by 4 different configurations: a reference with closed and open MOSE conditions, and the restoration intervention in closed and open MOSE conditions. We obtained 32 simulations for Significant wave height, 24 simulations for the sea level, and 24 for currents. At the end, the reference and the restoration intervention have been compared to assess the impact of the restoration intervention on the variable investigated.

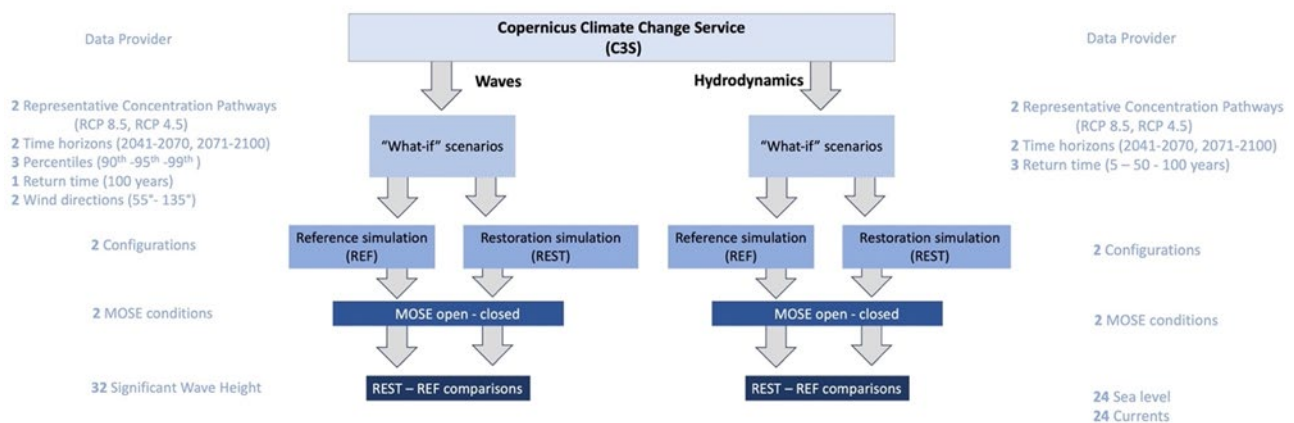


Figure 4.2. Schematic representation of the workflow adopted in this deliverable. The diagram summarizes all the simulations, variables, scenarios and configurations

4.2.1. "What-If" scenarios

Climate projections come with a range of uncertainties, stemming from various sources. Different emission scenarios lead to diverse climate outcomes, introducing uncertainty in predicting future climate conditions. Also, the future trajectory of greenhouse gas emissions depends on factors such as technological advancements, economic developments, and societal choices which are complicated to be predicted. In addition to that, some natural processes, such as volcanic eruptions, solar variability, and internal climate

oscillations, can influence short-term climate trends. Predicting the timing and magnitude of these events introduces uncertainties into long-term climate projections.

Climate models are complex representations of the Earth's climate system, but despite that, they have some simplifications or assumption which could introduce uncertainties in the solution. Some of the limitations are related to the model resolution, the representation of physical processes, and the inability to fully capture regional-scale variations. Understanding and quantifying these uncertainties are crucial but is out-of-the-scope of this task. To limit the uncertainty of our results, we did not provide numerical simulation for the future, but we provided a range of simulations forced by statistical descriptors of climate projections. This methodology is known as "what-if" scenarios. "What-if" scenarios are hypothetical situations or simulations that explore the potential consequences of certain changes or events in the oceanic system under specific environmental forcings. These scenarios are often used in climate projection studies to understand how various factors may influence the ocean environment. Some common "what-if" scenarios in oceanography include:

- Sea Level Rise Scenarios: Investigating the impact of different rates of sea level rise due to factors like melting ice caps and glaciers.
- Ocean Temperature Changes: Examining how alterations in global temperatures may affect ocean temperature profiles, leading to phenomena like ocean warming or cooling.
- Ocean Acidification Scenarios: Studying the potential consequences of increased carbon dioxide levels in the atmosphere on ocean pH levels and marine ecosystems.
- Changes in Ocean Circulation Patterns: Assessing the effects of alterations in ocean circulation patterns, such as shifts in major currents like the Gulf Stream.
- Extreme Events: Exploring the potential impact of increased frequency or intensity of extreme weather events, such as waves.

"What-if" scenarios are crucial in climate projection for several reasons:

- They help in the assessment of the risks associated with different climate change scenarios, allowing to identify potential vulnerabilities and impacts on both marine ecosystems and human activities.
- Scenario analysis assists policymakers in developing adaptive strategies and policies to mitigate or cope with the potential impacts of climate change on oceans.
- Understanding the consequences of different scenarios helps in sustainable resource management.
- Contribute to a better understanding of the complex interactions within the oceanic system, providing insights into the underlying mechanisms driving climate variability.

4.2.2. Climate change scenarios selection and description

The Copernicus Climate Change service (C3S) is the provider of the forcing data used for setting up the different scenarios. Two datasets were taken into account:

- Water level change indicator: <https://cds.climate.copernicus.eu/cdsapp#!/dataset/sis-water-level-change-indicators?tab=overview>
- Ocean wave indicator: <https://cds.climate.copernicus.eu/cdsapp#!/dataset/sis-ocean-wave-indicators?tab=overview>

These datasets provide information along all the European seas. For the purpose of this study, data closest to the boundaries of our models were extracted and utilized to force the simulations. This deliverable mainly focused on currents and sea-level which has the main impact on the Venice Lagoon, but also significant wave height is included in the study. For hydrodynamics six future scenarios were simulated. The climate simulations are based on Representative Concentration Pathways (RCPs), a set of four global carbon

emissions pathways developed for climate modelling. Of the four RCPs, which radiative forcings span from 2.6 to 8.5 W/m². The selection of the RCP is on related to what the authors of the C3S datasets consider most plausible. Following, their comment: “Due to the large climate variability in sea level, and the fact that extreme sea levels, takes multiple decades before the climate signal can be detected from the natural climate variability, we started our future climate simulations in 2040. At present global carbon emissions are tracking just above the RCP8.5 pathway. As such, regarding the mid-term future (2040-2070) we apply the RCP8.5 pathway. This is a high-emission scenario that assumes high population growth combined with relatively slow income growth with modest rates of technological change. However, countries across the world have committed to limit the global temperature change to 1.5 degree Celsius in the Paris Agreement. This requires very rigorous reductions in the global carbon emissions reductions. It is argued that RCP 2.6 is currently unfeasible, therefore, we apply the RCP 4.5 pathway to the long-term future (2070-2100). RCP4.5 is one of the more optimistic pathways that assumes human emissions of greenhouse gases will stabilize soon and then decline after a few decades”.¹

To model the distribution of the extreme values, we use the Gumbel distribution (Gumbel 1958) over the annual maxima values for each epoch. Each epoch/scenario consist of 29 years of data (2041-2070, 2071-2100), from which the annual maxima value for each station is computed. These 29 values are then fitted to the Gumbel distribution to derive the parameters defining the function, which can in theory be evaluated for any given return period. The starting value for low return periods will be strongly determined by the location's sea level rise and tidal range. While the Gumbel method is simple and widely used, the maximum return period for which the Gumbel function is evaluated here is 100 years. This is on the limits of the extrapolation capabilities of the method for a set of 30 years' sample values, as the uncertainty greatly increases for increasing return periods. Three return periods have been considered in this study, for taking into account common extreme events (5 years), rare extreme events (50 years) and very rare extreme events (100 years). The simulated scenarios for hydrodynamic conditions and related nomenclature are summarized in Table 3.1.

Table 3.1. Hydrodynamic condition scenarios simulated in this work. Acronym, climate scenarios with related temporal scenario, event return time, and simulation parameters are provided.

Experiment Name	Climate scenario	Temporal horizon	Return Time	Mean Sea Level [m]	Total water level [m]	Tidal Range [m]
H1	RCP 4.5	2071-2100	5 years	0.34	1.84	1.04
H2	RCP 4.5	2071-2100	50 years	0.34	2.26	1.04
H3	RCP 4.5	2071-2100	100 years	0.34	2.38	1.04
H4	RCP 8.5	2041-2070	5 years	0.25	1.62	1.03
H5	RCP 8.5	2041-2070	50 years	0.25	1.94	1.03
H6	RCP 8.5	2041-2070	100 years	0.25	2.02	1.03

To the main stressors of the Venice lagoon, circulation and sea level, we included in our set of numerical experiments also wave simulation. As shown in Deliverable 2.1, the very shallow depth of the lagoon (less than 1 m on average) and the limited fetch prevent the development of large wind-waves within the lagoon. Furthermore, due to the natural sheltering, swell from the Adriatic Sea cannot significantly penetrate the lagoon. As a result, it is necessary to generate waves within the lagoon by forcing them with wind, rather than by propagating extreme offshore wave conditions, as is typically done in “what-if” wave scenarios.

¹ <https://confluence.ecmwf.int/display/CKB/Product+user+guide+for+sea+level+and+ocean+wave+products++time+series+and+indicators>

Unfortunately, the dataset used for the climate projections provides only wave height, without any information on wave direction or the associated wind conditions. Therefore, each future wave height scenario was paired with a corresponding wave direction derived from a climatological analysis of historical data. In detail, we derived the main wave directions for extremes by investigating the climatic characteristic of the area, using Copernicus Marine Service (CMEMS) data for waves² and ECMWF-ERA5 (Hersbach et al., 2020) for wind. In Figure 4.3 the 99th percentiles both for wind and waves is shown. The climate assessment distinguished two main conditions for the area:

- The highest waves are SE oriented (while the prevalent waves are NE oriented).
- The highest winds are NE oriented.

These results indicated that the highest waves approaching the Venice lagoon are generated by the long fetch of the Adriatic Sea, but because of the sheltering, they are almost all dissipated at coast without affecting the lagoon. On the contrary, the highest waves inside the lagoon are generated under NE wind conditions, which is the strongest wind for the area. Thus, we included in our set of simulations both the conditions above mentioned.

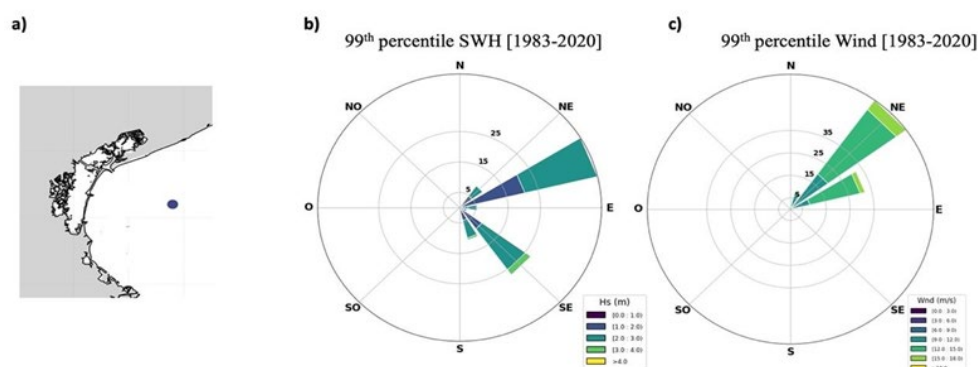


Figure 4.3. Wave and wind climate for the Venice lagoon pilot. Sub-plot (a) shows the location for the climate analysis, (b) shows the 99th percentile of SWH, (c) shows the 99th percentile for wind.

A preliminary assessment of the wave climate data projections (Figure 4.4) indicated that significant wave height (hereafter SWH) in the Northern Adriatic Sea is expected to show a slight negative trend ($\sim -7\text{mm}/10\text{years}$ under the RCP 4.5 scenario). The negative trend is even smaller under the RCP 8.5 scenario ($4\text{mm}/10\text{years}$). Since both scenarios suggest similar future conditions, the “what-if” simulations were carried out under a single RCP scenario. To adopt a conservative approach, we selected RCP 8.5, as it exhibits the lowest negative trend. Additionally, the C3S dataset does not provide waves statistics as those available for hydrodynamics, such as return time 5 and 50. The summary of the wave scenarios is provided in Table 3.2.

² https://data.marine.copernicus.eu/product/MEDSEA_MULTIYEAR_WAV_006_012/description

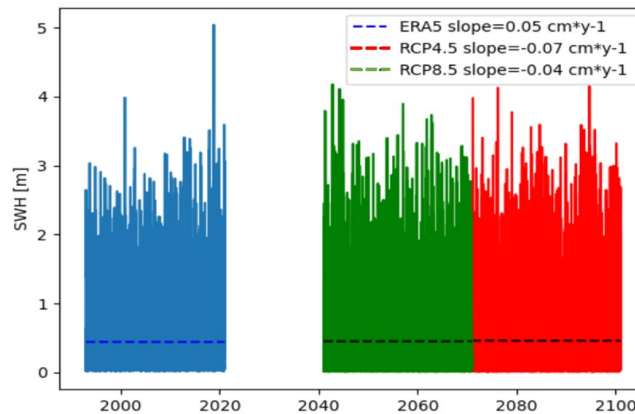


Figure 4.4. Significant wave height and related trends for past (1990-2020), RCP8.5 (2041-2070) and RCP4.5 (2071-2100) scenarios

Table 3.2. Wave condition scenario simulated in this work. Acronym, climate scenarios with related temporal scenario, considered statistics and simulation parameters are provided

Experiment Name	Climate scenario	Temporal horizon	Statistics	Wind direction
W1a	RCP 8.5	2041-2100	90 th perc.	135°
W2a	RCP 8.5	2041-2100	95 th perc.	135°
W3a	RCP 8.5	2041-2100	99 th perc.	135°
W4a	RCP 8.5	2041-2100	100 years	135°
W1b	RCP 8.5	2041-2100	90 th perc.	55°
W2b	RCP 8.5	2041-2100	95 th perc.	55°
W3b	RCP 8.5	2041-2100	99 th perc.	55°
W4b	RCP 8.5	2041-2100	100 years	55°

4.2.3. Numerical implementations

Every future scenario has been simulated with four different numerical configurations. The main configuration, which represents the benchmark for this study, is the ESS configuration (hereafter REF or reference configuration) we presented in the D2.1. The reference configuration set-up included both seagrass and salt marshes, which remained consistent across time evolution and scenarios. The second configuration (hereafter REST configuration) includes the future restoration activity planned in the Venice Lagoon and which will be carried out in the coming years, starting with the salt marsh restoration in the pilot site in 2023. This configuration is based on the Piano Morfologico (<http://provveditoratovenetia.mit.gov.it/introduzione.html>), focusing particularly on the restoration of morphological structures including the 8 salt marshes in the central-southern lagoon that are included in the REST-COAST project. The works are based on historical analyses of the morphological changes in the past century, on hydraulic optimization studies and reuse the dredged sediments from the channel excavation (Tagliapietra et al., 2018). Figure 4.5 shows the REF and REST configurations, with a magnification view at the pilot site to highlight the distinctions between the two configurations.

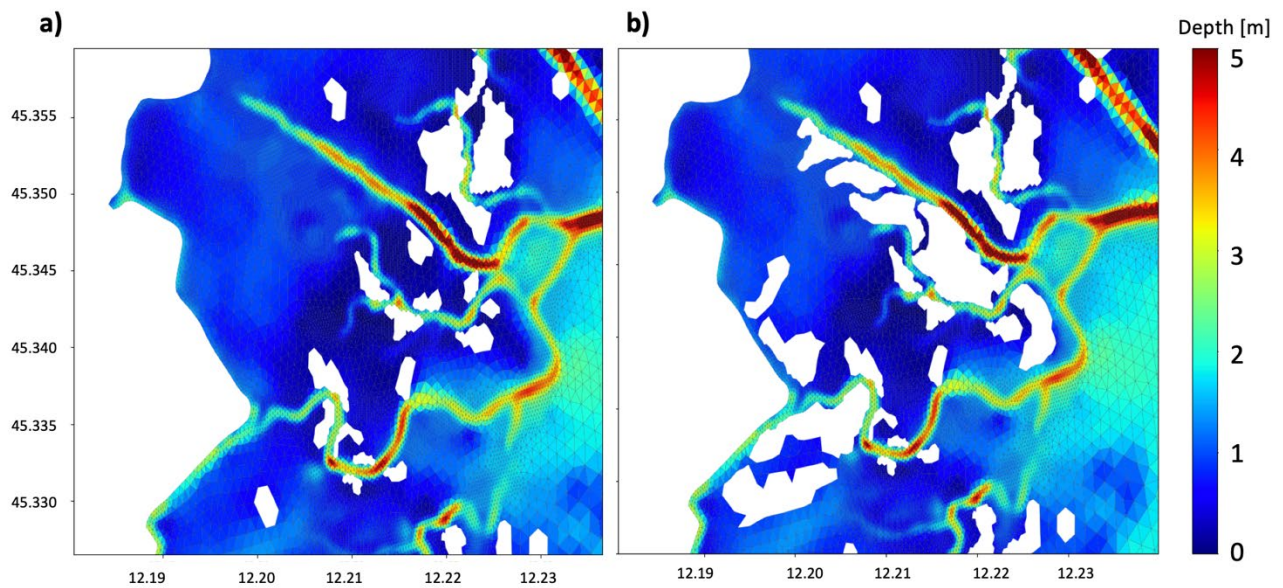


Figure 4.5. Magnification of the numerical grids and bathymetry on the pilot site. a) shows the REF configuration, b) shows the REST configuration

The REST simulation implementation allowed to study the effect of the restoration intervention on circulation and waves. The last two configurations included the MOSE infrastructure in both REF and REST. A summary of the numerical set-ups and related acronyms is presented in Table 3.3. The motivation for employing four configurations was to juxtapose the outcomes of REF and REST experiments, involving the computation of result differences. This approach provided an indirect means to evaluate the influence of the restoration intervention on hydrodynamics and waves within the pilot area through NBS. Furthermore, we investigated whether the closure of MOSE could yield different impacts on the pilot area in the REF and REST configurations.

Table 3.3 Summary of the four configurations used in the numerical simulations, with experiment name and related description.

Configuration	MOSE	Short description
REF	open	Benchmark configuration for both hydrodynamics and waves. Seagrass and salt marshes are included in the simulation. Further details about the configuration are described in deliverable D2.1
REST	open	As REF configuration with exception of the inclusion of the restoration intervention(NBS).
REF_MOSE	closed	As REF configuration, in which we simulated the MOSE barriers closure
REST_MOSE	closed	As REST configuration, in which we simulated the MOSE barriers closure

The last part of the study aims to understand if the effect of the restoration activity on hydrodynamics is affected by the MOSE barriers closure. For this reason, we compared the configurations REST and REF simulations both with closed MOSE barriers. This would correspond with the current conditions, as the MOSE can be activated when a surge is predicted to be at least +110 cm. The comparison further of open/closed MOSE barriers, despite being an interesting topic, goes beyond the objective of this work, and will not be investigated in depth here. In Figure 4.6 we presented a comparison between one example scenario (H3 in this case) with open 3.6a and closed 3.6b barriers, at lagoon scale, to provide an insight on the barriers effect on the sea level during an extreme storm surge.

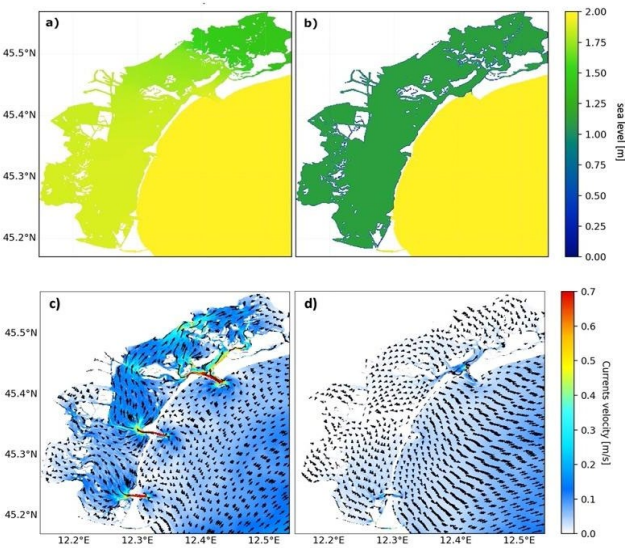


Figure 4.6. Comparison of extreme sea level with open (a) and closed MOSE (b) and corresponding current (c,d)

4.3. Results

4.2.1. Circulation

The results of the investigation of the currents are summarized comparing the simulations in two different locations (Figure 4.7 Location of the comparison between numerical configurations: the black dot indicates the pilot area, and the red dot shows the location of the Adriatic Sea.). The selection of the points aimed to have results from:

- the pilot area, which is the main topic of the project,
- the Adriatic Sea, as control of the forcing, and where the impact of the restoration should not be effective.

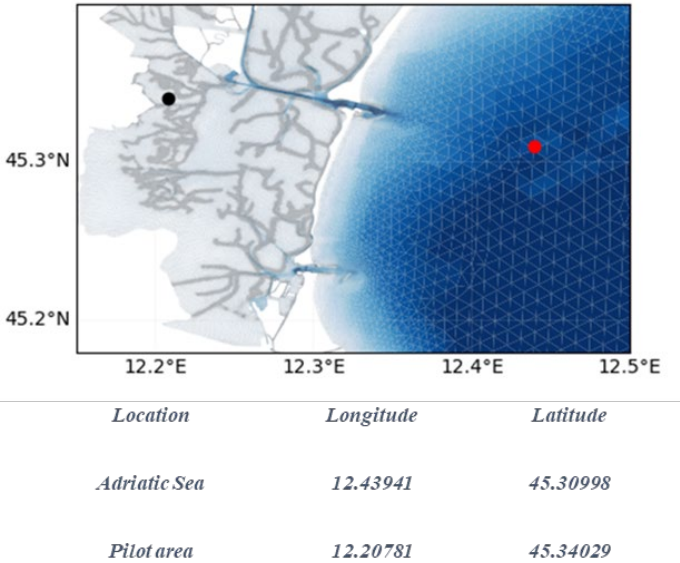


Figure 4.7. Location of the comparison between numerical configurations: the black dot indicates the pilot area, and the red dot shows the location of the Adriatic Sea.

In Figure 4.8a, we show the sea level at the Northern Adriatic Sea for the six simulations, representing different storm surges approaching the Venice lagoon, while in Figure 4.8c the water currents at the same location. These timeseries are from the REF simulation, which represent the benchmark for the study. Comparing the 3.8a-sub plot with the corresponding timeseries at pilot site 3.8b, it is evident a time lag in the occurrence of the extreme events around 3-4 hours, and a reduction in sea level elevation of ~15cm maximum. However, the reduction in elevation at the pilot site compared with the Adriatic Sea is more evident for higher sea-levels (H1, H6). The evaluation of water currents at the two locations 3.8c-d reveal more differences, mainly related to the fact that the open sea has higher velocity during the ebb phase of the events, while the pilot area reveals the currents peak during the flooding. The comparison of the results from the REST and REF configurations allowed to describe the effect of the restoration intervention. As expected, when the comparison is carried out at open sea, no difference is evident, thus we do not show the plot in this document. On the contrary, small difference, around ± 4 mm maximum, are shown by the sea level comparison 3.8e, and currents mainly increased in the REST configuration 3.8f, up to +3 cm/s. In detail, the differences in sea level is around ± 1.8 mm during the normal tidal cycle (before and after the extreme event occurs - up to hour 60 and after hour 84 in the timeseries), and here all the scenarios have almost the same difference between REST and REF configurations. After hour 60 the extreme event approaches to the lagoon and the difference REST-REF is sensitive to the magnitude of the event. Higher scenarios showed a higher increase of sea level (exceeding +4 mm in H3), but even a more rapid and intense decrease in water level: during the ebb phase H4 reaches ~ -3.5 at hour 86, while H3 reaches ~ -3.5 mm at hour 80 and ~ -5 mm at hour 86.

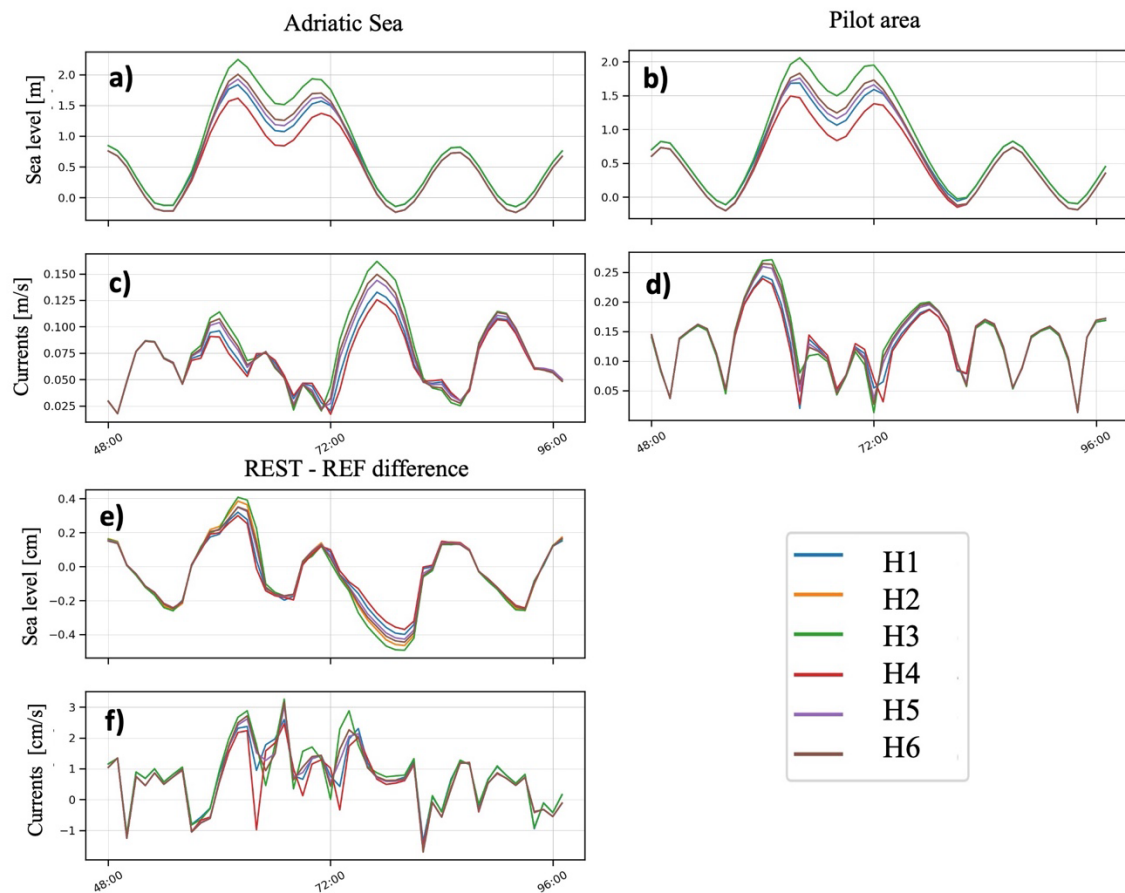


Figure 4.8. Timeseries of water level (a-b) and currents (c-d) at Adriatic Sea (a-c) and the pilot site (b-d) for the six scenarios. The difference between REST and REF configurations is shown in sub-plots (e) for sea level and (f) for currents.

The overall results showed how the restoration activity conducted at the pilot area has negligible significant effect on local sea level. The difference between the REST and REF configuration is of the order of few millimeters for all the simulated scenarios, and thus not appreciable in the timeseries. Despite that, we want to show this difference as map (Figure 4.9) to better highlight that the restoration intervention, i.e. the NBS, because of the presence of salt marshes, reduced the section for the water flow, has a lag time with respect to the upstream area. Consequently, this leads to a phase shift of the sea level oscillation and the intensification of currents between the restored salt marshes.

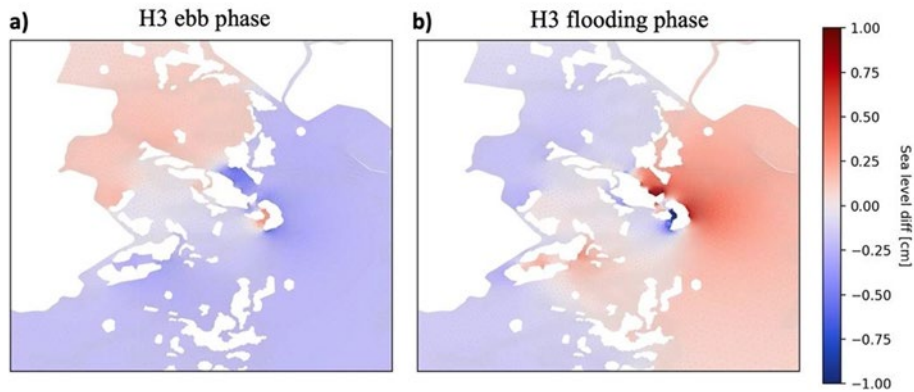


Figure 4.9. Sea level difference computed as REST - REF simulations for H3 during the ebb phase (a) and the flooding phase (b).

In Figure 4.10 we show the map for the lowest 3.10a and the highest 3.10b currents difference between REST and REF configurations. In the figure we show only one of the simulations because all of those revealed very similar pattern and intensity. The lowest difference in currents occurs in the slack phase, and from the map we observed a general reduction of circulation around the restored salt marshes, around $(-3, -5) \text{ cm s}^{-1}$. The highest difference is evident in the flooding phase, where some areas of reduced currents are evident about $(-5, -10) \text{ cm s}^{-1}$, reaching the highest currents reduction downstream the easternmost restored salt marshes, around -30 cm s^{-1} . On the contrary, all the funneling made up by the intervention increased the water velocity along these new channels of around $(10, 15) \text{ cm s}^{-1}$, with exception of the northernmost restored salt marshes where the currents increase up to 30 cm s^{-1} .

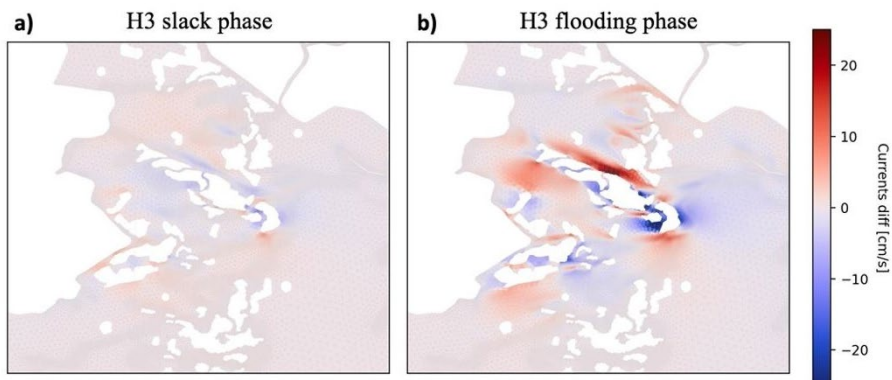


Figure 4.10. Currents difference for REST and REF configuration in the H3 simulation both on the slack phase (a) and the flooding phase (b).

Despite the primary focus of the study concerns the pilot site and the impact of the restoration activity, we recognize the broader importance of addressing the flooding risk for the entire Venice lagoon. To support this understanding, additional information about the land surface flooded during various storm surges for future scenarios in the entire lagoon is provided. For each of the six simulated scenarios, we calculated the maximum floodable area, which signifies the theoretical maximum surface that could be flooded during an event. We choose to reference this parameter with respect to the real simulated inundation for two reasons: i) the flooding is function of time. In our scenarios we set up the time of the extreme event growing phase to 6 hours, keeping the maximum value of the surge signal constant for 6 hours (with subsequent addition of the tidal component), and allowing for an 8-hour receding phase, and the receding phase of 8 hours. Naturally, the extreme events could have shorter surge peak and in-phase/ not in-phase tides-surge which significantly affects the flooded area; and ii) the flooding is function of land usage and coverage. These land characteristics are influenced by both human activities and natural processes (sometimes extreme conditions), making predictions challenging. The area potentially submerged by the most frequent extreme event we simulated for the time-period 2041-2070 ranges between 210 and 271 Km², while for the time-period 2071-2100 the area is sensibly larger, ranging from 262 and 371 Km². The maximum flooded area at lagoon scale, for every scenario, see Table 3.4.

Table 3.4 Maximum floodable areas for the six hydrodynamic “what-if” scenarios. The investigation is performed for the entire lagoon area.

Experiment Name	Maximum floodable area (Km ²)
H1	262
H2	365
H3	371
H4	210
H5	262
H6	271

4.2.2. Waves

Results from wave simulations (Figure 4.11) indicated how the restoration intervention significantly increased the local dynamics at the pilot area. For both the simulated directions, S-E (subplots 3.11a,c) and N-E (subplots 3.11b, d), within the numerical experiments of the same group (Wa and Wb), the difference in SWH showed the same distribution pattern, but with different intensity. It is noteworthy that under lower wave conditions (W1 and W2), REF simulations generally resulted in higher waves compared to REST simulations, with exception of the area located within the southern and northern groups of restored salt marshes. However, as the wave height increased (in W3 and W4 scenarios), the positive difference between the two simulations diminished, and the negative one intensified. For this reason, we showed in Figure 4.11 only the lowest (W1a and W1b) and the highest (W4a and W4b) conditions.

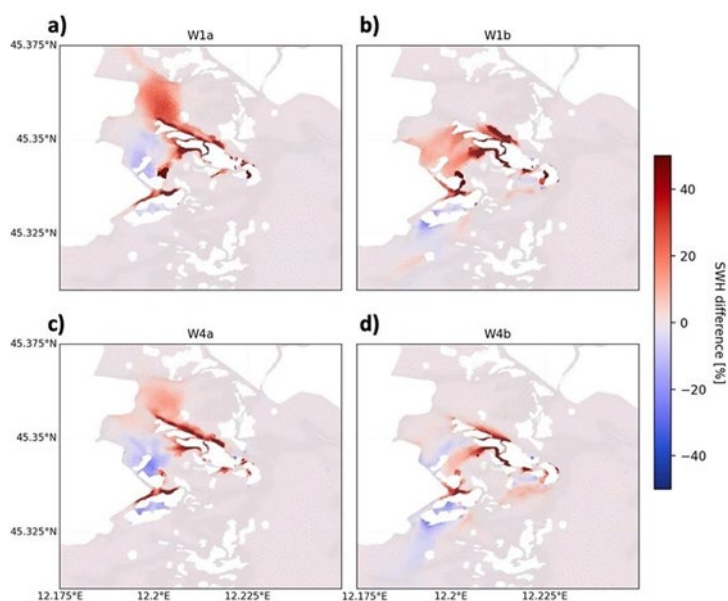


Figure 4.11. Significant wave height difference (expressed in percentage) computed as REST - REF configurations for the scenarios a) W1a, b) W1b, c) W4a and d) W4b.

In detail, concerning the distribution patterns (Figure 4.12) of the REST – REF difference we observed in Wa scenarios an increased SWH along the deep canals surrounding the salt marshes ($\sim +40\%$), and in the northern part of the restored salt marshes ($\sim +20\%$). On the contrary, it is highlighted a slight reduction ($\sim -10\%$) of SWH in the area located between the two groups of restored salt marshes. As anticipated, the area of SWH reduction is more evident for higher wave scenarios ($\sim -20\%$), while the northern part of the restored salt marshes revealed only $\sim +10\%$ in the higher scenarios. In the Wb scenarios, the increase of SWH in REF simulations along the deep canals of the pilot area is still evident, but at a lower extent compared to Wa scenarios. In lower waves conditions the central area between northern and southern groups of restored salt marshes showed $\sim +15\%$ of SWH in REF. On the contrary, when higher scenarios are considered, the difference reduced and becoming negative in some cases. In all the Wb scenarios, the southern group of restored salt marshes indicated a reduction of SWH ($\sim -10-20\%$). It is worth to notice that the magnitude of the SWH for REF configuration (Figure 4.12) is very low in the area ($\sim <40$ cm), and just on few canals traits SWH exceed 60 cm.

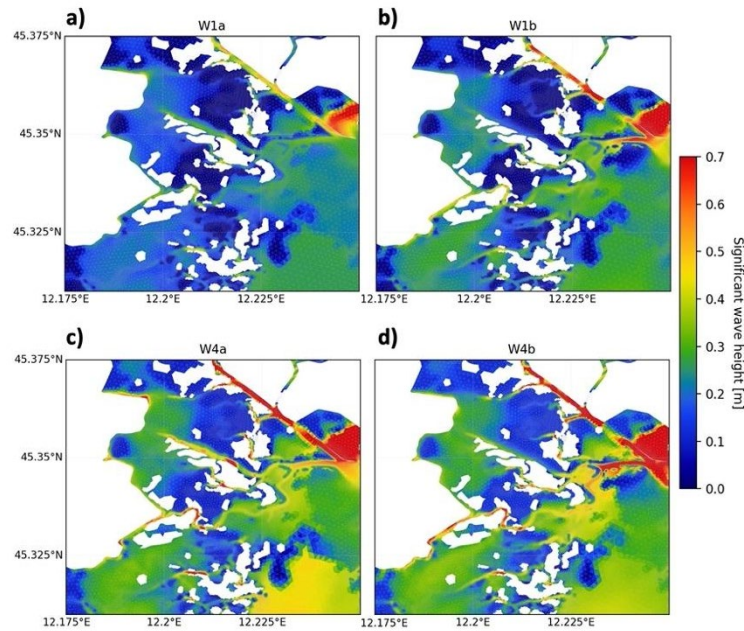


Figure 4.12. Significant wave height for the REF configuration and for the scenarios a) W1a, b) W1b, c) W4a, and d) W4b

4.2.3. MOSE barriers closure

The closure of the barriers is endeavored to limit the flooding of the low-lying lands around the lagoon, protecting the Venice city. The MOSE closure determines the sea level height inside the lagoon, which remains almost constant during the storms. The limitation of the water exchange between lagoon and North Adriatic Sea defines a net reduction of the lagoon circulation (Figure 4.6d). Our results revealed that the presence of the restoration intervention has negligible effect on sea level when the barriers are closed, as shown in Figure 4.13.

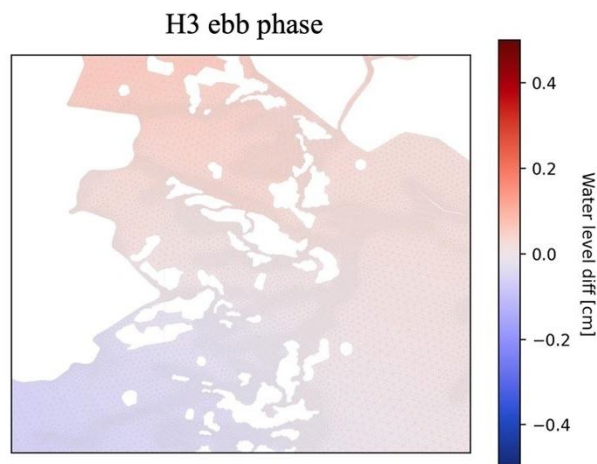


Figure 4.13. Water level difference between REST and REF configurations when MOSE barriers are closed.

Concerning the investigation on the wave field, the difference between the REST and REF configuration with closed MOSE mirrors precisely the difference observed in Figure 4.11, where the MOSE barriers were open. This parallel pattern arises due to the lagoon's confinement, preventing the influence of Adriatic Sea swell on the lagoon's wave dynamics. Consequently, the waves in the lagoon are predominantly driven by wind

forces and locally developed. This study revealed that the largest REST- REF difference occurs on currents (Figure 4.14), despite this is approximately one order of magnitude lower than the open MOSE condition. During slack phase (Figure 4.14a), currents exhibit no differences around the southern group of salt marshes while in the northern group is highlighted a reduction of circulation around the westernmost part, and an increase along their northern side. During the flooding phase (Figure 4.14b) there is a generalized increase of currents ($\sim 1 \text{ cm s}^{-1}$) at the pilot site, with the exception of the area between the two southernmost salt marshes, where currents show a reduced intensity.

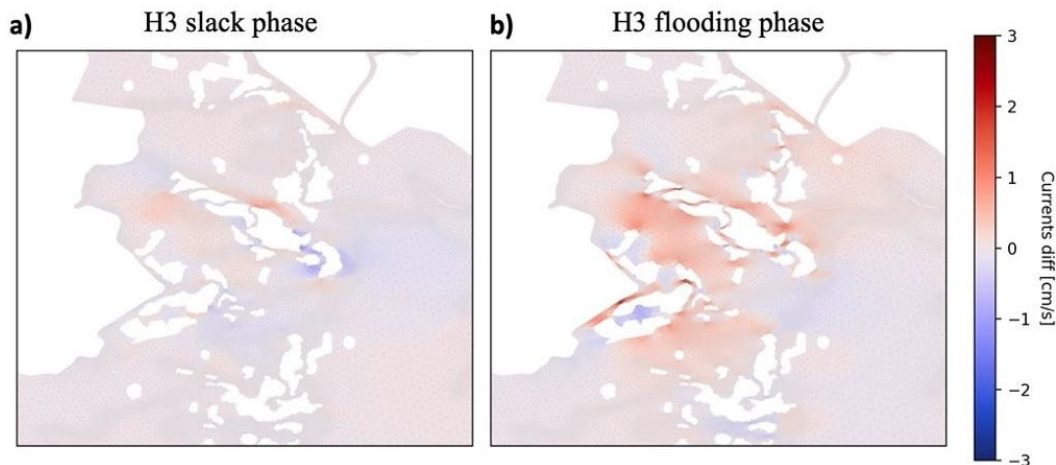


Figure 4.14. Currents difference for REST and REF configuration and closed MOSE barriers in the H3 simulation both on the slack phase (a) and the flooding phase (b).

4.4. Conclusions

This study provides a comprehensive assessment of the impact of salt marshes restoration intervention, i.e., NBS, on both hydrodynamics and wave conditions, under various storm surges affecting the Venice pilot site during the 2041-2070 and 2071-2100 scenarios. Despite the primary focus of the study concerns the pilot site and the impact of the restoration activity, we recognize the broader importance of addressing the flooding risk for the entire Venice lagoon. The analysis of maximum floodable areas underscores the varying scenarios, with a range of approximately 60 Km² observed for the period 2041-2070 and an expanded area of about 110 Km² for the 2071-2100 scenarios. The restoration intervention manifests its influence on hydrodynamics through changes in currents, particularly during the flooding phase. Sea level experiences a slight adjustment, typically within the range of $\pm 1 \text{ cm}$, primarily attributed to the restricted water flow caused by the presence of salt marshes.

Concerning the wave climate, the investigation of the projections suggests minimal alterations in wave conditions towards the end of the century. When examining the inclusion of restoration intervention, higher waves are more effectively attenuated by the restoration intervention. The placement of salt marshes emerges as a critical factor, with those close to deeper channels inducing significant increases in significant wave height (SWH) and currents. Notably, the western part of the northern group of salt marshes and the area between the two southernmost salt marshes present the lowest currents in the REST configuration. In addition, the southern group is identified as affected by wave reduction.

When the MOSE barriers are closed the lagoon undergoes to a remarkable reduction in currents by one order of magnitude. However, during the MOSE closure, the restoration intervention induces a general low ($\sim 1 \text{ cm s}^{-1}$) increase in currents at the pilot site, with a few small exceptions. This observation holds significance as it mitigates the anticipated reduction in currents induced by the barrier closure. The northern side of the

northern salt marshes group stands out as the most exposed area, experiencing an increase in significant wave height and currents velocity, whether MOSE is open or closed. This underscores the importance of meticulous positioning of salt marshes during restoration activities, especially considering their proximity to deep canals or channels, as it could lead to a significant increase in SWH and currents. Such insights are pivotal in refining restoration strategies for the Venice lagoon, ensuring a balanced and effective approach to hydrodynamic management.

4.5. Annexes

In the appendix are attached plots showing significant wave height, water level and currents from various simulations conducted in this study. For both wave height and water level the plots illustrate the REST configuration at the peak of each event. Currents plots refer to a different time step, specifically when the currents reach their maximum intensity. Additionally, for currents, also the REF configuration is shown. Last annex shows the maximum flooded area for every scenario at lagoon scale.

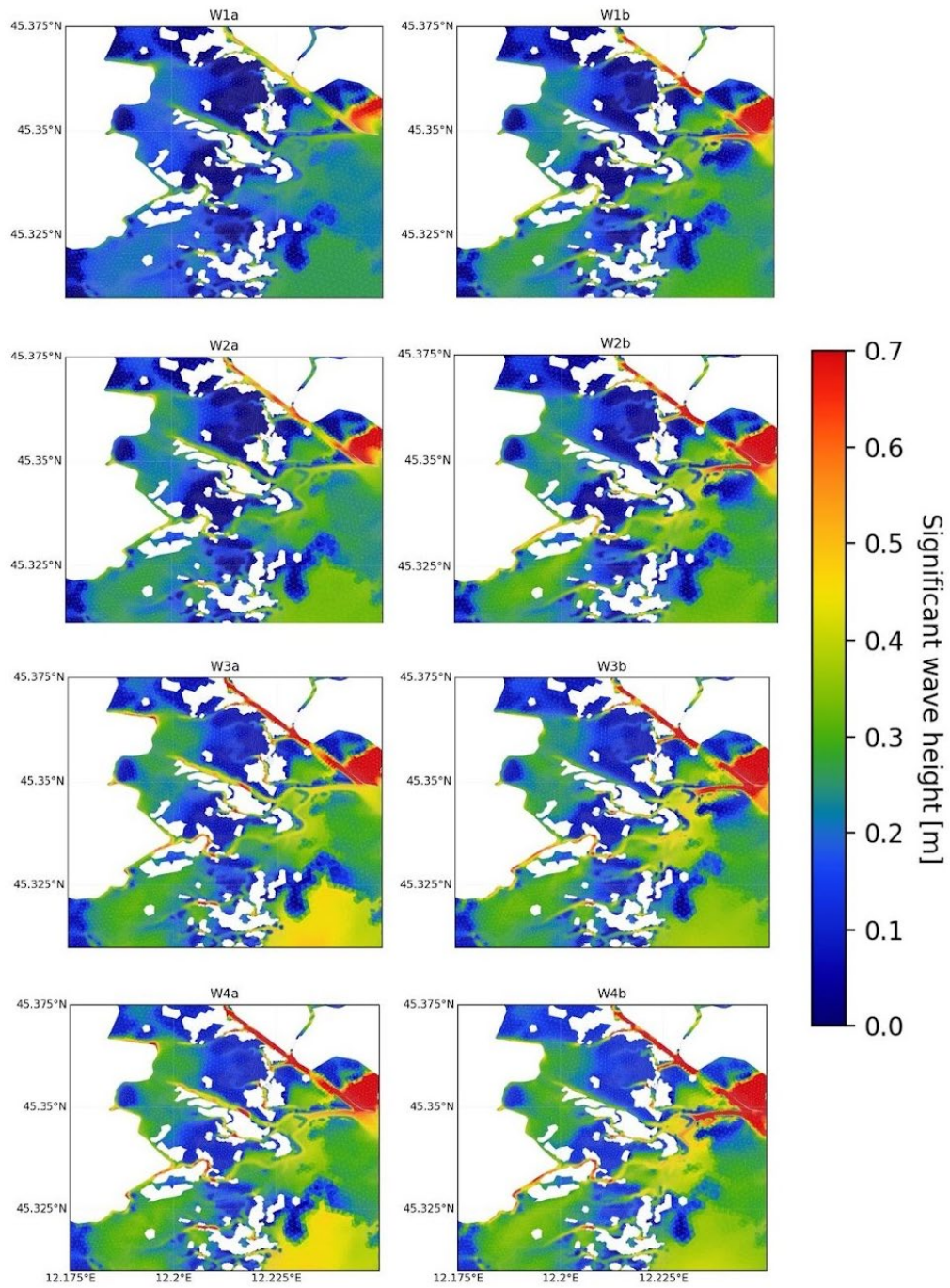


Figure 4.15. Annex 1: What-if scenarios of significant wave height at the pilot site

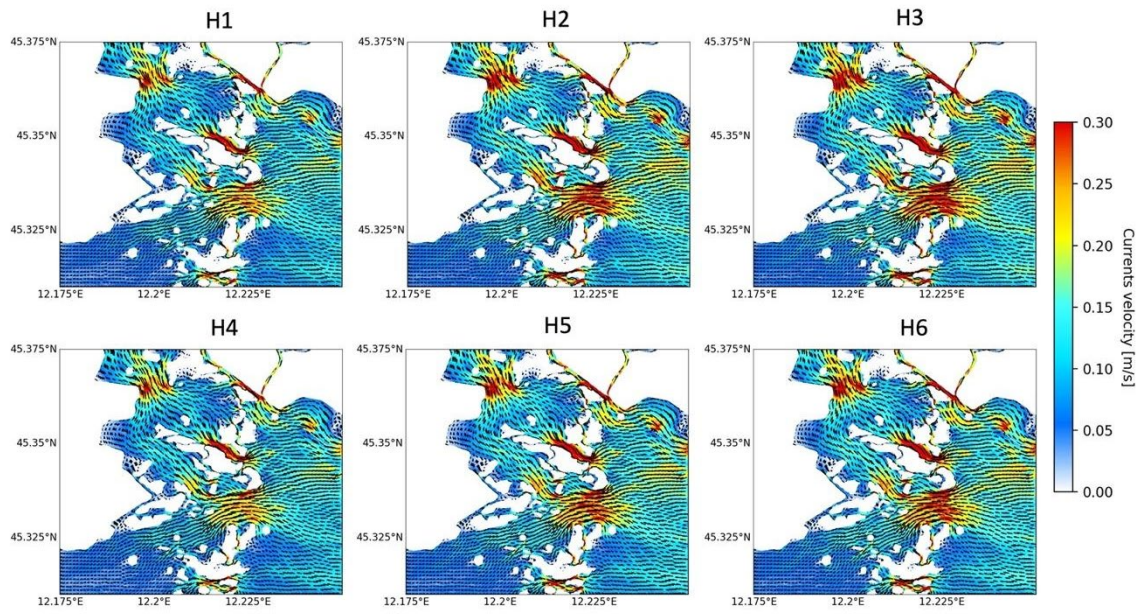


Figure 4.16. Annex 2: Currents for REST configuration

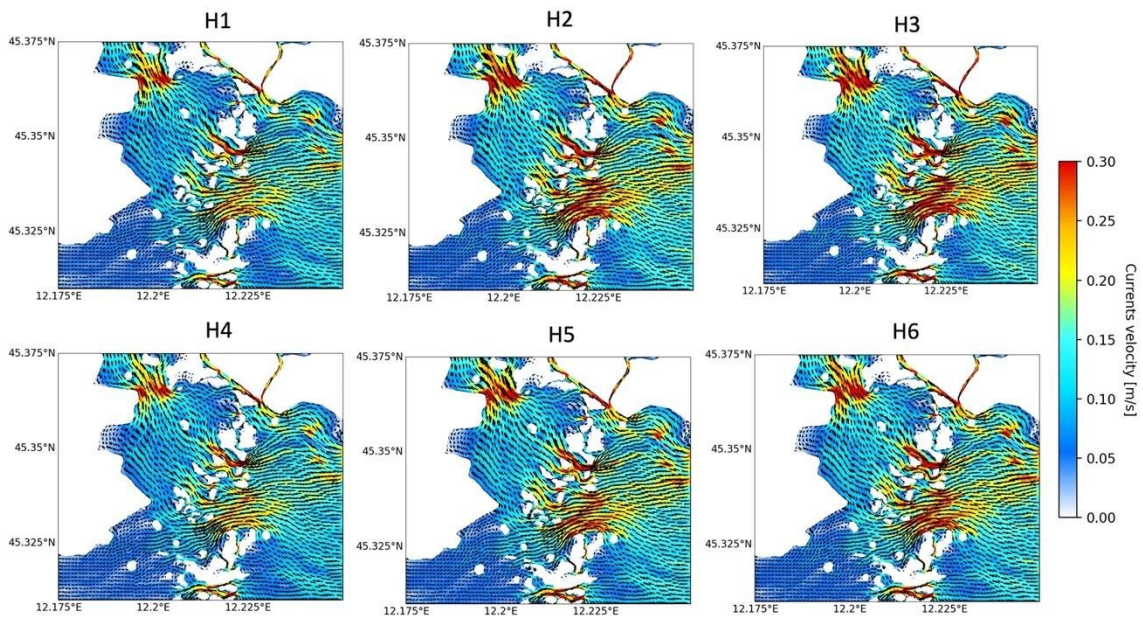


Figure 4.17. Annex 3: Currents for REF configuration

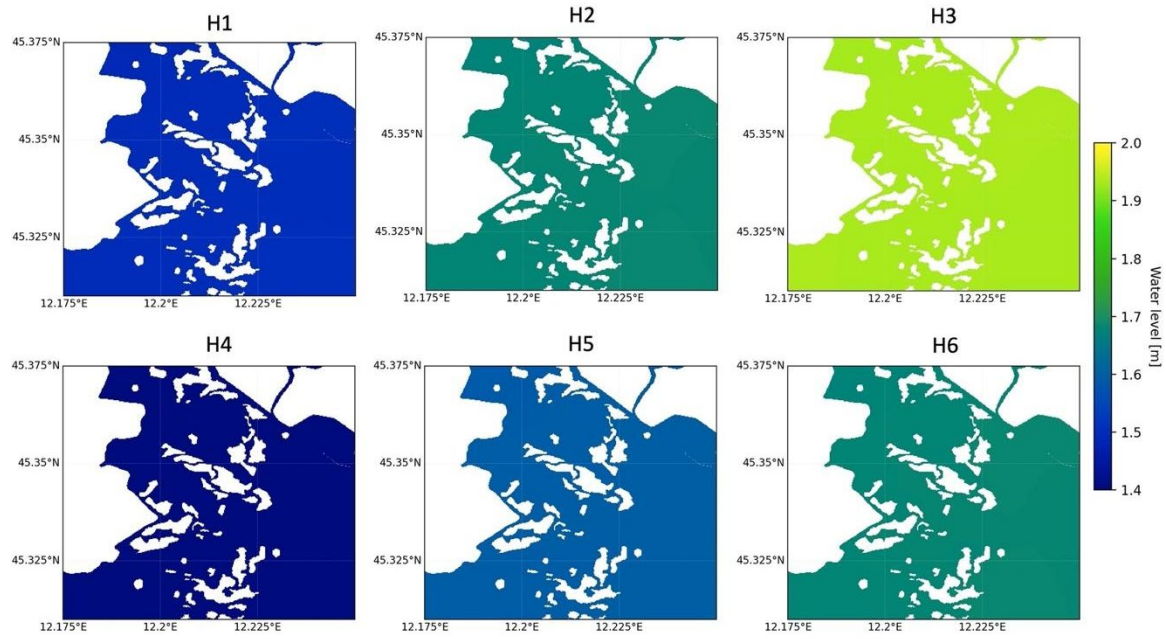


Figure 4.18. Annex 4: Water level for REST configuration

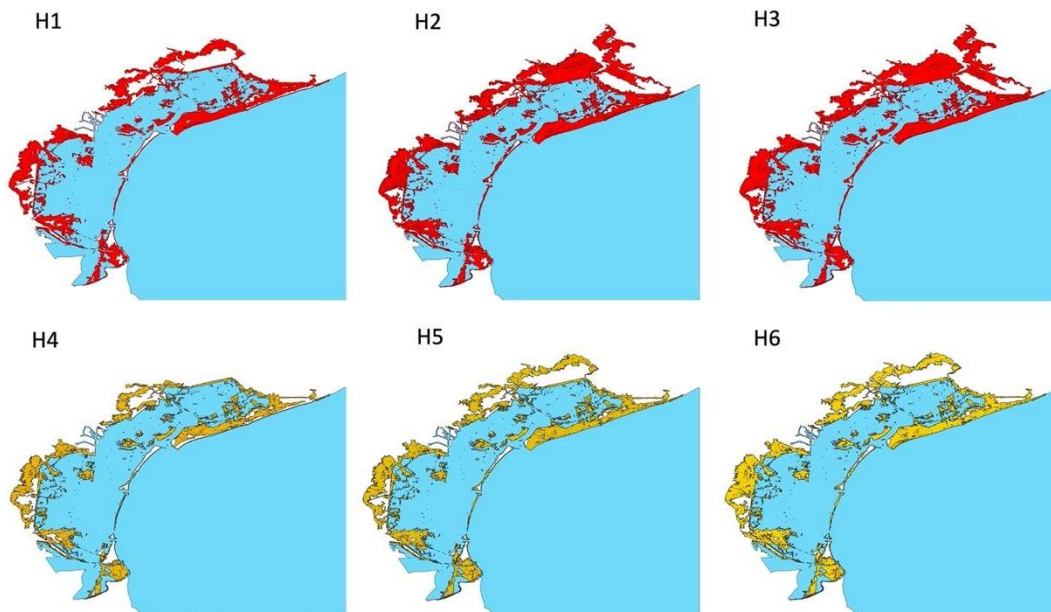


Figure 4.19. Annex 5: Maximum flooded area at lagoon scale for each of the six scenarios

5. Multi-risk projections and climate warnings with ESS in Arcachon Bay Pilot (EGIS, INR)

5.1. Introduction

5.1.1. Context

In the Arcachon Bay, seagrass is experiencing a chronic decline observed since the beginning of the 21st century (Auby et al. 2011). Consequently, the research in WP2 focuses on examining the impact of seagrass restoration on sediment dynamics and subsequent changes in coastal morphology through numerical modeling. This investigation aims to evaluate the potential reduction in coastal erosion risk and the corresponding socioeconomic benefits, such as decreased dredging requirements and improved navigability for fishing and tourism activities.

5.1.2. Objectives

To assess the risk reduction linked to various seagrass restoration approaches (to be executed in Task 2.3), the effects of seagrass on bio-physical and socio-economic factors in the Arcachon Bay are initially analyzed for the present baseline scenario and across different climatic projections (Task 2.2). Specifically, this study endeavors to characterize the socio-economic consequences related to enduring morphological shifts under diverse climatic circumstances, achieved through a combined eco-morphodynamic modeling methodology.

5.1.3. Methodology

Initially, a comprehensive socio-economic analysis is conducted for the Arcachon Bay, wherein the primary economic activities are identified and characterized. Specifically, this analysis delineates their interrelationships with each other and with the natural ecosystem.

Subsequently, the impacts are assessed utilizing the eco-morphodynamic model established in Task 2.1. This facilitates the identification of climatic signals and critical thresholds (tipping points) concerning key coastal parameters. To elaborate, the integrated eco-morpho model of the Arcachon Bay (developed in Task 2.1) is employed to project long-term variations in physical metrics, including erosion/deposition rates and sediment volume near harbor entrances. Moreover, various climatic scenarios are considered, and these physical metrics are quantified across multiple plausible future scenarios.

Finally, the interplay between each economic activity and the model-derived physical metrics is examined to gauge the sensitivity of different ecosystem service sectors to climate impacts.

5.2. Socio-economic analysis

5.2.1. General situation

The Arcachon Bay lies along the southwest coast of France, situated within the Nouvelle-Aquitaine region, covering an expanse of 150 km². Positioned at the southwestern extremity, it opens to the sea between Cap Ferret and Arcachon. Upon analyzing the land cover across the Arcachon Bay territory (as illustrated in the subsequent Figure 5.1), it becomes evident that within the initial 200 meters from the coastline (excluding

wetlands), artificial zones constitute approximately 75%, while forests and semi-natural areas account for roughly 20%, and agricultural lands occupy around 5%.

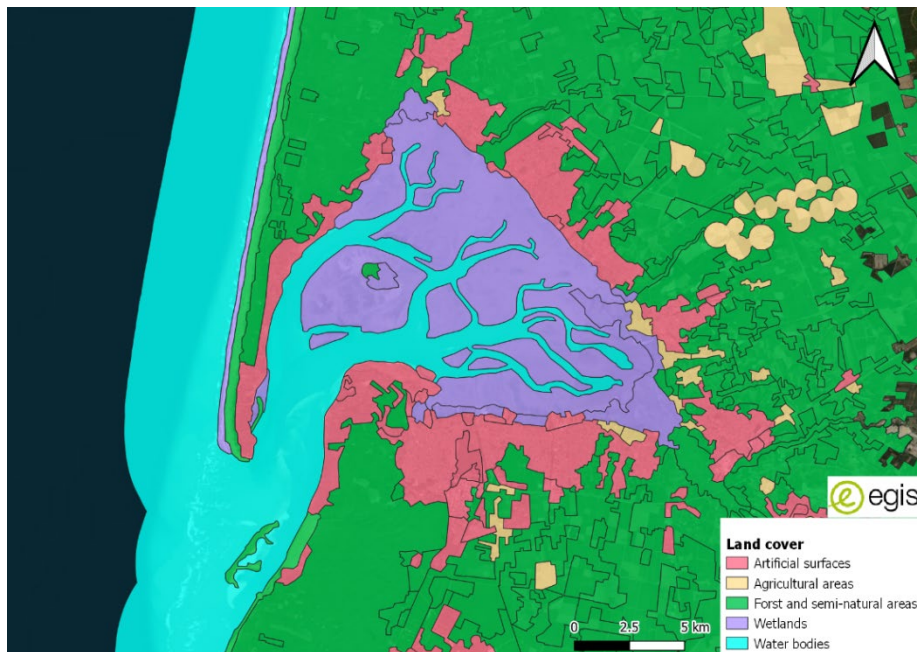


Figure 5.1. Land cover around the Bay (Corine Land Cover)

5.2.2. Port activities

5.2.2.1. Professional and non-professional fishery

The professional and non-professional fishing activities can be delineated and quantified as follows:

- As of 2014, the Bay accommodated approximately 400 professional fishermen (UICN France, 2014).
- The harbor of Arcachon hosts over 110 fishing vessels and annually trades 2600 tons of fish (geoimage.cnes.fr). Extrapolating from the revenue rate of the Gironde estuary, as reported by IUCN France (UICN France, 2014) at €11,500 per ton, this translates to €23 million solely for Arcachon.
- It is crucial to emphasize that fishing in the Bay is subject to regulation by public authorities, with prohibitions enforced near the Birds island, at Humeyre, and in the vicinity of the oyster farms.

The main impacts of professional and non-professional fishing activities on the different ecosystem services provided by *Zostera* seagrass are:

- On ESS water quality and ESS food provisioning: Fishery operations contribute to a significant number of navigation activities, exerting a widespread influence on the biosphere through noise pollution (impacting ecosystem service of food provisioning) and the introduction of hazardous substances (affecting water quality and subsequently, food provisioning). Navigation activities are linked to the concentration of irgarol in the water. Moreover, irgarol imposes constraints on specific phytoplankton populations and contributes to the deterioration of seagrass beds by disrupting photosynthesis processes (UICN France, 2014), (Auby I. et al., 2011).
- Direct impact on seagrass growth: Potential uprooting/crushing of seagrass (less predominant effect due to regulations).

As well, the influence of ecosystem services provided by *Zostera* seagrass on professional and non-professional fishing activities are:

- Impact of ESS erosion on sedimentation in channel, and therefore on navigability is evident (Balle Beganton et al., 2015).
- Professional fishermen capture fishes that take food from the seagrass meadows. Therefore, the link with the ESS food provisioning is then noticeable (Balle Beganton et al., 2015), but difficult to assess.

5.2.2.2. Dredging

To ensure good navigation operations, dredging activities are regularly planned at the harbor entrances within the Bay. Dredging activities in the Bay can be described as follows:

- Major dredging works are carried out roughly on a decadal basis for each channel entrance (Gironde.gouv.fr).
- Curing is done more regularly in specific limited areas: especially harbor entrances.
- The Table 5.1 provides information on the dredged volumes for the period 2018-2023, estimated from 2 000 m³ to 50 000 m³, for a cost of 15.8 €/m³ to 60.3 €/m³, depending on the dredging method. An estimated cost of 50€ is calculated for 1m³ of dredged material, accounting for all costs (tools, workers, before sediment treatment on land...). It corresponds to a mean cost of 1.5M€/yr on a 30 000 cubic meters dredged basis. No future trend for dredging is identified considering all the dependencies.

In recent years, dredging operations have been conducted at the harbors of Andernos-les-Bains, Arès, Gujan-Mestras, Lanton, Biganos, La Teste-De-Buch, and Arcachon, as reported on the Syndicat Mixte des Ports du Bassin d'Arcachon (SMPBA) website. Dredging is performed using either hydraulic dredge pumps or buckets, primarily for remedial purposes (see Figure 5.2). Additionally, the SIBA reports an annual availability of 30,000 cubic meters of sediment.



Figure 5.2. Hydraulic dredge (left) and mechanical dredge (right) [SIBA].



Figure 5.3. Location of the dredging works identified on the SMPBA website (SMPBA 2023)

Table 5.1. Data collected relative to dredging works for the period 2018-2023

City	Dredged volume (m3)	Year	Duration (month)	source	Cost (k€)	Cost /m3 (€/m3)
ANDERNOS	2000	2018	3	SMPBA- www.ecocitoyensdubassindarcachon.org	-	-
GUJAN	15000	2018	3	SMPBA-gironde.gouv.fr	237	16
ANDERNOS	-	2019	2	SMPBA	-	-
LA TESTE	50000	2021	5	SMPBA	-	-
LANTON	10000	2021	1	SPMBA	261	26
LANTON	8000	2022	-	SMPBA	326	41
ARES	10000	2022	1	SMPBA	-	-
LANTON	5800	2023	-	SMPBA	350	60

It is noted that the dredged material is recycled. Ten sediment settling basins are present for sediment recycling, for a total capacity of 78 000 m3. These materials can be used for backfilling for sewage works, creation of forest tracks, topsoil for landscaping.



Figure 5.4. Sediment settling basin (left) and their location (right) [SIBA].

The main impacts of dredging on the different ecosystem services provided by *Zostera* seagrass are :

- Impact on ESS water quality:
 - Dredging remobilizes sediment and therefore increases turbidity.
 - Tributyltin (TBT), an antifouling agent widely utilized in the past but banned since 1982, remains buried in the substrate and could potentially be released if the substrate is dredged too deeply (UICN France, 2014), leading to increased water pollution. TBT significantly impacts the biosphere, particularly affecting oysters. It is associated with mortality in bivalve larvae, reproductive disorders in certain gastropods, and shell malformations in oysters (IFREMER, 1997). Due to uncertainties regarding TBT concentration, substrate location, and dispersion, no quantification has been conducted.

Moreover, any dredging operation can potentially affect the surrounding environment, including habitat degradation, noise pollution, and the remobilization of other contaminants. The extent of these impacts varies depending on the type and scope of the dredging activity.

As well, the influence of ecosystem services provided by *Zostera* seagrass on dredging are:

- Impact of ESS erosion: Seagrass meadows contribute to increased sedimentation by slowing down the flow in their vicinity. Consequently, the necessity for dredging in the channels needs to be reevaluated.

5.2.3. Tourism and marine recreational activities

5.2.3.1. Pleasure boating and navigation

Pleasure boating and navigation in the Bay can be described as follows:

- Some navigation activities within the Bay are associated with fishing operations (as discussed earlier), while others pertain to recreational boating and tourism, such as shuttle services. It is estimated that approximately 12,000 boats traverse the Bay annually (UICN France, 2014).
- Shuttle boats traversing the Bay accommodate approximately 600,000 passengers annually, with up to 60 operations per day during the summer season (SIBA). These boats connect significant tourist destinations such as Arcachon/Moulleau-Cap Ferret and Arcachon-Andernos.
- Additionally, the Banc d'Arguin attracts around 250,000 visitors in July and August (located opposite the Dune du Pilat), making it one of the most popular tourist destinations within the Bay.

- Navigation represents 120 companies, 450 direct jobs and 127 M€ yearly revenue (SIBA, 2023).

The main impacts navigation and pleasure boating on the different ecosystem services provided by *Zostera* seagrass are:

- Impact on ESS water quality: In addition to fishing, navigation exerts a widespread influence on the biosphere through noise pollution and the introduction of hazardous substances.

As well, the influence of ecosystem services provided by *Zostera* seagrass on pleasure boating and navigation are:

- Impact of ESS erosion: Alterations in sedimentation levels within the channels will affect the draft. An adequate draft is essential for operations, particularly during low tide, as stated by SMPBA. This is not quantified.

5.2.3.2. Mooring

Mooring can be described and quantified as follows:

- In 2023, roughly 5000 moorings were available in the Bay, located mainly on the foreshore and in the river La Leyre (parc-marin-bassin-arcachon.fr, prefectorial decree, (Le Corre N. et al., 2015)). This figure has not changed significantly for the past 15 years (Figure 5.5).
- Mooring is regulated: it is forbidden in *Zostera* areas.
- The areas dedicated to mooring are regularly dredged. This was the case for example in 2022 in Arès, for the place called "Trou de Tracasse" (SMPBA). Over a period of two months, dredging operations removed 10,000 cubic meters of sediment from both the channel and the mooring area.

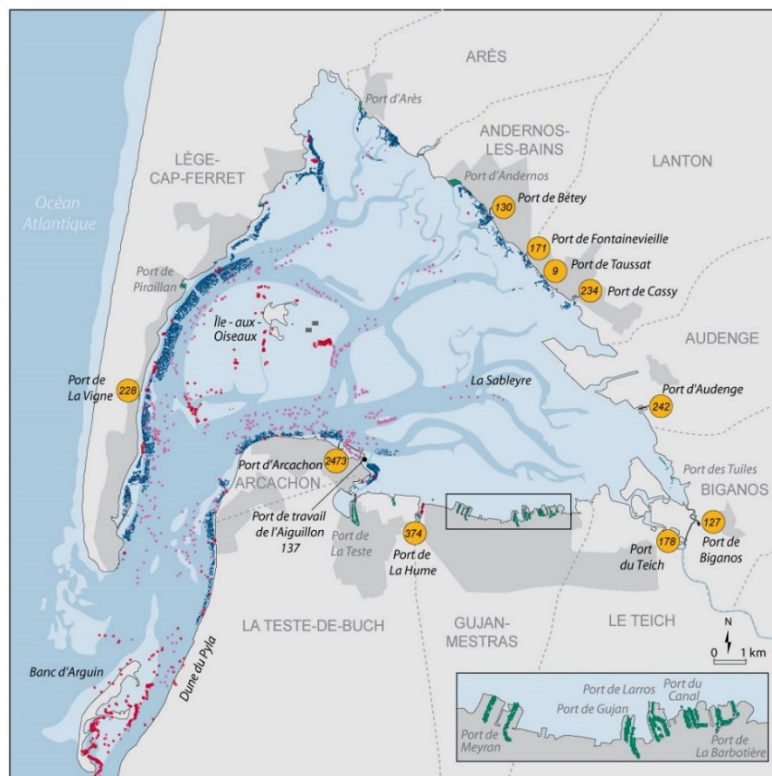


Figure 5.5. Location of moorings (mooring buoy in blue, anchor in red) observed in an afternoon in July 2008 (Le Corre N. et al., 2015)

The main impacts of mooring on the different ecosystem services provided by *Zostera* seagrass are:

- Mooring accounts for a significant portion of the boats navigating in the Bay, consequently influencing the ESS water quality as described before.

As well, the influence of ecosystem services provided by *Zostera* seagrass on mooring are:

- ESS flooding: Vegetation decreases both the flow and wave activity, thereby improving mooring conditions by reducing agitation.
-

5.2.3.3. Residential and general tourism

Residential and general tourism activity in the Arcachon lagoon can be quantified as follows:

- In 2020, the population of the Bay of Arcachon was 138,983, compared to 127,286 in 2014, indicating a growth of 9.2% over 6 years (INSEE).
- During the summer, the population in the area swells to around 400,000, according to SIBA data.
- The Dune du Pilat attracts approximately 1 million tourists annually (Banzo et al., 2018).
- The newly adopted SCOT of 2023 imposes restrictions on new construction, prohibiting development outside already urbanized areas within the first 100 meters from the shoreline, except for public services or specific economic activities. Additionally, the plan outlines demographic evolution objectives, aiming for a growth rate of +1.30% per year until 2030, followed by +1% per year until 2040.
- In 2022, tourism in the Bay represented 760 M€ (SIBA, 2013).

The main impacts of tourism on ecosystem services provided by *Zostera* seagrass are on water quality:

- Population pressure affects water treatment management, with three water treatment plants located in the Bay (SIBA). This pressure can impact water quality, indirectly affecting environmental conditions necessary for the growth of seagrass and the overall biosphere.
- Increased nutrient runoff from human activities and sewage can lead to eutrophication (UICN France, 2014), potentially harming *Zostera* seagrass beds and reducing their ability to provide habitat and food for marine species.

On the other side, the positive influence of ecosystem services provided by *Zostera* seagrass on tourism can be clearly established:

- Healthy *Zostera* seagrass beds contribute to improved water clarity and quality, enhancing the aesthetic appeal of the Arcachon lagoon for tourists (ESS water quality).
- *Zostera* seagrass beds support a diverse array of marine life, including commercially important fish species, which can attract recreational fishermen and contribute to the local economy.
- The presence of thriving seagrass ecosystems can provide natural coastal protection, reducing erosion and safeguarding infrastructure and property, thus supporting the long-term sustainability of tourism and residential development in the area.
- ESS flooding: Potential coastline stabilization favored by seagrass meadows can help preventing coastal areas prone to flooding to be flooded.

5.2.4. Oyster farming

Oyster farming in the Arcachon lagoon can be quantified as follows:

- The Bay of Arcachon hosts more than 300 oyster farming companies (Parc Marin).

- Oyster farming in the region provides employment for approximately 750 people on a permanent basis.
- The total area dedicated to oyster farms covers approximately 780 hectares.
- The oyster farming industry generates an annual revenue of €35 million and accounts for 8% of the French oyster production.

The main impacts of oyster farming on the ecosystem services provided by *Zostera* seagrass are:

- Oyster production relies heavily on water quality, which can be influenced by various factors including pollution and turbidity/sedimentation.
- Historically, the use of tributyltin (TBT) as an anti-fouling agent posed a threat to marine ecosystems, including *Zostera* seagrass beds, before its ban in 1982. Remobilization of TBT from subsoil deposits could potentially harm seagrass habitats and disrupt the ecosystem services they provide (UICN France, 2014).
- Sedimentation resulting from oyster farming activities can affect the light availability and sediment stability necessary for the growth and health of *Zostera* seagrass beds.

As well, the influence of ecosystem services provided by *Zostera* seagrass on oyster farming are clearly identified:

- *Zostera* seagrass beds play a crucial role in maintaining water quality by filtering pollutants and stabilizing sediments, thereby indirectly supporting the health and productivity of oyster farming operations.
- The presence of healthy *Zostera* seagrass habitats can enhance local biodiversity, providing important nursery and foraging grounds for various marine species that contribute to the ecological balance of the Bay of Arcachon.
- *Zostera* seagrass beds help to mitigate coastal erosion by trapping sediment and dampening wave energy, which can protect oyster farming infrastructure and ensure the long-term sustainability of the industry in the face of changing environmental conditions.

5.2.5. Conclusion

The socio-economic analysis conducted earlier is summarized in the table below, preceding the impact assessment in the subsequent section.

Table 5.2. Summary of socio-economic analysis

Activity	Estimated yearly economic significance	Main impacts of activity on ESS	Main impact of ESS on activity
Fishing	>23 M€ revenue	ESS Water quality ESS food provisioning	ESS erosion ESS food provisioning
Dredging	1.5M€ cost	ESS water quality	ESS erosion
Boating and navigation	127 M€ revenue	ESS water quality	ESS erosion
Mooring			
Residential and tourism	760 M€ revenue (200 M€ in touristic housing only)	ESS water quality	ESS water quality ESS flooding
Oyster farming	35M€ revenue	ESS water quality ESS erosion	ESS water quality ESS erosion

5.3. Impact assessment

5.3.1. Method

Following the above socio-economic description of the Arcachon Bay, numerical model results obtained using the eco-morphodynamic D-FM model are used to assess the impacts on the various socio-economic indicators associated to changing forcing conditions (climate scenarios).

The model and its characteristics in terms of physical and numerical considerations, forcings, extents, processes represented, etc. has been detailed in the previous deliverable D2.1. The coupled eco-morphodynamic model has been calibrated and validated for the period 2016-2019, representing correctly the trends and order of magnitude of the morphological changes that occurred. Two main models have been implemented:

- an eco-morpho-hydro model aiming at representing morphological changes and functioning with a morphological acceleration factor,
- an eco-wave-hydro model aiming at calculating water renewal time, plume dispersion, storm impacts, etc.

For this deliverable D2.2., the focus was on utilizing the first model to estimate the bio-physical indicators necessary for assessing damages in future scenarios. Additionally, preliminary findings from the second model are provided, which assess water renewal and flushing times.

The following sections are more specifically addressing the definition of the forcing conditions, the assessment of indicators in terms of sediment dynamics (mainly related to ESS erosion) and their sensitivity to changing climate conditions.

5.3.2. Current and climatic forcing conditions

To align with the methodologies adopted in other pilot sites, the focus was placed on projecting future scenarios for the years 2050, 2070, and 2100. From a modeling standpoint, these future horizons involve translating changes in environmental forces (such as wind, waves, tide, etc.) and defining climate conditions based on global climate scenarios. Two global climate scenarios were chosen: "business-as-usual" SSP2-4.5 and "pessimistic" SSP5-8.5.

5.3.2.1. Water levels

Anticipated rising sea levels are poised to directly influence the hydrodynamic circulation within the Arcachon Bay, thereby impacting water renewal, wave dynamics, and erosion/sedimentation patterns, consequently leading to morphological alterations within the bay.

Figure 5.6 shows the regional projections of water level rise, as reported by IPCC AR6 for the North-European Atlantic coast, with projected sea level rises of 0.21 / 0.23, 0.34 / 0.39 and 0.53 / 0.79 m for the years 2050, 2070, and 2100 respectively, compared to the current level (mean 1995-2014) and for the two selected climate scenarios (SSP2-4.5 / SSP5-8.5).

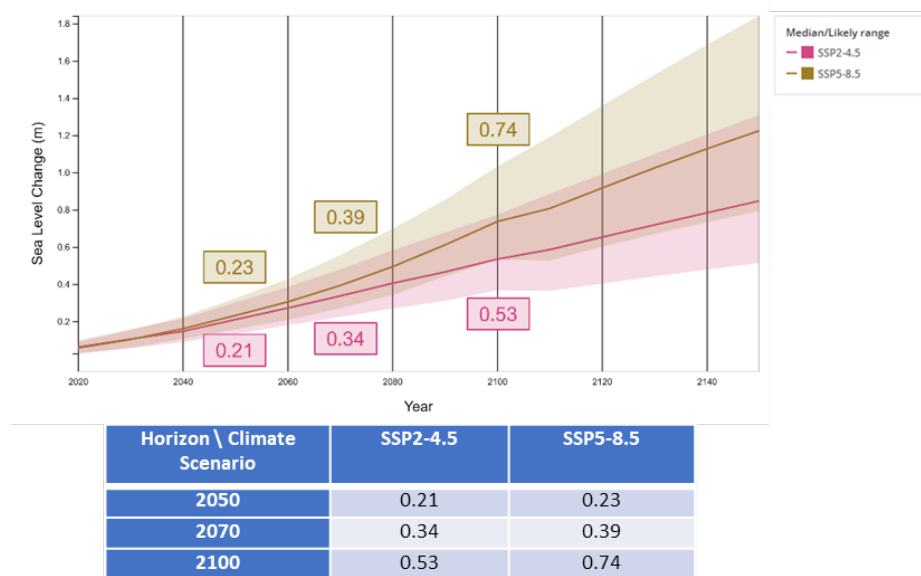


Figure 5.6. Sea level rise projections (m), median and likely range, for two climate scenarios: SSP2-4.5 and SSP5-8.5. Extracted from "<https://sealevel.nasa.gov>".

5.3.2.2. Wind

IPCC projections regarding wind magnitude are represented in Figure 5.7, suggesting a decrease of the mean surface wind (-2.6% by 2100 for scenario SSP5-8.5).

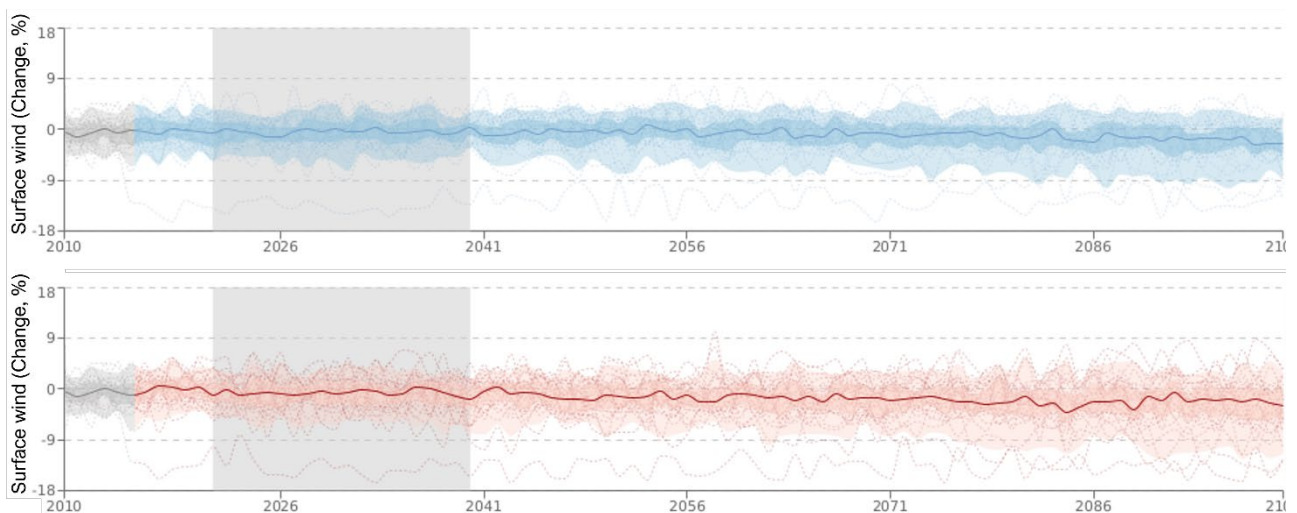


Figure 5.7. Surface wind projections (% of change). Ensemble mean (solid line) and confidence interval are represented for climate scenarios SSP2-4.5 (blue) and SSP5-8.5 (red).

Based on meteorological data collected from the Météo-France station situated in Cap Ferret, general projections can be derived through the analysis of trends observed over the past decades.

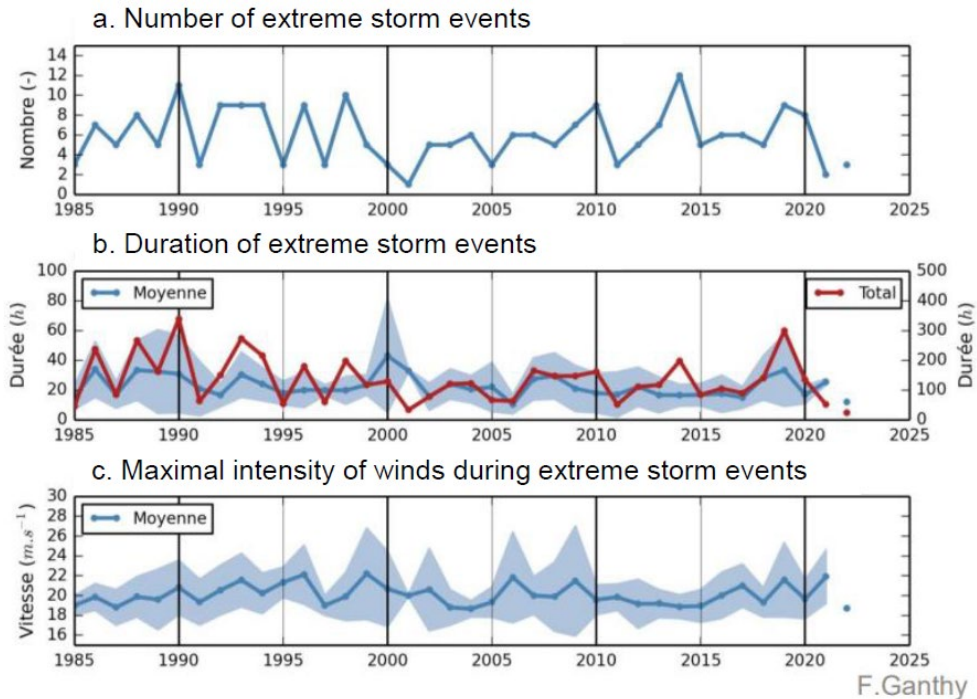


Figure 5.8. Storm events analysis in term of number (a), duration (b) and intensity (c). From Ganthy F., Ifremer (personal communication).

After examining extreme wind events dating back to 1985, no significant trend in the frequency or duration of these events is evident. However, a minor uptick in the intensity of maximum wind speeds can be observed. Despite these observations, the extreme values utilized in the preceding deliverable D2.1 remain applicable for future climate scenarios

5.3.2.3. Waves

The analysis of meteorological data indicates a lack of discernible trends in storm events affecting the Arcachon Bay. Unlike offshore waves, which are typically impeded by the passes situated at the bay's entrance, Arcachon Bay experiences more pronounced impacts from changes in water levels and wind phenomena (Parisot et al., 2008). Consequently, for this study, the wave conditions for future scenarios are assumed to remain consistent with current conditions, as outlined in deliverable D2.1.

5.3.2.4. Bathymetry

The coupled eco-morpho model has been validated using bathymetric surveys conducted in 2016 and 2019, demonstrating its capability to accurately assess morphological changes over a three-year period in this intricate coastal estuarine setting. However, this validation period is insufficient for predicting morphological changes over multiple decades. Forecasting long-term trends in morphological changes poses challenges and prompts inquiries into the existence and nature of morphological equilibrium. Nevertheless, attaining such equilibrium is elusive due to the constant evolution of external conditions (Dronkers 1986; Dam et al., 2016). The potential for reliable predictions in realistic environments remains uncertain (De Vriend et al. 1993; Haff 1996, 2013; Stive and Wang 2003; Dam et al. 2016).

In this context, various methodologies have been explored to evaluate morphological projections for the Bay, including considerations of tidal asymmetry (not reported here). However, due to the uncertainties inherent in these projections, a more straightforward approach has been adopted. The current methodology involves shorter simulations spanning a three-year period, utilizing a morphological acceleration factor. The initial bathymetry remains the same for each scenario, except for the inclusion of sea level rise (SLR). Subsequently, the effects of varying SLR scenarios are examined after a three-year simulation period to assess various biophysical indicators outlined in this study.

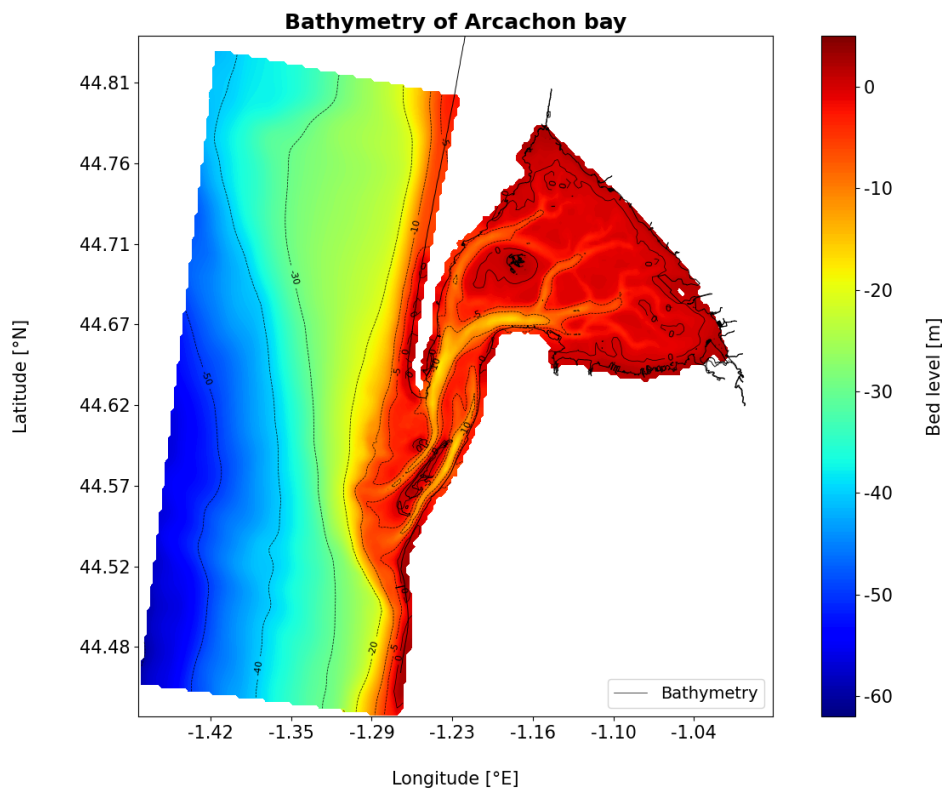


Figure 5.9. Initial bathymetry applied in the model (m with respect to current MSL).

5.3.3. Sediment dynamics

Seagrass meadows, acting as genuine ecological engineers in marine coastal regions, directly influence sediment dynamics. The influence of seagrass on sediment dynamics can be delineated across various aspects:

- Stabilization of the seabed within restored seagrass areas
- Alterations observed in the vicinity of existing seagrass zones
- Influence on channel morphology
- Impact on sediment grain size distribution
- Assessment of sedimentation patterns within port environments

Each of the aforementioned aspects is associated with quantifiable indicators that can be assessed using the sophisticated modeling tool. These indicators include erosion and sedimentation rates within seagrass areas, mudflats, and channels, as well as turbidity, water renewal time, sediment granulometry, and sedimentation around harbors.

Initially, the model incorporates the influence of seagrass on hydrodynamics, attenuating currents and waves as described in deliverable D2.1. Reduced currents in vegetated regions typically result in increased sedimentation within and around those areas. Consequently, higher vegetation density is expected to enhance currents within channels, leading to elevated flow velocities and subsequently, greater transport rates. Secondly, the vegetation module reduces bed shear stress and consequent sediment transport in vegetated zones, thereby stabilizing the seabed.

5.3.3.1. Impact on seabed stabilization in seagrass areas

Seagrass plays a crucial role in capturing sediment from the water column, thereby reducing water turbidity. This dual effect promotes both the growth of seagrass and extends its depth range. As turbidity diminishes, light can penetrate deeper into the water column, facilitating seagrass growth at greater depths (Maxwell, P. et al., 2016). This dynamic creates a positive feedback loop that enhances seagrass growth.

5.3.3.2. Impact in the vicinity of seagrass area

The presence of the seagrass meadow influences adjacent areas, particularly by altering hydrodynamic patterns (see deliverable D2.1).

We can examine three key aspects:

- The effect on salt marshes
- The impact on mooring capacity
- The influence on coastline stabilization

These aspects will be further elaborated upon without specific quantification at this stage.

Impact on salt marshes

Reeves et al. (2019) and Donatelli et al. (2018) show that salt marsh systems can be significantly influenced by the adjacent seagrass dynamics. Indeed, the amount of sediment delivered to the salt marshes are dependent of the state of the seagrass meadow, and this coupled evolution is on large time scales of decades to centuries. Seagrass meadows trap more sediment when prograding because of shear stress reduction, implying less suspended sediment available for deposition on the salt marshes. On the contrary, if vegetation on meadows dies, sediment is liberated and can go from the meadows to the salt marshes. Therefore, when salt marshes prograde, seagrass meadow tend to decline, and this interaction tends to be enhanced. Conversely, if seagrass meadows grow, salt marshes tend to decline, allowing for seagrass meadow progradation. This constitutes a positive feedback loop, which is especially pronounced when sediment is preserved within a relatively confined environment or back-barrier setting.

Impact on mooring capacity

The zones designated for mooring undergo regular dredging maintenance. If sedimentation decreases in the vicinity of seagrass areas, there may be a reduction in the need for dredging in mooring zones. Consequently, this could potentially increase mooring capacity, leading to positive effects on recreational boating and tourism. Furthermore, seagrass meadows tend to diminish current velocities, which could result in reduced agitation in mooring areas and potentially extend their operational timeframe.

Impact on coastline stabilization

Potential change in wave height and direction, as well as currents, can induce a change in longshore transport. Therefore, the extent of coastline retreat may vary depending on the orientation of the coastline and the alterations in environmental conditions.

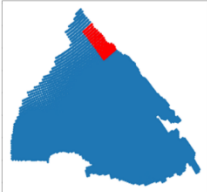
Seagrass meadows help reducing wave agitation (Dinu et al., 2013). Deriving the change in wave energy from the change in wave height allows to estimate the change in longshore transport. For example, on the study case of a part of the southern Romanian coast conducted with SWAN model, a reduction of 5% in wave height has led to a 12% decrease in longshore transport. This is especially influenced by the extent of the vegetation meadow (and its proximity to the coastline), the wave climate and the local bathymetry.

5.3.3.3. Impact on sediment size

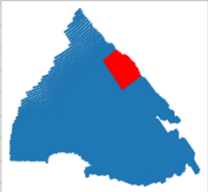
Seagrass meadows, when dense, captures fine material by reducing turbulence and increasing deposition. Therefore, sediment distribution in high-density seagrass meadows tends to become muddier. However, in low-density seagrass meadows, turbulence increases at the edges of the meadows putting small sediment in suspension and then increasing the mean sediment size (Maxwell, P. et al., 2016).

Table 5.2. Mudfraction change (%) between the beginning and the end of the run (3 years simulation) for current (reference) and future horizons. Location of each area considered (red) on following maps.

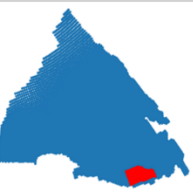
SSP5-8.5					
Future horizon		2020	2050	2070	2100
Areas around harbors	Ares	16.30	15.80	15.23	15.28
	Andernos	12.47	13.07	12.99	13.42
	Gujan	15.18	15.54	14.92	13.96
	La Teste	18.37	19.04	17.89	15.15
Mudflats		6.48	6.56	6.21	6.42
Bottom of the Bay		5.48	5.62	5.02	5.01



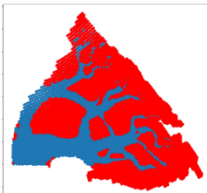
Ares




Andernos



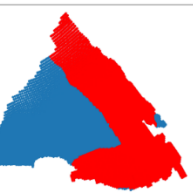
Gujan



Mudflats



La Teste



Bottom of the Bay

The evolution of the mud fraction for a 3-years period has been simulated, for different areas, and different horizons. The modelling results (Table 5.3) support the increase of mud fraction for the bottom part of the Bay and the mudflats, in line with historic observations (Cognat, 2019). Concerning the evolution around harbor entrances, except for Ares, the mud fraction is predicted to increase quicker in 2050 and slower in 2070 and 2100, than in the current state. In Ares, the difference between the beginning and the end of the run decreases at each horizon with SLR increase.

A trend is difficult to predict with those results, as changes between horizons are insignificant. However, it seems that higher mean sea level reduces the deposition of mud in the vicinity of harbors. The evolution for mudflat is stable and no real impact of SLR is noticeable.

5.3.3.4. Erosion/sedimentation of channels

The impact on sedimentation within the channel is analyzed for both primary and secondary channels. Considering the model configuration and assumptions, only channels wider than 200 meters are taken into consideration. These channels are highlighted in blue on the "Mudflat" map provided in Table 5.2.

The variation in sedimentation across different scenarios is determined by comparing the bathymetric changes from the beginning to the end of the three-year simulation period. This difference allows for the assessment of the percentage increase or decrease in sedimentation, as well as an estimation of the corresponding volume change

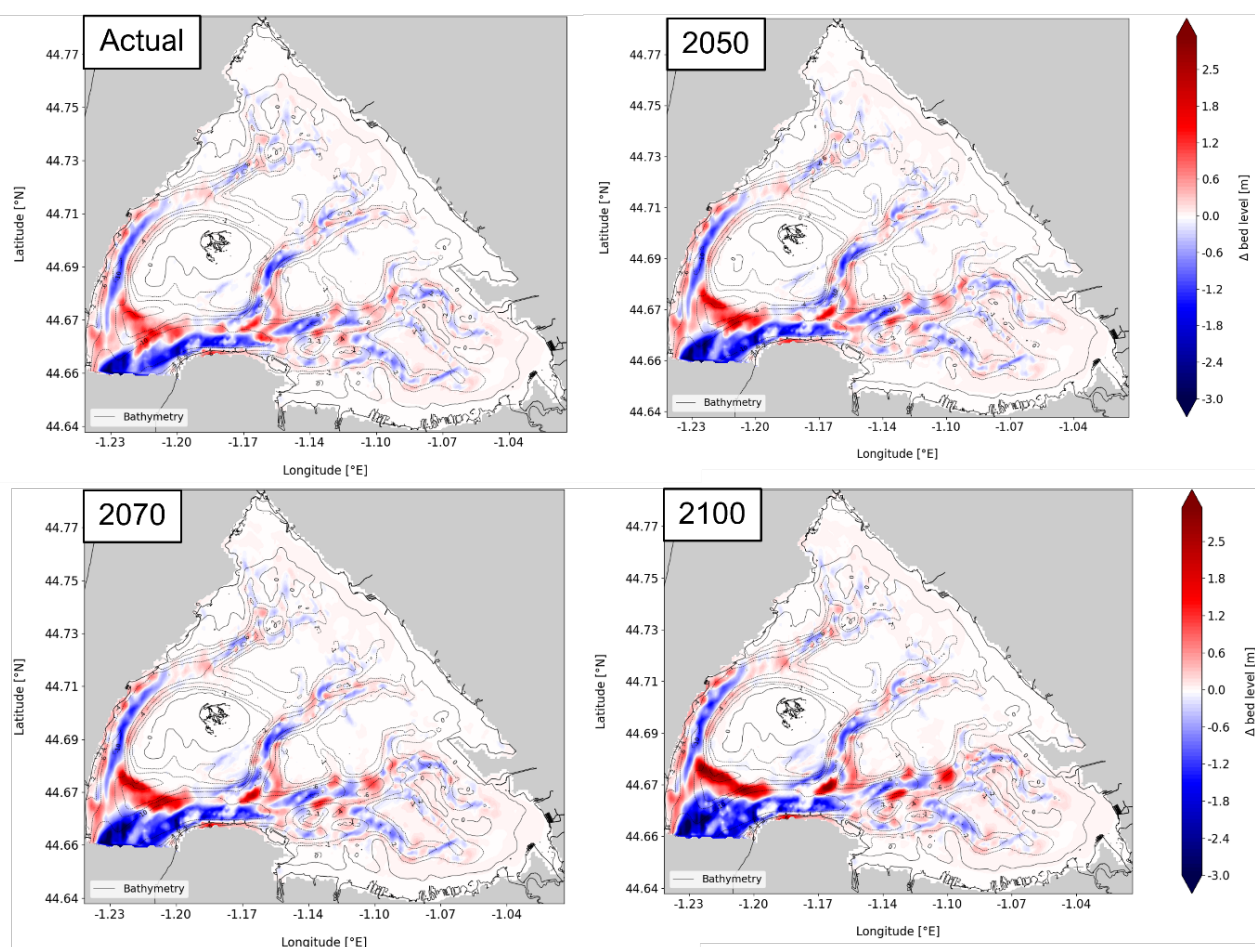


Figure 5.10. Morphological changes (m), calculated over 3 years for future horizons and corresponding SLR.

The morphological changes simulated over three years for the various targeted horizons reveal consistent trends (Figure 5.10). These trends indicate erosion in the channel east of Arcachon, sedimentation in the southwestern portion of Ile aux Oiseaux, and noticeable erosion/sedimentation patterns within the main and secondary channels. Sedimentation is also observed on the mudflats near the river mouth of La Leyre. Across the entire bay, the average bed evolution rates for channels are -3.1, -3.6, -3.9, and -4.4 cm per year for the current state, 2050, 2070, and 2100 respectively. For mudflats (see Table 6-3, "Mudflats"), rates of +0.4, +0.5, +0.6, and +0.7 cm per year are recorded. Regarding the secondary channel situated at the highest part of the bay, the mean bed evolution rates are -2.0, -1.9, -1.9, and -1.1 cm/year for the current, 2050, 2070, and 2100 horizons respectively.

In summary, with an increase in sea level rise (SLR), erosion and sedimentation rates become more pronounced, and the areas affected by erosion or sedimentation remain comparable to those in the current situation.

5.3.3.5. Impact on modification of draft

The decrease in sedimentation within the channel (particularly post-dredging) results in an augmentation of the draft, which can prove advantageous, particularly during low tide. This connection and its implications for various uses have been recognized by SMPBA.

5.3.3.6. Sedimentation in the vicinity of ports

Following the global overview detailed in section 5.3.3.3, a more thorough analysis of the Bay's innermost part has been conducted to forecast potential changes associated with dredging requirements near harbor entrances. The subsequent Table 6.4 displays the outcomes in terms of sediment deposition volume (expressed as a relative difference over a three-year period in percentage) for areas situated near four harbor entrances.

Table 5.4. Relative difference over 3 years (%) in term of volume deposited for areas around harbors entrances for current, 2050, 2070 and 2100 horizons.

SSP5-8.5				
Horizons	2020	2050	2070	2100
Ares	1.04%	1.13%	1.20%	1.32%
Andernos	0.82%	0.84%	0.86%	0.84%
Gujan	1.74%	1.85%	1.94%	2.08%
La Teste	0.56%	0.57%	0.53%	0.44%

Ares
Andernos
Gujan
La Teste

The change in deposited volume around harbors remains relatively constant, with a peak of +0.3% observed for Gujan between the year 2100 and the current situation. Within the chosen areas, no notable influence of sea level rise (SLR) could be identified, and the deposited volume is not anticipated to decrease with SLR.

5.3.4. Water quality

Seagrass meadows play a significant role in influencing the water quality within the Bay, contributing to changes in suspended sediment concentration, according to Arias (2022). Studies by Pelisson (2019) and Arias

(2022) employing modeling approaches have indicated that current levels of suspended sediment concentration are 2 to 10 times higher compared to concentrations prior to the regression of seagrass. This section examines water renewal by studying the overall renewal time of the Bay and the dispersion of potential pollutants originating from harbors under future climate conditions

5.3.4.1. Water renewal

The study of water renewal in Arcachon Bay relies on the calculation of flushing time using the model. According to Plus et al. (2009), flushing time is defined as the duration required for a significant portion of a water parcel to be replaced by water originating from outside the lagoon boundaries. In this study, a passive tracer is introduced with a theoretical concentration set at 1.0 (or 100%) throughout the Bay. The time taken for the tracer concentration to decrease below 37% of the initial concentration (i.e., e^{-1}) is noted, representing a threshold for the replacement of the water parcel. Employing this approach, Plus et al. (2009) calculated a water flushing time in the bay as 18.9 days under current conditions. By applying similar forcings (i.e., tidal currents and excluding wind waves and Leyre flow), our model yields flushing times of 20.0, 19.6, 19.6, and 19.2 days for current, 2050, 2070, and 2100 conditions, respectively. The difference between computed water flushing times may be associated to the influence of vegetation on hydrodynamics, that is incorporated in our modelling approach.

Flushing time calculations are also conducted in proximity to harbor zones (Figure 5.11). The objective is to evaluate the potential rate of water renewal around these potentially contaminated regions. These renewal times are assessed across various climate scenarios to comprehend the potential impact of sea level rise (SLR). It is observed that increasing water levels generally result in a quicker pace of water renewal, indicated by a faster decline in tracer concentration. The disparities between scenarios are more noticeable for Gujan, Lanton, and Ares. For instance, at Gujan harbor, tracer concentration reaches zero on day 4 for the 2100 scenario, while it takes less than 10 days to reach zero in the current situation.

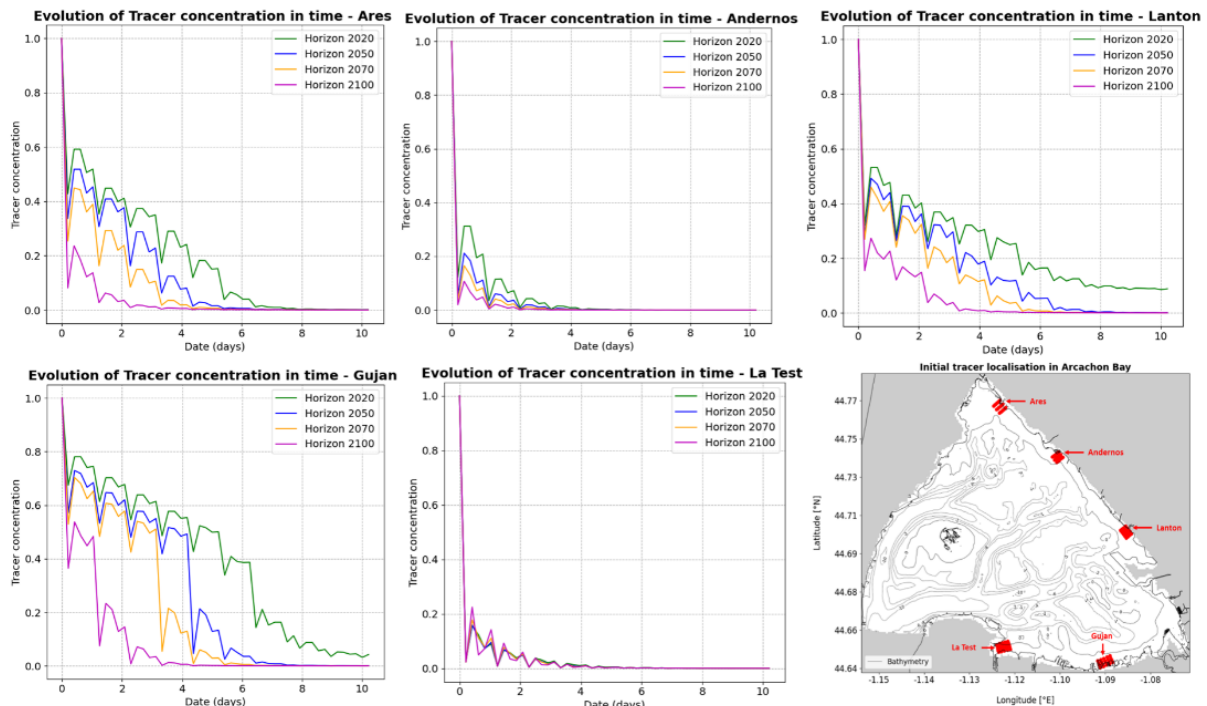


Figure 5.11.. Evolution of tracer concentration (1 initially) for 5 harbors and 4 horizons over 10 days of simulation.

5.4. Sensitivity of ESS to climate forcing and multi-impact chains

Further below, each subsection focuses on a specific ecosystem service (ESS) potentially provided by the seagrass meadow. The interactions depicted in the sketches between various processes (represented as boxes) are elaborated upon, with processes being described and, if possible, quantified using the model or literature as previously outlined. Uncertainties and further questions arising from the study are also addressed. Processes may be interconnected between different ESS, and if so, this is indicated.

While there is a particular emphasis on ESS erosion, the impact of various climate forcing on the ESS water quality is also depicted based on an understanding of the system, although specific links have not been quantified.

5.4.1. Sediment management

The ESS Erosion facilitated by seagrass is a complex and multifaceted mechanism. Seagrass meadows exert influence on sedimentation, impacting sediment size, seabed stabilization within seagrass meadows, in areas adjacent to seagrass, and within channels. The assessment of impacts conducted in section 5.3 enables the evaluation of the sensitivity of these impacts to changing climatic conditions.

As mentioned previously, while the impact of vegetation has not yet been fully assessed (as it will be in Task2.3), there is a climate change sensitivity regarding channel filling and sedimentation in mudflat zones. Channel erosion increases with higher sea level rise (SLR) across the entire bay, although establishing a trend at the bay's innermost part is more challenging. This directly affects dredging requirements and changes in draft, impacting navigation-related activities, as illustrated in the diagram (Figure 5.12). Changes in navigation duration (for pleasure boating, tourism, and fishing) and direct costs associated with dredging operations are affected. The diagram underscores the indirect impacts on seagrasses through water quality deterioration (potential remobilization of TBT and increased presence of toxic substances as navigation intensifies).

Currently, within the innermost part of the bay, SLR does not appear to significantly affect sedimentation. Therefore, vegetation restoration could prove beneficial in influencing dredging needs near harbor entrances. The link between changes in sedimentation and alterations in navigation duration has been noted by SMPBA. For instance, in 2021 at La Teste-De-Buch, dredging of 50,000 cubic meters of sediment resulted in fishing professionals and pleasure boaters experiencing an increase of 1.5 to 2 hours of navigation time around low tide. It can be inferred that reduced sedimentation, leading to increased draft, allows for longer navigation operations, thereby generating positive economic impacts. Specifically, an increase in draft could benefit pleasure boating, tourism, and fishing activities.

With higher SLR, sedimentation on mudflats is anticipated to surpass current levels. This could impact coastline stabilization by increasing sediment deposition near the coast, as elucidated in the impact assessment section. Consequently, the intrusion of seawater may be affected, establishing a connection with flood control and impacting land cover and tourism.

The summarized diagram outlining the impacts of ESS erosion facilitated by seagrass is provided below:

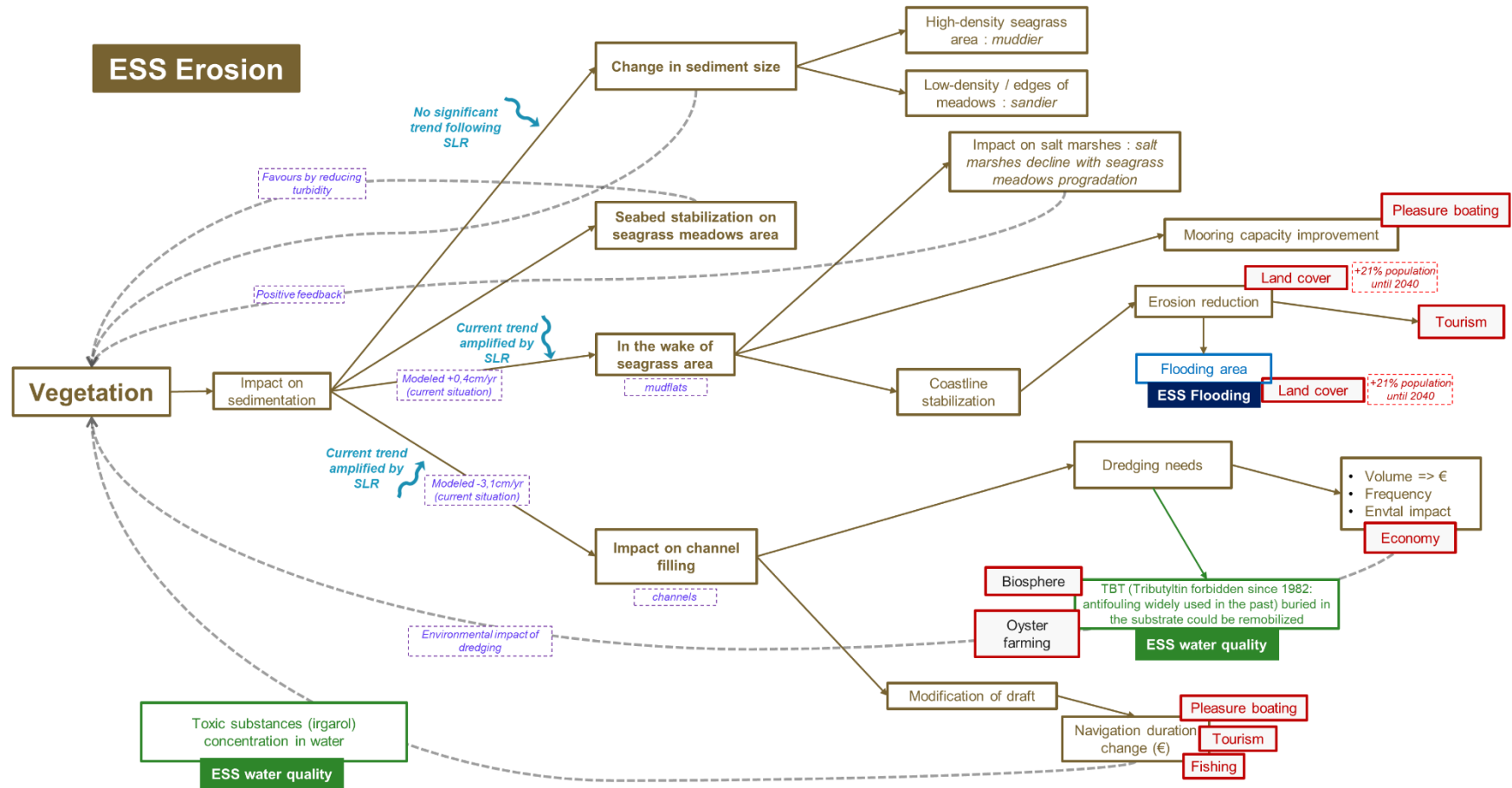


Figure 5.12. Multi-impact chain and climate sensitivity for ESS erosion.

5.4.2. Water quality

The impact of climate change on the ESS water quality provided by seagrass meadows manifests in alterations to renewal times in the Bay. It has been modelled that renewal time for the whole Bay is expected to decrease by 4% until 2100. The renewal time for areas close to harbors is also expected to decrease when already important in the current situation: it would be divided by 3 until 2100 for Arès, Lanton, and Gujan, due to sea-level-rise.

Numerous feedback mechanisms are also highlighted in the literature:

- *Zostera* seagrasses possess the ability to absorb toxic substances (such as irgarol), thereby aiding in reducing their concentrations in the water (UICN France, 2014). Irgarol is particularly associated with navigation activities (fishing, tourism, pleasure boating), and an increase in irgarol concentration can lead to a restriction of phytoplankton populations.
- *Zostera* contributes to the natural regulation of nitrogen concentrations originating from wastewater (UICN France, 2014), via eutrophication.
- High-density seagrass, especially in sheltered environments, absorbs more ammonium, thereby reducing toxicity and promoting seagrass growth, thus establishing a positive feedback loop (Maxwell, P. et al., 2016).
- Another positive feedback loop is associated with sediment trapping: *Zostera* limits the suspension of fine particles, thereby enhancing water transparency.
- Nevertheless, negative feedback mechanisms are also identified in the literature (Maxwell, P. et al., 2016). One such mechanism is sediment sulfide toxicity: high-density seagrass traps organic matter, which decomposes and releases sulfide, impairing seagrass growth. This mechanism becomes more pronounced with higher temperatures.
- Additionally, photosynthesis leads to elevated pH levels, which inhibit seagrass growth in sheltered environments.

As evidenced by the impact assessment, changes in climate forcing will impact the renewal time of chemicals and pollutants. The synthetic diagram linking ESS water quality and socio-economic impacts is depicted below:

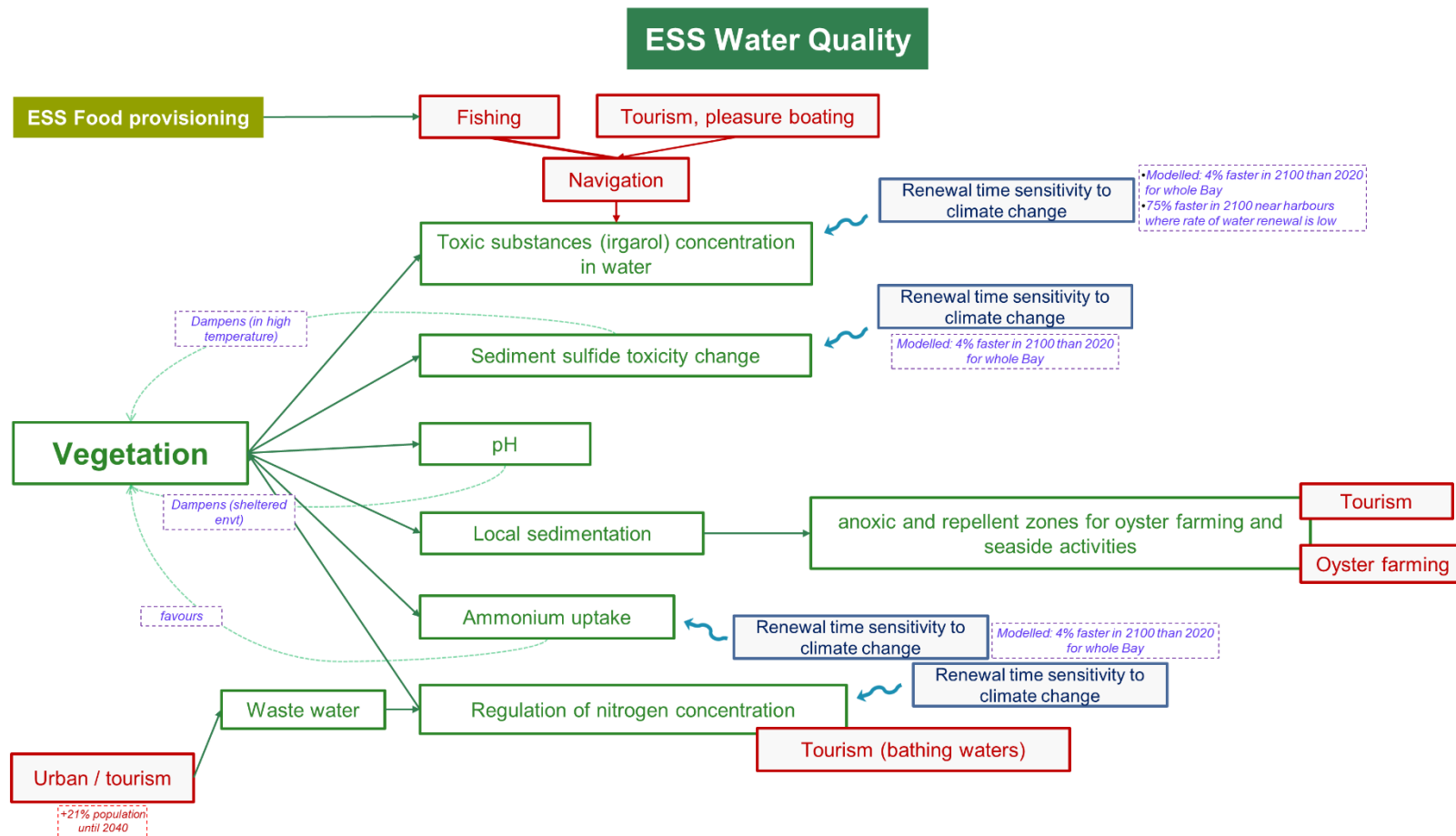


Figure 5.13. Multi-impact chain and climate sensitivity for ESS water quality

5.5. Conclusion

The aim of the current deliverable is to assess the projections of ecosystem-services (ESS) provided by seagrass meadows within the Arcachon Bay for different future horizons: 2050, 2070 and 2100. In particular, this study characterizes the socio-economic consequences related to enduring morphological shifts under diverse climatic circumstances, achieved through a modeling approach.

After a comprehensive socio-economic analysis, the main economic activities have been identified. The impacts are then assessed using the eco-morphodynamic model. When possible, the quantification of bio-physical indicators needed for assessing sensitivity of ESS to climate forcings is presented. In the last section, the interplay between each economic activity and the model-derived physical metrics is examined. This work led to the conception of multi-impact chains for the main ESS aimed: Sediment management and Water quality.

In conclusion, the modeling tool helped to assess some trends for sediment management, linked with SLR. With higher SLR, sedimentation on mudflats is anticipated to increase, with a consequence on flood control. However, the erosion of channels, connecting harbors to the Bay, could benefit pleasure boating, tourism and fishing activities. SLR, and morphological changes associated, have a noticeable effect on water renewal times. Modeling results show an increase in water renewal, leading to an improved water quality in the Bay.

This modular approach we developed helps to estimate the risk reduction from ESS as a function of projection time horizon, and enables the future introduction of restoration scenarios to be executed in Task 2.3.

6. Multi-risk projections and climate warnings with ESS in Sicily Lagoon Pilot (UC)

The University of Catania (UC) is leading research activities within the REST-COAST project to evaluate the effectiveness of a suite of coastal restoration measures at the Sicily pilot site, focusing on the Cuba-Longarini coastal lagoon system, part of the Natura 2000 network under the Lagoons of the South-East of Sicily. The study area is characterized by complex challenges, including flood and erosion risks affecting the village of Granelli and ongoing anthropogenic pressures that threaten lagoon biodiversity and water resources.

To address these issues, UC collaborates with local site managers to assess restoration strategies aimed at enhancing biodiversity and increasing the delivery of ecosystem services linked to coastal risk mitigation. In addition to ongoing pro-biodiversity interventions—such as the construction of artificial islands and improved hydraulic connectivity between lagoon sectors—further measures under investigation include: (i) revegetation of the dune belt between Granelli and the sea, and (ii) expansion of the existing seagrass meadow along the Granelli coastline.

The performance of these solutions is evaluated through numerical modelling, which simulates system responses to extreme events under current and projected climate scenarios. This includes considerations of sea level rise and changes in wave climate, with the goal of quantifying the impact and resilience of restoration strategies. In the present contribution, results of the abovementioned numerical models are discussed, and performance of NbS is evaluated through simple efficacy indicators.

A detailed description of the hydrodynamic scenarios, the input datasets, as well as the model setup and validation procedures adopted in this study, can be found in Deliverable 2.1 of the REST-COAST project.

6.1 Plan of simulations

By combining a full set of hydrodynamic scenarios (explained in D2.1) with the three restoration configurations—namely the no-NbS (NN), dune revegetation (DR), and seagrass meadow reconstruction (SR)—a total of 45 numerical simulations were carried out using the eco-hydro-morphodynamic modelling chain. The plan of the simulations is shown in Table 6.1.

6.2 Performance of the Nature-Based solutions under different climate scenarios

In the present section, results from the simulations are shown and performance of the investigated Nature-based Solutions to reduce coastal hazard is evaluated by means of simple efficiency indicators. To assess the performance of the solution to reduce flooding risk, efficiency of flooding reduction E_f is evaluated:

$$E_f = \frac{A_{f,NN} - A_{f,NbS}}{A_{f,NN}} \cdot 100 \quad (6.1)$$

where $A_{f,NN}$ is the flooded area due to inundation in no-NbS conditions, $A_{f,NbS}$ is the flooded area due to wave storm considering an NbS option (dune revegetation or seagrass revegetation). An efficiency indicator for flooding reduction for the city area E_{fc} is also computed, which is calculated analogously to E_f , but including the flooded areas due to inundation in the city area only. Flooding efficiency indicators E_f and E_{fc} are schematized in Figure 6.1a and 6.1b respectively.

Table 6.1. Plan of simulations

id	T_r [years]	Restoration scenario	Climatic scenario	H_s [m]	T_p [s]	SLR [m]
1	5	Current state (no NbS)	Present (SP)	4.26	9.65	0.00
2			S4.5-2070	5.68	10.42	0.37
3			S4.5-2100	5.16	10.14	0.57
4			S8.5-2070	5.22	10.20	0.48
5			S8.5-2100	5.48	10.34	0.78
6	5	Dune revegetation	Present (SP)	4.26	9.65	0.00
7			S4.5-2070	5.68	10.42	0.37
8			S4.5-2100	5.16	10.14	0.57
9			S8.5-2070	5.22	10.20	0.48
10			S8.5-2100	5.48	10.34	0.78
11	5	Seagrass revegetation	Present (SP)	4.26	9.65	0.00
12			S4.5-2070	5.68	10.42	0.37
13			S4.5-2100	5.16	10.14	0.57
14			S8.5-2070	5.22	10.20	0.48
15			S8.5-2100	5.48	10.34	0.78
16	50	Current state (no NbS)	Present (SP)	5.61	10.37	0.00
17			S4.5-2070	8.06	11.52	0.37
18			S4.5-2100	7.21	11.16	0.57
19			S8.5-2070	6.67	10.95	0.48
20			S8.5-2100	8.36	11.68	0.78
21	50	Dune revegetation	Present (SP)	5.61	10.37	0.00
22			S4.5-2070	8.06	11.52	0.37
23			S4.5-2100	7.21	11.16	0.57
24			S8.5-2070	6.67	10.95	0.48
25			S8.5-2100	8.36	11.68	0.78
26	50	Seagrass revegetation	Present (SP)	5.61	10.37	0.00
27			S4.5-2070	8.06	11.52	0.37
28			S4.5-2100	7.21	11.16	0.57
29			S8.5-2070	6.67	10.95	0.48
30			S8.5-2100	8.36	11.68	0.78
31	100	Current state (no NbS)	Present (SP)	6.01	10.56	0.00
32			S4.5-2070	8.70	11.77	0.37
33			S4.5-2100	7.75	11.39	0.57
34			S8.5-2070	6.97	11.09	0.48
35			S8.5-2100	9.18	12.00	0.78
36	100	Dune revegetation	Present (SP)	6.01	10.56	0.00
37			S4.5-2070	8.70	11.77	0.37
38			S4.5-2100	7.75	11.39	0.57
39			S8.5-2070	6.97	11.09	0.48
40			S8.5-2100	9.18	12.00	0.78
41	100	Seagrass revegetation	Present (SP)	6.01	10.56	0.00
42			S4.5-2070	8.70	11.77	0.37
43			S4.5-2100	7.75	11.39	0.57
44			S8.5-2070	6.97	11.09	0.48
45			S8.5-2100	9.18	12.00	0.78

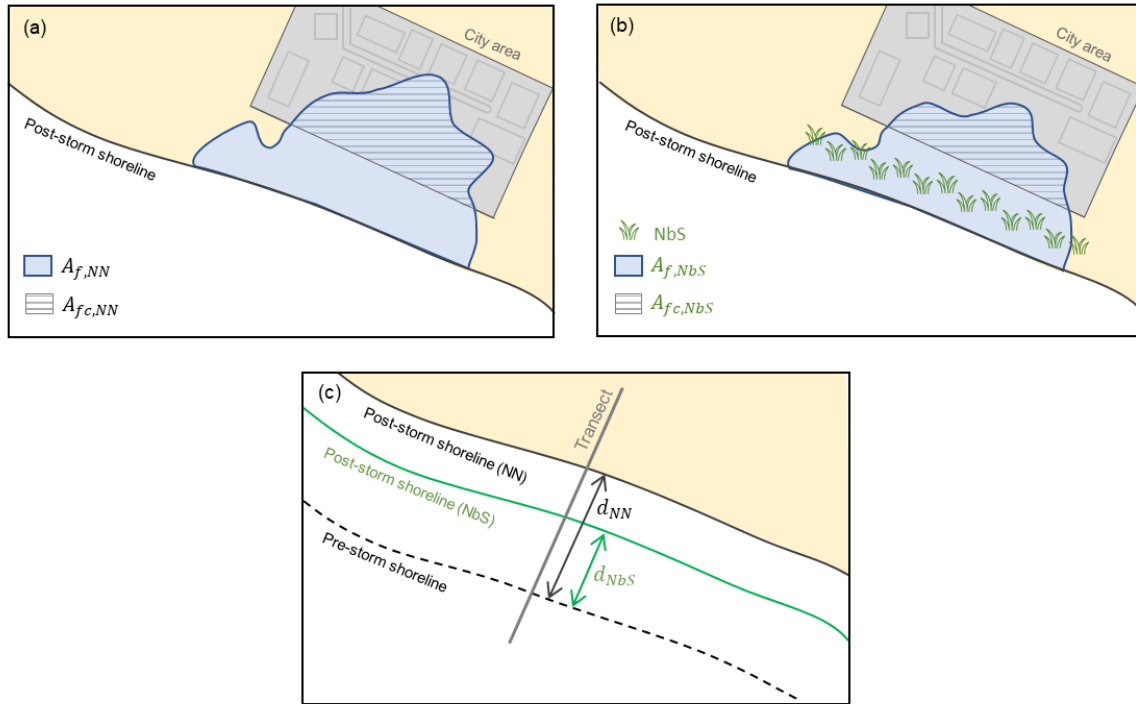


Figure 6.1. Schematization of the terms used within the efficacy indicators: Flooded areas without or with NbS (a and b respectively); shoreline retreat (c).

Figure 6.2 shows the inundation map for the present scenario (SP, SLR = 0.00 m), no-NbS, with 100 years return period storm conditions ($H_s = 6.01$ m, $T_p = 10.56$ s). The figure shows the maximum water levels $z_{w,max}$ reached during the simulation due to wave storm. A significant inundation of the low-lying area in the proximity of the Longarini lagoon discharge channel is observed on the left side of the map. The city area (bounded by the gray line) appears to be not significantly affected by inundation, with limited water levels mainly in the western part of the city, close to the Longarini discharge channel, and inbetween the two central city blocks, which however hosts a plain land lot which can presently absorb the flooding. The total flooded area is 0.229 km^2 , whereas the city flooded area is 0.019 km^2 .

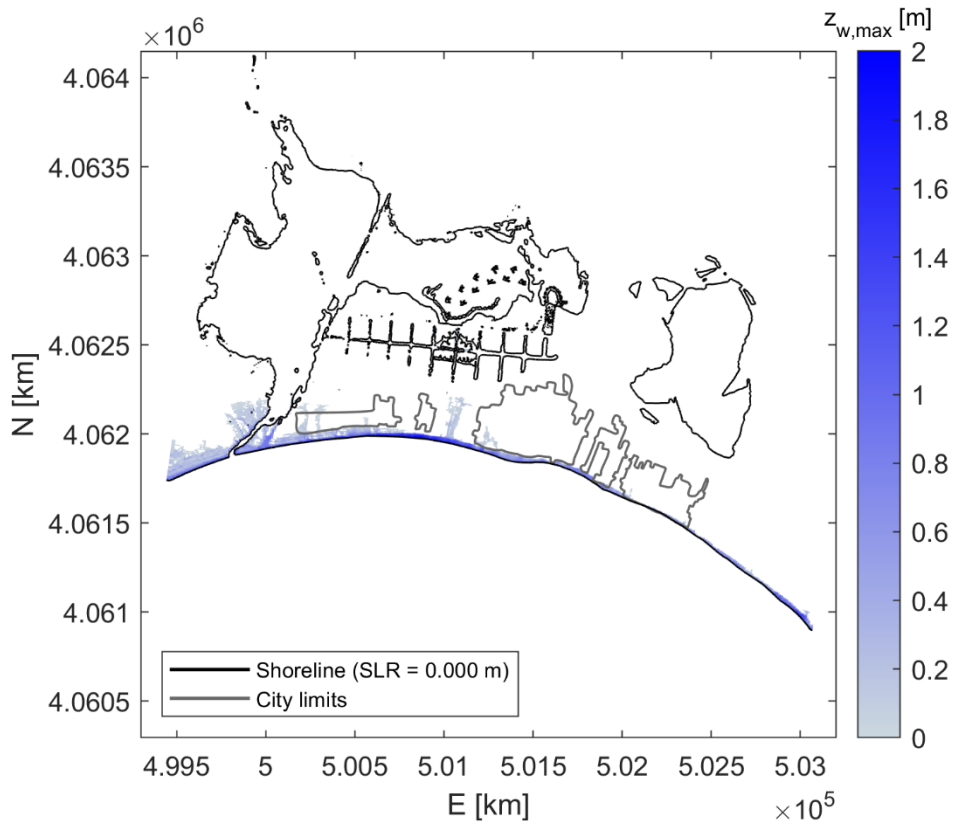


Figure 6.2. Inundation map for present scenario (SP), $Tr = 100$ years, no-NbS, $H_s = 6.01$ m, $T_p = 10.56$ s, $SLR = 0.000$ m.

Figure 6.3 shows the S4.5-2100 simulation, no-NbS, for 100 years return period storm wave conditions ($H_s = 7.75$ m, $T_p = 11.39$ s) and $SLR = 0.57$ m. The increase in sea level leads to significant extension of the area covered by the two lagoons, leading to an opening of a second channel to the Longarini lagoon area. Low-lying land lots between city and lagoons, now lie below the mean sea level, with some of them hydraulically connected with the lagoons. In this scenario, the inundated area significantly increases reaching 0.361 km^2 over the whole investigated domain and 0.095 km^2 within the city area (23% of the total city area). Furthermore, the city area results to be threatened by the increase of the lagoon water level.

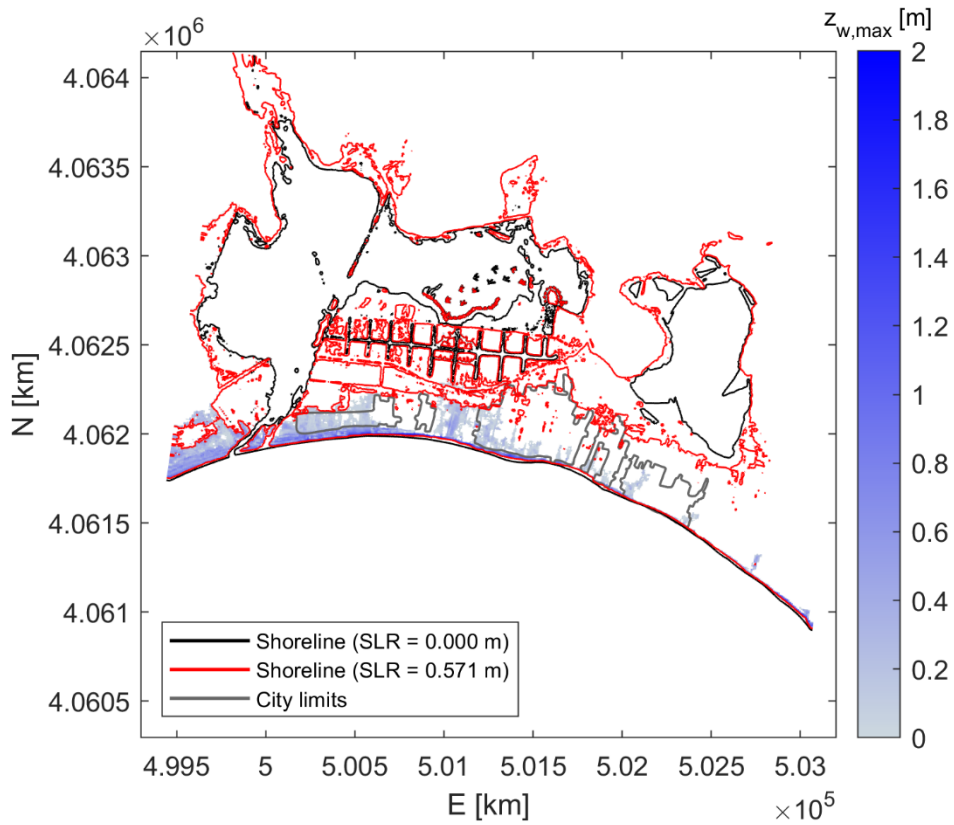


Figure 6.3. Inundation map for simulation S4.5-2100 ($T_r = 100$ years) scenario, current state, $H_s = 7.75$ m, $T_p = 11.39$ s, $SLR = 0.369$ m

Figure 6.4 shows the inundation maps, with a zoom on the city area, for simulated scenario S4.5-2100 with 100 years T_r storm wave conditions ($H_s = 7.75$ m, $T_p = 11.39$ s) and $SLR = 0.571$ m, for no-NbS (subpanel 6.4a), dune revegetation (subpanel 6.4b), seagrass reconstruction (subpanel 6.4c). From the comparison between the subpanels, the two interventions both reduce flooded areas due to waves, especially in the eastern part of the domain reaching a flooding reduction efficiency for the whole investigated domain E_f of 10.05% and 22.09% for dune revegetation and seagrass revegetation respectively. The eastern city blocks are the ones that benefit the most from the flooding reduction in the city, with E_{fc} of 20.45% and 52.57% for dune revegetation and seagrass revegetation respectively.

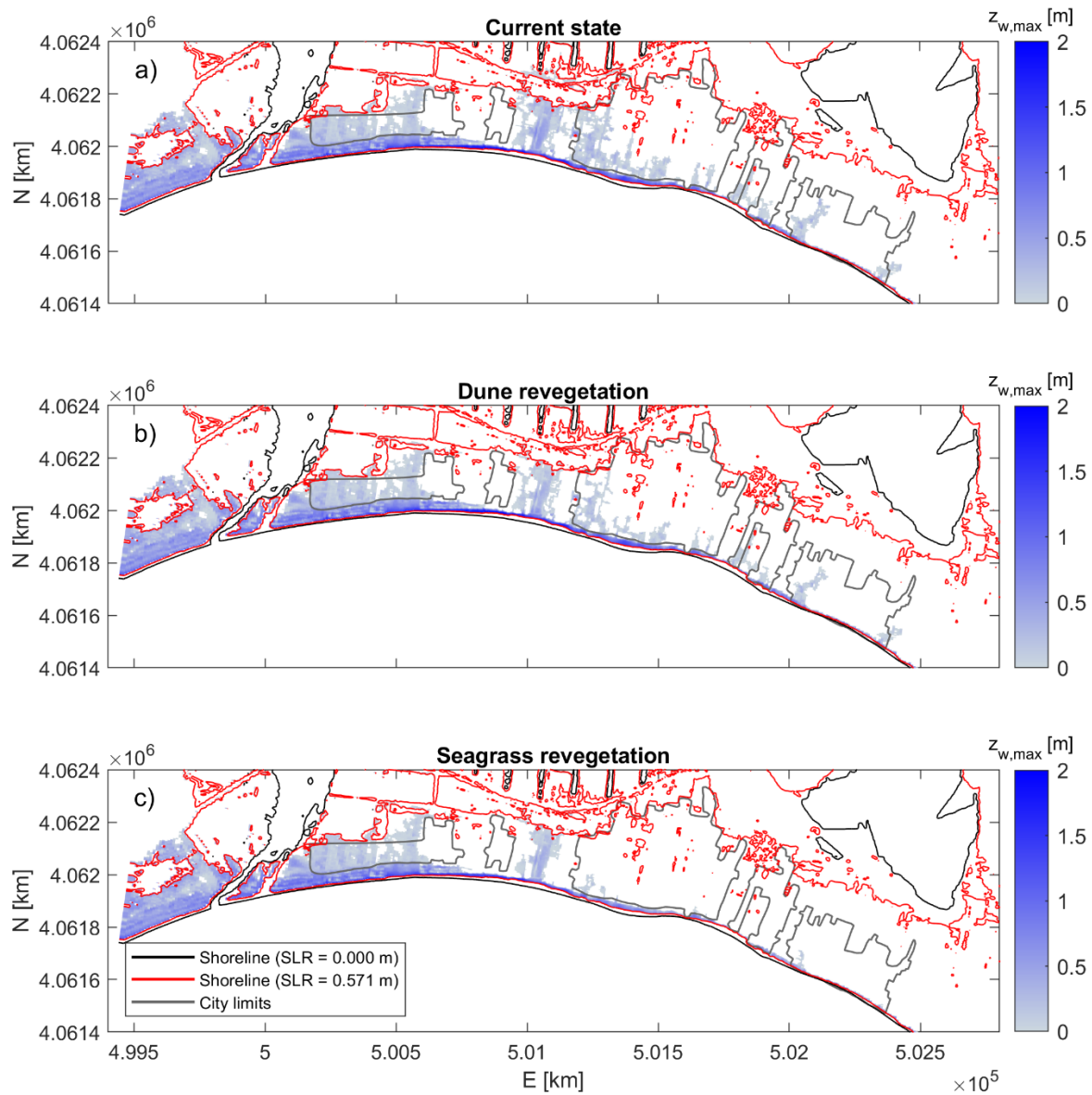


Figure 6.4. Inundation maps for simulation scenario S4.5-2100, $T_r = 100$ years ($H_s = 7.75$ m, $T_p = 11.39$ s, $SLR = 0.369$ m): a) current state, b) dune revegetation, c) seagrass revegetation.

To provide an overall view of the efficiency of the investigated NbS, the bar plot in Figure 6.5a illustrates the flooded areas due to inundation in the city area for all the simulations with $T_r = 100$ years. Figure 6.5a reveals that the most severe scenario in terms of flooded city areas is the S8.5-2100, with 0.238 km^2 of flooded area, 59% of the city area. In all the investigated scenarios, the proposed NBS contribute to reduction of inundated areas, with flooding reduction efficiency indicator ranging from 11 to 24% for dune revegetation and from 51% to 57% for seagrass revegetation (Figure 6.5b).

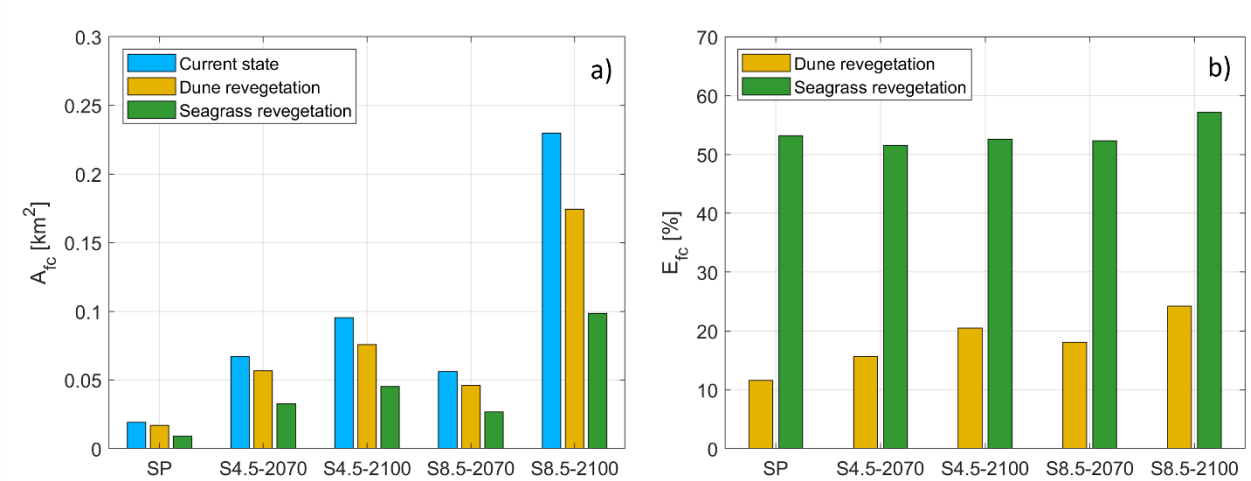


Figure 6.5. a) Flooded areas due to wave storm ($T_r = 100$ years) in the city area; b) Flooding reduction efficiency percentage due to proposed NbS

Concerning the capability of the NbS to reduce erosion due to wave storm, an erosion reduction efficiency indicator E_e is computed as:

$$E_e = \frac{d_{NN} - d_{NbS}}{d_{NN}} \cdot 100 \quad (6.2)$$

where d is the distance between the shoreline position at time 0, to the position of the shoreline at the end of the simulation ($t = 1800$ s). The distance is measured along 30 100-meters long transects shown in Figure 6.6. By the abovementioned indicator, shoreline retreat is a positive value, whereas a shoreline advancement will result in a negative value (Figure 6.1c). The subscript NN indicates a no-NbS (current state) simulation, whereas NbS indicates a simulation with an implemented NbS.

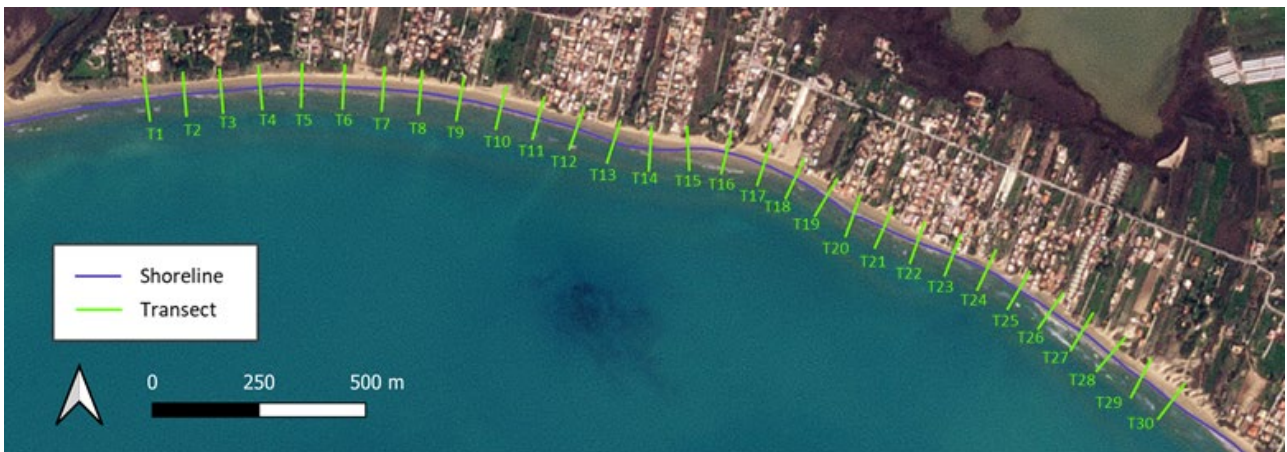


Figure 6.6. Position of the 30 transects along which the shoreline retreat is computed

To provide an overview of the performance of the Nature-based Solutions (NbS) in reducing storm-induced shoreline retreat, Figure 6.7a, c, e, g, and i (left column) shows the shoreline retreat across 30 transects for all scenarios.

Given that the dune revegetation (DR) intervention is located onshore, it appears not to significantly contribute to the reduction of shoreline retreat. This is evident from the shoreline retreat plots in the left column, which largely overlap with the no-NbS scenario, and the negligible values of the E_e indicator shown in the right column.

The seagrass revegetation (SR) intervention shows varying effectiveness depending on the section of the beach being analyzed. In the western section, specifically transects T1 to T7, the contribution of the SR intervention is negligible, consistent with the eroded volume results. In contrast, for the central and eastern transects (T12–T30), the SR intervention appears to reduce shoreline retreat (see subpanels a, c, g and b, d, h), by approximately 2 to 4 meters.

The average reduction effectiveness along these transects, as measured by the E_e indicator, is as follows for the different hydrodynamic scenarios: SP: $E_e = 31\%$, S4.5-2070: $E_e = 31\%$, S4.5-2100: $E_e = 23\%$, S8.5-2070: $E_e = 29\%$, S8.5-2100: $E_e = 24\%$.

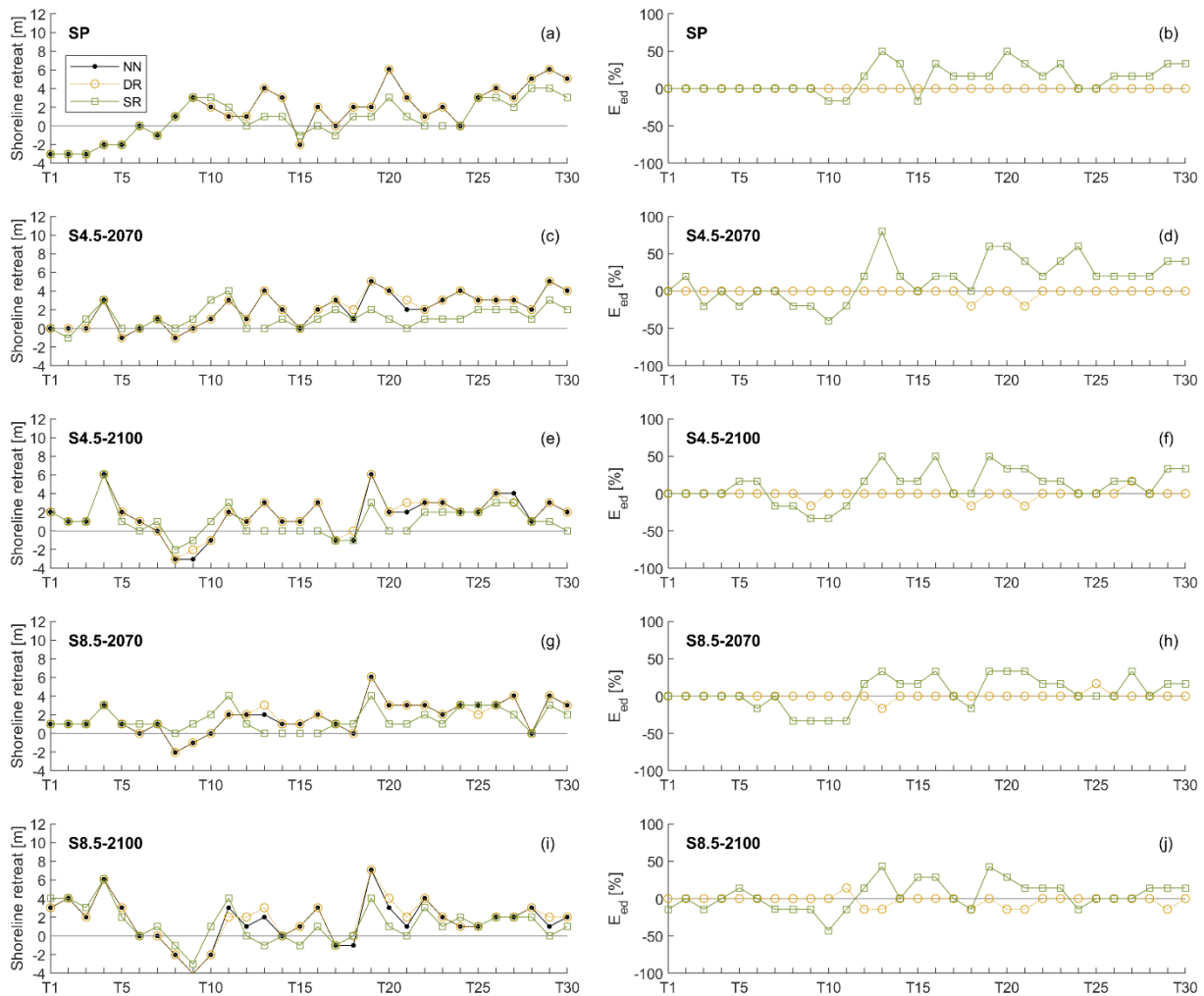


Figure 6.7. Shoreline retreat for no-NbS (NN, black dots), dune revegetation (DR, orange circles) and for seagrass meadow reconstruction (SR, green squares) along transects T1-30 (location in Figure 6.7c) for present (a) and future (c,e,g,i) hydrodynamic scenarios; shoreline erosion reduction efficacy E_e of DR and SR for present (b) and future (d,f,h,j) hydrodynamic scenarios.

6.3 Conclusions

To conclude, both the proposed additional Nature-based Solutions, specifically addressed to coastal risk reduction, seem to provide a notable contribution in mitigating both wave-induced coastal flooding and erosion in the urbanized area. However, the SLR projections, even for the less severe condition, foresee scenarios in which the area potentially occupied by the lagoon increases significantly and reaches the city area. This has also consequences for the biodiversity, as the sea level would eventually (i) deepen the water level in the lagoon, making it potentially unsuitable for some species of wading birds to prosper; (ii) submerge the artificial islands purposely made for birds to nest, and favour higher wave energy due to decreasing lagoon shallowness; (iii) increase saltwater exchange with the sea, which is not a biodiversity threat per se, but may have consequences for fresh groundwater quality in the surrounding area. Further studies will focus on including rain precipitations and river discharges due to extreme events, to include the full wetland dynamics and to assess consequences of compound floodings in present and projected scenarios.

7. Multi-risk projections and climate warnings with ESS in Foros Bay Pilot (BAS)

The Foros Bay is a part of the Burgas Bay, the largest Bulgarian bay. Together with adjacent low-laying wetland, it represents a biodiversity hotspot. The area is one of the most protected from wave action along the Bulgarian coast, and is a centrepiece for both unique natural diversity (landscape, habitat, and species) and human uses. The area is protected under the NATURA 2000 network (both Birds and Habitat) – BG0000271 Mandra-Poda; The Foros Bay is a part of an important place from ornithological point of view (“Mandra-Poda Complex”) and lays on the Via Pontica bird migratory route.

Several dramatic changes have occurred on the bay and its watershed area since 1920. Previously, the coastal area bordering the bay was a wetland almost completely covered with hygrophytes and hydrophytes; there were sand dunes and a dry land never had been flooded by the nearby lake that was used as vineyards. Subsequently, a part of the swamp was dried out to gain land for city development transforming it into settling (stabilization) basins and damming part of Mandra Lake to serve the oil refinery (Birdlife International, 2002).

The area is an important centre for community engagement into environmental protection – there is a visiting centre for bird watching. Also, educational programmes for volunteers and children were developed. Being the most wave protected part of the coast with a sandy bottom, the area offers suitable conditions for wave-sensitive species (such as seagrasses and other submerged aquatic plants) to accommodate and persist. The spatial distribution of the soft-bottom vegetation is limited by high turbidity and macroalgae mats that cover a part of the bottom. The habitats are vulnerable to both marine and land-based activities (point and diffuse sources) or processes (river floods). The adjacent low-lying wetland is also vulnerable to river floods and, despite of being less wave exposed, to coastal floods and erosion associated with extreme hydrometeorological events. Moreover, the expected climate impact would result in the coastal environment change; hence, flooding and erosion hazards due to sea level rise would cause even more severe consequences.

7.1. Study framework

Methodology framework in use is designed to reveal the impact of extreme events on the pilot and in particular to elucidate the mitigating role of vegetation. More precisely, the seagrass effect on damping of system energy and subsequent resilience increase to coastal erosion and flooding were investigated. To this end, we applied the event approach by considering three design events with return periods of 20, 50 and 100 years. The study framework is schematised in Figure 7.1.

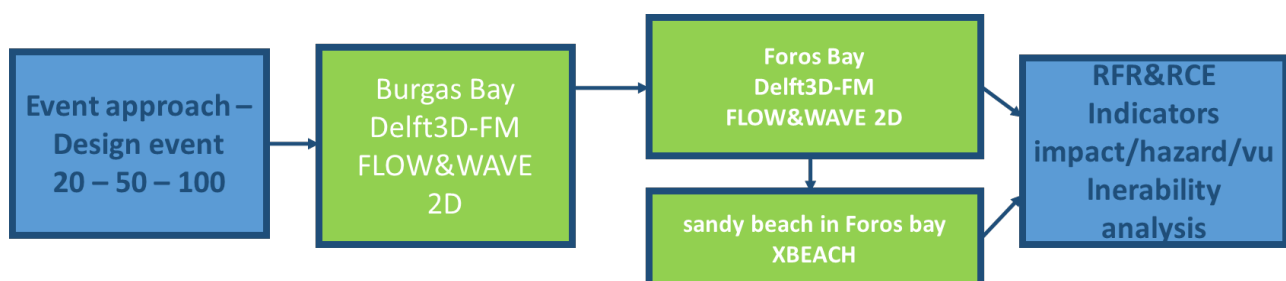


Figure 7.1. Schematization of the study framework

7.2. Data

7.2.1. Bathymetry & Topography

Different data types were used to generate a composite terrain model of Burgas Bay and Foros Bay. The wide Burgas Bay was mapped with a multibeam sonar in 2022. During 2023, additional bathymetric data for Foros Bay with a resolution of 3 m/cell size were obtained. For depths between 4 and 25 m, a seabed model with 7 m/cell size resolution was compiled. In the shallowest part of the Foros Bay, in 2023, bathymetric surveys were carried out using a boat mounted single-beam echo sounder. As a result, the entire Uzungeren Lake was mapped. The shallows were mapped by unmanned aerial photogrammetry, which also provides topography data. The UAS provided higher resolution data for the composite model allowing generation very high resolution digital surface model (20 cm/pix).

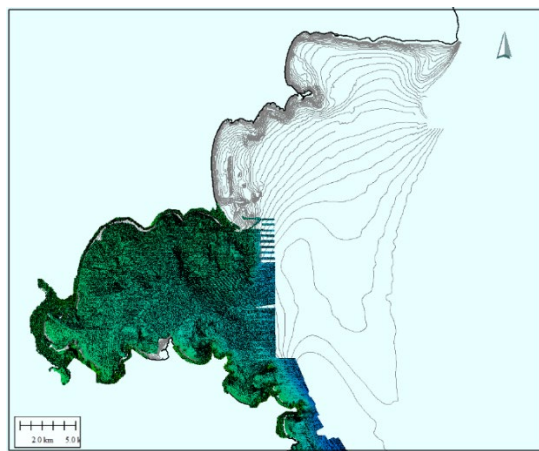


Figure 7.2. Bathymetry and topography compiled datasets used in the study

7.2.2. Waves and surge

Datasets for waves, currents and surge level used in the study can be described as follows:

- Wave properties extracted from the wave hindcast covering the period 1980 – 2020 (Valchev et al., 2010; Valchev et al., 2012) in order to reproduce recent past to present conditions (Figure 7.3)
- Surge level coming from Copernicus Climate Change Service as boundary conditions for the Foros Bay domain

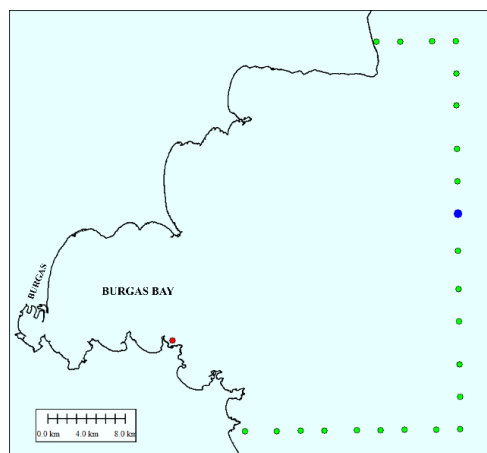


Figure 7.3. Location of points for which wave and wind properties were extracted from a hindcast dataset

7.2.3. Bottom sediments

The bottom sediments in Foros Bay, including the inner part of the bay and the entrance to the Usungeren Lake were surveyed in January 2023. The granulometry of a total of 13 samples were analyzed. According to the Wentworth classification, sediment type varies with depth decrease from fine sand through very coarse silt to very fine silt. D50 varies between 157 and 6 μm . Additional data available in IO-BAS gathered in 2022 show that the bottom sediments in the deeper parts of the Foros bay and Port of Burgas water area are presented mostly silts including also medium sands and clays. D50 varies between 245 and 0.03 μm . The locations of bottom sediment samples are presented in Figure 7.4.



Figure 7.4. Location of bottom sediment samples collected for the needs of REST-COAST Project (red dots) and those of supplementary samples (green dots).

7.2.4. Vegetation

The Foros Bay accommodates soft-bottom vegetation with a total area of 39 ha. The dominant species is the seagrass *Zostera noltei*, *Hornemann* but other aquatic species are also present, e.g. *Zannichellia palustris* L. and *Stuckenia pectinata* (L.) Börner, macroalgae - *Ulva* sp., *Ceramium* sp., *Cladophora coelothrix* Kützinger etc. The distribution of seagrass meadows is shown in Figure 7.5. The envisioned areas of seagrass restoration are also included in the figure.



Figure 7.5. Location of the seagrass meadow present in Foros Bay (light green polygon A) and the envisioned area of seagrass restoration (dark green polygons B and C)

7.3. Models and methods

Methodology framework was designed to reveal the impact of extreme events on the pilot and in particular to define the energy attenuation role of vegetation. Therefore, the event approach was employed by reconstructing three design events with return periods of 20, 50 and 100 years. Hydrodynamic conditions in terms of waves, currents, surge and winds corresponding to the recent past and present were obtained by means of probabilistic analysis of available data.

7.3.1. Design of extreme hydrometeorological events

In order to design a realistic extreme event, first, peak over threshold (POT) analysis was used to identify the individual coastal storms applying a threshold of 2 m for significant wave height, which were exceeded for a time-span longer than 18 hours considering (Valchev et al., 2016). Thus, a total of 215 events were identified, each represented by significant wave height maxima (H_s) with associated values of peak wave period (T_p), wave direction, event duration as well as wind speed maxima (V_{max}) during the event.

Furthermore, Extreme Value Analysis (EVA) was applied to calculate return values of design properties relevant for selected return periods serving as boundary conditions for Burgas Bay Delft3D-FM model. Time series for all points located along the open boundaries of Burgas Bay Delft3DFM domain were statistically analysed (Figure 7.3). It was found that significant wave height, peak wave period and wind speed behave in a similar manner following the growth, developed and decay phase of the event. All events were driven by winds with direction turning from NNW to ESE in the course of event, with an average of 42.2°N (NE). The results from EVA application are shown in Table. 7.1.

Table. 7.1. Return values of wave properties and wind speed for selected design events

TR	H_s , m	T_p , s	V_{max} , m/s
TR020	8.4	10.9	20.9
TR050	10.5	11.4	21.6
TR100	12.5	11.8	22.0

Results reported in Valchev et al. (2012) were used to determine the event duration, wave and wind direction behaviour for the storm event prototype. Thus, the event duration was set to 110 hours, with duration of growth phase - 17 hours, developed phase - 55 hours and decay phase - 38 hours.

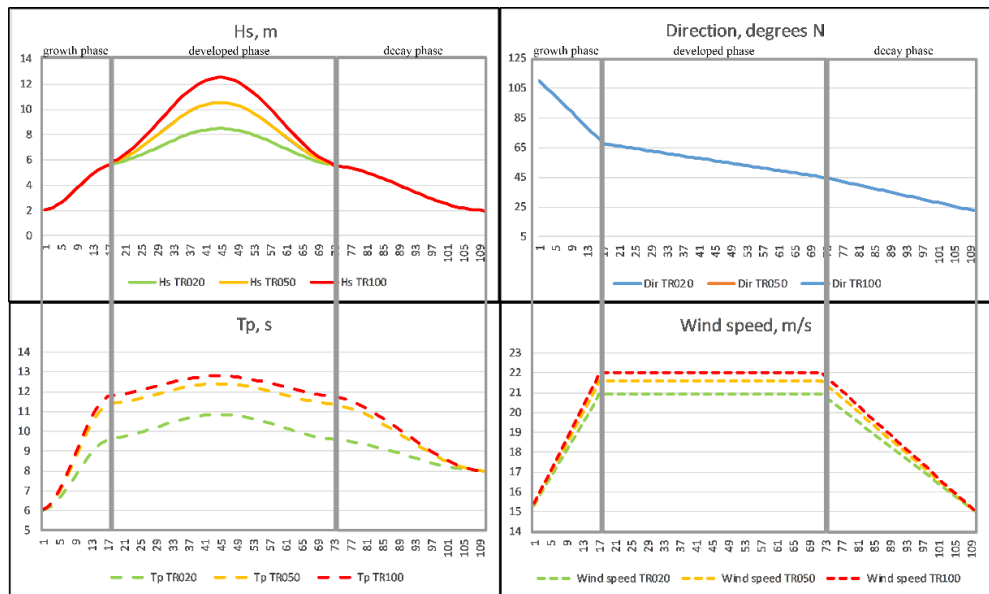


Figure 7.6. Extreme events' pattern for selected return periods

The waves and wind direction were set to vary in the event course: from ESE to ENE during the growth, from ENE to NE during the developed sea and from NE to NNE during the decay. The time series of Hs and Tp were calculated for each storm phase using the formula $s = S \sin(\pi \frac{t}{T_d})^2$, where S is the property maximum, T_d - event duration, t - time. The overall extreme event's pattern for selected return periods is shown in Figure 7.6. Such time series were constructed for each boundary point according to the local statistics.

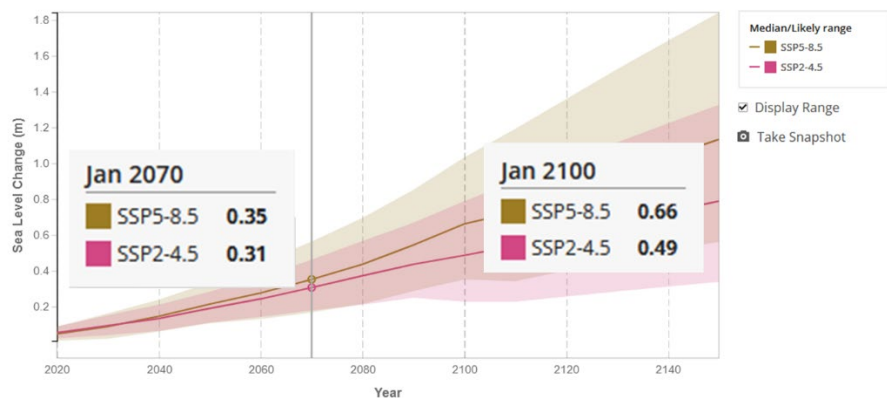


Figure 7.7. Sea level rise scenarios and projections (<https://sealevel.nasa.gov/ipcc-ar6-sea-level-projection-tool>)

The future conditions were addressed by making use of existing climate scenarios, more specifically middle and high-end ones RCP4.5 (SSP2-4.5) and RCP8.5 (SSP5-8.5). Considered projections were 2070 and 2100. According to predictions of IPCC AR6 (2023) sea level rise for Burgas would vary between 0.31 and 0.66 cm, according to the corresponding scenarios and projections (Figure 7.7). Surges relevant for Burgas were taken from Copernicus climate change services (<https://cds.climate.copernicus.eu/>). The values used are presented in Table 7.2.

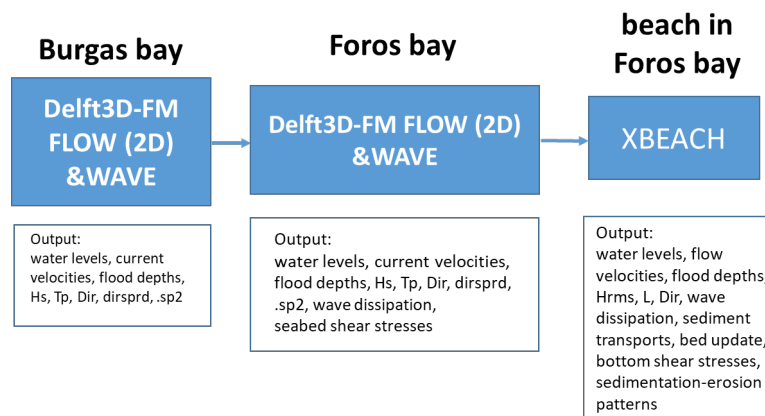
Table 7.2. Return values of future surge level and for selected design events

TR	Surge, m	
	RCP4.5	RCP8.5
TR025	0.603	0.640
TR050	0.653	0.700
TR100	0.702	0.757

As for waves, a recent study concludes that the projected changes in the mean wave properties in middle future are more significant under RCP8.5. Moreover, possible effects seem to be more pronounced with respect to the extreme wave heights: 100-year return period growth is 5% for the western and 25% for the eastern Black Sea (Islek et al., 2022). Therefore, we hypothesized that there will be no change in the future wave conditions; the more so, our recent past to present estimates tend to exceed the projected values provided by Copernicus climate change services (<https://cds.climate.copernicus.eu/>).

7.3.2. Modelling system

The modelling system consists of two Delft3D-FM domains – Burgas Bay and Foros Bay. Additionally, XBeach model was implemented on a domain comprising a low-laying coastal stretch represented by a sandy beach and adjacent underwater area located within the Foros bay. All elements of the system are coupled offline (Figure 7.8).

*Figure 7.8. Modelling system scheme.*

The Burgas Bay Delft3D-FM domain (Figure 7.9) was implemented by online coupling of flow and wave processes. The flow module uses unstructured grid with spatial resolution varying from 500m at the offshore boundary to 20 m for the shallower than 20 m depths. The grid consists of 537276 cells. The wave module uses regular grid with horizontal resolution of 100 m. The model resolution is high enough to allow for a very good representation of the hydrodynamics and wave dynamics within the coastal area of complex bathymetry.

D2.2 Good practice criteria Multi-variable risk projections

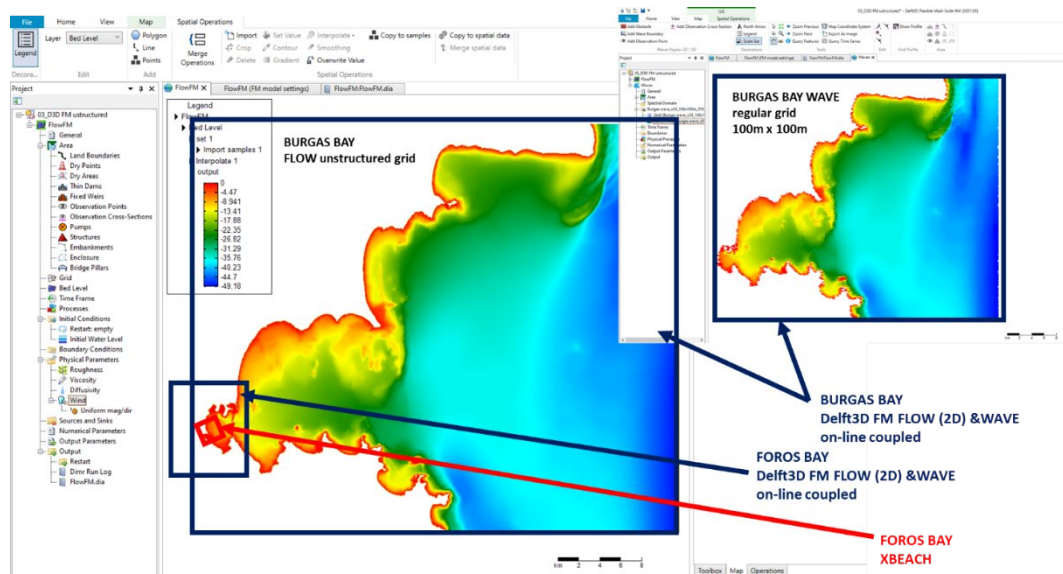


Figure 7.9. Burgas Bay Delft3D-FM FLOW&WAVE domain and location of the other elements of the modelling chain

The Foros Bay Delft3D-FM domain is of higher spatial resolution and covers Burgas port infrastructures, the Poda protected area and Uzungeren Lake within Foros Bay as well as surrounding low-laying area and the located nearby Port of Burgas (Figure 7.10). The flow module is set on unstructured grid with cell sizes varying from 50 m at the offshore boundary to 20 m in the nearshore part of the grid. The wave grid is regular with spatial resolution of 20 m. The flow grid consists of 83237 cells, while the wave grid comprises 157156 cells. The offshore boundary conditions for the flow grid consist of water levels. The wave module boundary points are located at every grid node at the offshore boundary.

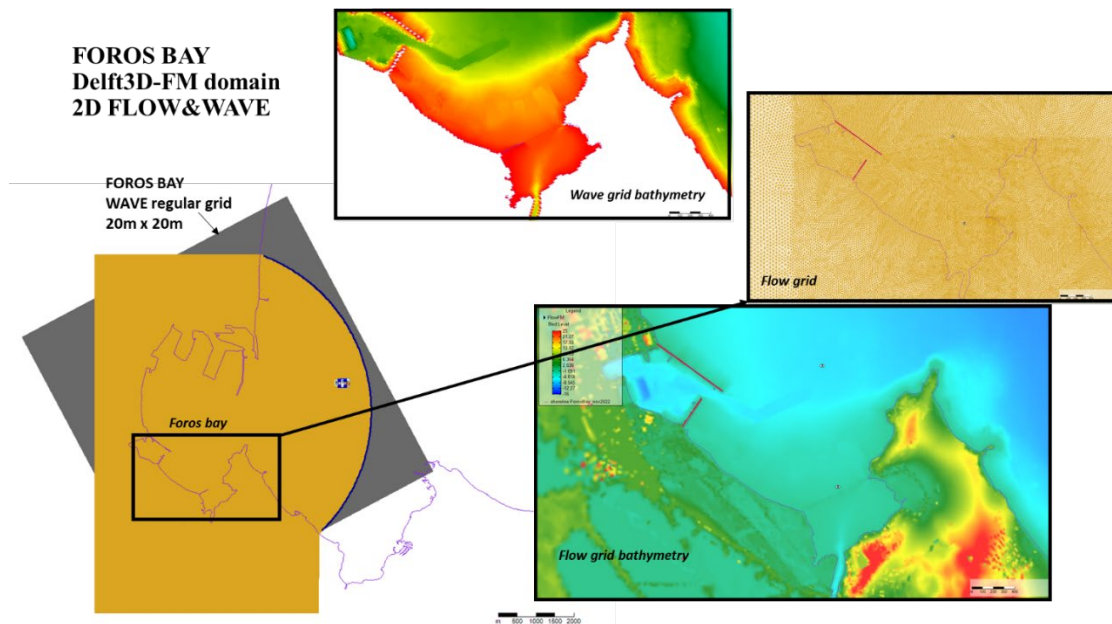


Figure 7.10. Foros Bay Delft3D-FM domain setup. Unstructured flow grid and regular wave grid (left). Water depths (wave module) and bathymetry (flow module) and a fragment of the unstructured flow grid (right). The offshore boundary conditions points (water levels) for the flow grid are depicted by blue dots (left).

The presence of seagrasses into the model domain was implemented into the model as area trachytopes, using the formula of Baptist (2005). The formulae require following input parameters: vegetation height (h_v), density (n), drag coefficient (C_D) and alluvial bed roughness (C_b). The values applied in the model set-up are summarized in Table 7.3.

Table 7.3. Input parameters used for seagrasses implementation into the model

h_v [m]	n	C_D [-]	C_b
0.3	6.5	1.8	62

Two polygons of seagrass meadows corresponding to present and restored areas are shown in Figure 7.11. The situation of the area planned for seagrass restoration was selected considering the depth limitation posed to the community spread. Thus, the offshore boundary was restrained to the 6 m depth contour. The simulations performed are listed in Table 7.4.

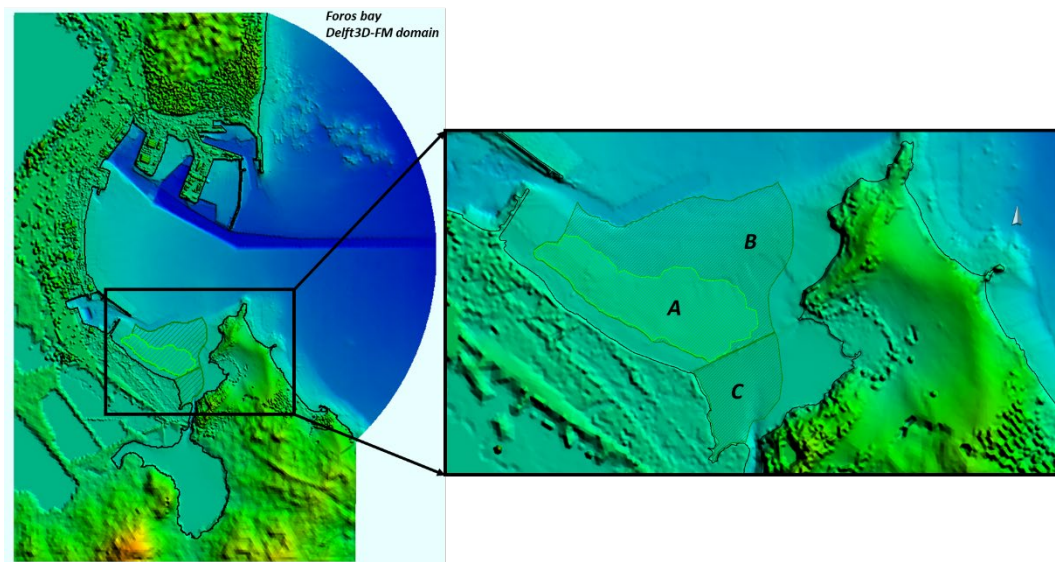


Figure 7.11. Location of the seagrass meadows within Foros Bay Delft3D-FM domain existing to present delineated by light green polygon (A) and the planned area of seagrass restoration delineated by dark green polygons (B and C).

Table 7.4. Simulations overview for Foros Bay domain (P – present, R – restored)

Alternative	SLR	Waves	Surges	Vegetation	No. of simulations
A0 (Baseline)	-	WAV_P	SS_P	VEG_P	3
A1	-	WAV_P	SS_P	VEG_R	3
A2 (Do nothing)	SLR_4.5 (2H)	WAV_P	SS_4.5	VEG_P	6
A3 (Do nothing)	SLR_8.5 (2H)	WAV_P	SS_8.5	VEG_P	6
A4	SLR_4.5 (2H)	WAV_P	SS_4.5	VEG_R	6
A5	SLR_8.5 (2H)	WAV_P	SS_8.5	VEG_R	6

The 2DH morphodynamic model XBeach (Roelvink et al., 2009) is implemented at the south-western part of the Foros Bay (Figure 7.12). The domain is limited landward by the international road E87 and covers a costal stretch presented by low-laying area, a part of natural protected area Poda with maximum elevation of 6m. It includes a narrow subaerial beach, together with the bottom slope up to 7m depth. The grid is regular non-

equidistant with varying cell sizes cross-shore – from 14m to 2m at the middle of the grid – and regular 5m-resolution along-shore, resulting in 151145 nodes. The model was run in surfbeat mode using cyclic lateral boundary and bedfriction manning coefficients map with value of 0.02 for the bottom slope and 0.04 for the terrestrial part of the domain. The model is fed by hourly wave parameters and water levels at the offshore boundary coming from the Foros Bay Delft3D-FM model output. Waves at the boundary are expressed as JONSWAP spectra through the wave parameters H_s , T_p , wave direction, directional spreading, as the random seed for waves in the model is set to 0 for comparison purposes. The morphological acceleration factor (morfac) is set to 10, the sediments are homogeneous with D_{50} of 0.0001m and D_{90} of 0.0002m.

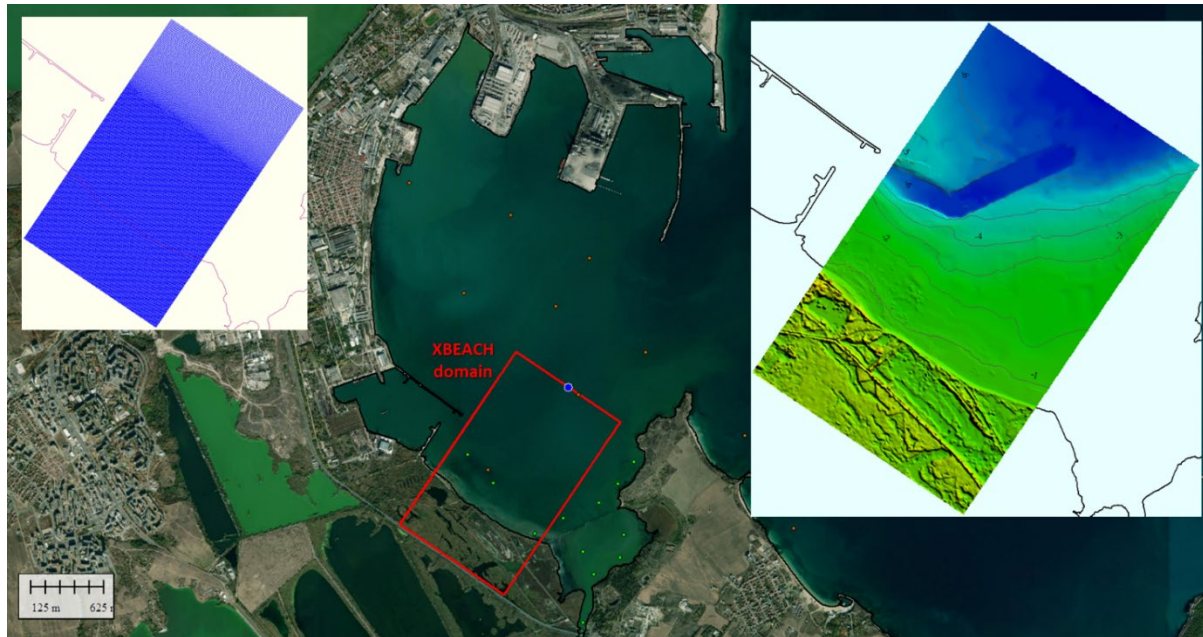


Figure 7.12. Location of XBeach model domain within Foros Bay delineated by red line (left) and bathymetry of the domain (right). The blue dot at the XBeach boundary allocates the output model location of Foros Bay Delft3D-FM model used for XBeach boundary conditions

The seagrass meadows – both existing to present and planned for restoration – are incorporated into the model using the vegetation module of XBeach (Van Rooijen et al., 2015). It was set up with following parameters: vegetation stem diameter of 0.005m, vegetation density – 130/sq.m, and vegetation height of 0.30m. The spatial coverage of two variants of seagrass patches within the domain are presented using grid map files (Figure 7.13). The simulations performed are listed in Table 7.5.

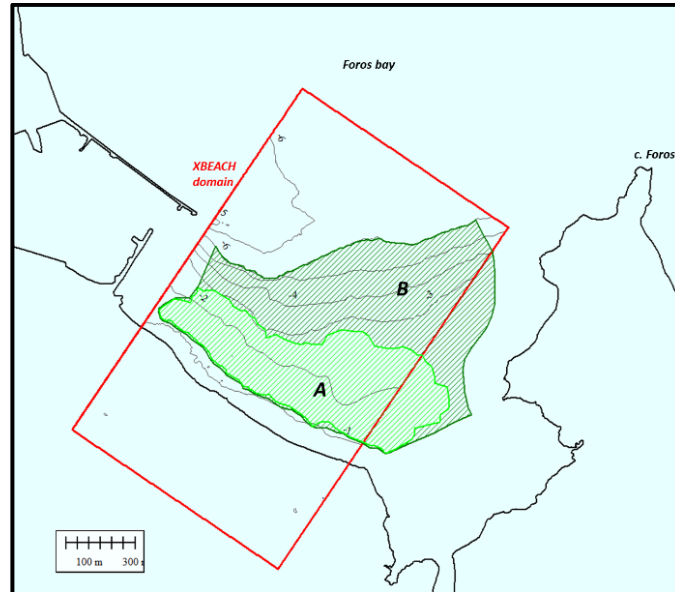


Figure 7.13. Distribution of seagrasses into the XBeach domain (red polygon). The seagrass meadow existing to present is delineated by light green polygon (A) and the planned area of seagrass restoration is delineated by dark green polygon (B).

Table 7.5. Simulations overview for Foros Bay beach (P – present, R – restored)

Alternative	SLR	Waves	Surges	Vegetation	No. of simulations
A0 (Baseline)	-	WAV_P	SS_P	VEG_P	3
A1	-	WAV_P	SS_P	VEG_NO	3
A2	-	WAV_P	SS_P	VEG_R	3
A2 (Do nothing)	SLR_4.5 (2H)	WAV_P	SS_4.5	VEG_P	6
A3 (Do nothing)	SLR_8.5 (2H)	WAV_P	SS_8.5	VEG_P	6
A5	SLR_4.5 (2H)	WAV_P	SS_4.5	VEG_NO	6
A6	SLR_8.5 (2H)	WAV_P	SS_8.5	VEG_NO	6
A7	SLR_4.5 (2H)	WAV_P	SS_4.5	VEG_R	6
A8	SLR_8.5 (2H)	WAV_P	SS_8.5	VEG_R	6

7.3.3. Nature-based solution (NbS) and related Ecosystem Services (ESS)

Nature-based solution taken into account is *restoration of seagrass meadow*. The effort considers assisted reintroduction of a *Zostera Noltei* dominated ecosystem, which is currently degraded due to multiple anthropogenic stressors, such as eutrophication, contamination, poor light conditions and presence of opportunistic species. For both present and future conditions *two ecosystem services* were assessed – *Reduction of Flood Risk (RFR)* and *Reduction of Coastal Erosion (RCE)*. The indicators are based on result of the hydrodynamic and morphodynamic modelling described above. The RFR assessment is using model results of Foros Bay Delft3D-FM FLOW&WAVE model, while the RCE is using the results from XBeach model domain. The RFR indicator is flooded area (sq.km) calculated for the Foros Bay and the surrounding wetland solely, with a threshold of 1cm of water layer thickness. Two indicators are employed for RCE analysis – eroded volumes and eroded areas – calculated for the entire model domain. The erosion area are outlined using a threshold of 1cm sediment layer thickness.

7.4. Results and discussion

7.4.1. Hydrodynamic modelling

Analysis of the preliminary model results showed that restored seagrasses do not have a noticeable impact on the flow and wave pattern and the overall energy reduction in the system in comparison with the contribution of the existing meadow. Therefore, we decided to conduct model studies without any seagrasses as a baseline in order to prove their ESS.

The overall model results show that the prevailing flow pattern does not change significantly for all modelled conditions. A reduction of flow velocities is observed which is very well pronounced over the area of both present and restored seagrass in particular for lower energy conditions (TR020 design event) (Figure 7.14). However, this effect decays with the increase of energy input of the system accompanied by the sea level rise for both climate change scenarios into consideration.

The general circulation pattern during extreme events shows presence of a large anticyclonic eddy, which follows the coastal contour from cape Fors through the inner part of the bay. This facilitates the channeling of polluted and highly eutrophicated waters into the seagrass area. In calm hydrometeorological conditions, the reverse flow is observed (e.g. in Figure 7.5), i.e. discharge of these waters from the interior of the bay past c. Fors to open waters. For that reason, the narrow coastal strip along the eastern side of the bay is not suitable for seagrass restoration because the probability of their survival is very low, both in strong and weak conditions.

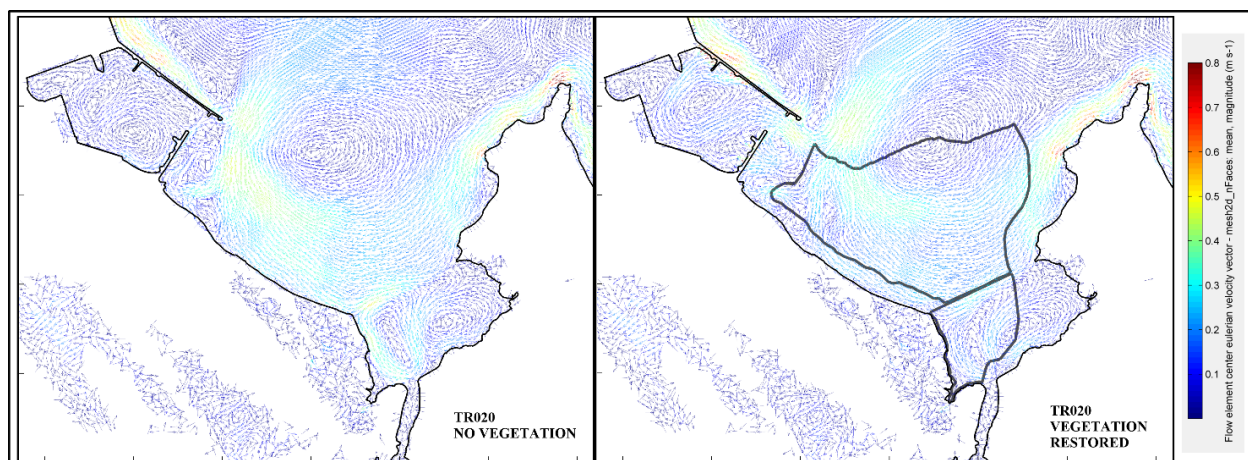


Figure 7.14. Flow pattern calculated for TR020 design event (present climate conditions) for the case of no vegetation (left) and in presence of existing and restored seagrass meadows.

Concerning the waves, the model results show a decrease of significant wave height over the area occupied by seagrasses, which is more pronounced in the shallower part of the meadow, as well as in the inner bay. This is corroborated by the wave energy dissipation (Figure 7.15). Similarly to the flow behaviour, this effect vanishes with the increase of energy input in the system.

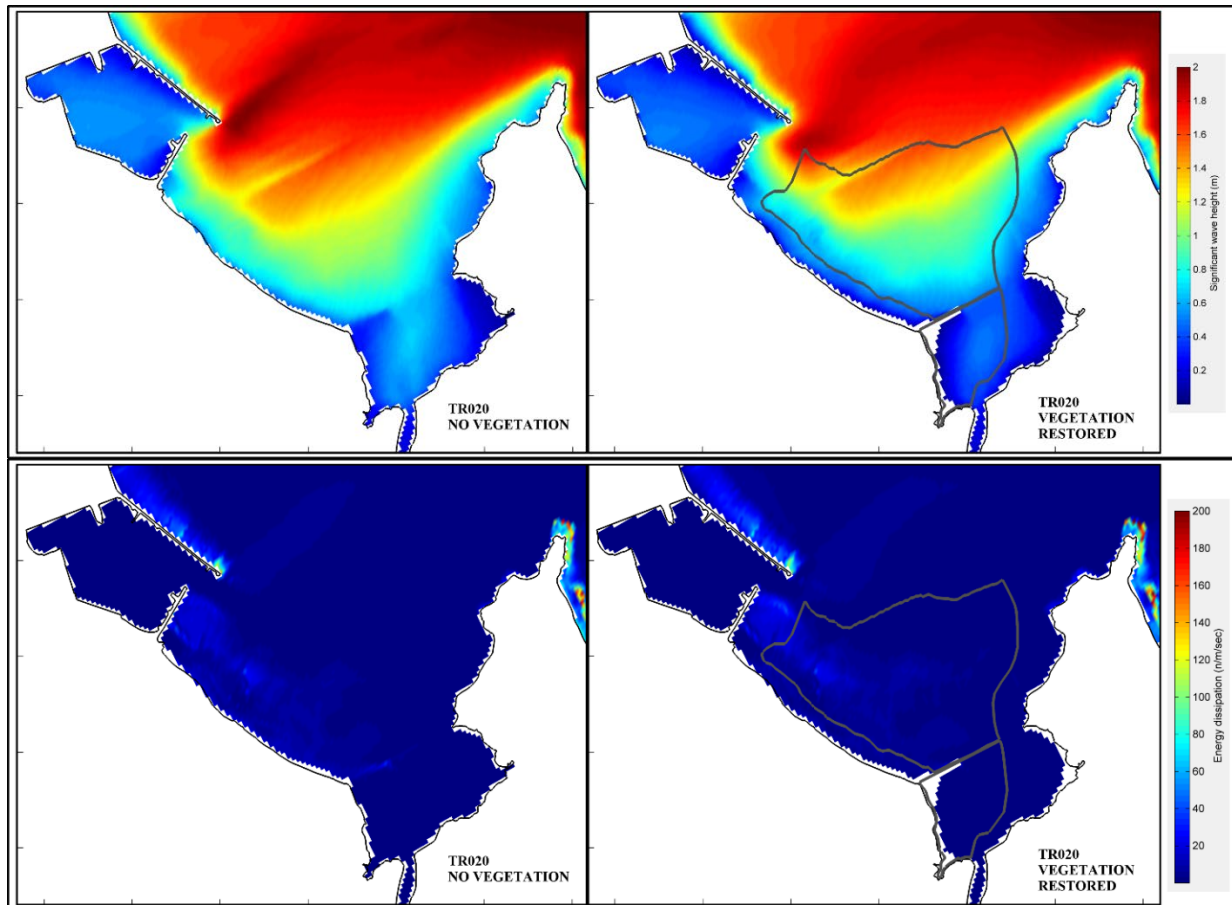


Figure 7.15. Significant wave height (upper panel) and wave energy dissipation (lower panel) for TR020 design event (present climate conditions) for the case of no vegetation (left) and in presence of existing and restored seagrass meadows.

The model results for present climate conditions show that part of Poda protected area, as well as the narrow strip along the coastline including Usungeren Lake, Poda swamp and small parts of the settling basins of the oil refinery are flooded for all return periods. With the rise of sea level and surges due to climate change, the flooded areas increase significantly covering the larger part of Poda protected area and the whole settling basins behind the wetland (Figure 7.16). The same applies for the low-laying areas situated in the eastern coast of the bay. The analysis of the entire set of simulations show that the seagrasses have insignificant effect on reduction of flooding.

Flood areas for all design events concerning present conditions and two considered horizons of RCP4.5 and RCP8.5 are presented in Table 7.5. The percentage of flood increase with respect to TR020 present conditions shows that there is a slight increase of flood area for the rest of design events (6-8%) due to the wave action and surge. However, the flood area increases drastically for selected climate scenarios and projections as the percentage varies between 62% (RCP4.5 H2070) and 84% (RCP8.5 H2100) owing to the sea level rise.

Table 7.5. Flood areas [sq. km] for all design events concerning present conditions and two considered horizons of RCP4.5 and RCP8.5. Right panel presents the percentage of flood increase due to climate change with respect to present conditions

Return period	Flood areas [sq. km]					Percentage of flood increase with respect to TR020 present conditions				
	Present climate conditions	RCP4.5 H2070	RCP4.5 H2100	RCP8.5 H2070	RCP8.5 H2100	Present climate conditions	RCP4.5 H2070	RCP4.5 H2100	RCP8.5 H2070	RCP8.5 H2100
TR020	0.996	1.611	1.724	1.643	1.802	100	162	173	165	181
TR050	1.054	1.640	1.753	1.666	1.814	106	165	176	167	182
TR100	1.074	1.662	1.765	1.687	1.832	108	167	177	169	184

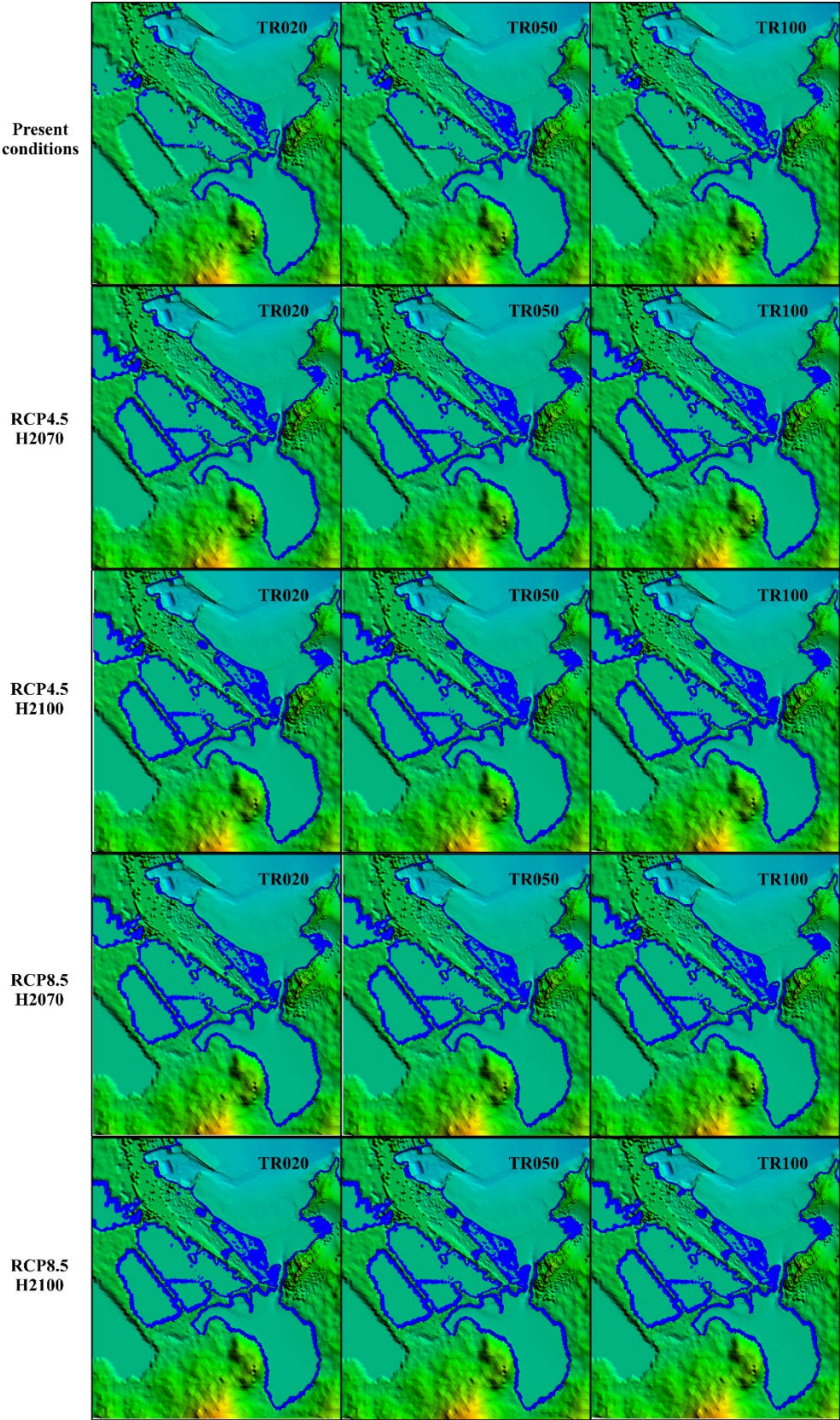


Figure 7.16. Flooded areas for considered return periods concerning present conditions and two considered horizons of RCP4.5 and RCP8.5.

7.4.2. Morphodynamic modelling

Similarly to hydrodynamic modelling strategy, model studies were conducted without any seagrasses as a baseline in order to prove their ESS. Further, two variants of seagrass distribution were modelled related to the existing and planned for restoration meadows.

Considering the results of all modelled simulations it can be stated that, the presence of seagrasses affect significantly the erosion-accumulation pattern (Fig7.17 and 7.18). The most considerable erosion volumes are observed along the coastline while within the surf zone and wetland the intensity of erosion process decreases. Breaching and accumulation fans occur at coastline and wetland, while seaward in the surf zone, the morphodynamic pattern is marked by alternation of erosion-accumulation strips of a small layer thickness up to 5 cm expanding to 3 m depth. Erosion processes aggravate with the sea level rise as the area of interaction shifts towards the wetland.

In presence of seagrasses, their protection effect on the bottom slope is substantial for both present and future conditions, whereas on the coastline and wetland this effect is notable only for lower sea level. Concerning design event TR020, breaching takes place in case of 0.49m (RCP4.5 H2100) and 0.66m (RCP8.5 H2100) sea level rise. In former case, the seagrasses manage to prevent occurrence of coastline breaching located in the middle of modelled area in case of (Figure 7.17), which is not observed in the latter. Concerning design event TR050, the situation is similar but in both cases the seagrasses cannot cope with reduction of erosion processes. Concerning design event TR100, the breaching of the coastline occurs already in H070 (sea level 0.31m) for both climate change scenarios. In presence of seagrasses, the erosion subsides for above mentioned cases but fails in case of H2100 for both scenarios (Figure 7.18). The effect of the restored seagrass meadow is discernible only on the bottom slope affecting considerably the erosion area.

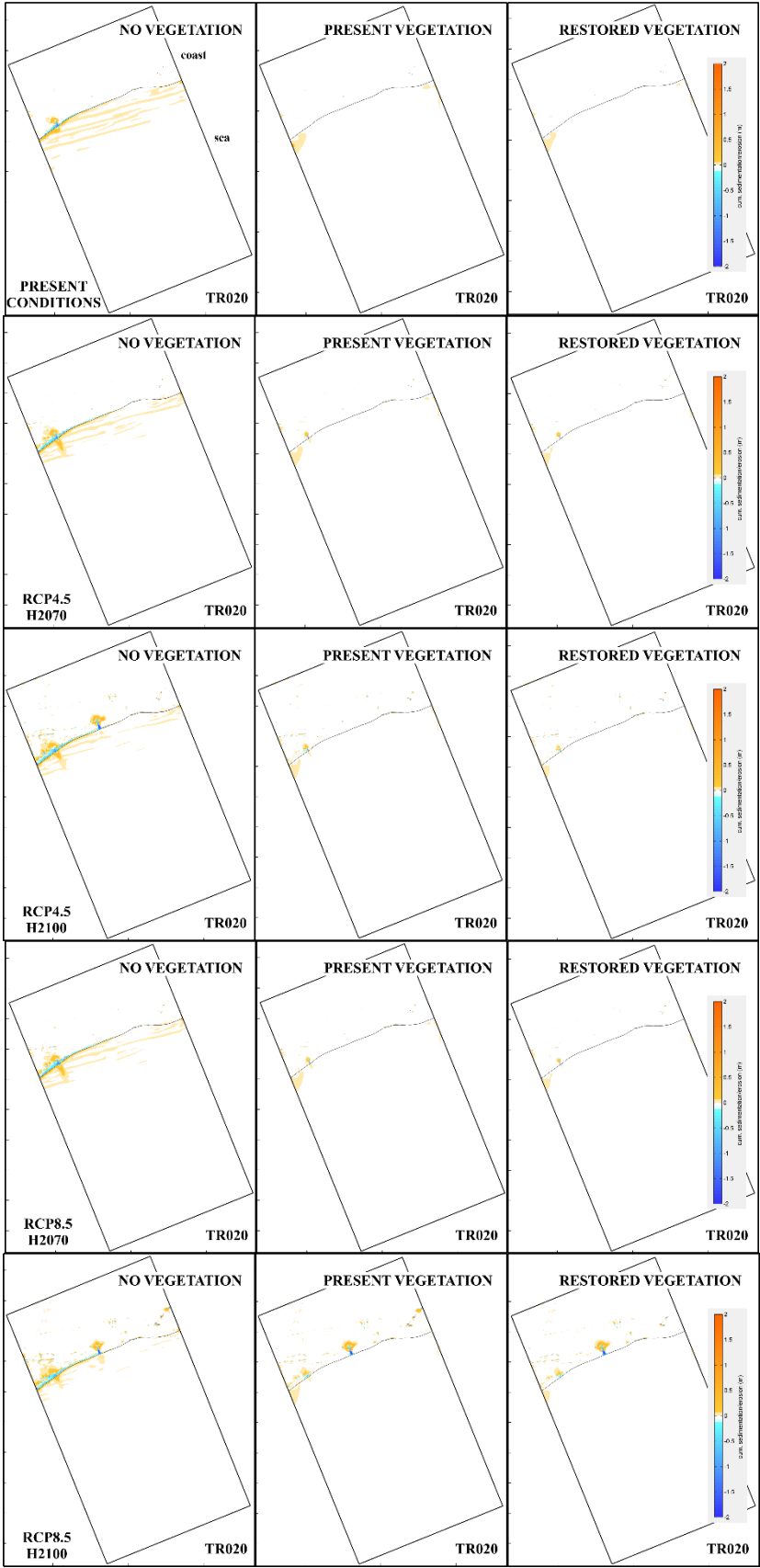


Figure 7.17. Sedimentation – erosion patterns calculated for TR020 storm event for present climate conditions and future climate change under RCP4.5 and RCP8.5, horizons 2070 and 2100

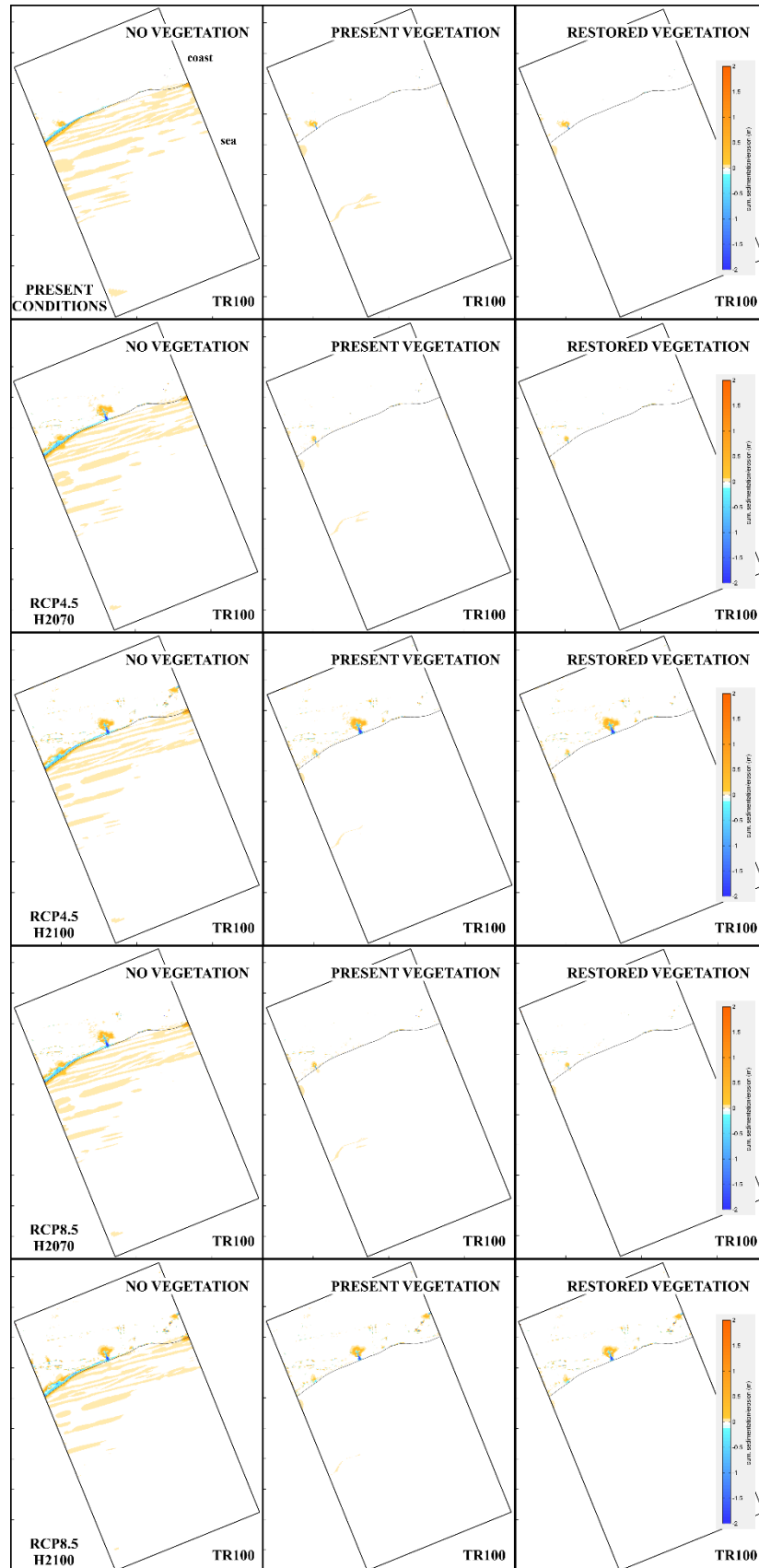


Figure 7.18. Sedimentation – erosion patterns calculated for TR100 storm event for present climate conditions and future climate change under RCP4.5 and RCP8.5, horizons 2070 and 2100.

7.4.3. Assessment of ecosystem services

Two ecosystem services were assessed – Reduction of Flood Risk (RFR) and Reduction of Coastal Erosion (RCE) – for both present and future conditions.

Flood area (in sq.km) was employed as indicator for RFR ESS assessment, which was calculated for the Foros Bay and the surrounding wetland solely. Flood areas concerning present conditions and two considered horizons of RCP4.5 and RCP8.5 for all design events are presented in Figure 7.19. The flood area increases drastically for selected climate scenarios and projections owing to the sea level rise. The percentage varies between 62% (RCP4.5 H2070) and 84% (RCP8.5 H2100). The result implies that the seagrass presence has insignificant effect on reduction of flooding risk. Hence, this ESS is not relevant for the case of Foros pilot since the rising level is the main source of flooding, which seagrasses could not possibly influence on. The differences due to the direct wave impact and surges are similar and vary within a small range of 3-8% of the flood area as the difference decreases with sea level growth for future scenarios. Moreover, this behaviour is reproduced for all climate change conditions into consideration.

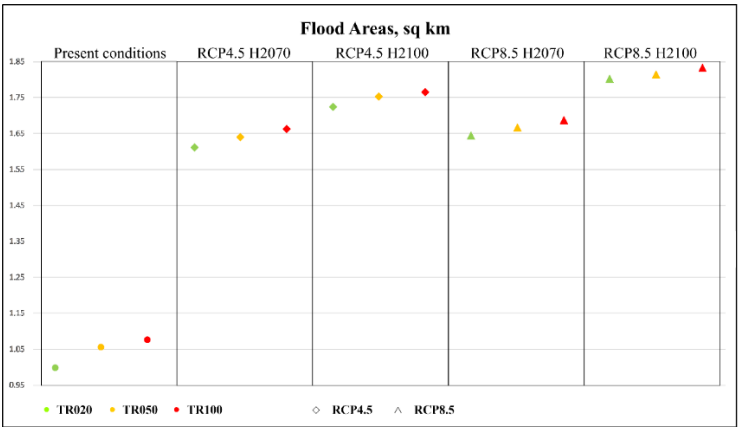


Figure 7.19. Flood areas concerning present conditions and two considered horizons of RCP4.5 and RCP8.5 calculated for all design events.

As for the analysis of RCE ESS, two indicators were employed – eroded volumes and eroded areas – which were calculated for the entire XBeach model domain. Erosion volumes and area for cases of no vegetation, present and planned for restoration concerning present conditions and two considered horizons of RCP4.5 and RCP8.5 calculated for all design events are presented in Figure 7.20 and Figure 7.21, respectively.

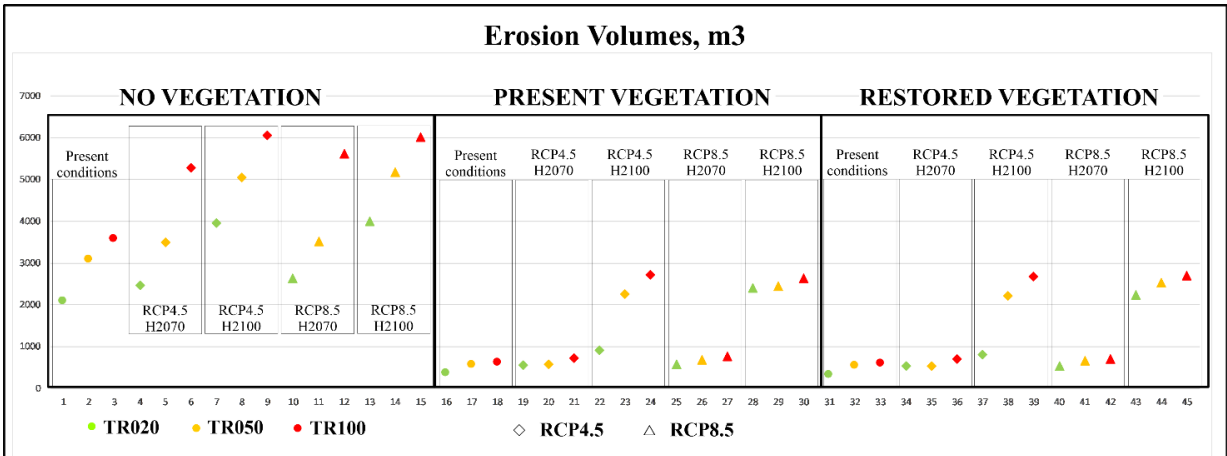


Figure 7.20. Erosion volumes for cases of no vegetation, present and planned for restoration concerning present conditions and two considered horizons of RCP4.5 and RCP8.5 calculated for all design events.

In case of no vegetation, the erosion volumes are in the range 2000 - 6000 m³. In presence of seagrasses, the erosion volumes decrease substantially by 1.7 to 7.9 times, as they are below 1000 m³ for all cases except for RCP4.5 H100 (TR050 and TR100) and RCP8.5 H100 (all return periods). The contribution of the restored seagrass meadow over the present vegetation is estimated to be 5% on the average as the maximum one 11.4% is calculated for case of TR020 RCP4.5 H2100 (Figure 7.20).

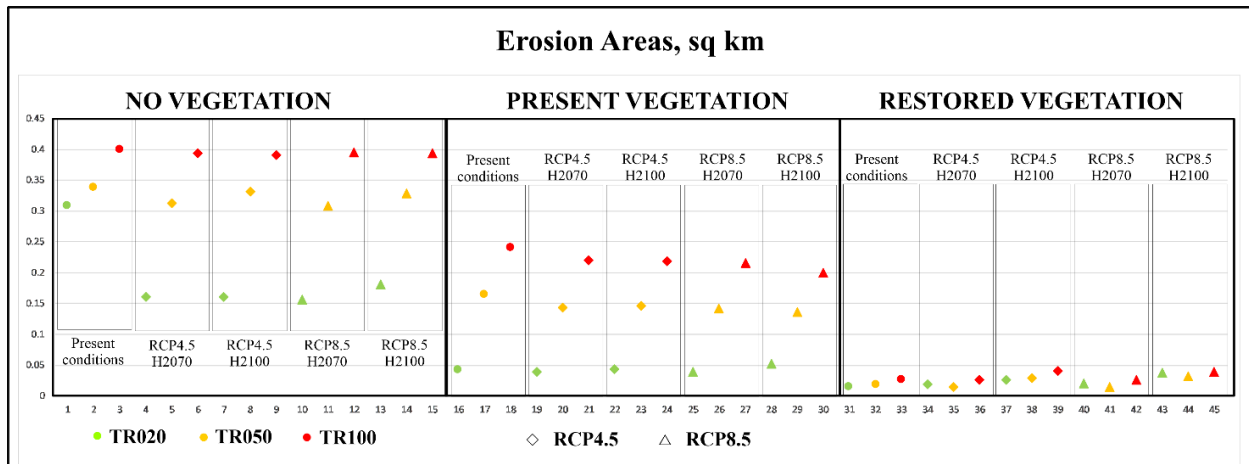


Figure 7.21. Erosion area for cases of no vegetation, present and planned for restoration concerning present conditions and two considered horizons of RCP4.5 and RCP8.5 calculated for all design events.

The behaviour of erosion area indicator shows slightly different trend. It displays the increasing contribution of seagrasses, as the ecosystem service is most valued considering the impact of restored vegetation (Figure 7.21). It should be reminded that this indicator includes also erosion areas of very thin eroded layer since the imposed threshold is set to 1cm sediment layer thickness.

In absence of vegetation, the areas affected by erosion vary between 0.16 and 0.40 sq. km. The existing vegetation contributes to the erosion mitigation by decreasing of the affected area by 1.7 – 7.4 times, whilst the contribution of restored meadows appears to be even more impacting – effected areas decrease by 4.8 – 21.6 times. The contribution of restored seagrass meadow over the present vegetation is estimated to be 72% on the average as the maximum one 90% is calculated for case of TR050 RCP4.5 H2070 (Figure 7.21).

The overall results suggest that the tipping point for contribution of ecosystem services towards reduction of erosion lies between climate change scenarios RCP8.5 H2070 and RCP4.5 H2100 with the major role of sea level rise within the range 0.35-0.49m.

7.5. Conclusions

The presented study reveals the impact of extreme events in combination with climate change projections of sea level rise on the Foros pilot and in particular estimates the ecosystem services of existing and planned for restoration seagrass vegetation. It is based on the results of hydrodynamic and morphodynamic modelling performed using Delft3D-FM FLOW&WAVE and XBeach models. The event approach was applied by considering three design events with return periods of 20, 50 and 100 years. The future conditions were addressed by making use of existing climate scenarios, more specifically middle and high-end ones RCP4.5 (SSP2-4.5) and RCP8.5 (SSP5-8.5). Considered projections were 2070 and 2100.

The hydrodynamic model results show that the prevailing flow pattern does not change significantly for all modelled conditions. A reduction of flow velocities is observed, which is very well pronounced over the area of both present and restored seagrass in particular for lower energy conditions. However, this effect decays with the increase of energy input of the system accompanied by the sea level rise for both climate change scenarios into consideration. Concerning the waves, a decrease of significant wave height over the area occupied by seagrasses was observed, which is more pronounced in the shallower part of the meadow, as well as in the inner bay corroborated by the wave energy dissipation pattern. Similarly to the flow behaviour, this effect vanishes with the increase of energy input in the system.

For both present and future conditions two ecosystem services were assessed – Reduction of Flood Risk (RFR) and Reduction of Coastal Erosion. The RFR indicator is flooded area (sq.km) while two indicators are employed for RCE analysis are eroded volumes and eroded areas. It is very important which indicator would be considered as more indicative, because the analysis depends on the targeted process and would lead to different valuation of ESS.

Concerning present conditions, the flood area indicator shows a slight increase of 6-8% for TR050 and TR100 compared to TR020 due to the wave action and surge. However, the flood area increases drastically for the selected climate scenarios and projections as the percentage varies between 62% (RCP4.5 H2070) and 84% (RCP8.5 H2100) mainly due to the sea level rise. The result implies that the seagrass presence has insignificant effect on reduction of flooding risk. Hence, this ESS is not relevant for the case of Foros pilot since the rising level is the main source of flooding, which seagrasses could not possibly influence on.

With respect to the RCE, it can be concluded that the presence of seagrasses affect significantly the erosion-accumulation pattern. The most considerable erosion volumes are observed along the coastline while within the surf zone and wetland the intensity of erosion process decreases. In case of no vegetation, the erosion volumes are in the range 2000 - 6000 m³, while in presence of seagrasses, they decrease substantially by 1.7 to 7.9 times. The contribution of the restored seagrass meadow over the present vegetation is estimated to be 5% on the average as the maximum one 11.4% is calculated for case of TR020 RCP4.5 H2100.

On the other hand, the erosion area indicator displays the increasing contribution of seagrasses with respect to the case of no vegetation, as the ecosystem service is most valued considering the impact of restored seagrass meadows. In absence of vegetation, the areas affected by erosion vary between 0.16 and 0.40 sq. km. The existing vegetation contributes to the erosion mitigation by decreasing of the affected area by 1.7 – 7.4 times, whilst the contribution of restored meadows appears to be even more impacting – effected areas decrease by 4.8 – 21.6 times. The contribution of restored seagrass meadow over the present vegetation is estimated to be 72% on the average as the maximum one 90% is calculated for case of TR050 RCP4.5 H2070.

The overall results suggest that the tipping point for contribution of ecosystem services towards reduction of erosion lies between climate change scenarios RCP8.5 H2070 and RCP4.5 H2100 with the major role of sea level rise within the range 0.35-0.49m.

8. Multi-risk projections and climate warnings with ESS in Vistula Lagoon (IBW)

8.1 Vistula Lagoon context

Vistula Lagoon is generally isolated from direct effects of sea level rise and increasing storminess, being separated from the Baltic Sea by a very strong, ca. 1.5 km wide coastal barrier with several strips of high dunes (up to 20 m high), additionally protected by forests and other vegetation. The barrier is sheltered from the most powerful waves being located inside the Gulf of Gdańsk. Hence, even the most extreme climatic scenarios (RCP 8.5) do not project the breaching of that barrier. Second, the Vistula Lagoon has a very mild wave climate due to its shallow bed (ca. 2.5 m on average). The main hydrodynamic forcings are produced by wind driven storm surges, which can be very high and exceed 1.5m. The most exposed areas, located in the SW corner of the Lagoon, see Figure 8.1, are heavily protected, but they remain outside the REST-COAST project. In all, the effects of sea level rise will be generally static for most banks of the Lagoon. As they are largely uninhabited and pristine, the ensuing permanent flooding will be acceptable. Another issue is the ice action during winter; ice often develops due to very shallow depth of the Lagoon. It can exert tremendous forces on any man-made structures. In this context, studies on risk projections and climatic warnings are mainly focused on the limits of application of NbS during erection and operation of the currently constructed artificial island – Vistula Lagoon pilot in the REST-COAST project, intended to serve as biodiversity restoration effort by creating a habitat for birds hatching on meadows, water birds and waders, see Figure 8.1.



Figure 8.1. Location of artificial island – study site in the Polish part of Vistula Lagoon: source – public domain, adapted by G. Różyński.

8.1.1. Criteria to define efficiency of risk reduction

High end IPCC sea level rise predictions along the Polish coast, located at the southernmost part of the Baltic Sea Baltic, are in the range of 0.7 – 0.9 m by the end of 21st Century, incl. the glacial isostatic adjustment. It will impact the western corner of the Lagoon - depression pertaining to Vistula Lagoon River Delta – cf. Figure 8.1. This vast issue is beyond the REST-COAST project – dikes securing the delta are being refurbished now and will have to be elevated further to secure future safety and ensure sustainable farming in the delta. Hence, IBW does not plan any studies related to remediation of sea level rise aftermaths in the delta. Second, breaching of the barrier separating the Lagoon from the Baltic Sea is very unlikely as well, incl. the highest seawater levels. Thus, this problem is also beyond the scope of the studied pilot site.

The criteria that determine the efficiency of risk reduction at Vistula Lagoon pilot are concentrated on: (1) maximization of NbS approach to the construction of the rim of the island, (2) minimization of impact of the placement of the island on hydrodynamics that controls local sediment transport patterns and adjacent morphodynamics, which is a form of respecting the NbS approach as well, and (3) harnessing secondary by-effects, resulting from the erection of the island, namely gradual, spontaneous appearance of reed fields around the rim (aimed at creation of additional spawning grounds for local fish populations) and partial denitrification of water returning to the Lagoon after deposition of dredged sediment. The main criterion regarding the rim is the required resilience against ice action. The main rationale regarding the island location is minimum change of wave and current fields forced by winds blowing from directions producing the largest fetch, i.e. NE and SW. The harnessing of by-effects is also consistent with the NbS approach.

8.1.2. Risk reduction

8.1.2.1. Ad. 1 The rim

The initial concept consisted in prioritization of the use of natural materials for the rim. This idea is presented in Figure 8.2, showing geo-tubes located at the inner and outer foot and on the top of the rim. The core is composed of sand and the whole structure is topped with a heavy stone armor resisting ice action.

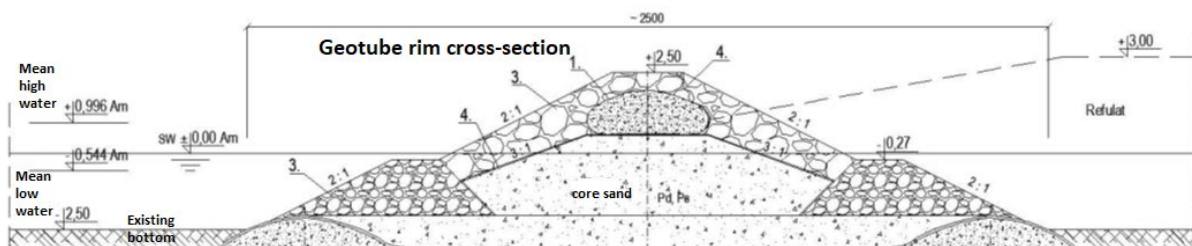


Figure 8.2. Initial concept of rim employing geo-tubes with local sediment, source Maritime Office Gdynia

This bold idea had to be discarded after the execution of strength tests of lagoon bed soil samples. They featured clays and silts with sizable admixtures of organic material (ca. 3% – 5%). Consequently, their natural water content is very high (between 50% - 120%) resulting in very low strength parameters against structural loads. Therefore, implementation of the concept shown in Figure 8.2 would certainly trigger very high and

uneven subsidence of the rim, so traditional engineering methods had to be used to construct the rim, cf. Figure 8.3. Simultaneously, limitations of NbS solutions in basins where the bed is composed of thick layers of organic sediments were identified and could be highlighted.



*Figure 8.3. Rim under construction, made of two rows of sheet piles with stone armor gradually forming the crest between them:
source - courtesy NDI group.*

The rim is ca. 5000 m long. It consists of two rows of Larsen sheet piles (each unit is 13 m long: 9 m driven through organic soils down to a stable sand layer, 2 m across the water column and 2 m above mean water level in Vistula Lagoon). Both rows are braced together on top and the space between them is filled with stone armor to resist ice action as one robust structure. The length of units demonstrates difficulties related to ultra-low strength parameters of the Lagoon's bed; they had to be driven to a depth securing safe contact with sand underlying thick organic sediments to ensure structural stability of the rim. The completed rim is presented in Figure 8.4. Heavy stone armor provides safety from sea level rise, and predominantly, from tremendous forces generated by ice in winters. The need for such robust structure also demonstrates limitations of NBS solutions in shallow basins in moderate latitudes, where ice action in winter is still a frequent phenomenon.



Figure 8.4. The rim of artificial island, Sept. 2023: source - REST-COAST

8.1.2.2. Ad. 2 Placement of the island

Hydrodynamic simulations were executed to evaluate the change of wave and current fields in the Lagoon after construction of the island. The DELFT3D package was used for this purpose. The location of the island was selected using trial-and-error methodology, guided by engineering experience of IBW team. It was intended to: (1) minimize changes of hydrodynamic regimes, (2) bearing in mind minimum disturbances to wildlife in the Lagoon, (3) minimizing construction costs of the island. Hence, the island had to be located away from the adjacent spawning areas for populations of fishes living in Vistula Lagoon. Economic considerations favored locations near the new navigation channel to the Baltic Sea. Figure 8.5 shows an exemplary simulation of alterations to the wave climate for NE wind speed of 10 m/s. Figure 8.6 presents the concomitant alterations for surface currents. As can be seen the alterations are very low, i.e. the ESS in the Lagoon will not be impacted. Importantly, the NE direction corresponds to the longest fetch in Vistula Lagoon and the resultant very low impacts can be primarily attributed to the shallow seabed, significantly limiting wave parameters. In all, the results present successful risk reduction achieved by minimization of alterations to local hydrodynamics; in this way the related morphodynamic changes were minimized as well.

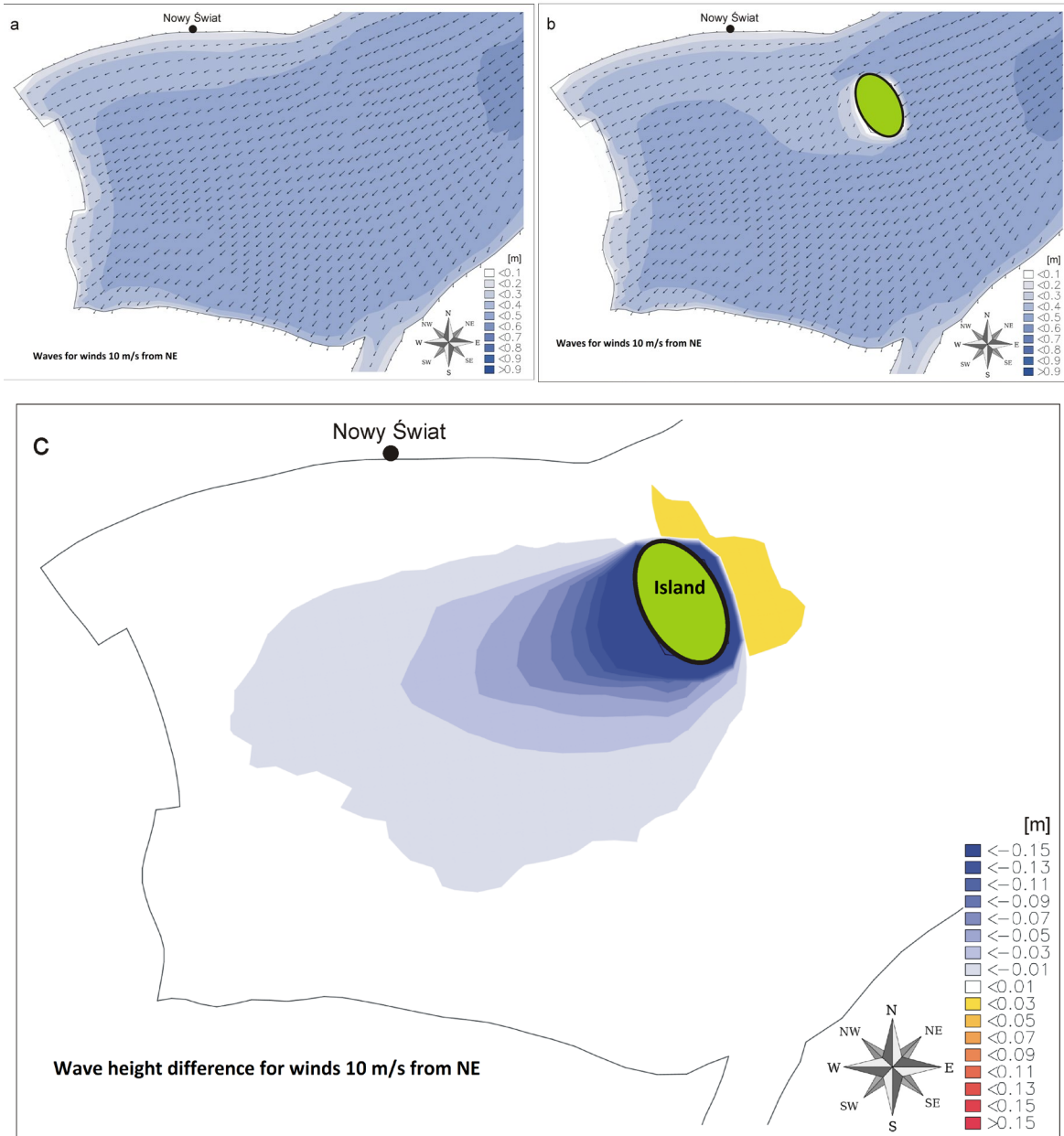


Figure 8.5. Wave heights for wind $v = 10$ m/s from NE: (a) without artificial island, (b) with the island, (c) differences in wave height: source – IBW PAN.

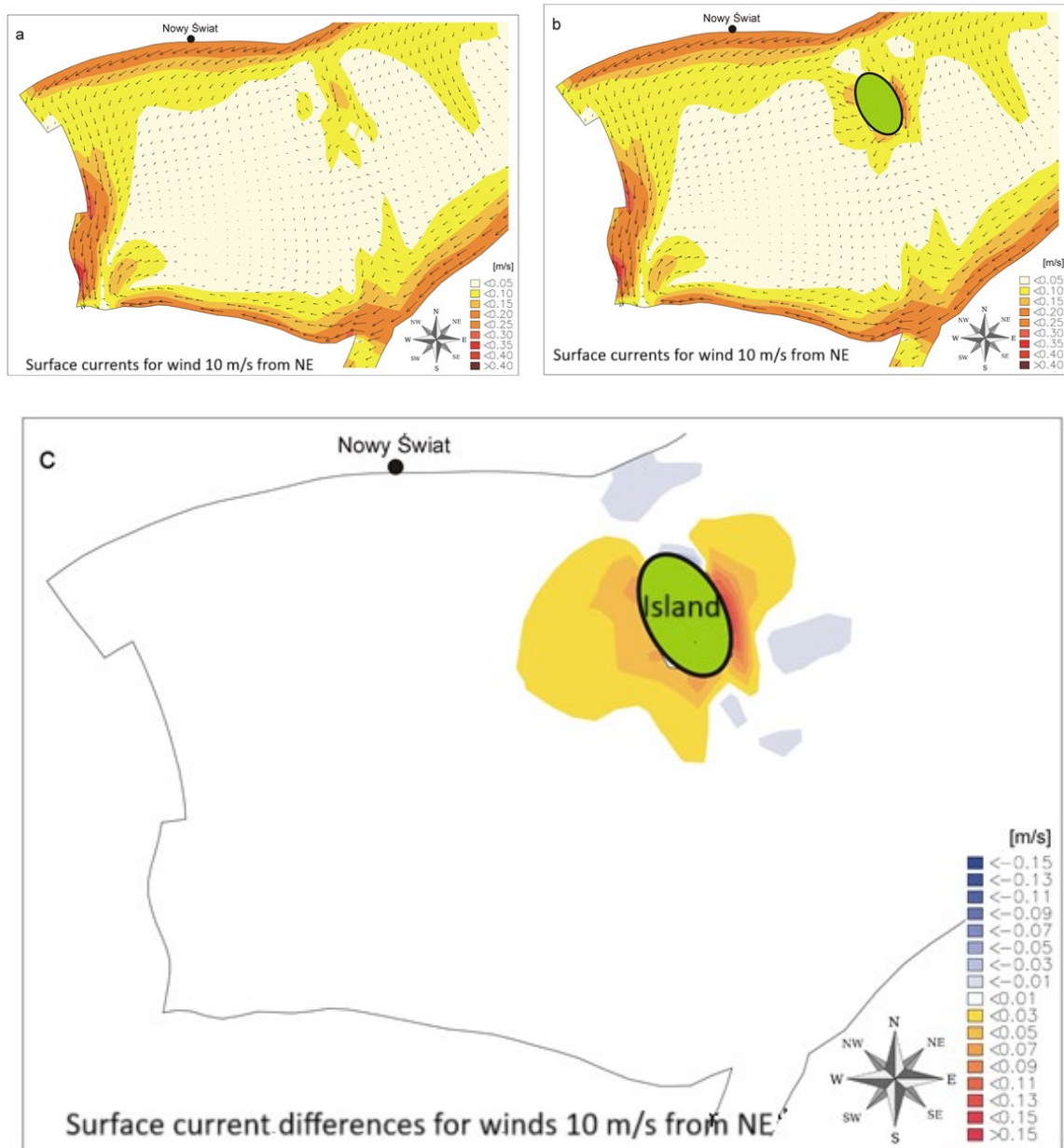


Figure 8.6. Surface currents for wind $v = 10$ m/s from NE: (a) without artificial island, (b) with the island, (c) differences in currents – IBW PAN.

8.1.2.3. Ad. 3 By-effects

Upon consultations with ichthyologists it was determined that reeds will gradually appear spontaneously around the island rim. Given its length of ca. 5000 m and conservatively assuming the width of 20 m we can expect additional spawning grounds of $5000 \cdot 20 = 100000 \text{ m}^2$ (10 ha). Other associated ESS will include formation of habitat for insects in the reeds on which both juvenile fish and birds living on the island will feed.

The other by-effect consists in extra denitrification of effluent returning to the Lagoon after delivering sediment to the island. This benefit will be occurring in sedimentation tanks for the effluent, where very fine

particles are separated from it. The effluent will be passing through jute rollers containing vegetation capable of its partial denitrification, see Figure 8.7. Upon trial-and-error the following plants were found suitable for this task: sweet flag (*Acorus calamus* L.), greater tussock-sedge (*Carex paniculata* L.), great manna grass (*Glyceria maxima* [Hartm.] Holmb.), common rush (*Juncus effusus* L.), lesser bulrush (*Typha angustifolia* L.) and common bulrush (*Typha latifolia* L.).

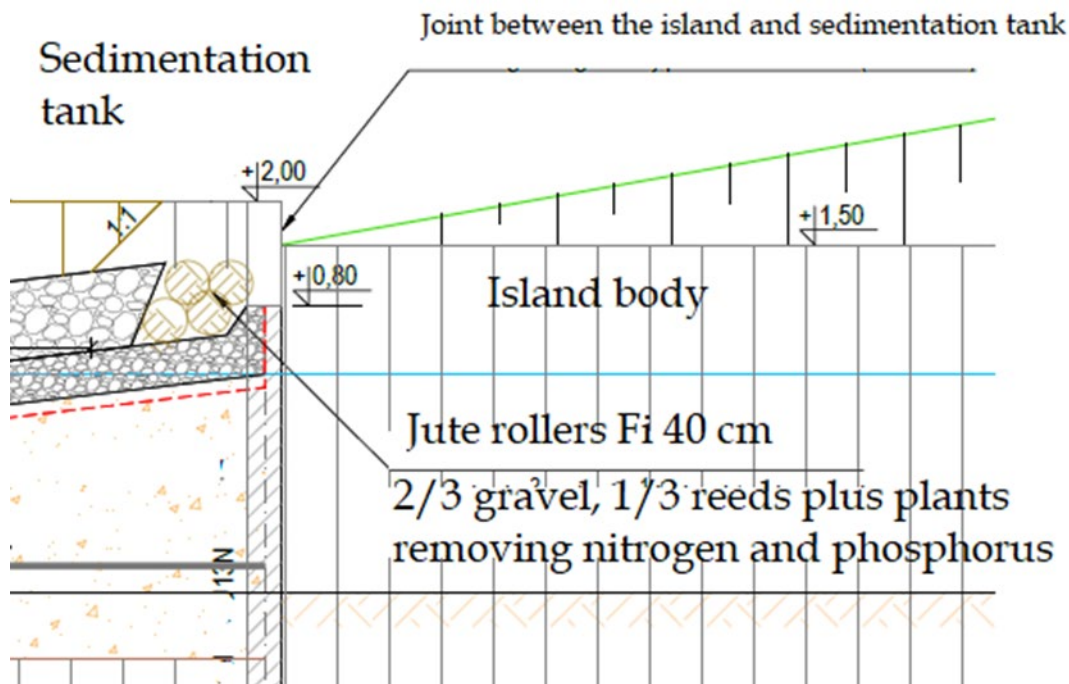


Figure 8.7. Denitrification by jute rollers containing reeds that denitrify effluent returning to Vistula Lagoon after deposition of sediment

8.1.3. Efficiency at long term under different climate projections

As Vistula Lagoon is generally sheltered from the effects of climate change (sea level rise and increased storminess) the focus of analyses presented herein was concentrated on the limits of NbS applied in shallow coastal lagoons. The study revealed that thick layers of organic sediments that form the beds of many shallow coastal lagoons are a serious impediment in implementation of NbS in structural design of marine structures. For this reason, traditional engineering solutions had to be applied during construction of the rim of artificial island. On the other hand, the island will serve as safe haven for birds hatching on meadows by artificial harvesting (or natural pasturing) of vegetation on the island to ensure the maintenance of grassland there. This solution can be recommended in all areas where a need for safe bird habitat emerges, irrespectively of climate change consequences.

The process of determination of optimum placement of the island is a legacy applicable to any similar site for all climatic scenarios as well. Importantly, it is consistent from the point of view of NbS rationale by minimization of impacts of the new island on adjacent hydrodynamics. Also, it respects ecological considerations by prior determination of existing spawning grounds and ultimate placement of the island away from them. Finally, the economic aspect was incorporated by locating the island at minimum possible costs related to the required engineering and hydraulic (dredging) works.

When schemes like the artificial island on Vistula Lagoon are considered, one should always incorporate their potential positive by-effects. The improvement of water quality of effluent returning to the lagoon after deposition of sediment on the island can be recommended under any climatic scenario. Also, spontaneous formation of reed fields around the island leading to the appearance of new spawning grounds should be viewed positively; new grounds will be functioning under any climatic scenario. The only aspect that requires attention is a possible appearance of alien fishes in future, which can be climate change related: such developments may necessitate carefully planned interventions.

8.1.4. Conclusions

This pilot site is primarily aimed at biodiversity restoration and conservation of birds deemed important elements of the local ecosystem. Vistula Lagoon is both NATURA 2000 area for both birds (PLB280010) and habitats (PLH280007). This explains the efforts aimed at biodiversity restoration. Simultaneously, one of key characteristics of the Lagoon is its almost perfect sheltering from climate change consequences, apart from its south western corner, which is entirely outside the REST-COAST project. Therefore, climate change consequences are of secondary importance at the study site, since occasional inundations of the island under sea level rise are considered natural at seaside meadows, maintained on the island. The main lesson learned are the identified limitations of NBS at sites featured by thick layers of organic soils. Considerations regarding the placement of the island can serve as blueprint for similar analyses elsewhere. Also, positive utilization of by-effects can be recommended in future (biodiversity) restoration efforts.

9. Integrated conclusions

The aim of the current deliverable is to assess the projections of ecosystem-services (ESS) provided by effective coastal restoration, combining sediment management (e.g. dunes reconstruction) with reconstruction of salt marsh and seagrass meadows within different REST_COAST pilot sites. The main conclusions for the more advanced Pilots (in terms of restoration) and under future horizons are summarized in what follows.

This deliverable provides an integrated assessment of future scenarios for ecosystem service (ESS) delivery associated with coastal restoration interventions in REST-COAST pilot sites. Building upon the storm-based modelling efforts reported in D2.1, this report focuses on the projections of long-term performance of Nature-Based Solutions (NbS) under sea level rise (SLR), storm intensification and changing sediment dynamics.

Restoration of **salt marshes** for ESS in Wadden Sea and Venice Lagoon:

- In **Wadden Sea**, NbS involving salt marsh restoration demonstrate a significant capacity to modify hydrodynamic behavior and sediment transport. The presence of salt marshes delays both the rise and fall of water levels, favoring sediment deposition, though this effect is sensitive to storm intensity and spatial location. Modelling results show a clear reduction in sediment export beyond the marsh edges and lower bed evolution within the vegetated areas. During storm events, sediment export into Ley Bay is reduced in scenarios with NbS, confirming the protective role of restored salt marshes in reducing erosion.
- In **Venice Lagoon**, salt marshes affect circulation patterns, particularly during flood phases, producing slight sea level adjustments (± 1 cm) due to flow restriction. While wave conditions show limited alteration in projected climate scenarios, restoration interventions enhance attenuation of high-energy wave events. The spatial configuration of restored areas plays a critical role; marshes positioned near deeper channels are associated with increased significant wave height (SWH) and current intensity, while sheltered sectors demonstrate marked reductions. These effects collectively underscore the importance of design and placement in NbS planning.

Restoration of **seagrass meadows** for ESS in Foros Bay and Arcachon Bay:

- In the **Foros Bay**, seagrass restoration contributes to a measurable reduction in flow velocities and wave heights under low-energy conditions. These effects are more pronounced in shallow zones and inner parts of the bay. However, their effectiveness diminishes under higher energy input or SLR-driven scenarios. Although seagrass has limited impact on flood mitigation, it plays a significant role in modifying erosion–sedimentation patterns, especially along the coastline. The results suggest that restored seagrass meadows enhance sediment stability, particularly in the surf zone and adjacent wetland areas.
- The **Arcachon Bay** restoration modelling incorporates socio-economic analysis to link biophysical processes with key local activities such as tourism, boating and fisheries. Sediment management and water quality emerge as primary ESS. Under increased SLR, the modelling indicates greater sedimentation on mudflats and enhanced water renewal in the lagoon, improving water quality. Conversely, deeper channels may promote navigability. This modular approach supports decision-making by projecting ESS sensitivity across different future time horizons.

Restoration by **effective sediment management** for ESS in Sicily Lagoon, Vistula lagoon and Ebro Delta:

- In **Sicily Lagoon**, the combination of dune reconstruction and vegetative stabilisation demonstrates potential to reduce erosion and wave-induced flooding near urban areas. Nevertheless, SLR projections—even under moderate scenarios—suggest that lagoon expansion could encroach into inhabited zones. This shift may impact biodiversity through habitat loss, submersion of artificial nesting islands, and increased salinity intrusion, with possible effects on groundwater quality.
- **Vistula lagoon**, is primarily focused on biodiversity restoration, with particular attention to bird habitats within designated Natura 2000 sites. Given the lagoon’s natural protection from open sea influences, climate change impacts are expected to remain limited, and occasional inundation is seen as ecologically compatible. The risk assessment therefore emphasises ecosystem functionality and habitat connectivity over direct hazard mitigation.
- In the **Ebro Delta**, projected reductions in river discharge threaten the sediment supply required for long-term delta maintenance. Under current abstraction levels, sediment transport capacity may decrease significantly, further exacerbating delta retreat. Modelling of coastal dynamics suggests that classical beach nourishment is less effective over time due to sediment loss and high maintenance requirements. In contrast, alternating dune systems, which allow storm energy dissipation while preserving internal dune volumes, perform better in long-term scenarios. These structures combine ecological stability with technical effectiveness, especially under intense SLR and storm conditions

Overall, the results presented in this deliverable highlight the potential of NbS to deliver multiple ESS under future climate scenarios. While effectiveness varies by site and intervention type, the modelling frameworks developed under WP2 offer a robust platform for comparing restoration alternatives and guiding long-term adaptation planning. The incorporation of ecological functionality, morphological response, and socio-economic relevance into a unified risk-based approach marks a significant advancement in ecosystem-based coastal resilience strategies.

Taken together, the pilot site results confirm that Nature-Based Solutions offer measurable benefits in reducing coastal risks and enhancing ecosystem functioning, even under uncertain future conditions. By integrating ecosystem service projections into advanced modelling frameworks, this deliverable provides the analytical foundation for designing adaptive, locally tailored strategies that complement or replace conventional hard infrastructure. The cross-site insights gained in D2.2 are intended to inform both site-specific restoration actions and broader governance frameworks, reinforcing the role of ecosystem-based adaptation in European coastal resilience policy.

10. References

- Alberti, T., Anzidei, M., Faranda, D., Vecchio, A., Favaro, M., & Papa, A. (2023). Dynamical diagnostic of extreme events in Venice lagoon and their mitigation with the MoSE.
- Anderson, R.S.(2002) Modeling the tor-dotted crests, bedrock edges, and parabolic profiles of high alpine surfaces of the Wind River Range, Wyoming. *Geomorphology* 46, 35–58.
- Auby I., Bost C.A., and Budzinski H. (2011). Régression des herbiers de zostères dans le Bassin d’Arcachon : état des lieux et recherche des causes. Rapport Ifremer RST/LER/AR/11.007, 195p.
- Arias A. (2022). Modélisation des interactions macrophytes-dynamique sédimentaire : Application aux herbiers de zostères du Bassin d’Arcachon et à leur régression récente. MSc manuscript, Université de Bordeaux, Ifremer, 52p.
- Ballé-Béganton J., J. Herry, M. Philippe, R. Pasco, B. Angst, M. Urien, D. Bailly, M. Cassé (2015). Les services écosystémiques en soutien à la gestion des herbiers de zostères du golfe du Morbihan. Projet Interreg IVA Manche VALMER, 14p.
- Banzo M., C. Cazals et V. André-Lamat (2018). Le bassin d’Arcachon entre attractivité et protection. *Sud-Ouest européen*, 45, 13-24.
- Baptist, M., 2005. Modelling floodplain biogeomorphology, PhD Dissertation, TU Delft library, <http://resolver.tudelft.nl/uuid:b2739720-e2f6-40e2-b55f-1560f434cbee>.
- Baptist, M. J., Van Der Wal, J. T., Folmer, E. O., Gräwe, U., & Elschot, K. (2019). An ecotope map of the trilateral Wadden Sea. *Journal of Sea Research*, 152, 101761.
- Batalla R.J., Vericat D. (2011) Hydrology and Sediment Transport. The Ebro River Basin. *Handbook of Environmental Chemistry* 13, 21–46, D. Barcelo and M. Petrovic (eds.)
- Benedet, L., Dobrochinski, J. P. F., Walstra, D. J. R., Klein, A. H. F., & Ranasinghe, R. W. M. R. J. B. (2016). A morphological modeling study to compare different methods of wave climate schematization and evaluate strategies to reduce erosion losses from a beach nourishment project. *Coastal engineering*, 112, 69-86.
- Bladé, E., Cea, L., Corestein, G., Escolano, E., Puertas, J., Vázquez-Cendón, E., Dolz, J., Coll, A. (2014) Iber: Herramienta de simulación numérica del flujo en ríos. *Rev. Int. Métodos Numér. Cálculo. Diseño Ing.*, 30, 1–10.
- Boucher J.-M., Delteril J.-P., Manaud F., Maurer D. and Trut G. (1997). Étude intégrée du bassin d’Arcachon. Rapport Ifremer, Brest, France, 129p.
- Bouma, H., De Jong, D.J., Twisk, F., Wolfstein, K., 2005. A Dutch Ecotope System for Coastal Waters (ZES.1). Middelburg, report RIKZ/2005.024. English version June 2006.
- Caires, S., & Yan, K. (2020). Ocean surface wave time series for the European coast from 1976 to 2100 derived from climate projections. Copernicus Climate Change Service (C3S) Climate Data Store (CDS).
- Cea, L., Puertas, J., Vázquez-Cendón, M.E. (2007) Depth Averaged Modelling of Turbulent Shallow Water Flow with Wet-Dry Fronts. *Arch. Comput. Methods Eng.*, 14, 303–341.
- Chen, W., Staneva, J., Jacob, B., Sanchez-Artus, X. and Wurpts, A., What-If Nature-Based Storm Buffers on Mitigating Coastal Erosion. *Science of the Total Environment* (under review) Available at SSRN 4463184.

- Church J. A., Clark P. U., Cazenave A., Gregory J. M., Jevrejeva S., Levermann A., et al. (2013). "Sea level change'," in *Climate change 2013: The physical science basis. contribution of working group I to the fifth assessment report of the intergovernmental panel on climate change*. Eds. Stocker T. F., Qin D., Plattner G.-K. (Cambridge; New)
- Chytrý, M., Tichý, L., Hennekens, S. M., Knollová, I., Janssen, J. A., Rodwell, J. S., ... & Schaminée, J. H. (2020). EUNIS Habitat Classification: Expert system, characteristic species combinations and distribution maps of European habitats. *Applied Vegetation Science*, 23(4), 648-675.
- Cognat M. (2019). Rôles des facteurs environnementaux et des interactions biomorphodynamiques sur l'évolution spatio-temporelle des herbiers de zostères dans une lagune mésotidale. PhD thesis, Université de Bordeaux.
- Colosimo, I., van Maren, D. S., de Vet, P. L. M., Winterwerp, J. C., and Van Prooijen, B. C., 2023. Winds of opportunity: The effects of wind on intertidal flat accretion. *Geomorphology*, 108840. doi.org/10.1016/j.geomorph.2023.108840
- Coles, S., 2009. An introduction to statistical modeling of extreme values. 3. print., Springer series in statistics. Springer: London, United Kingdom.
- Dam, G., M. van der Wegen, R. J. Labeur, and D. Roelvink (2016). Modeling centuries of estuarine morphodynamics in the Western Scheldt estuary. *Geophys. Res. Lett.*, 43, 3839-3847.
- Dean, R. G., & Yoo, C. H. (1992). Beach-nourishment performance predictions. *Journal of waterway, port, coastal, and ocean engineering*, 118(6), 567-586.
- Delft3D, 2023. Delft3D-Flow User Manual: Delft3D-FLOW User Manual (deltares.nl), p. 252-261 and 627-630.
- De Vriend, H. J., M. Capobianco, T. Chesher, H. E. de Swart, B. Latteux, and M. J. F. Stive (1993). Approaches to long-term modelling of coastal morphology: A review. *Coast. Eng.*, 21(1-3), 225-269.
- Dinu I., Monclus i Bori A., Gràcia V., Garcia-Leon M., Lin-Ye J., Stanica A. and Sanchez-Arcilla A. (2023). Assessing the coastal protection role of seagrass meadows along a barrier beach, southern Romanian coast. *Journal of Sea Research*, 191, 102329.
- Dissanayake, P. and Wurpts, A., 2013. Modelling an anthropogenic effect of a tidal basin evolution applying tidal and wave boundary forcing: Ley Bay, East Frisian Wadden Sea, *Coastal Engineering* 82, 9-24.
- Dissanayake, P., Wurpts, A., Winter, C., 2019. Storm Classification and the Investigation of Impacts on Beach/Dune. In: Goseberg, Nils; Schlurmann, Torsten (Hg.): *Coastal Structures 2019*. Karlsruhe: Bundesanstalt für Wasserbau. S. 632-641. https://doi.org/10.18451/978-3-939230-64-9_063.
- Dolch, T., Folmer, E. O., Frederiksen, M. S., Herlyn, M., van Katwijk, M. M., Kolbe, K., ... Westerbeek, E. P. (2017). Seagrass. In *The Wadden Sea Quality Status Report*
- Donatelli C., Ganju N. K., Fagherazzi S. and Leonardi N. (2018). Seagrass Impact on Sediment Exchange Between Tidal Flats and Salt Marsh, and The Sediment Budget of Shallow Bays. *Geophysical Research Letters*, 45(10), 4933-4943.
- Dronkers, J. (1986). Tidal asymmetry and estuarine morphology. *Neth. J. Sea Res.*, 20(2/3), 117-131.
- Elias, E., Alonso, A.C., van Maren, B. (2021). Morfologische veranderingen Eems-Dollard en Groninger Wad.

Deltares report 11203742-000-ZKS-0003

- Elmilady, H., van der Wegen, M., Roelvink, D., & van der Spek, A. (2020). Morphodynamic evolution of a fringing sandy shoal: From tidal levees to sea level rise. *Journal of Geophysical Research: Earth Surface*, 125, e2019JF005397. <https://doi.org/10.1029/2019JF005397>
- Esselink, P., van Duin, W.E., Bunje, J., Cremer, J., Folmer, E.O., Frikke, J., Glahn, M., de Groot, A.V., Hecker, N., Hellwig, U., Jensen, K., Körber, P., Petersen, J., Stock, M., 2017. Salt marshes, In: Wadden Sea Quality Status Report 2017. Eds: Kloepper, S. et al., Common Wadden Sea Secretariat, Wilhelmshaven, Germany. Last updated 21.12.2017.
- Faranda, D., Ginesta, M., Alberti, T., Coppola, E., & Anzidei, M. (2023). Attributing Venice Acqua Alta events to a changing climate and evaluating the efficacy of MoSE adaptation strategy. *npj climate and atmospheric science*, 6(1), 181.
- Fernández-Montblanc, T., Duo, E., & Ciavola, P. (2020). Dune reconstruction and revegetation as a potential measure to decrease coastal erosion and flooding under extreme storm conditions. *Ocean & Coastal Management*, 188, 105075.
- Garner, G. G., T. Hermans, R. E. Kopp, A. B. A. Slangen, T. L. Edwards, A. Levermann, S. Nowicki, M. D. Palmer, C. Smith, B. Fox-Kemper, H. T. Hewitt, C. Xiao, G. Aðalgeirsdóttir, S. S. Drijfhout, T. L. Edwards, N. R. Golledge, M. Hemer, R. E. Kopp, G. Krinner, A. Mix, D. Notz, S. Nowicki, I. S. Nurhati, L. Ruiz, J-B. Sallée, Y. Yu, L. Hua, T. Palmer, B. Pearson, 2021. IPCC AR6 Sea-Level Rise Projections. Version 20210809. PO.DAAC, CA, USA. Dataset accessed [2023-11-26] at <https://podaac.jpl.nasa.gov/announcements/2021-08-09-Sea-level-projections-from-the-IPCC-6th-Assessment-Report>.
- Garzon, J. L., Miesse, T., & Ferreira, C. M. (2019). Field-based numerical model investigation of wave propagation across marshes in the Chesapeake Bay under storm conditions. *Coastal Engineering*, 146, 32-46.
- Golledge N. R. (2020). Long-term projections of sea-level rise from ice sheets. *Wiley Interdiscip. Reviews: Climate Change* 11 (2), e634. doi: 10.1002/wcc.634
- Gorría, H. (1877) Desecación de las marismas y terrenos pantanosos denominados de Los Alfaques. Tech. Rep., Ministerio de Agricultura. Madrid
- Gracia, V., García, M., Grifoll, M., & Sánchez-Arcilla, A. (2013). Breaching of a barrier under extreme events. The role of morphodynamic simulations. *Journal of Coastal Research*, (65), 951-956.
- Grases, A., Gracia, V., García-León, M., Lin-Ye, J., & Sierra, J. P. (2020). Coastal flooding and erosion under a changing climate: implications at a low-lying coast (Ebro Delta). *Water*, 12(2), 346.
- Haff, P. K. (1996), Limitations on predictive modeling in geomorphology, in *The Scientific Nature of Geomorphology*. Edited by B. Rhoads and C. Thorn, pp. 337-358, Wiley, New York.
- Haff, P. K. (2013), Prediction in geology versus prediction in engineering, *Geol. Soc. Am. Spec. Pap.*, 502, doi:10.1130/2013.2502(06).
- Hargrove, W. W., Hoffman, F. M., & Hessburg, P. F. (2006). Mapcurves: a quantitative method for comparing categorical maps. *Journal of Geographical Systems*, 8, 187-208.
- Hausfather, Z., & Peters, G. P. (2020). RCP8. 5 is a problematic scenario for near-term emissions. *Proceedings of the National Academy of Sciences*, 117(45), 27791-27792.

- Hersbach, H., Bell, B., Berrisford, P., Hirahara, S., Horányi, A., Muñoz-Sabater, J., ... & Thépaut, J. N. (2020). The ERA5 global reanalysis. *Quarterly Journal of the Royal Meteorological Society*, 146(730), 1999-2049.
- Holthuijsen, L. H., Booij, N., & Herbers, T. H. C. (1989). A prediction model for stationary, short-crested waves in shallow water with ambient currents. *Coastal engineering*, 13(1), 23-54.
- Houser, C., Hapke, C., & Hamilton, S. (2008). Controls on coastal dune morphology, shoreline erosion and barrier island response to extreme storms. *Geomorphology*, 100(3-4), 223-240.
- Houwing, E. J., Tanczos, I.C., Kroon, A., De Vries, M.B., 2000. Interaction of submerged vegetation, hydrodynamics and turbidity; analysis of field and laboratory studies, Conference Proc. INTERCOH2000.
- Ibàñez C., Prat N., Canicio A. (1996) Changes in the hydrology and sediment transport produced by large dams on the lower Ebro river and its estuary. *Regulated Rivers: Research and Management*, 12, 51-62.
- Islek, F., Yüksel, Y. and Sahin. C. 2022. Evaluation of regional climate models and future wave characteristics in an enclosed sea: A case study of the Black Sea. *Ocean Engineering*, Volume 262, 112220, ISSN 0029-8018, <https://doi.org/10.1016/j.oceaneng.2022.112220>
- IPCC SIXTH ASSESSMENT REPORT (AR6) "CLIMATE CHANGE 2023" (<https://www.ipcc.ch/report/ar1/wg1/sea-level-rise/>), 2023
- Jacob, B., Dolch, T., Wurpts, A., & Staneva, J. (2023). Evaluation of seagrass as a nature-based solution for coastal protection in the German Wadden Sea. *Ocean Dynamics*, 73(11), 699-727
- Istituto Idrografico della Marina (2019), Nautical charts, Panels 20-21, Genova.
- Janowski, L., Madricardo, F., Fogarin, S., Kruss, A., Molinaroli, E., Kubowicz-Grajewska, A., & Tegowski, J. (2020). Spatial and temporal changes of tidal inlet using object-based image analysis of multibeam echosounder measurements: A case from the Lagoon of Venice, Italy. *Remote Sensing*, 12(13), 2117.
- Jiménez, José A., and Agustín Sánchez-Arcilla. (2004). "A long-term (decadal scale) evolution model for microtidal barrier systems." *Coastal Engineering* 51.8-9: 749-764.
- Kaiser, R.; Knaack, H.; Miani, M.; Niemeyer, H.D., 2010. Examination of Climate Change adaptation strategies for Coastal Protection. In: MCKEE SMITH, J. and LYNETT, P. (ed.): Proceedings of the 32nd International Conference on Coastal Engineering, 2010, Shanghai. <http://journals.tdl.org/icce/index.php/icce/issue/view/154/showToc>
- Kaspar, F., Niermann, D., Borsche, M., Fiedler, S., Keller, J., Potthast, R., Rösch, T., Spanghel, T., and Tinz, B.: Regional atmospheric reanalysis activities at Deutscher Wetterdienst: review of evaluation results and application examples with a focus on renewable energy, *Adv. Sci. Res.*, 17, 115-128. <https://doi.org/10.5194/asr-17-115-2020>, 2020
- Knutson, P. L., Brochu, R. A., Seelig, W. N., & Inskeep, M. (1982). Wave damping in *Spartina alterniflora* marshes. *Wetlands*, 2, 87-104.
- Korres, G., Ravdas, M., & Zacharioudaki, A. (2019). Mediterranean sea waves analysis and forecast (CMEMS MED-Waves).
- Kriegler, F. J. (1969). Preprocessing transformations and their effects on multispectral recognition. In

Proceedings of the Sixth International Symposium on Remote Sensing of Environment (pp. 97-131).

Lang A., Mikolajewicz U. (2020). Rising extreme sea levels in the German bight under enhanced CO₂ levels: A regionalised large ensemble approach for the north Sea. *Clim Dyn* 55, 1829–1842. doi: 10.1007/s00382-020-05357-5

Le Corre N., Le Berre S., Peuziat I., Brigand L. and Courtel J. (2015). Approche des espaces de la pratique nautique par l'analyse de la fréquentation : l'exemple du bassin de navigation arcachonnais. *VertigO*, vol. 15(3), online.

Lesser, G., Roelvink, J.A., Van Kester, J.A.T.M., Stelling, G.S., 2004. Development and validation of a three-dimensional morphological model. *Coastal Engineering*, 51, 883–915.

Management Plan of Protected Area "Poda" for the period from 2002 - 2010", Birdlife International, 2002

Mathis M., Mikolajewicz U. (2020). The impact of meltwater discharge from the Greenland ice sheet on the Atlantic nutrient supply to the northwest European shelf. *Ocean Sci.* 16 (1), 167–193. doi: 10.5194/os-16-167-2020

Mascioli, F., Piattelli, V., Cerrone, F., Gasprino, D., Kunde, T., Miccadei, E., 2021. Feasibility of objective seabed mapping techniques in a coastal tidal environment (Wadden Sea, Germany), *Geosciences*, 11(2), 49.

Maxwell, P. J. S. Eklof, M. M. van Katwijk, K. R. O'Brien, M. de la Torre-Castro, C. Boström, et al. (2016). The fundamental role of ecological feedback mechanisms for the adaptive management of seagrass ecosystems - a review. *Biological Reviews*, pp. 0-0.

Mayer, A., & Silver, W. L. (2022). The climate change mitigation potential of annual grasslands under future climates. *Ecological Applications*, 32(8), e2705.

Mendoza, E. T., Jimenez, J. A., & Mateo, J. (2011). A coastal storms intensity scale for the Catalan sea (NW Mediterranean). *Natural Hazards and Earth System Sciences*, 11(9), 2453-2462.

Mikolajewicz U., Sein D. V., Jacob D., König T., Podzun R., Semmler T. (2005). Simulating Arctic sea ice variability with a coupled regional atmosphere-ocean-sea ice model. *Meteorologische Z.* 14 (6), 793–800. doi: 10.1127/0941-2948/2005/0083

Mudd, S.M., Furbish, D.J. (2004) Influence of chemical denudation on hillslope morphology. *J. Geophys. Res. Earth Surf.*, 109. doi:10.1029/2003JF000087.

Murphy, A. H., & Epstein, E. S. (1989). Skill scores and correlation coefficients in model verification. *Monthly weather review*, 117(3), 572-582.

Nepf, H. M., & Vivoni, E. R. (2000). Flow structure in depth-limited, vegetated flow. *Journal of Geophysical Research: Oceans*, 105(C12), 28547-28557.

Niemeyer, H. D., Berkenbrink, C., Ritzmann, A., Knaack, H., Wurpts, A., Kaiser, R., 2014. Evaluation of Coastal Protection Strategies in Respect of Climate Change Impacts. In: *Die Küste 81*. Karlsruhe: Bundesanstalt für Wasserbau. S. 565-577.

Nguyen, H. M., Bryan, K. R., Zhou, Z., & Pilditch, C. A. (2022). Modeling the effects of aerial temperature and exposure period on intertidal mudflat profiles. *Continental Shelf Research*, 245, 104802.

Oberrecht, D., 2020. Development of a numerical modeling approach for large-scale fluid mud flow in estuarine

- environments. Hannover: Gottfried Wilhelm Leibniz Universität, Diss., 2020, xvi, 118 S. DOI: <https://doi.org/10.15488/10488>
- Palmer M. D., Gregory J. M., Bagge M., Calvert D., Hagedoorn J. M., Howard T., et al. (2020). Exploring the drivers of global and local sea-level change over the 21st century and beyond. *Earth's Future* 8, e2019EF001413. doi: 10.1029/2019EF001413
- Palmer M., Howard T., Tinker J., Lowe J., Brichenno L., Calvert D., et al. (2018). UKCP18 marine report. Met Office Hadley Centre, Exeter, United Kingdom, 133pp.
- Paola, C., Voller, V.R. (2005) A generalized Exner equation for sediment mass balance. *J. Geophys. Res. Earth Surf.*, 110. doi:10.1029/2004JF000274.
- Parisot J.-P., J. Diet-Davancens, A. Sottolichio, E. Crosland, C. Drillon, and R. Verney (2008). Modélisation des agitations dans le bassin d'Arcachon. *Xèmes Journées Sophia Antipolis*, pages 435-444.
- Pein, J., Staneva, J., Mayer, B., Palmer, M. D., & Schrum, C. (2023). A framework for estuarine future sea-level scenarios: Response of the industrialised Elbe estuary to projected mean sea level rise and internal variability. *Frontiers in Marine Science*, 10, 1102485.
- Pelisson C. (2019). Modélisation de la dynamique sédimentaire dans le Bassin d'Arcachon en lien avec la dynamique temporelle des herbiers de zostères. MSc manuscript, Université Bretagne-Sud, Ifremer, 50p.
- Plus M., Dumas F., Stanisière J.-Y. and Maurer D. (2009). Hydrodynamic characterization of the Arcachon Bay, using model-derived descriptors. *Continental Shelf Research* 29, 1008-1013.
- Pries, A. J., Miller, D. L., & Branch, L. C. (2008). Identification of structural and spatial features that influence storm-related dune erosion along a barrier-island ecosystem in the Gulf of Mexico. *Journal of Coastal Research*, (24), 168-175.
- Reeves I. R. B., L. J. Moore, E. B. Goldstein, A. B. Murray, J. A. Carr et al. (2019). Impacts of Seagrass Dynamics on the Coupled Long-Term Evolution of Barrier-Marsh-Bay Systems. *JGR Biogeosciences*, 125(2), e2019JG005416.
- Rodríguez-Santalla, I., & Navarro, N. (2021). Main threats in Mediterranean coastal wetlands. The Ebro Delta case. *Journal of Marine Science and Engineering*, 9(11), 1190.
- Roelvink, D., Reniers, A., Van Dongeren, A. P., De Vries, J. V. T., McCall, R., & Lescinski, J. (2009). Modelling storm impacts on beaches, dunes and barrier islands. *Coastal engineering*, 56(11-12), 1133-1152
- Roland A, Zhang YJ, Wang HV, et al (2012). A fully coupled 3D wave-current interaction model on unstructured grids. *Journal of Geophysical Research: Oceans* 117(C11). <https://doi.org/10.1029/2012JC007952>
- Santillán, D., Cueto-Felgueroso, L., Sordo-Ward, A., Garrote, L. (2020) Influence of Erodible Beds on Shallow Water Hydrodynamics during Flood Events. *Water*, 12, 3340, doi:10.3390/w12123340
- de Schipper, M. A., Ludka, B. C., Raubenheimer, B., Luijendijk, A. P., & Schlacher, T. A. (2021). Beach nourishment has complex implications for the future of sandy shores. *Nature Reviews Earth & Environment*, 2(1), 70-84.
- Scheel, F. (2017). Memo Input Reduction Tool - Description and User Manual. Deltares memo 1221439-000-HYE-0004. https://svn.oss.deltares.nl/repos/openearthtools/trunk/matlab/applications/tools/input_reduction_tool/D

escription_and_user_manual_input_reduction_tool.pdf

- Schrijvershof, R. A., van Maren, D. S., Torfs, P. J., & Hoitink, A. J. F. (2023). A Synthetic Spring-Neap Tidal Cycle for Long-Term Morphodynamic Models. *Journal of Geophysical Research: Earth Surface*, 128(3), e2022JF006799.
- Shields, A. (1936). Anwendung der Aehnlichkeitsmechanik und der Turbulenzforschung auf die Geschiebebewegung. Mitteilung der Preussischen Versuchsanstalt für Wasserbau und Schiffbau, Heft 26, Berlin.
- SIBA (2013). Recueil de données tourisme sur le Bassin d’Arcachon. Online documentation, 17p., consulted in December 2023.
- SIBA (2023). Recueil de données touristiques, Bassin d’Arcachon. Bassin d’Arcachon, un monde à part. Région Nouvelle Aquitaine, updated in June 2023, 30p.
- Soulsby, R.L., Whitehouse, R.J.S. (1997) Threshold of Sediment Motion in Coastal Environments. Pacific Coasts and Ports '97: Proceedings of the 13th Australasian Coastal and Ocean Engineering Conference and the 6th Australasian Port and Harbour Conference, Volume 1
- Stive, M. J. F., and Z. B. Wang (2003). Morphodynamic modeling of tidal basins and coastal inlets, in *Advances in Coastal Modeling*. Elsevier Oceanogr. Ser., vol. 67, edited by V. C. Lakhan, pp. 367-392, Elsevier, Amsterdam.
- Sutherland, J., Peet, A. H., & Soulsby, R. (2004). Evaluating the performance of morphological models. *Coastal engineering*, 51(8-9), 917-939.
- Suzuki, T., Hu, Z., Kumada, K., Phan, L. K., & Zijlema, M. (2019). Non-hydrostatic modeling of drag, inertia and porous effects in wave propagation over dense vegetation fields. *Coastal Engineering*, 149, 49-64.
- Suzuki, T., Zijlema, M., Burger, B., Meijer, M. C., & Narayan, S. (2012). Wave dissipation by vegetation with layer schematization in SWAN. *Coastal Engineering*, 59(1), 64-71.
- Tagliapietra, D., Baldan, D., Barausse, A., Buosi, A., Curiel, D., Guarneri, I., Pessa, G., Rismondo, A., Sfriso, A., Smania, D., & Volpi Ghirardini, A. (2018). *Protecting and restoring the salt marshes and seagrasses in the lagoon of Venice*. <http://journal.um-surabaya.ac.id/index.php/JKM/article/view/2203>
- Tanino, Y., & Nepf, H. M. (2008). Laboratory investigation of mean drag in a random array of rigid, emergent cylinders. *Journal of Hydraulic Engineering*, 134(1), 34-41.
- Tena A., Batalla R.J., Vericat D., Lopez–Tarazón J.A. (2011) Suspended sediment dynamics in a large regulated river over a 10-year period (the lower Ebro, NE Iberian Peninsula). *Geomorphology*, 125, 73–84.
- UICN France (2014). Panorama des services écologiques fournis par les écosystèmes français - étude de cas : les écosystèmes marins et côtiers d'Aquitaine. Paris, France, 48p.
- Van Leer, B. (1979) Towards the Ultimate Conservative Difference Scheme, V. A Second Order Sequel to Godunov’s Method. *J. Comput. Phys.*, 32, 101–136.
- Van Loon-Steensma, J. M., Hu, Z., & Slim, P. A. (2016). Modelled impact of vegetation heterogeneity and salt-marsh zonation on wave damping. *Journal of Coastal Research*, 32(2), 241-252.
- Van Maren, D. S., Oost, A. P., Wang, Z. B., & Vos, P. C. (2016). The effect of land reclamations and sediment

- extraction on the suspended sediment concentration in the Ems Estuary. *Marine Geology*, 376, 147-157.
- Van Maren, D. S., van Kessel, T., Cronin, K., & Sittoni, L. (2015). The impact of channel deepening and dredging on estuarine sediment concentration. *Continental Shelf Research*, 95, 1-14.
- Vanoni V. A., Brooks N. H. (1957) Laboratory studies of the roughness and suspended load of alluvial streams. Sedimentation Laboratory, California Institute of Technology, Pasadena, Calif.
- Van Rijn, L.C. (1984a) Sediment Transport, Part I: Bed Load Transport. *J. Hydraul. Eng.*, 110, 1431–1456.
- Van Rijn, L.C. (1984b) Sediment Transport, Part II: Suspended Load Transport. *J. Hydraul. Eng.*, 110, 1613–1641.
- Van Rijn, L.C. (1987). Mathematical modelling of morphological processes in the case of suspended sediment transport. Delft: Delft Hydraulics Communications #382.
- Van Rooijen, A. A., Van Thiel de Vries, J. S. M., McCall, R. T., Van Dongeren, A. R., Roelvink, J. A., & Reniers, A. J. H. M. (2015, June). Modeling of wave attenuation by vegetation with XBeach. In E-proceedings 36th IAHR World Congress (pp. 1-7).
- Valchev N., E. Trifonova, N. Andreeva. 2012. Past and recent trends in the western Black Sea storminess, *Nat. Hazards Earth Syst. Sci.*, 12, 961–977, 2012, doi:10.5194/nhess-12-961-2012
- Valchev, N, N. Andreeva, P. Eftimova, B. Prodanov, I. Kotsev, Assessment of vulnerability to storm induced flood hazard along diverse coastline settings, 3rd European Conf. on Flood Risk Manag. FLOODrisk 2016, E3S Web of Conferences 7 10002, 2016 (URL: <DOI: 10.1051/e3sconf/20160710002>).
- Vuik, V. (2017). POV Waddenzeedijken; effectiviteit voorlanden HR - Stabiliteit van vegetatie. HKV memo PR3365.30.
- Winterwerp, J. C., Zhou, Z., Battista, G., Van Kessel, T., Jagers, H. R. A., Van Maren, D. S., & Van Der Wegen, M., 2018. Efficient consolidation model for morphodynamic simulations in low-SPM environments. *Journal of Hydraulic Engineering*, 144(8), 04018055.
- WMO, 2008. Guide to Meteorological Instruments and Methods of Observation, No. 8. CWOP-WMO8.pdf (weather.gov)
- York: Cambridge University Press), 1137–1216. Available at: http://www.climatechange2013.org/images/report/WG1AR5_Chapter13_FINAL.pdf.
- Zijl, F., Groenenboom, J., Laan, S. & Zijlker, T. (2022). DCSM-FM 100m: a sixth-generation model for the NW European Shelf: 2022 release. Deltares rapport 11208054-004-ZKS-0002.
- Zhang Y, Ye F, Stanev E et al (2016) Seamless cross-scale modelling with SCHISM. *Ocean Modelling* 102. <https://doi.org/10.1016/j.ocemod.2016.05.002>